Development of Hydrate Inhibition Monitoring and Initial Formation Detection Techniques

Saeid Mazloum Vajari

Submitted for the degree of Doctor of Philosophy

Heriot-Watt University

Institute of Petroleum Engineering

February 2012

ABSTRACT

Prevention of gas hydrate blockages is a major challenge posed to the petroleum industry because uncontrolled formation of hydrate may result in plugging of transport pipelines, causing considerable production loss and personnel safety hazard. Injection of hydrate inhibitors is the most common option to prevent hydrate formation.

In current industrial practice the dosage of hydrate inhibitor is estimated and injected upstream without much downstream measurements. Therefore, hydrate blockages are still encountered in the oil and gas industry due to lack of any hydrate monitoring measures against unexpected changes.

In this thesis, novel techniques have been developed for monitoring hydrate inhibition and detecting early signs of hydrate formation based on downstream sample analysis and online measurements. The main achievements of this study can be categorised as follow:

1. **Hydrate Inhibition Monitoring Techniques:** Three techniques, i.e. conductivity-velocity (C-V) technique, water activity technique and water content technique, have been developed for determining optimising inhibitor injection rates
2. **Initial Hydrate Formation Detection Techniques:** The main objective of detecting early signs of hydrate formation is to give the operators adequate time to prevent hydrate formation and start remediation actions. Two techniques including the onset of hydrate formation and compositional change have been developed for detecting initial hydrate formation
3. **Development of prototypes:** Following the above fundamental studies, prototypes of the CV and water activity methods have been developed

The development of hydrate inhibition monitoring and early hydrate formation detection techniques opens a novel flow assurance approach for the oil and gas industry. The developed hydrate monitoring techniques like the C-V technique, water activity and content techniques can be used to optimise hydrate inhibitor injection. In the near future, further development of the investigated early hydrate formation detection techniques like gas compositional change technique could provide an effective measure to minimise the risk of hydrate blockage.

Dedicated to my parents

ACKNOWLEDGEMENTS

I would like to express my sincere gratitude to Professor Bahman Tohidi for providing me the opportunity to do this research and also for his outstanding supervision, guidance and support throughout my thesis. He was always accessible and willing to help me with my study. On personal side, he did not hesitate to invite me to become an extended part of his family.

I wish to deeply thank Dr. Jinhai Yang and Dr. Antonin Chapoy for their supervision and technical advice and helpful discussions during the course of this thesis and furthermore for their critical comments on this thesis. My profound thanks are also extended to Ross Anderson, Rod Burgess who helped me constantly with their valuable suggestions and patiently dealt with all my questions. I am also grateful to all my friends and colleagues at the Centre for Gas Hydrate Research and Hydrafact Ltd who made my stay in Edinburgh very pleasant and memorable. Especial thanks go to Roghieh Azarinezhad who has been a friend and was there whenever I needed her help no matter time or day.

I greatly appreciate the reviewers and examiners of this thesis, Dr. Anne Sinquin and Dr. Arfan Ali for their precious times and valuable suggestions.

Additionally, I would like to thank the members of mechanical and electrical workshop who were responsible for manufacture and maintenance of the experimental equipments designed and used as part of this study.

This study is a part of research Project "Hydrate Monitoring and Early Warning System", sponsored by JIP (Joint Industrial Project). The JIP programme is jointly sponsored by BP, Chevron, Petronas, Statoil, Petronas, NIGC and TOTAL, whose support is gratefully acknowledged.

Last but not least, I express my heartfelt appreciation to my family for their love, moral support and patience during my absence.

DECLARATION STATEMENT

ACADEMIC REGISTRY
Research Thesis Submission

Name*:*	Saeid Mazloum Vajari		
School/PGI:	Institute of Petroleum Engineering		
Version: *(i.e. First, Resubmission, Final)*	First	Degree Sought (Award **and** Subject area)	PhD in Petroleum Engineering

Declaration

In accordance with the appropriate regulations I hereby submit my thesis and I declare that:

1) the thesis embodies the results of my own work and has been composed by myself
2) where appropriate, I have made acknowledgement of the work of others and have made reference to work carried out in collaboration with other persons
3) the thesis is the correct version of the thesis for submission and is the same version as any electronic versions submitted*.
4) my thesis for the award referred to, deposited in the Heriot-Watt University Library, should be made available for loan or photocopying and be available via the Institutional Repository, subject to such conditions as the Librarian may require
5) I understand that as a student of the University I am required to abide by the Regulations of the University and to conform to its discipline.

* *Please note that it is the responsibility of the candidate to ensure that the correct version of the thesis is submitted.*

Signature of Candidate*:*		Date:	

Submission

Submitted By *(name in capitals):*	Saeid Mazloum Vajari
Signature of Individual Submitting:	
Date Submitted:	

For Completion in the Student Service Centre (SSC)

Received in the SSC by *(name in capitals):*			
Method of Submission *(Handed in to SSC; posted through internal/external mail):*			
E-thesis Submitted (*mandatory for final theses)*			
Signature:		Date:	

TABLE OF CONTENTS

Abbreviations

AA	Anti-agglomerates
AAD	Average absolute deviation
ABS	Absolute value
AC	Alternating current
ANN	Artificial neural network
Aw	Water activity
C	Electrical conductivity
d	Molecular diameter
DC	Direct current
DSO	Digital oscilloscope
EG	Ethylene glycol
EM	Electromagnetic
EoS	Equation of state
FIR	Far infrared
FP	Freezing point
FPGA	Field programmable gate arry
GASPT	Gas property measurement
GHD	Gas hydrate deposit
GUI	Graphical user interface
HMI	Human-machine interface
HSB	Hydrate stability boundary
HSZ	Hydrate stability zone
HWHYD	Heriot-Watt hydrate prediction software
HYDRAFLASH	Hydrate and PVT Prediction Commercial Software
IR	Infrared
KI	Kinetic inhibitor
LDHI	Low dosage hydrate inhibitor
MEG	Mono ethylene glycol
MW	Micro wave
NIR	Near infrared
TOHSZ	Temperature outside hydrate stability zone
PE	Peltier element
ppm	Part per million
PRT	Platinum resistance temperature probe
PTFE	Poly(tetrafluoroethylene)
PVCap	Polyvinylcaprolactam
PVT	Pressure-volume-temperature
PVTX	Pressure-volume-temperature and concentration
RTD	Resistance thermometer device
SCADA	Supervisory control and data acquisition systems
sH	Structure H gas hydrate
sI	Structure I gas hydrate
sII	Structure II gas hydrate
SoS	Speed of sound

TDLAS	Tuneable diode laser absorption spectroscopy
TE	Thermoelectric module
UV	Ultraviolet
V	Speed
VIS	Visible

List of Publications by the Candidate

Some of the results of this research have been published in the following peer reviewed journals and conferences. Two patens also has been filed as a result of the research.

Mazloum, S., Yang, J., Chapoy, A., and Tohidi, B., 2011. A New Method for Hydrate Early Warning System Based on Hydrate Memory. *7th International Conference on Gas Hydrates*. Edinburgh, Scotland, United Kingdom, 17-21 July 2011.

Mazloum, S., Chapoy, A., Yang, J., and Tohidi, B., 2011. A Simple Correlation for Calculating the Hydrate Suppression Temperature Based on Water Activity. *7th International Conference on Gas Hydrates*. Edinburgh, Scotland, United Kingdom, 17-21 July 2011.

Mazloum, S., Chapoy, A., Yang, J., and Tohidi, B., 2011. Developing a Robust Hydrate Early Warning System. *7th International Conference on Gas Hydrates*. Edinburgh, Scotland, United Kingdom, 17-21 July 2011.

Mazloum, S., Chapoy, A., Yang, J., and Tohidi, B., 2011. Online Monitoring of Hydrate Safety Margin. *7th International Conference on Gas Hydrates*. Edinburgh, Scotland, United Kingdom, 17-21 July 2011.

Mazloum, S., Yang, J., Chapoy, A., and Tohidi, B., 2011. A Novel Technique for Optimising Hydrate Inhibitor Injection Rates. *Offshore Technology Conference*. Rio de Janeiro, Brazil, 4-6 October 2011.

Chapoy, A., Mazloum, S., Burgass, R., Haghighi, H., and Tohidi, B., 2012. Clathrate Hydrate Equilibria in Mixed Monoethylene Glycol and Electrolyte Aqueous Solutions. *The Journal of chemical Thermodynamics*, **48**, pp:7-12.

Mazloum, S., Chapoy, A., Yang, J., and Tohidi, B., 2012. Developing a Hydrate Early Detection System. *Proceedings of the 3rd International Gas Processing Symposium*. Doha, Qatar, 5-7 March 2012.

Haghighi, H., Chapoy, A., Burgass, R., Mazloum, S., and Tohidi, B., 2009. Modelling of Phase Equilibria for Petroleum Reservoir Fluids Containing Water and Aqueous

Methanol Solutions: Experimental Measurements and Modelling Using the CPA Equation of State. *Fluid Phase Equilibria*, **278**, pp:109-116.

Yang, J., Chapoy, A., Mazloum, S. and Tohidi, B., 2012. Improving the Reliability of Hydrate Prevention Techniques. *Proceedings of the 3rd International Gas Processing Symposium*. Doha, Qatar, 5-7 March 2012.

Yang, J., Chapoy, A., Mazloum, S. and Tohidi, B., 2011. Development of a Hydrate Inhibition Monitoring System by Integration of Acoustic Velocity and Electrical Conductivity Measurements. *Exploration & Production - Oil & Gas Review*. Volume 9 Issue I.

Bonyad, H., Zare, M., Mosayyebi, M. R., Mazloum, S. and Tohidi, B., 2011. Field Evaluation of A Hydrate Inhibition Monitoring System. *Offshore Mediterranean Conference OMC*. Ravenna, Italy, 23-25 March 2011.

Yang, J., Chapoy, A., Mazloum, S. and Tohidi, B., 2011. A Novel Technique for Monitoring Hydrate Safety Margin. *SPE EUROPEC/EAGE:Annual Conference and Exhibition*. Vienna, Austria, 23-26 May.

Macpherson, C., Glenat, P., Mazloum, S. and Young, I., 2012. Successful Deployment of a Novel Hydrate Inhibition Monitoring Systems in a North Sea Gas Field. *Oil Field Chemistry Symposium*. Oslo, Norway, 18-21 March.

Patents:

"A Method for Water Treatment Specifically, for Removing KHIs from Produced water". UK patent application no. 1202743.9

"Early Warning System for Hydrate or Clathrate Materials". UK patent application no. 1108224.5

CHAPTER 1. INTRODUCTION

The growing demand for oil and natural gas combined with a rise in oil and gas prices has forced the industry to develop new fields in increasingly deeper waters and longer tiebacks worldwide. Production at these extremes has raised a great concern with flow assurance issues. The high pressure and low temperature conditions in these regions provide favourable conditions for gas hydrate formation. Gas hydrate management is considered to be one of the most critical aspects of flow assurance design strategies because hydrate blockages commonly cause serious problems to oil & gas transport pipelines, processing facilities, and deep-water drillings. It impedes hydrocarbon flow and even exposes personnel safety at danger (Barker and Gomez, 1989; Sloan, 2000). It can completely stop production for several days. The recent (April 2010) BP failing attempt to place a containment chambers on their severed oil pipe in the Gulf of Mexico is a vivid example of equipment failure due to formation of hydrates. In addition, the removal of hydrate plugs is generally difficult to achieve and could cause considerable damage to production facilities such as line rupture and could create a serious safety and environmental hazard. For these reasons, hydrate plug formation should be prevented effectively and economically to guarantee that pipelines operate normally.

The chapter starts with an overview of gas hydrates, a brief review of the existing flow assurance solutions and their limitations for tackling these problems. The main objective of this chapter is to introduce the concept of "Hydrate Inhibition Monitoring and Initial Hydrate Formation Detection Techniques". This concept forms the basis of novel techniques which have been developed and intensively investigated in this thesis in order to optimise hydrate inhibitor injection and minimise the risk of hydrate blockage. The application of these techniques can be further expanded by implementing them in SCADA (Supervisory Control And Data Acquisition) systems being used in advanced monitoring and managing systems in oil and gas productions. The rest of the chapter presents the outline of the thesis.

1.1. GAS HYDRATES

Gas hydrates are ice-like crystalline structures formed by hydrogen bonded water molecules and stabilised by the presence of guest molecules within the lattice cavities. Without the support of the trapped molecules, the lattice structure of hydrate clathrates would collapse into conventional ice crystal structure or liquid water. The molecules commonly found in natural gas that occupy the cavities are light alkanes (C1-C4), carbon dioxide, nitrogen and hydrogen sulphide. Three main structural types of gas hydrates that form naturally in gas/water mixtures are structure I (sI), structure II (sII) and structure H (sH). These structures have been characterised using neutron or X-ray diffraction techniques. sI and sII hydrate crystals were determined in the late 1940s and mid 1950s (von Stackelberg et al., 1949; von Stackelberg et al., 1954). Structure H was determined by Ripmeester (Ripmeester 1987). The type of the structure formed depends primarily on the size of the guest molecules. Small and round molecules like methane and carbon dioxide form structure I. While typical natural gas mixture containing C_1-C_4 components will preferentially form structure II hydrate. For inclusion of larger molecules such as n-butane which can go into the large cavities of sII, the presence of a smaller 'help' gas such as methane is required to fill small cavities and stabilise the structure. sH is capable of trapping much larger molecules, such as methylcyclohexane. Figure 1.1 shows the three common hydrate unit crystal structures and geometry of the cages. Each structure is a combination of small and larger cages. When a minimum number of cavities are occupied, crystals become stable and hydrate forms. Gas hydrates can form at temperatures well above the

freezing point of water depending on the pressure. If all the cages are occupied, the ratio of water molecules to hydrocarbon molecules would be 5.67 to 5.75 depending on the formed structure. A detailed description of the molecular structure has been given by (Sloan and Koh, 2008).

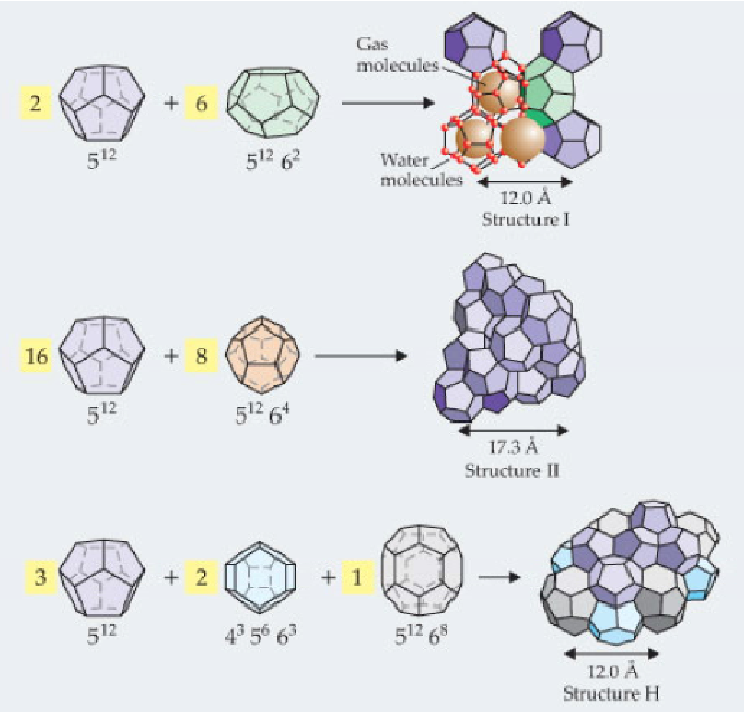

Figure 1.1 The three common hydrate crystal structures illustration and geometry of cages (Drawn from http://www.eoearth.org)

1.2. GAS HYDRATE STABILITY ZONE (HSZ)

Gas hydrates can form in conditions where water and gas molecules exist under favourable pressure and temperature. The set of pressures-temperatures at which hydrate can form is called hydrate stability zone (HSZ). The boundary of hydrate stability zone depends upon composition of aqueous and hydrocarbon phases. For a given composition of hydrocarbons and aqueous phase, a curve of temperature and pressure can be measured and/or predicted from statistical thermodynamics using modern thermodynamic computer programmes. This curve is called hydrate phase boundary (Figure 1.2). The area to the right of the curve will be free of hydrates, whereas the area to the left represents conditions where hydrates can form. In this figure, natural gas hydrate phase boundary has been predicted for different aqueous

systems, i.e. systems containing 10 mass% of salt or different thermodynamic inhibitors using HWHYD 2.1 software, which is developed by the Centre for Gas Hydrate Research at Heriot-Watt University. As can be seen, the addition of thermodynamic inhibitors such as salt, methanol and ethylene glycol to the aqueous phase shifts the curves to lower temperatures (or higher pressures). This is the most common way of preventing gas hydrate formation which will be discussed in more detail later in this chapter.

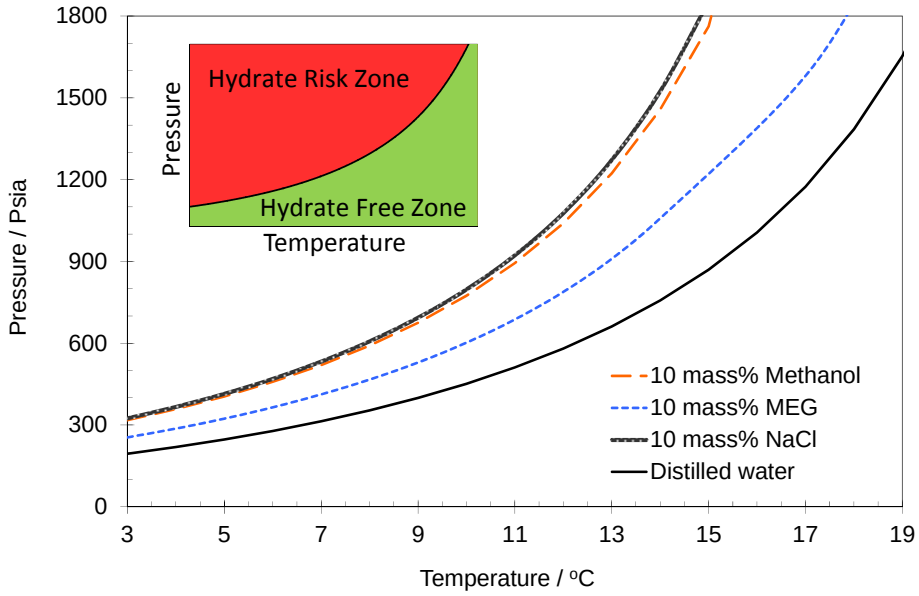

Figure 1.2 Predicted hydrate phase boundary for a typical standard natural gas using HWHYD2.1 and effect of different thermodynamic inhibitors and salt on hydrate forming condition.

1.3. GAS HYDRATE CONTROL AND PREVENTION

In principle, there are two options to avoid hydrate blockage with regard to the nature of gas hydrate formation. One option is to remove one of the elements that are essential for hydrate formation. For example, the hydrocarbon fluids in a pipeline can be kept outside the hydrate stability zone by thermal insulation or active heating, or by lowering the operating pressure, or by reducing water content. However, these techniques may not be feasible and/or economical for some conditions, especially in offshore and deep-water environments because of high cost of insulation, heating, and dehydration (Sloan, 2005).

Application of hydrate inhibitors is the second option to prevent hydrate blockage or reduce the risk of hydrate blockage. Hydrate inhibitors are divided into two categories, i.e., thermodynamic hydrate inhibitors (THIs) and low dosage hydrate inhibitors (LDHIs). Thermodynamic inhibitors like methanol (MeOH), mono ethylene glycol (MEG) and ethanol are such chemical additives that shift the hydrate phase boundary to a lower temperature and/or higher pressure by reducing the water activity. Therefore, the system can be operated safely outside the hydrate stability region. Selection of the thermodynamic inhibitors often involves comparison of many factors including required dosage, possibility of regeneration, safety and environmental issues, capital/operating cost, physical properties (such as viscosity, volatility and solubility in liquid hydrocarbon phase), gas dehydration capacity and corrosion inhibition effect. As can be seen in Figure 1.2, methanol inhibits hydrate formation more than an equivalent mass percentage of glycol in the aqueous phase. Though more effective, methanol does have safety issues as it is a volatile and flammable liquid and is known to be toxic to living organisms. From an industrial view point, methanol increases the corrosion tendencies of pipes and equipment (Hoppe et al, 2006). Typically, methanol is not recovered due to its high volatility and low costs, therefore, the economic of methanol recovery are not favourable in most cases. But since glycols are expensive inhibitors, there is a definite need for extra, costly and space consuming, onshore or offshore plants for their regeneration (Mokhatab et al., 2007). Methanol injection leads to a high operational expenditure and also needs large storage facilities. MEG injection needs installation of reboilers for regeneration as well as storage requirement. Glycol is non-flammable. In addition to hydrate inhibition, MEG can act as a dehydration means for gas system. Only a negligible amount of MEG is lost to the gas phase as it is not very volatile. It does not also contaminate the oil due to its low solubility. But it is significantly more viscous than methanol, especially at low temperatures. This means that a MEG injection system requires stronger pumps and larger diameter lines. It is not rare that a high concentration up to 60 mass% of MeOH or MEG in the aqueous phase may be needed to have sufficient inhibition effect. For high water-cut systems the large volume of MeOH and MEG requires huge storage areas on the platform with limited space and/or separate pipeline, may result in significant increase in CAPEX and OPEX, as well as negative impact on the environments (Brustad et al., 2005 and Cowie et al., 2005). As a result, in the past two

decades, LDHIs have been developed rapidly (Lederhos et al., 1996; Notz et al., 1996; Mitchell and Talley, 1999; Argo et al., 2000 and Fu et al., 2002). LDHIs include kinetic hydrate inhibitors (KHIs) and anti-agglomerants (AAs). LDHIs are so called as they can be efficiently used at dosages far lower than those of thermodynamic hydrate inhibitors. Generally they are effective at 0.5 – 3 mass% in water, whereas methanol and glycol are generally used between 10 – 60 mass% in water. These new hydrate inhibitors form the basis of a technique that allows the system to operate inside the hydrate stability zone, contrary to the previous described methods. In fact, LDHIs act at the early stages of hydrate formation by interfering with the process of nucleation/growth and/or modifying the rheological properties of the system. It is generally believed that KHIs delay hydrate nucleation and hinder hydrate growth within certain degree of subcooling, while AAs allow hydrate formation but prevent hydrate crystals from agglomeration, thus hydrate crystals can be transported as slurry at reasonable viscosity. By 2005 there were 50-70 field applications of LDHIs, the majority of them related to KHIs. The commercial deployment of AA started a little later than KHI due to environmental and operational concerns. However, the number of AA applications is now increasing rapidly (Kelland, 2006).

In current industrial practice the amount of a hydrate inhibitors (i.e., thermodynamic inhibitors, KHIs and AAs) is determined based on the predicted or measured hydrate phase boundary for the specific fluid composition (gas or oil and water), water-cut, worst temperature and pressure conditions, and the estimated inhibitor loss to non-aqueous phases. In addition to the above a safety factor is also considered when calculating the inhibitor dosage and/or pump rate. Consequently, it is usual that excessive dose of an inhibitor has to be applied to minimize the risk of hydrate blockages, which causes unnecessarily more cost and severer environmental impact. However, despite all these measures, hydrates do still form and cause serious operational and safety concerns. Their formation often takes place due to problems with injection pumps, a sudden increase in the water cut (water content of the fluid in the system), reducing the concentration of inhibitor, a change in fluid flow rate, emergency shut-downs, problems associated with start-ups, lack of reservoir fluid samples, lack of information on the composition of produced water, changes in the system temperature and pressure, uncertainty concerning the performance of the utilised inhibitor(s), and deleterious synergy between various inhibitors.

For these reasons, hydrate inhibition and formation should be controlled and monitored effectively to guarantee that pipelines operate normally and economically. In general, systematic ways of controlling and monitoring along the pipeline and/or downstream to examine the degree of inhibition and warns initial hydrate formation are very limited. Therefore new techniques are necessary. In this thesis, novel techniques have been developed for monitoring hydrate inhibition and initial hydrate formation detecting based on downstream sample analysis and online measurements.

1.4. MONITORING HYDRATE INHIBITION TECHNIQUES

The aim of this part of the work is developing few techniques that can provide an accurate and timely data of the degree of hydrate inhibition in the pipeline or processing facilities, i.e., how far away the operating conditions are from the HSZ. The techniques perform measurements of physical parameters of produced fluids which are then used to either directly calculate hydrate phase boundary or indirectly through inhibitors concentrations. The determined phase boundary of produced fluids is compared with the operational conditions of the production unit in which the measurements take place. Hydrate safety margin was introduced to describe the degree of hydrate inhibition. It is defined as the temperature difference between the actual fluid temperature and the hydrate dissociation temperature at a given pressure. The determined hydrate safety margin can be used as traffic lights to help the operators have an appropriate control of hydrate inhibition. In Figure 1.3, a red light can be shown if the determined hydrate safety margin is negative, which alarms the operator that the pipeline conditions are inside the HSZ, i.e., the pipeline has already been exposed to hydrate formation risk, therefore, more hydrate inhibitor must be injected into the pipeline immediately; a green light indicates that the system is safe from hydrate formation and the current injection rate of the inhibitor is appropriate; an amber light reminds the operator that the system is close to the HSZ and the inhibitor injection rate needs to be increased a bit; finally, a blue light means over inhibition, therefore, the inhibitor injection rate should be reduced. Furthermore, the increment or decrement of hydrate inhibitors can be quantitatively estimated using the determined hydrate safety margin.

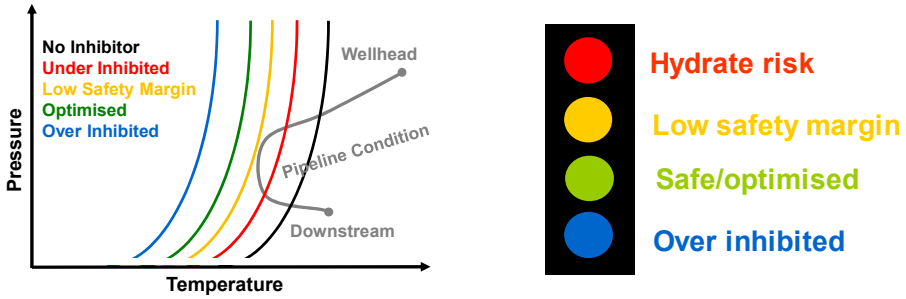

Figure 1.3 Hydrate safety margin determined by the developed hydrate inhibition monitoring techniques could be used as traffic lights to help the operators have a better control of hydrate inhibition.

1.5. INITIAL HYDRATE FORMATION DETECTION TECHNIQUES

The main objective of detecting early signs of hydrate formation is to give the operators adequate time to prevent hydrate formation and start remediation actions. Early warning sign of hydrate formation in pipeline and also in onshore processes and platforms is very important to ensure appropriate measure is taken to prevent the blockage and rupture of pipeline and vessels. Sloan (Sloan, 2000) pointed out that no one indicator gives the best warning of hydrate formation. In general, there are several methods for warning of hydrate formation which are applied and considered for testing. These are pigging return, changes in fluid rates and compositions at the separator, pressure drop increases, acoustic detection, thermocamera and gamma ray densitometer. However, each of this method has its own limitation.

Pigging Returns: The flexible plastic balls or cylinders called pigs are launched through the pipeline by pressure driven to sweep debris from the pipeline into a pig trap. The pig trap provides valuable information about solid deposition in the pipeline such as hydrates, wax, scale and sand. In the case of hydrate, frequently hydrate particles are found in pig traps before hydrate blockages occur in the pipelines. Pigging returns is carefully examined for evidence of hydrate particles. Hydrate masses are stable even at atmospheric pressure in a pig receiver discharge. The endothermic process of hydrate dissociation causes released water to form ice, which inhibit rapid dissociation. Although onshore pigging is commonly done to keep lines clear, it may be very expensive to provide offshore pigging either through a mobile pigging vessel over the well or from the wellhead without round trip pigging

capability. Therefore, high costs limit the frequent examination of offshore pigging returns.

Changes in Fluid Rates of Composition at Separators: When the water production is small, it may be possible to monitor the rate of water production. If the water arrival decreases significantly at the separator, hydrate may be forming in the line. This has been reported by Corrigan et al (Corrigan et. al., 1996) on the controlled experiment by British Petroleum for 13.7 miles gas line in the southern North Sea. This case study showed that after methanol injection was stopped, no increase in accumulation of water production for 30 hours after the start of test while gas flow rates remained steady and the pressure drop did not change. The first significant increase in line pressure was observed 46 hours after the start of the test and large fluctuation in the gas flow rate observed 74 hours after the start of the test concurrent with further increase in pressure. In this case, separator water rate provides an early indication of hydrate formation by 16 hours in a gas line that has no oil/condensate and little water production. However, when water production is substantially higher or intermittent, this technique will not be applicable as early warning. The monitoring of changes in gas composition is not being widely reported. Therefore this technique is explored further in this thesis.

Pressure drop increases: A less direct flow indicator is line-pressure drop build-up, which differs for hydrates and for paraffin wax. Hydrate formation at the wall in the gas pipeline will cause the pressure drop (Δp) increases and the flow rate decrease due to decrease in the pipe diameter. Pressure drop increases are usually more noticeable than flow rate changes. The change in Δp is more sensitive than the change in flow because the Δp in pipes is proportional to the square of turbulent flow rates. However, in the presence of hydrate, a large restriction may be necessary over a long length before a substantial pressure drop occurs. In addition, the Δp trace usually contains substantial noise making it difficult to observe small changes or trends in Δp as an early warning.

Acoustic Sensing Along Subsea Pipeline: This technique has been widely used for sand monitoring by detecting sand impingement on pipe. Application of acoustic sensor for hydrate particles is limited to onshore pipeline. However, this unit has yet to be field tested in a subsea application (Sloan, 2000).

Thermocamera: It is a hand-held device that measures the infrared spectral transmission as an indicator of system temperature (Sloan, 2000) only onshore or topside offshore. This device enables determination of temperature variations in the system, particularly at points where hydrates might form but where a thermocouple is not provided such as downstream of a valve. The limitation is that this thermocamera is very sensitive to pipe coating, variation in wall thickness and pipe roughness.

Gamma Ray Densitometers with Temperature Sensing: A gamma ray densitometer uses an emitter and sensor on opposite external of pipe walls. The transmission of the gamma ray to the sensor is a function of the density of the pipe contents. This technique is based on combined gamma ray densitometry with the temperature downstream of densitometry to indicate changes in conditions that could be hydrate present. This combination is needed since the gamma ray alone will not be able to discriminate density of water and hydrate. Hydrates are indicated by a low temperature (owing to the Joule-Thomson effect) and an increase in density, whereas the water temperature is similar to that of gas. A high-density, low temperature mass in the pipeline is likely to be hydrates, whereas a high density slug without a temperature drop is probably water. This technique is useful tool for onshore but it could not be applied to subsea due to limitation on temperature sensing requirement.

The aim of initial hydrate formation detection techniques in this work is to provide timely signs of initial hydrate formation in the pipeline and/or processing facilities. These techniques provide measurements of physical parameters of fluids flow and/or fluids samples which are then used to determine whether the initial hydrate formation took place in the system. The provided measurements can detect changes in the water structure referred as hydrate water memory or the changes in the composition of gas phase and gas released from aqueous phase. The techniques are designed to give the operator adequate time to initiate remedial steps prior to massive hydrate formation/build up which could result in pipeline/facilities blockage.

1.6. THESIS OUTLINE

In this thesis, a number of novel techniques have been developed for monitoring hydrate inhibition and detecting early signs of hydrate formation based on downstream sample analysis and online measurements. Figure 1.4 illustrates structure of the thesis

and subcategorises different investigation conducted for developing each technique. Each group of these techniques have been detailed in appropriate chapters as follow.

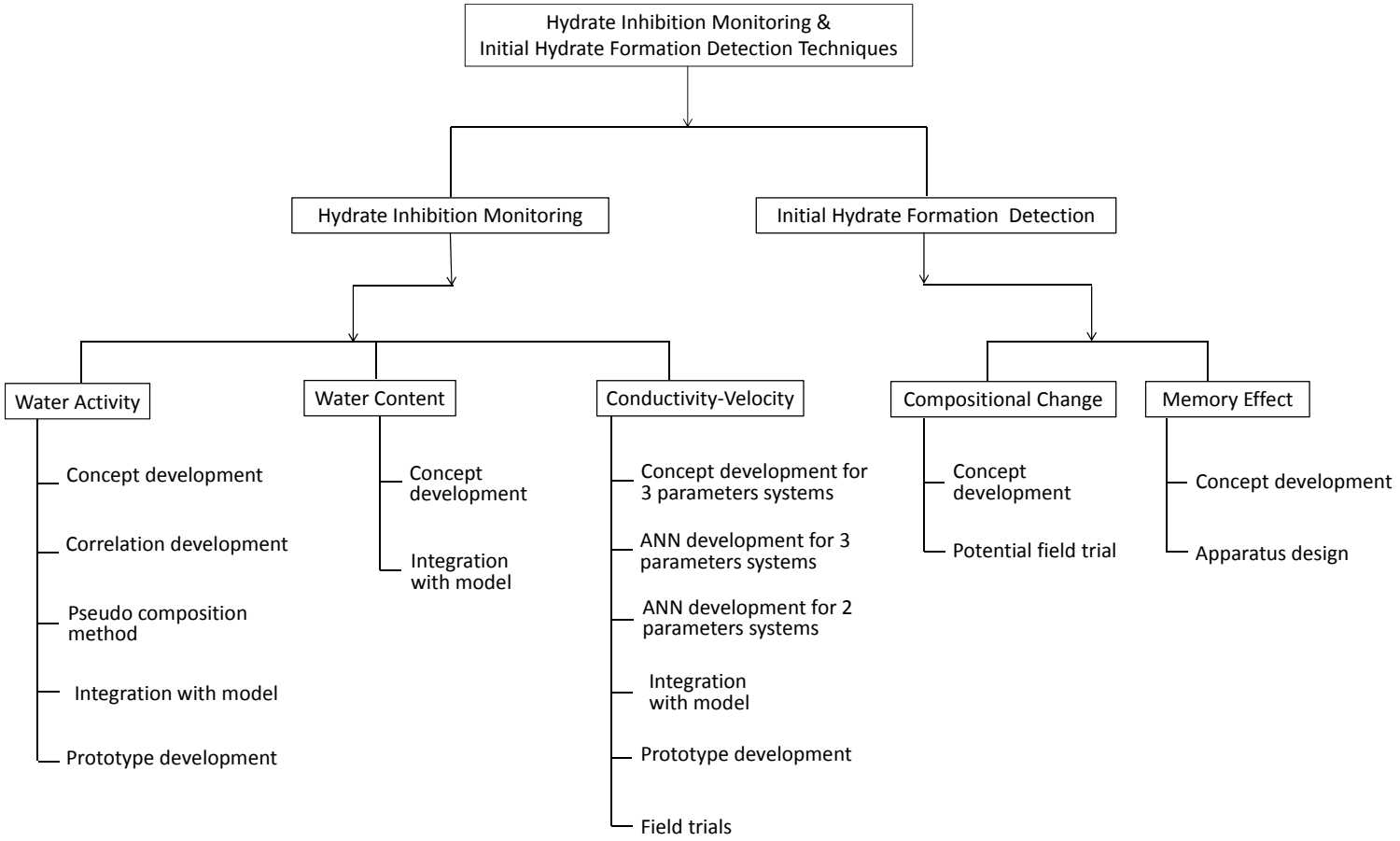

Figure 1.4 Workflow chart illustrating the structure of the thesis and subcategorising different investigations conducted for each technique developed in this work.

This thesis consists of seven chapters. The current chapter introduce the concept of hydrate inhibition monitoring and initial hydrate formation detection techniques, presenting the main definitions and principal of the work and summarising different hypothesis investigated and developed in this work.

Under "monitoring hydrate inhibition" category, three techniques, i.e. conductivity-velocity (C-V) technique, water activity technique and water content technique, have been developed for determining the hydrate risk free zones and optimising inhibitor injection rates. C-V technique has been detailed in Chapter 2 and water activity technique along with water content technique has been presented in Chapter 3. It is essential to understand the fundamentals behind the desired techniques. As a result, the effect of different hydrate inhibitors (e.g. MEG, Ethanol, Methanol, AA, KHI, and salts), thermodynamic conditions (temperature and pressure) on the physical properties of downstream fluids were intensively investigated including, electrical conductivity, acoustic velocity and conductivity/velocity thermal coefficients, water activity, and water content in appropriate chapters.

In C-V technique, downstream fluid properties, i.e. conductivity, acoustic velocity and conductivity/velocity thermal coefficients, were correlated to the corresponding salt and inhibitor concentrations using pre-trained Artificial Neural Network (ANN). Therefore, by online/downstream measurements of physical properties of fluid, the salt and inhibitor concentrations can be determined. These concentrations were then linked to an in-house thermodynamic model to predict hydrate stability zone of the system under study. This technique was further extended to three parameter systems where there are three unknown concentrations, e.g. salt, thermodynamic inhibitor and KHI. The three parameter method is very useful in the field during changeover of inhibitor types (e.g. exchange from methanol injection to KHI injection) or during restart of the LDHI inhibited field where the system should be treated with thermodynamic inhibitor to prevent hydrate formation upon restart. Obviously, salt is usually the third unknown parameter in these cases.

In Chapter 3, the water activity of liquid phase or the water content of vapour phase was correlated to the suppression of hydrate dissociation temperature due to the presence of salts and hydrate inhibitors without the need to know the specific type of the salts and thermodynamic inhibitors. Thermodynamic modelling was also performed to predict the water activity and water content for the experimentally tested inhibition systems to evaluate the experimental measurements.

"Initial hydrate formation detection" category includes the onset of hydrate formation (hydrate memory) and compositional change techniques (composition of gas phase and gas released from aqueous phase). The results of investigating and developing these two techniques are presented in Chapters 4 and 5 respectively.

Onset of hydrate formation technique is based on detecting hydrate formation memory. The principle of the technique is that hydrate forms more easily from a solution with hydrate memory than from a freshly prepared gas-water mixture. Therefore, if the produced water has experienced hydrate formation in production facilities, the hydrate memory can be detected in downstream. For the hydrate memory technique, the effect of hydrate memory on the onset of hydrate formation was investigated for different systems containing salt, methanol, MEG, KHI and produced water. The dependence of hydrate memory on various parameters was also experimentally tested, such as the retaining time, temperature outside the hydrate stability zone, pressure, depressurisation, and changes in gas compositions. A purpose-build apparatus was also designed and built as part of this thesis to make it possible to use thermoelectric modules for cooling and heating in development of hydrate memory-based early warning device which could facilitate its application in field condition.

For the compositional change techniques, the changes in the composition of gas phase and gas released from aqueous phase were investigated for detecting hydrate history. These techniques are based on the fact that composition of gas in both gas and hydrate (and consequently aqueous phase resulted from dissociation of hydrate) phases

significantly changes due to hydrate formation. The effects of different parameters on the gas compositional change were experimentally tested, such as hydrate saturation, retaining time, temperature outside the hydrate stability zone, and the presence of different inhibitors and salts. Different measuring/sampling procedures and methods were also investigated to facilitate application of the compositional change technique. In collaboration with the project sponsors a field evaluation is being planned for this technique.

Following the above fundamental studies, prototypes of the C-V and water activity techniques have been developed. The developed C-V prototype can determine salt and hydrate inhibitor concentrations simultaneously by an artificial neural network (ANN) correlation using the measured conductivity and velocity, and can also predict the hydrate stability zone with an in-house thermodynamic model using the determined salt and inhibitor concentrations given that the hydrocarbon composition is known. The autocorrelation approach was applied to improve the accuracy and reliability of the C-V prototype. The C-V prototype has been commercialised after intensive evaluation in our lab and under field conditions by some oil and service companies. A water activity correlation was developed to determine the suppression of hydrate dissociation temperature using the measured water activity over a wide range of temperature and pressure for salt systems and salt-MEG systems. Pseudo salt and inhibitor concentrations were introduced to improve the accuracy of water activity technique. The developed water activity prototype can determine hydrate suppression temperature and stability zone using the measured water activity by integration with our in-house thermodynamic model and a commercial water activity meter. Chapter 6 details the developed prototypes.

The main conclusions drawn from this thesis along with a number of recommendation for future work has been presented in the last chapter, Chapter 7.

CHAPTER 2. INTEGRATED C-V TECHNIQUE FOR HYDRATE INHIBITION MONITORING

2.1. INTRODUCTION

This chapter details development of a novel hydrate inhibition monitoring/optimising system named conductivity-velocity (C-V) method based on acoustic velocity and electrical conductivity measurements of an aqueous sample. C-V method determines concentrations of both salt and inhibitors with high accuracy, however the embedded C-V method also predict hydrate stability zone of the system when hydrocarbon composition and operation temperature and pressure are known.

C-V method was developed successfully in this laboratory (Yang et al., 2011) for two parameters systems (systems with two unknown salt and/or inhibitor concentrations), i.e., MeOH or MEG or KHI systems in the presence of salts. In this study, as a continuation of the work, the two parameter C-V method was extended to systems containing AA, KHI or ethanol in the presence of salt, and further developed for three parameters systems (systems with three unknown salt and two inhibitors). This chapter details these developments and the results.

2.2. METHODOLOGY

Hydrate safety margin under a pipeline pressure can be defined as a temperature difference between the actual fluid temperature and the hydrate dissociation temperature for a specific composition of the gas or oil in the pipeline. It was previously reported that the hydrate suppression temperature (i.e., dissociation temperature shift) of salt aqueous solution can be determined by measuring the electrical conductivity of an aqueous sample (Mohammadi, et al., 2007). Henning et al. (2000) developed an acoustic multi-sensor system for accurate measurements of concentrations of chemicals like MeOH and MEG. However, in most cases, there are salts and one inhibitor at least in the aqueous phase in a pipeline. To be able to determine both inhibitor and salt concentrations simultaneously two physical properties are at least to be known. Sandengen and Kaasa (2006) developed an empirical correlation that determined MEG concentration and NaCl concentration based on measurements of the density and electrical conductivity of water samples under examination. However, the requirement of high accuracy of the density measurement makes it hardly applicable to real produced water samples that usually contain solid particles (sands and clays) and oil droplets.

In general, to determine any number of unknown parameters, the same number of equations will be needed. In the other words, equal to the number of unknown parameters in a system, the same number of independent measurements will be conducted to be able to determine the unknown parameters. The aim of this work was to accurately determine concentration of one inhibitor in the presence of salt (two parameters system) and also to further develop this method for systems containing two inhibitors and salt (three parameters system). Therefore, in the former case, measurement of two independent parameters and in the later case, three independent parameters are required. To be able to determine these concentrations, measuring sound velocity and electrical conductivity were selected for two parameter measurements whilst for three parameters systems, temperature slope of sound or conductivity was used as the third property to be determined. The following section defines these properties.

2.2.1. Electrical Conductivity

Electrical Conductivity is the ability of a material to conduct electric current. The basic principle by which instruments measure conductivity is simple, two plates are placed in the sample, a potential is applied across the plates (normally a sine wave voltage), and the current that passes through the solution is measured. Conductivity (G), the inverse of resistivity (R), is determined from the voltage and current values according to Ohms law:

$$G = \frac{I(amps)}{E(volts)} = \frac{1}{R} \qquad \text{Equation 2.1}$$

Since the charge on ions in solution facilitates the conductance of electrical current, the conductivity of a solution is proportional to its ion concentration. In some situations, however, conductivity may not correlate directly to concentration. Figure 2.1 illustrates the relationship between conductivity and ion concentration for two common solutions. It should be noted that the graph is linear for sodium chloride solution, but not for highly concentrated sulphuric acid (Wright, 2007). Ionic interactions can alter the linear relationship between conductivity and concentration in some highly concentrated solutions. The C-V technique was only developed in the linear region.

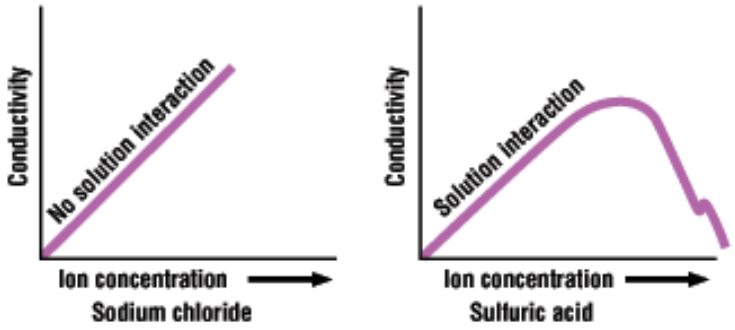

Figure 2.1 Example chart for electrical conductivity and ion concentration for NaCl and sulphuric acid

The basic unit of conductance is the siemens (S), formerly called the mho. Since cell geometry affects conductivity values, standardized measurements are expressed in specific conductivity units (S/cm) to remove the effect of variations in electrode dimensions. Figure 2.2 shows a schematic of a conductivity cell with two electrodes.

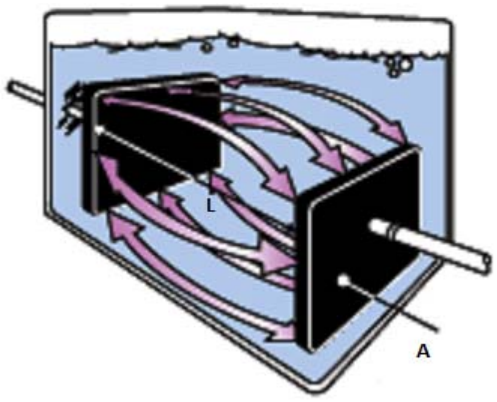

Figure 2.2 Schematic of a conductivity measurement cell with two electrodes

Specific conductivity (C) is product of measured conductivity (G) and the electrode cell constant K (L/A), where L is the length of the column of liquid between the electrodes and A is the area of the electrodes.

$$C = G * \frac{L}{A} \qquad \text{Equation 2.2}$$

If the cell constant (K) is 1 cm^{-1}, the specific conductivity is the same as the measured conductivity of the solution. Cell constant is calculated using Equation 2.2. To be able to measure electrical conductivity the measurement cell must be calibrated against a standard solution. It should be mentioned electrical conductivity is highly temperature dependent, the degree to which temperature affects conductivity varies from solution to solution and can be calculated using the following formula:

$$G_t = G_{tcal} * \{1 + \alpha * (t - t_{cal})\} \qquad \text{Equation 2.3}$$

Where G_t is conductivity at any temperature t in °C, G_{tcal} is conductivity at calibration temperature t_{cal} in °C and α is temperature coefficient of solution at t_{cal} in °C.

To determine temperature coefficient for a solution, conductivity should be measured over a range of temperature; by plotting the change in conductivity versus the change in temperature and dividing the slope of the graph by G_{tcal}, α can be determined. It should be mentioned that the value for α is known for the reference solutions and there is no need for calculations. To remove the temperature effect, usually a temperature measurement is incorporated with conductivity measurement device.

There are different types of conductivity measurement cells, e.g. two electrodes (two poles), three electrodes or four electrodes. The most popular method for measuring electrical conductivity is platinised four electrodes cell. Figure 2.3 shows a simplified diagram of a four-pole conductivity cell.

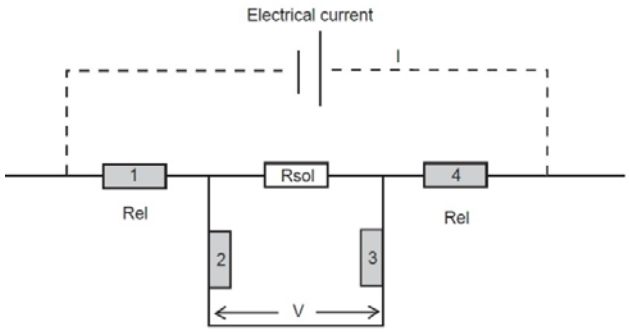

Figure 2.3 Simplified diagram of a 4-pole (electrodes) conductivity cell

In a four-pole cell, current is applied to outer electrodes (1 and 4) in such a way that a constant potential difference is maintained between the inner electrode (2 and 3). As this voltage measurement takes place with a negligible current, these two electrodes are not polarised (R2 = R3 = 0). The conductivity will be directly proportional to the applied current. The geometry of four-pole cells with an outer tube minimises the beaker field effect, due to the measurement volume being well defined within the tube. Therefore, the position of the conductivity cell in the measuring vessel or the sample volume has no influence on the measurement. To further minimise the polarisation effect and error, the electrodes are covered with a platinum black. Hence, the surface of the pole is increased and the current density is decreased; and consequently the polarisation effect is less and measurement will be only affected by resistance of the sample R_{sol}.

Conductivity measurements could be affected by polarisation, contamination, geometry, cable resistance, cable capacitance, frequency change and temperature. To avoid polarization (accumulation of ions on the electrode and increase in resistance), it four-electrodes cells are usually constructed with platinum black coating surface as well as using alternate current with the right frequency. Using a four-electrodes cell also could prevent the effect of contamination, geometry and polarisation. Apart from using four electrodes cell, adjusting the cable parameters (compensation factors) and

choosing a right measurement frequency could improve the effect of cable resistance, capacitance (Radiometer Analytical, 2004).

2.2.2. Sound Velocity

The second property must be independent of the conductivity technique. In other words, it is not correlated with the electrical conductivity in any way. Furthermore, the corresponding test technique should also be sensitive enough to identify the change in hydrate inhibitor concentrations and salt concentrations. Preferably, the technique is robust for potential online application. Acoustic velocity (acoustic property) is such a parameter that does not have necessary correlation with the electrical conductivity (electrical property). It is well known that the sound propagation can be directly related to salt concentration (Clay and Medwin, 1977). In the recent years acoustic velocity has been successfully applied to investigate a variety of solutions, even composition of binary gas mixtures (Jerie, et al., 2004; Vibhu, et al., 2004; Goodenough, et al., 2005; Vyas, et al., 2006). In addition, ultrasound can penetrate metal wall of pipelines, and are not easily interfered by unexpected waves like common sound and low frequency vibration. Therefore, measuring ultrasound velocity can be an ideal technique for online application contains solid particles (sands and clays) and oil droplets.

In principle, the speed of sound is the distance travelled during a unit of time by a sound wave propagating through an elastic medium. In general, the speed of sound (compressional wave) c is given by the Newton-Laplace equation (Povey, 1997).

$$c = \sqrt{\frac{p}{\rho}} \qquad \text{Equation 2.4}$$

where p is a coefficient of stiffness, and ρ is the density. This general equation could be specified for liquid and gas as below:

$$c_{fluid} = \sqrt{\frac{K}{\rho}} \qquad \text{Equation 2.5}$$

where K is the bulk modulus of a substance, it measures the substance's resistance to uniform compression (Padmini and Rao, 1961). It is defined as the pressure increase needed to decrease the volume by a factor of 1/e. Its base unit is the Pascal.

$$K = -V\frac{\partial P}{\partial V} \qquad \text{Equation 2.6}$$

Where V and P denote volume and pressure respectively. From these equations, it can be concluded that speed of sound in liquid is mainly dependent on the density and compressibility of the liquid. Since these two parameters are also related to temperature as well, therefor, speed of sound in liquid will be also a function of temperature. The density of a solution is the summation of mass (massic) concentrations of the components of that solution. So density could be calculated from the following equation:

$$\rho = \sum_i \rho_i \qquad \text{Equation 2.7}$$

Where ρ_i is density of each component in solution. This equation shows that the density of a solution depends on its composition, while it is well known that the bulk modulus of a solution also strongly depends on the molecular composition of a solution. As a result, the measured speed of sound will be representative of the mixture solution.

2.2.3. Thermal Coefficients of Sound Velocity and Electrical Conductivity

To be able to determine a third unknown (another inhibitor in a solution), a third independent measurement is required. Previous experiments found that the temperature slope of the measured acoustic velocity and electrical conductivity is independent of the velocity and conductivity, therefore can be used as the third parameter. Equation below shows this calculation:

$$S_{SoS} = \frac{V_{T_2} - V_{T_1}}{T_2 - T_1} \qquad \text{Equation 2.8}$$

where S_{SoS} is the thermal coefficient of velocity and V_{T1} and V_{T2} are the measured sound velocities at temperatures of T_1 and T_2.

$$S_{Cond} = \frac{C_{T_2} - C_{T_1}}{T_2 - T_1} \qquad \text{Equation 2.9}$$

where S_{Cond} is the thermal coefficient of conductivity and C_{T1} and C_{T2} are the measured conductivities at temperatures of T_1 and T_2.

2.2.4. Artificial Neural Network

A Artificial neural network is a useful approach for correlating a limited quantity of experimental data with required variables in some specific cases where is temporarily lack of fundamental understanding of the necessary relationship between the variables under examination, or the analytical or empirical correlation is possibly not conventional to be actually applied

An artificial neural network consists of large numbers of computational units called neurons, connected to each other by means of direct weighted communication links as shown in Figure 2.4. The input layer of the network receives all the input data and introduces scaled data to the network. The data from the input neurons are propagated through the network via weighted interconnections. Every *i* neuron in a *k* layer is connected to every neuron in adjacent layers. The *i* neuron within the hidden *k* layer performs the following tasks: summation of the arriving weighted inputs (input vector $Ii = [I_{i,1},\ldots I_i,N_{k-1}]$) and propagations of the resulting summation through a non-linear activation function *f* to the adjacent neurons of the next hidden layer or to the output neuron(s). In this work, the activation function is a sigmoid function:

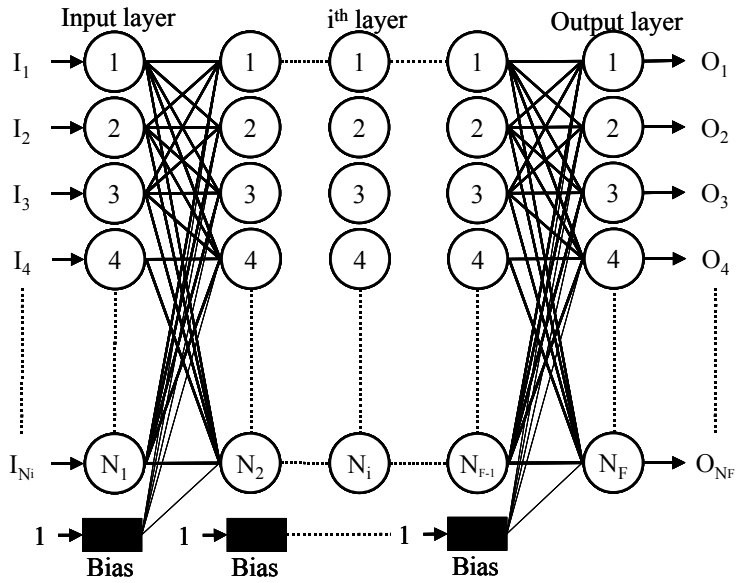

Figure 2.4 Architecture of a multi-layer feed forward artificial neural network

$$f(x) = \frac{1}{1+e^{-x}} \qquad x \in [0,1] \qquad \text{Equation 2.10}$$

A bias term, b, is associated with each interconnection in order to introduce a supplementary degree of freedom. The expression of the weighted sum, S, to the i^{th} neuron in the k^{th} layer ($k \geq 2$) is:

$$S_{k,i} = \sum_{j=1}^{N_{k-1}} \left[(w_{k-1,j,i} I_{k-1,j}) + b_{k,i} \right] \qquad \text{Equation 2.11}$$

Where w is the weight parameter between each neuron-neuron interconnection. Using this simple feed-forward networks with non-linear sigmoid activation functions, the output, O, of the i neuron within the hidden k layer is therefore:

$$O_{k,i} = \frac{1}{1+e^{-\left(\sum_{j=1}^{N_{k-1}} \left[(w_{k-1,j,i} I_{k-1,j}) + b_{k,i} \right]\right)}} = \frac{1}{1+e^{-S_{k,i}}} \qquad \text{Equation 2.12}$$

For the use with the neural network, the input data, X, were normalized and centred:

$$X_i^l = 0.1 + 0.8 \frac{X_i^l - X_{i,\min}}{X_{i,\max} - X_{i,\min}} \qquad \text{Equation 2.13}$$

Where X_i^l is the l^{th} values of the input data fed to the input neuron i, and $X_{i,min}$ is the minimal value of the input data fed to the same i neuron and inversely $X_{i,max}$ is the maximal value. To achieve a better stability and to have output of the same order of magnitude, the following scaling rule was applied to salt and inhibitor concentrations before normalisation:

$$X_{Network} = \ln(X_{\exp}) \qquad \text{Equation 2.14}$$

During the training, input variables are fed to the network and the difference between the experimental outputs and the calculated outputs is used as a criterion for adjustment of network's synaptic weights. All synaptic weights and biases are first initialised randomly. The network is then trained, its synaptic weights are adjusted by an optimisation algorithm, until it correctly emulates the input/output mapping, by minimizing the average root mean square error. The optimisation method chosen in this work is the Levenberg-Marquardt algorithm (Levenberg, 1944; Marquardt, 1963). The Levenberg-Marquardt optimisation algorithm consists in modifying the network's synaptic weight by the following formula:

$$w_j = w_{j-1} - [\bar{H}(w_{j-1}) + \mu_j \bar{I}_d]^{-1} \nabla J(w_{j-1})$$ Equation 2.15

With

$$\bar{H}(w_j) = \sum_{k=1}^{N} \left(\frac{\partial err^k}{\partial w_j} \right) \left(\frac{\partial err^k}{\partial w_j} \right)^T + \sum_{k=1}^{N} \left(\frac{\partial^2 err^k}{\partial w_j \partial w_j^T} err^k \right)$$ Equation 2.16

Where err^k, μ, J, N are the residue vector, the step values of the Levenberg-Marquardt method Equation 2.10 and Equation 2.11, the Jacobian matrix of the first derivative of global error to weight and the number of feed inputs , respectively. err^k is defined by:

$$err^l = Y^l_{\text{exp.}} - Y_{cal}{}^l$$ Equation 2.17

Finally, inhibitor concentrations are then re-transformed to their original scale.

2.2.5. Determination of Hydrate Phase Boundary

An in-house thermodynamic model (Tohidi, et al., 1996; Østergaard, et al., 2005) and chapter three of this thesis) was employed to determine the hydrate phase boundary. To determine the hydrate phase boundary, the model is fed with the salt concentration and the inhibitor concentrations determined by the ANN correlation and the composition of the hydrocarbon fluids (oil or gas) in the pipeline.

Figure 2.5 shows the methodological chart of the hydrate inhibition monitoring system for a three parameters system. The acoustic velocity, electrical conductivity and thermal coefficients (acoustic velocity or electrical conductivity) are functions of the salt concentration, the inhibitor concentrations, and temperature. The velocity, conductivity, thermal coefficients and temperature of the aqueous sample under examination are measured and fed to a pre-trained ANN correlation. The salt concentration and the inhibitor concentrations are determined by the ANN correlation. By feeding the thermodynamic model with the composition of the hydrocarbon fluids, the hydrate phase boundary can be determined by the thermodynamic model (for THI systems). The hydrate safety margin is determined by the definition given that the pipeline temperature and pressure are known.

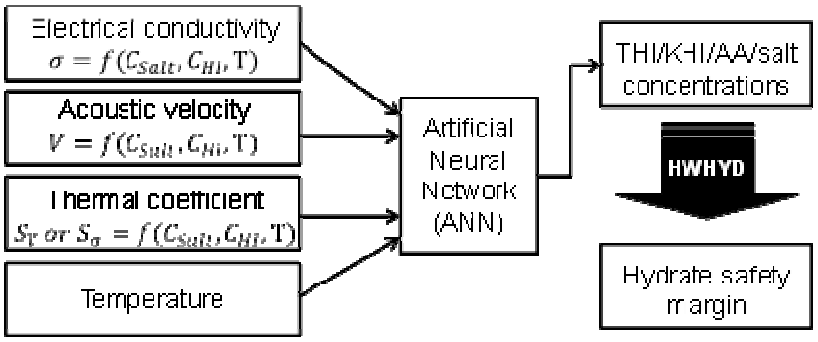

Figure 2.5 Methodological chart of the hydrate inhibition monitoring system

2.3. EXPERIMENTAL EQUIPMENT

2.3.1. Electrical Conductivity Meter

Electrical conductivity was measured using a CDM230 Conductivity Meter with a four-pole conductivity cell (supplied by Meterlab Radiometer Analytical). The conductivity metre has a nominated accuracy of 0.2% in 0.1 uS to 400 mS (conductance) and a working temperature range from –9.9 ^{o}C to 99.9 ^{o}C. It has a built-in temperature sensor with 0.1 ^{o}C of temperature resolution. The four-pole cell consists of 4 platinum rings. Alternating currents at different frequencies are applied to the two outer rings and the voltage is measured on the two inner rings. Figure 2.6 shows the conductivity meter and the conductivity cell.

Figure 2.6 Picture of conductivity meter and conductivity cell

2.3.2. Ultrasound Pulse Generator

A Panametrics 5077PR pulser-receiver is used to generate desired pule for agitating the ultrasound transducer and emitting the sound wave. This pulser is equipped with a

receiver which could amplify and filter the received signal for more convenient processing in case of weak or noisy signals. This device is also equipped with a knob which could be used for adjusting the voltage level and is able to generate negative pulsed up to -400 V. The adjustable frequency selector is designed to select proper frequency (up to 35 MHZ) depending on the transducer. An adjustable synchronised signal is generated on each pule to make sampling equipment in sync with the generated pulse. Figure 2.7 shows the pulse generator.

Figure 2.7 Picture of Panametrics 5077PR pulser-receiver

2.3.3. Ultrasound Transducer

A pair of Panametrics V104 ultrasound transducers was used in the setup for generating and receiving the ultrasound pulse. This transducers has a central frequency of 1MHZ.

2.3.4. Data Acquisition Board

A high frequency data acquisition board from Link Instruments was used to capture the received ultrasound signals for analysis. This equipment is able to acquire signals at 500 MHZ. A trigger input is designed for this equipment which gives ability to be synchronised with the pulse generator.

2.3.5. Measurement Cell

A stainless steel cell (Figure 2.8) was used to equilibrate the samples at desired temperatures and also to perform the measurements. It is surrounded with a jacket connected to a cryostat cooling/heating bath for adjusting the sample temperature. The

two ultrasound transducers housed in two end caps are fitted on the two end of the cell. A lid is specially designed to hold the conductivity probe at the top of the cell without hitting the sound wave. A drain valve is designed under the cell for easy cleaning of the cell after each measurement. Figure 2.9 shows a schematic of the C-V setup.

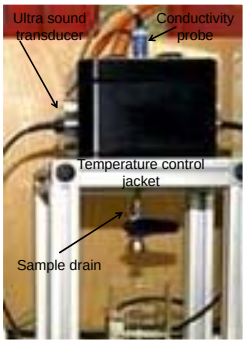

Figure 2.8 Picture of the measurement cell

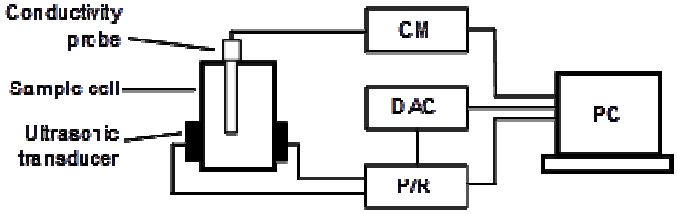

Figure 2.9 Schematic diagram of the C-V device

2.4. EXPERIMENT PROCEDURE

The prepared aqueous solutions (about 120 ml) were charged into the C-V cell. A thermostat connected to a cooling jacket surrounding the sample cell was used to control the measurement temperature. The conductivity and velocity were measured at 0, 4, 15, and 25 ºC for two-parameter measurement method and at 10 and 20 ºC for three-parameter method. The test samples were kept at each temperature for at least one hour to reach thermal equilibrium. All the measurements were conducted under atmospheric pressure.

To ensure the accuracy of measurements, the conductivity meter was calibrated using the 0.1D KCl standard solution supplied by Meterlab Radiometer Analytical, whilst

the velocity measurement was calibrated using deionised water against literature velocity data.

2.4.1. Speed of Sound Measurements and Calibration

To be able to measure speed of sound, the distance which sound wave travels and the time of this travel are measured.

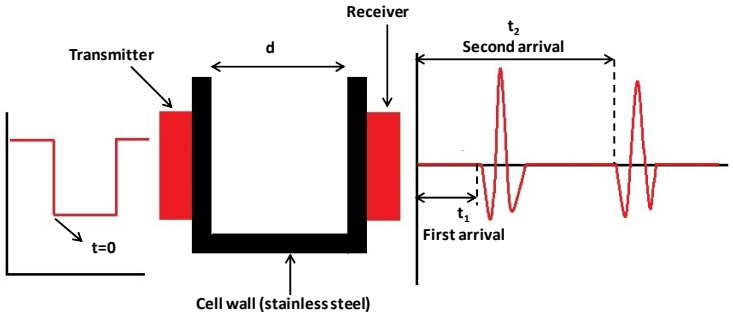

Figure 2.10 Schematic of the C-V cell and sound velocity measurement

Figure 2.10 shows a diagram illustrating how the acoustic velocity is measured. For measuring the speed of sound, two parameters, i.e. distance (d) and time delay (t_0), should be defined before the experiments. The distance, d, directly depends on the distance between inner side walls of the cell. t_0 is the time delay which takes for the wave to pass through the stainless steel wall of the cell and depends on the thickness of the wall. The true travelling time is equal to the difference of the measured time t and the time delay t_0. Although the distance between the walls is approximately known, in order to measure sound velocity with a required accuracy, it needs to be determined precisely. In this work determining d and t_0 is referred as sound calibration. The calibration was conducted using fluids with known speed of sound, i.e. deionised water. A correlation was developed to relate sound velocity in deionised water to temperature using literature data. In this work the average value of the sound velocities reported by Clay and Medwin (1977) and NPL UK (2000) has been used as reference values for sound calibration.

To be able to measure the distance, another cell parameter should be measured which is t_0. Based on Figure 2.10, t_0 can be calculated from the following equation.

$$t_0 = t_1 - \frac{t_2 - t_1}{2} \qquad \text{Equation 2.18}$$

where t_1 is the travel time of the first arrival wave and t_2 is the second arrival travel time. As distance (d) and t_0 are cell specifications, so they would not change until a physical change or maintenance is required and performed. These two parameters, d and t_0 have been determined for all the measurement cells used in this study and therefore, are assumed to be known here after. To calculate sound velocity for any solution, actual travelling time was determined by subtracting t_0 from the measured first arrival time t_1. The sound velocity of the solution will be calculated by dividing the distance and the actual travelling time.

2.4.2. Noise Reduction in Speed of Sound Measurements

Electronic measurements are usually involved with noise. In this work, the captured acoustic signal is also highly affected by noise. Figure 2.11 shows the acoustic signal is buried under noise(the blue colour signal). It was found that the noise distribution is a normal Gaussian distribution so averaging can reduce the noise level significantly. A real time averaging shown in Equation 2.19 has been used for this purpose. As one can see in Figure 2.11 the averaged signal is a clear signal and the first and second arrival can be found more accurately

$$f_{avg}(n) = \frac{1}{n}\sum_{i=1}^{n} f(i)$$

$$f_{avg}(n+1) = f_{avg}(n) + \frac{f(n+1) - f_{avg}(n)}{n+1} \qquad \text{Equation 2.19}$$

where $f(n)$ is the wave form array, n is the n^{th} wave form and f_{avg} is the average wave form. The digitised waveform size was very big (about 1mega byte for each wave form) so it was not possible to store the wave for future averaging. This real time averaging method helped to save the memory space and time with a better performance.

The only week point for this method is that it usually takes about 2 to 3 minutes to capture the signals and average them. In calibration stage it is not a big issue but for the prototype it could be a frustrating for each measurement. To overcome this problem and improve the developed prototype a new processing method was suggested and applied which will be discussed in Chapter 6.

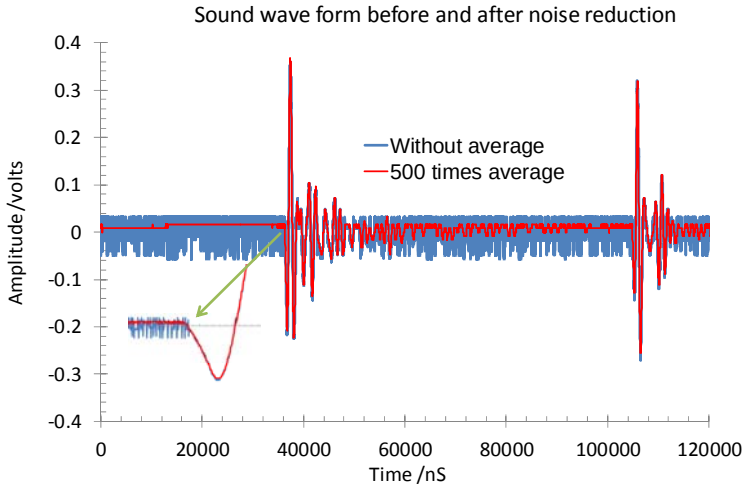

Figure 2.11 Sound waveform before and after noise reduction using real time averaging

2.5. EXPERIMENTAL MATERIALS

Materials used in this part of the work were:

- Deionised water
- Thermodynamic inhibitors: ethanol with 99.9% purity and ethylene glycol (MEG) with 99% purity both from Sigma-Aldrich
- Salts: NaCl with 99.5% purity supplied by Aldrich
- KHI: commercial KHI supplied by Clarient
- AA: commercial water-soluble AA supplied by Baker Hughes and oil-soluble AA supplied by Champion

2.6. RESULTS AND DISCUSSIONS

The applicability of C-V device has been examined for all three groups of hydrate inhibitors, i.e. thermodynamic hydrate inhibitor, KHIs and AAs in the presence and absence of salt. For thermodynamic inhibitors, following the previous success for methanol and ethylene glycol, in this work ethanol was tested. For the KHI group, a commercial KHI supplied by Clarient was examined. The applicability of the C-V method for AAs were also evaluated with two commercial AAs, one oil-soluble AA from Champion and one water-soluble AA from Baker Hughes. Finally, the C-V

method was further developed for measuring three unknown concentrations simultaneously, a system containing MEG, the KHI and NaCl. In each of the mentioned systems, a large data base of the conductivity and sound velocity data were generated and an ANN was trained. The following sections will detail the results.

2.6.1. Oil-soluble AA Systems with Salt

The conductivity and velocity of solutions containing different salt and AA concentrations were measured over a temperature range from 0 to 25 °C. Initially, it was intended to do the measurements for a typical AA concentration from 0 to 3 mass% and salt concentration from 0 to 10 mass%. However, precipitation of the AA was observed in the solutions containing certain concentration of salt, as shown in Figure 2.12. Therefore, it was decided to reduce the concentration of salt from 10 mass% to 3 mass% where the AA started to come out of the solution.

3 mass% AA + 1 mass% NaCl 1 mass% AA + 3 mass% NaCl

Figure 2.12 Precipitation of the oil soluble AA in the presence of NaCl

2.6.1.1. Conductivity Measurements

Table 2.1 shows the actual measurements of electrical conductivity for systems containing different concentrations of the oil-soluble AA and salt. .

Table 2.1 The measured conductivity of the aqueous AA solutions in the presence of salt, in mS/cm

NaCl	T	AA/ mass%					
mass%	ºC	0.2	0.5	1.0	1.5	2.0	3.0
0	0	0.28	0.73	1.14	1.73	2.10	2.87
	4	0.31	0.90	1.30	1.92	2.32	3.19
	15	0.42	1.28	1.64	2.26	2.90	4.23
	25	0.47	1.72	2.04	2.80	3.41	4.92
1	0	11.68	11.05	11.08	10.45	9.57	7.67
	4	12.85	12.46	12.18	11.50	10.33	8.41
	15	18.09	17.05	16.56	15.33	14.52	13.00
	25	23.22	22.19	21.93	21.14	20.85	20.10
2	0	21.87	17.93	17.50	N/A	N/A	N/A
	4	24.62	20.10	19.70	N/A	N/A	N/A
	15	33.14	26.74	26.47	N/A	N/A	N/A
	25	41.40	33.30	32.90	N/A	N/A	N/A
3	0	31.37	27.80	25.80	N/A	N/A	N/A
	4	34.60	30.20	28.60	N/A	N/A	N/A
	15	43.83	36.90	34.90	N/A	N/A	N/A
	25	54.06	43.90	40.20	N/A	N/A	N/A

As one can see for higher concentration of NaCl and AA, AA starts to come out of the solution and the measured conductivity and velocity values were not valid any more. These values are shown as N/A in the table.

Effect of temperature on the conductivity measurement

To be able to develop an ANN correlation which covers temperature in full range from 0 to 25 °C, the conductivity data have been plotted for each salt and AA concentration against temperatures separately. This makes it possible to drive a relation between temperature and conductivity. Figure 2.13 illustrates conductivity versus temperature for different salt and AA concentrations.

As it was expected, by increasing temperature, electrical conductivity increases in all systems. In the systems without AA or containing very low concentration of AA, conductivity increases linearly with temperature. However, at higher AA concentrations especially in the presence of salt, the relation between conductivity and temperature is not very linear (the second figure, 1 mass% NaCl). This can be

attributed to a specification of AAs that are multiple components and different components might be precipitated at different temperatures.

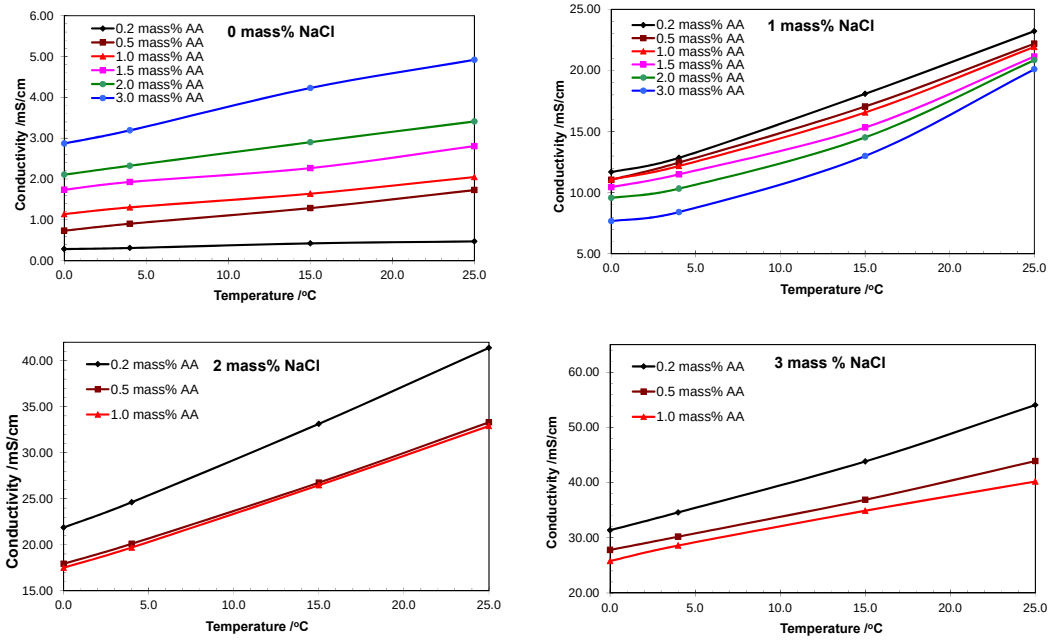

Figure 2.13 Effect of temperature on electrical conductivity for different salt and oil-soluble AA concentration

Effect of coexistence of AA and NaCl on the conductivity

To investigate the effect of the oil-soluble AA on conductivity values, the results have been plotted against the AA concentration for each temperature and salt concentrations separately as shown in Figure 2.14.

As can be seen from this figure, the conductivity changes with the AA concentration in a very similar way, which means that the effect of the AA on the conductivity is independent of temperature. The conductivity behaviour versus AA concentrations does not follow a similar trend for different salt concentrations. This could be attributed to the complex behaviour of AA or interactions between NaCl and AA. However, it was not possible to find out the reasons as the chemical composition was not disclosed by the supplier.

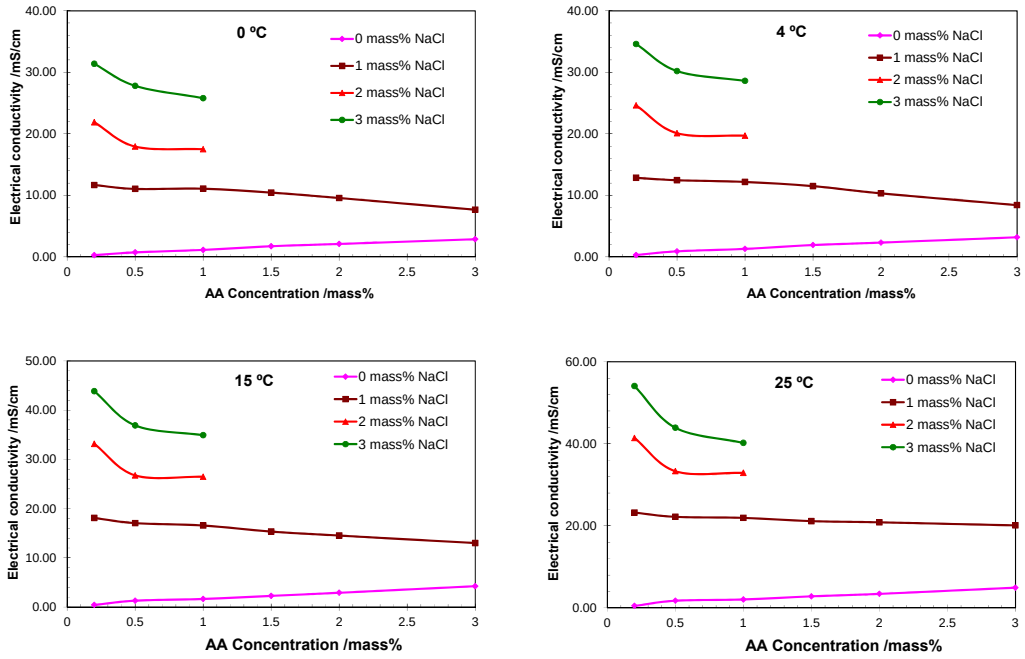

Figure 2.14 Effect of the AA on electrical conductivity

In Figure 2.14, for the systems without NaCl, the conductivity increases with the AA concentration. This suggests that the presence of some salts (ions) in the AA. For solutions containing 1 mass% NaCl, the conductivity decreases with the AA concentration. In the systems containing 2 and 3 mass% NaCl, the conductivity decreases however for higher AA concentration the conductivity is almost constant. Visual observation found that at these points some AA slightly appeared in the solution. Therefore, these odd behaviours could be due to the interaction between NaCl and the AA ions, which could not be specified due to lack of the chemical composition of the AA.

Figure 2.15 shows the conductivity changes with NaCl concentrations. As it was expected, the conductivity increases with salt concentration. Same results observed for other temperatures as well.

2.6.1.2. Speed of Sound Measurements

Speed of sound is the second parameter used for developing the ANN correlation. Similarly, speed of sound was measured within a temperature range of 0 to 25 ºC. AA

and NaCl concentration ranges were the same as conductivity measurements. Table 2.2 shows the results of these measurements.

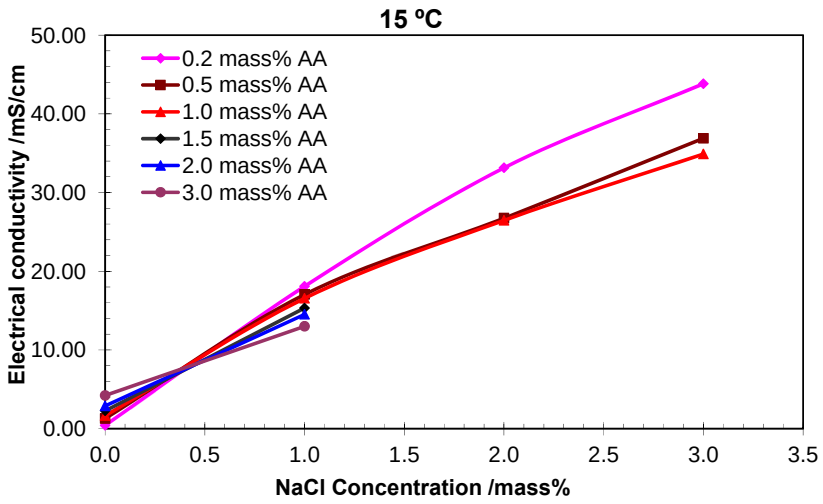

Figure 2.15 Effect of NaCl on electrical conductivity

Table 2.2 The measured speed of sound in the aqueous oil-soluble AA solutions, in m/s

NaCl mass%	T °C	AA/ mass%					
		0.2	0.5	1.0	1.5	2.0	3.0
0	0	1405.3	1406.4	1408.4	1410.0	1411.9	1415.5
	4	1423.6	1425.2	1427.3	1428.9	1430.5	1433.0
	15	1467.9	1468.8	1470.1	1471.1	1472.2	1474.0
	25	1496.9	1498.3	1498.7	1499.2	1500.1	1501.4
1	0	1417.9	1419.6	1421.6	1423.2	1425.2	1428.5
	4	1435.9	1437.9	1440.0	1441.7	1442.9	1445.8
	15	1478.8	1480.1	1481.0	1481.8	1483.6	1485.8
	25	1507.9	1508.7	1509.1	1509.6	1511.0	1511.9
2	0	1429.3	1430.9	1432.6	N/A	N/A	N/A
	4	1446.3	1448.8	1450.9	N/A	N/A	N/A
	15	1488.1	1490.2	1491.6	N/A	N/A	N/A
	25	1516.5	1517.8	1518.8	N/A	N/A	N/A
3	0	1441.8	1443.3	1445.0	N/A	N/A	N/A
	4	1459.3	1461.1	1462.8	N/A	N/A	N/A
	15	1500.3	1501.0	1501.4	N/A	N/A	N/A
	25	1528.0	1528.5	1529.4	N/A	N/A	N/A

Effect of temperature on sound velocity

As with the conductivity data, the sound velocity data has been studied to drive a relation between sound velocity and temperature. Figure 2.16 shows the sound velocity changes with temperature.

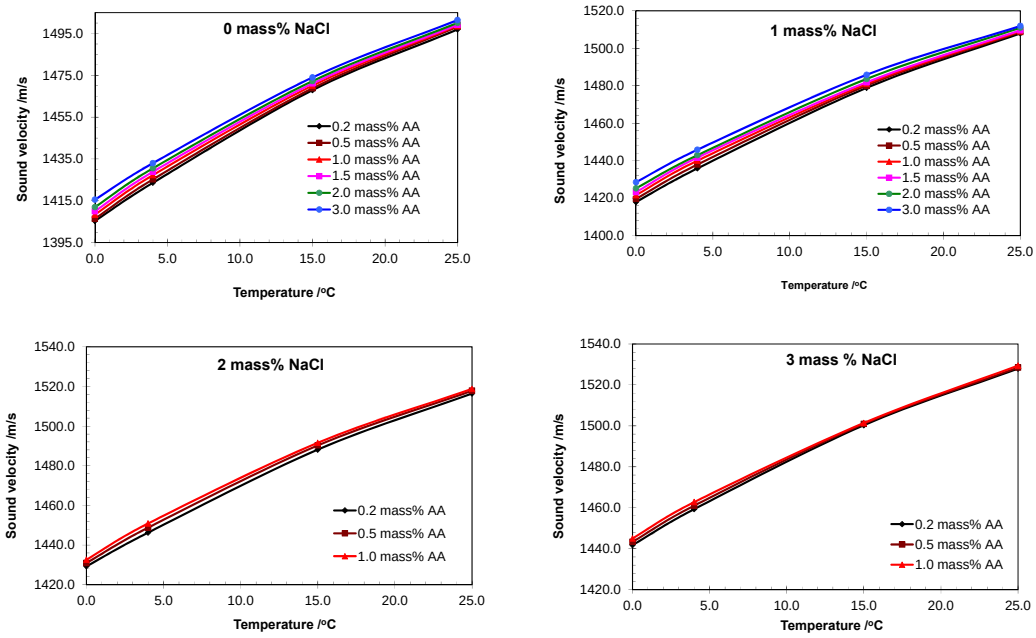

Figure 2.16 Effect of temperature on sound velocity

As one can see from these graphs, sound velocity increases with increase in temperature. These changes are not liner but they are monotonic, which make it easy to fit a cure and interpolate data for full temperature range at an interval of 1 ºC.

Effect of coexistence of AA and NaCl on sound velocity

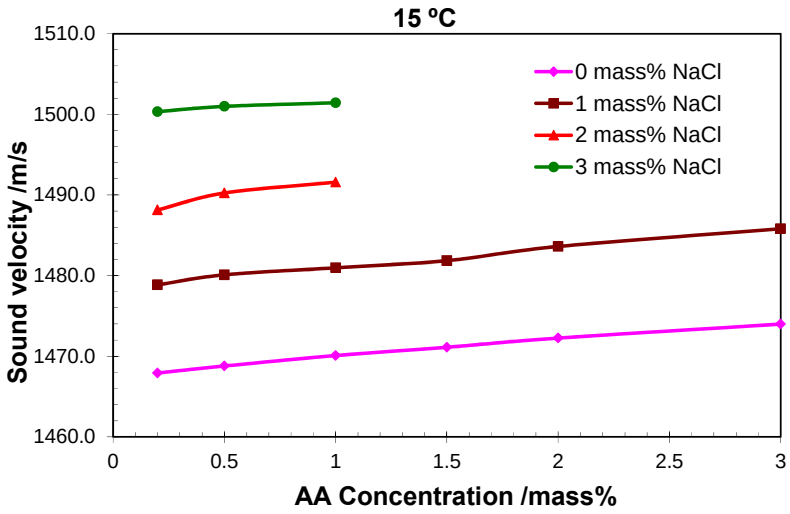

Figure 2.17 Effect of the oil-soluble AA on sound velocity when NaCl concentrations and temperature are constant.

Figure 2.17 shows that sound velocity increases by increasing AA concentration in the solution. However, solutions with higher NaCl concentration, i.e. 3 mass%, do not exactly follow this trend and smaller changes observed, which could be due to precipitation of the AA. It should be mention that the changes in sound velocity with AA concentration are not very significant.

Figure 2.18 shows the sound velocity changes with NaCl concentrations. As it was expected, by increasing NaCl concentration in solution, sound velocity increases. This increase is linear. However, at the point of 3 mass% NaCl, there is a deviation from linearity, which could again be related to precipitation of the AA.

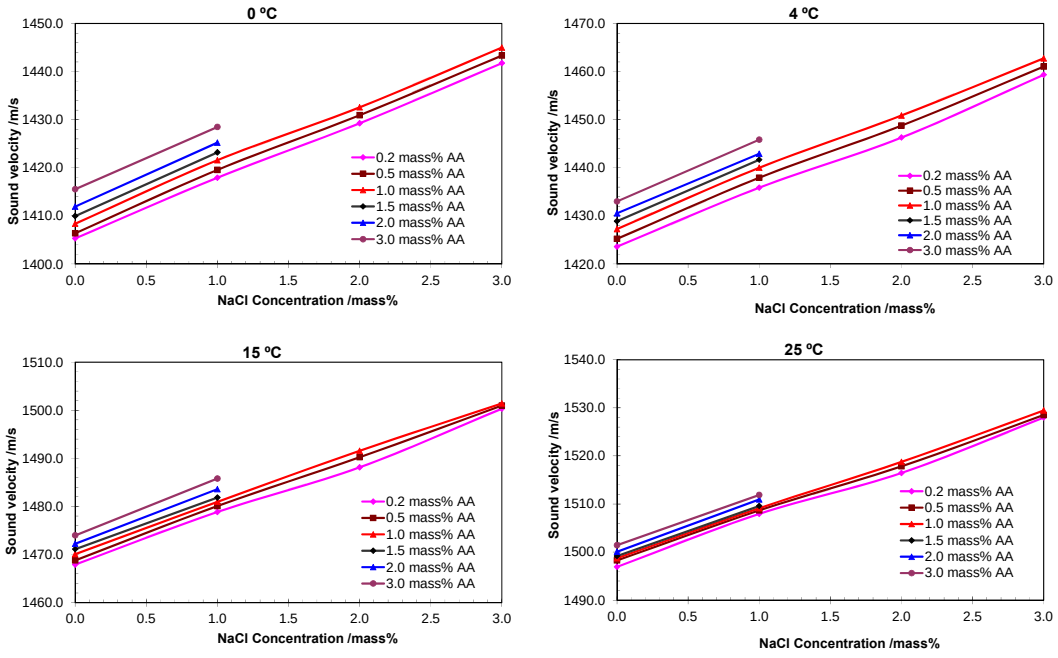

Figure 2.18 Effect of NaCl on sound velocity

2.6.1.3. ANN Development for Oil Soluble AA Systems

The aim of measuring electrical conductivity and sound velocity was to create a required database for developing an ANN correlation for determining AA and NaCl concentrations of aqueous solutions. To achieve this, different types of ANN with different neurons and hidden layers were tried. The AA precipitation made it difficult to have an desired ANN to fit the measured results. Among all the tried results the best ANN was selected with 3 inputs, 1 hidden layer with 7 neurones to output AA and salt concentrations. Figure 2.19 shows the schematic of this network.

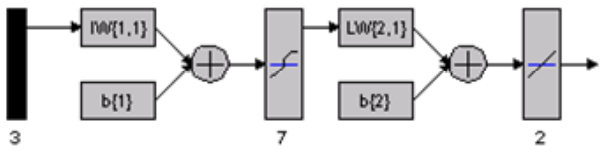

Figure 2.19 Schematic of the developed ANN for the oil soluble AA

To develop the ANN, a feed-forward network was used. The transfer functions for the input layer was TANSING and for the output PURELINE has been used in Matlab. ANN results have been shown in Figure 2.20 and Figure 2.21. The validation points are generated using data that are randomly selected from the database created for developing the ANN and the testing points are generated using independent data that were measured separately and used in developing the ANN. The NaCl and AA concentrations of the independent data were (NaCl=1.5, AA=0.6), (NaCl=2.8, AA=0.9), (NaCl=0.5, AA=2.5) and (NaCl=1.8, AA=1.7) mass% respectively.

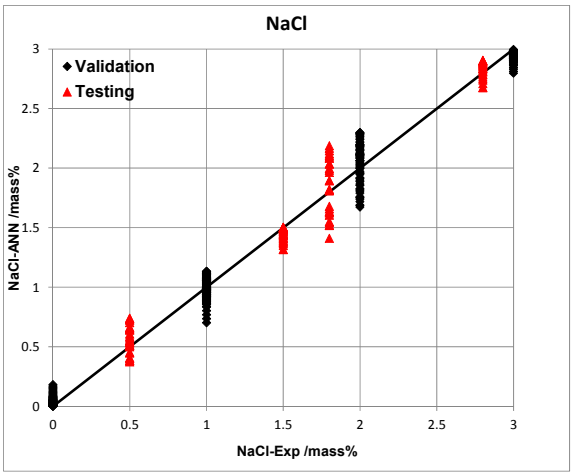

Figure 2.20 Performance of ANN correlation in determining NaCl concentration.

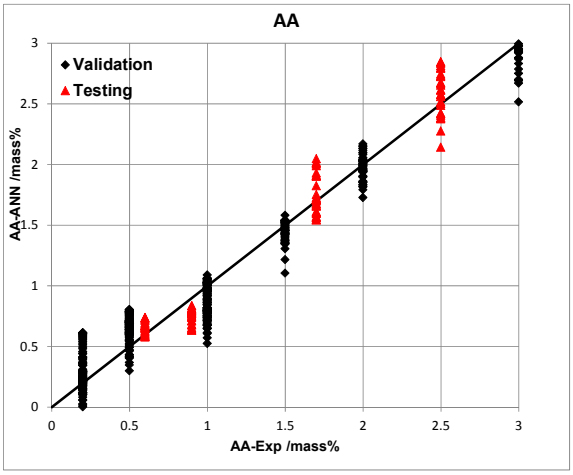

Figure 2.21 Performance of ANN correlation in determining concentrations of the oil-soluble AA.

The ANN results have been analysed and the error values have been determined for testing and validation results. As can be seen from these figures, the ANN results for NaCl shows better accuracy due to stronger effect of NaCl on conductivity and sound velocity. Table 2.3 shows the maximum, and average values from the developed ANN for independent data over the temperature range. The independent results show slightly bigger deviation than what was expected in other inhibition systems (Yang, 2011). However, it seems still in acceptable error range and the C-V method could be applied for AA systems. Table 2.4 summarises the accuracy of this ANN for both validating and testing data.

Table 2.3 ANN testing results for independent data

System		Temperature/ ºC			
		0	4	15	25
NaCl	Exp	0.50	1.50	1.80	2.80
	Max	0.73	1.50	2.18	2.90
	Ave	0.56	1.43	1.83	2.82
AA	Exp	2.50	0.60	1.70	0.90
	Max	2.84	0.73	2.04	0.83
	Ave	2.58	0.65	1.70	0.75

Table 2.4 ANN absolute deviation in AA and NaCl concentrations for testing and validation data

	Maximum AD	Average AD
NaCl	0.38	0.07
AA	0.48	0.12

2.6.2. Water-Soluble AA Systems with Salt

It was seen that precipitation of the oil-soluble AA limited the working range of the ANN and also resulted in undesired ANN accuracy. To confirm the applicability of the C-V method a commercial water-soluble AA has been examined in this section. A new ANN correlation has been developed and evaluated for the water-soluble AA over a temperate range of 0 to 25 ºC.

The visual solubility tests showed that, this AA is completely soluble in deionised water in the absence of salt. By adding more than 1 mass% NaCl, AA/some AA components started coming out of the solution. Figure 2.22 shows two examples of solutions with different AA and NaCl concentrations. The amount of precipitations in the water-soluble AA solutions was less than the previous oil-soluble AA solutions. Vigorous mixing dissolves the AA back in the solution and the water-soluble AA solution became transparent again. The water-soluble AA also takes longer time to comes out of the solution after mixing is stopped.

Based on the visual observations for solubility, it was decided to train the ANN for the systems with 0 to 3 mass% of water-soluble AA and NaCl.

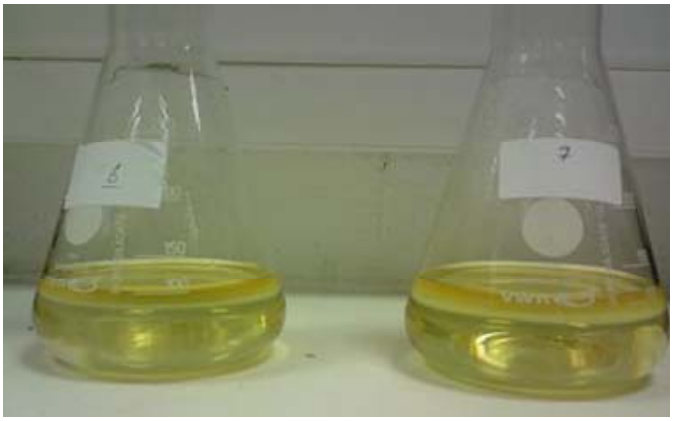

3 mass% AA + 1 mass% NaCl 1 mass% AA + 3 mass% NaCl

Figure 2.22 Visual observation of the precipitation of the water-soluble AA in the presence of NaCl

2.6.2.1. Conductivity Measurements

Table 2.5 summarises the measured electrical conductivities for the tested water-soluble AA solutions with and without NaCl over 0 to 3 mass% concentrations of both AA and NaCl at 0, 4, 15 and 25 °C.

Table 2.5 The measured electrical conductivity values of the aqueous water-soluble AA solutions, in mS/cm

NaCl mass%	T °C	AA/ mass%						
		0.2	0.5	1	1.5	2	2.8	3
0	0	0.09	0.19	0.329	0.43	0.55	0.73	0.78
	4	0.10	0.21	0.37	0.49	0.75	0.84	0.94
	15	0.14	0.29	0.49	0.68	1.08	1.18	1.33
	25	0.18	0.36	0.63	0.88	1.39	1.53	1.81
1	0	9.53	9.54	9.72	9.42	9.36	9.33	9.31
	4	10.78	10.85	11.14	10.65	10.61	10.60	10.57
	15	14.53	14.51	14.48	14.27	14.28	14.31	14.24
	25	18.32	17.94	17.56	17.85	17.91	17.93	17.75
3	0	26.29	26.12	25.83	25.83	25.36	25.18	24.98
	4	29.57	29.36	29.11	29.14	28.59	28.30	28.09
	15	39.18	38.94	38.68	38.44	38.09	37.60	37.60
	25	48.68	48.51	48.34	48.17	47.51	46.93	46.83

Effect of temperature on the measured conductivities

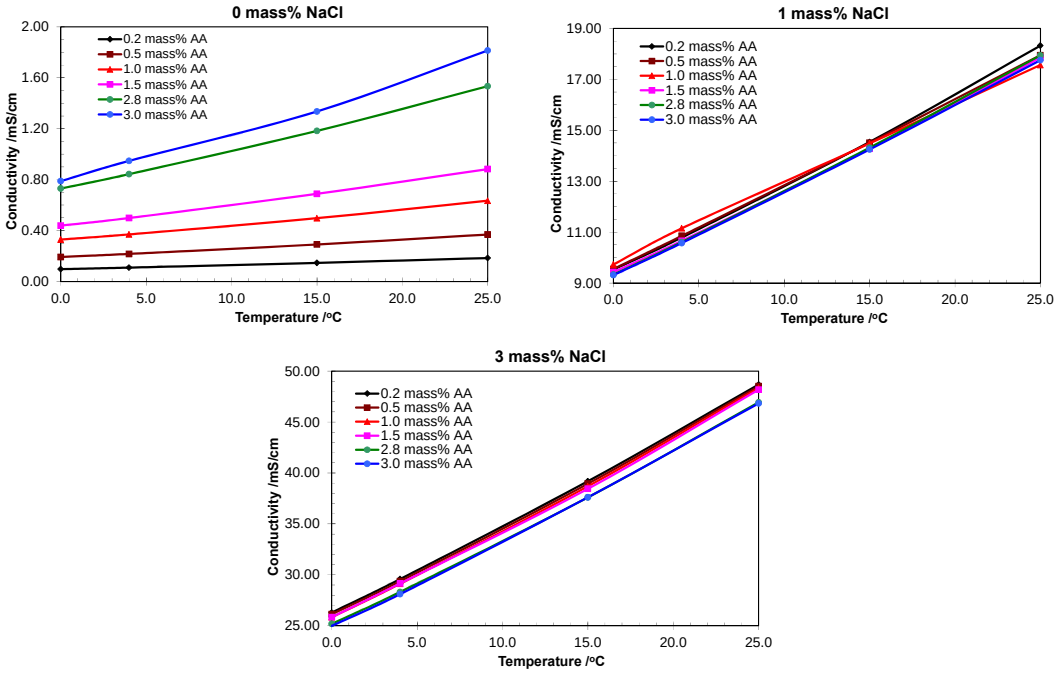

Figure 2.23 Effect of temperature on electrical conductivity of the water-soluble AA solutions

Figure 2.23 illustrates the effect of temperature on the conductivity of aqueous water-soluble AA solutions. A similar to the oil-soluble AA solutions, an increase in temperature caused almost a liner increase in electrical conductivity. The changes in temperature caused a monotonic change in conductivity. This behaviour was observed even when salt concentration was 3 mass %. However because of small effect of AA on conductivity, conductivity results for solution with same salt concentration are very close to each other and some point are not distinguishable. Based on these plots, for each concentration of salt a curve was fitted to interpolate the conductivity data at a temperature interval of 1 °C. These data were used for training and validating the ANN correlation.

Effect of coexistence of the water-soluble AA and NaCl on conductivity

The effect of the AA on electrical conductivity was investigated in the presence and absence of salt. This kind of study gives a better understanding of the physical property of the systems under test, therefore, makes data preparation much easier for developing ANN. Figure 2.24 illustrates the measured conductivities plotted against AA concentration for each temperature and salt concentration.

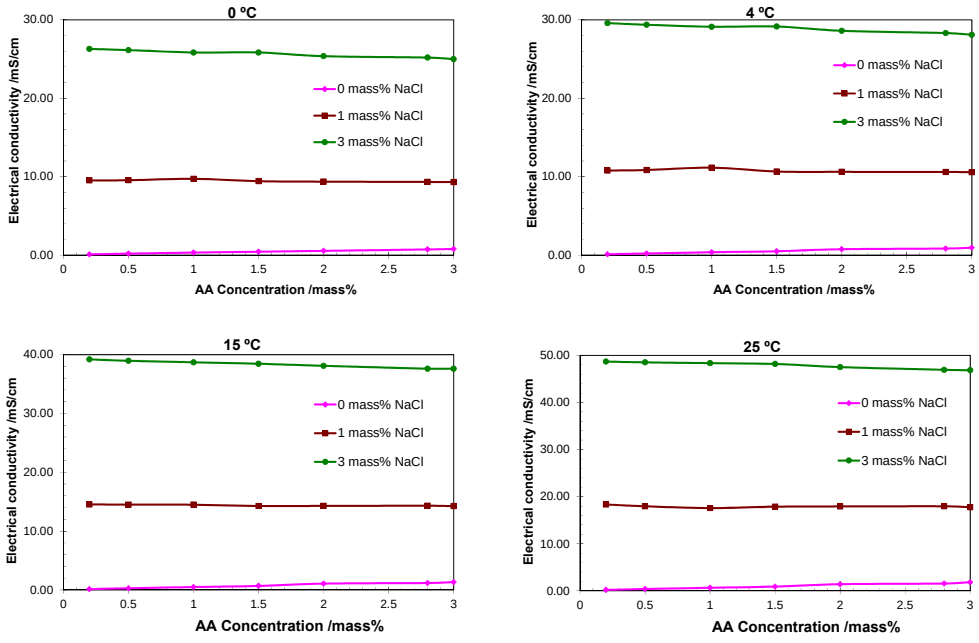

Figure 2.24 Effect of the water-soluble AA on electrical conductivity

As can be seen from these graphs, in the absence of NaCl, the electrical conductivity of the solution is very low. With increase in the AA concentration in this system, the conductivity starts to increase. Although the increase is very small, it is still measurable by the conductivity meter. Similar behaviour can be seen at different temperatures, suggesting that this water-soluble AA contains a low concentration of some ions. In the presence of 1 and 3 mass% NaCl, the conductivity slightly decreases as the AA concentration increases.

To investigate the conductivity changes with NaCl concentrations, the results have been plotted in Figure 2.25. These results show that electrical conductivity is significantly increasing by increase in salt concentration. Due to small effect of AA on conductivity, in this figure the curves looks not distinguishable (because of large scale very fine changes due to AA effect) however there are fine changes which can clearly be seen in Table 2.5. Similar behaviour observed for other temperatures.

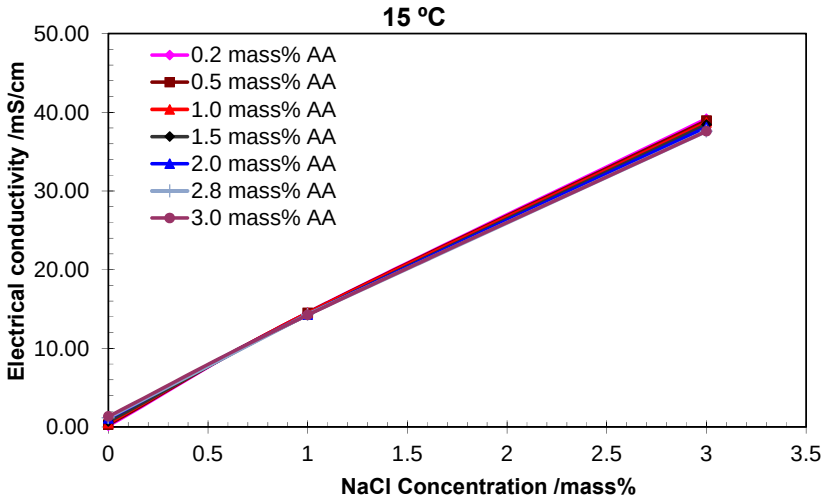

Figure 2.25 Effect of NaCl on electrical conductivity

2.6.2.2. Speed of Sound Measurements

Sound velocity as a second parameter was measured for determining concentrations of salt and the water-soluble AA over the temperature range from 0 to 25 °C. The results of these measurements are tabulated in Table 2.6.

Table 2.6 The measured sound velocity of the aqueous water-soluble AA solutions, in m/s

NaCl	T	AA/mass%						
mass%	°C	0.2	0.5	1	1.5	2	2.8	3
0	0	1402.7	1404.1	1405.8	1408.0	1409.1	1412.2	1413.5
	4	1421.9	1423.5	1424.5	1426.7	1427.9	1430.3	1431.6
	15	1466.7	1467.9	1468.6	1470.4	1471.4	1472.9	1473.7
	25	1497.5	1498.3	1499.2	1499.9	1500.5	1502.1	1502.3
1	0	1415.9	1416.9	1418.6	1420.5	1421.9	1424.5	1424.9
	4	1434.8	1435.6	1437.6	1438.9	1440.4	1443.0	1443.3
	15	1478.7	1478.9	1480.8	1481.5	1482.7	1485.0	1485.6
	25	1508.1	1508.1	1508.8	1509.9	1509.9	1511.7	1511.9
3	0	1444.0	1444.9	1446.4	1448.6	1449.3	1451.3	1452.6
	4	1460.9	1461.8	1463.6	1465.2	1466.2	1467.7	1468.4
	15	1501.3	1501.9	1503.7	1504.0	1505.2	1506.0	1505.9
	25	1530.2	1530.2	1531.3	1530.6	1531.3	1532.1	1532.1

Effect of temperature on sound velocity

To interpolate the sound velocity data for temperatures between the measured temperature points, sound velocity data were plotted versus temperature at constant salt and AA concentrations. Figure 2.26 shows these plots. the sound velocity monotonically increases as the temperature rises. This monotonic increase was observed in different concentrations of AA and NaCl. For each curve with constant AA and salt concentrations, a curve was fitted to interpolate sound velocity data for the temperatures at a temperature interval of 1 °C between the measured points in order to have fine temperature distribution of data for ANN training. This monotonic behaviour made it possible to achieve a very good interpolation for a desired ANN correlation.

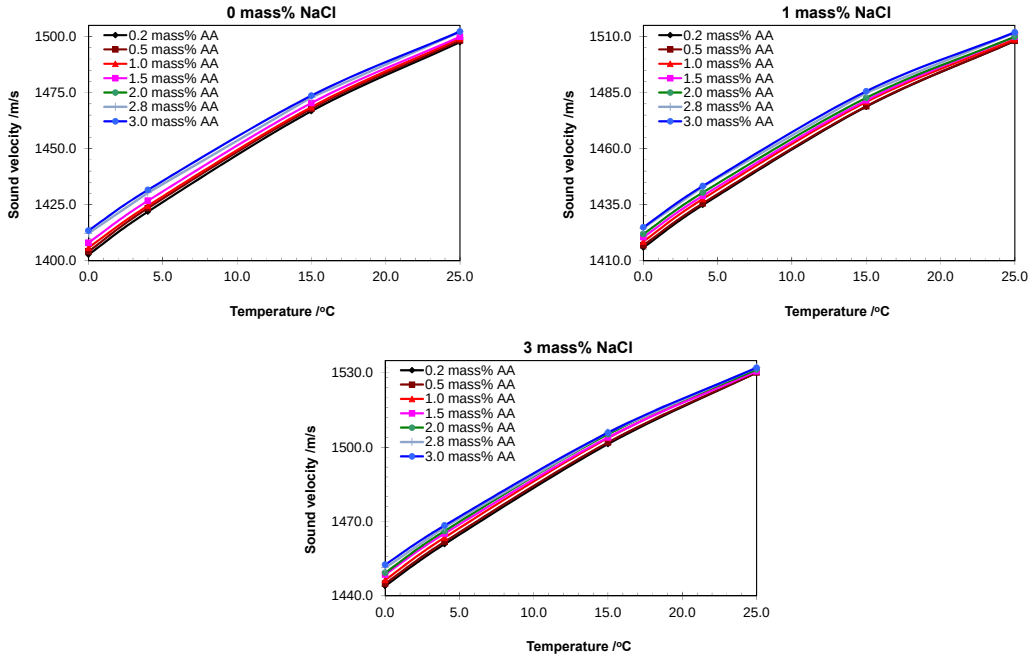

Figure 2.26 Effect of temperature on sound velocity when NaCl is in the aqueous water-soluble AA solutions

Effect of coexistence of the water-soluble AA and NaCl on sound velocity

Figure 2.27 illuminates the effect of the water-soluble AA on sound velocity. According to these graphs, sound velocity increases as the AA concentration increases. The general increase trend is liner, although there was some points fluctuating around the linear trend. This fluctuation is within the sound velocity measurement error range (0.5 m/s).

Figure 2.28 shows sound velocity against NaCl concentrations at constant temperatures and AA concentrations. As it was expected, sound velocity increases with increasing NaCl concentration in the solution. A good linearity is observed in these graphs, which results in more accurate ANN correlation than that for the oil-soluble AA systems.

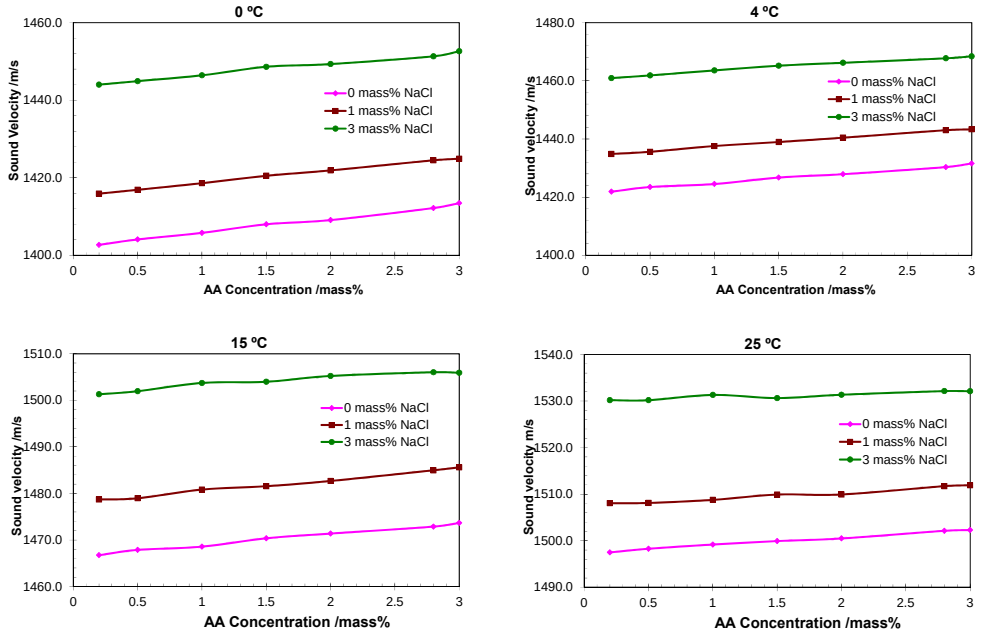

Figure 2.27 Effect of the water-soluble AA on sound velocity when NaCl concentration and temperature are constant.

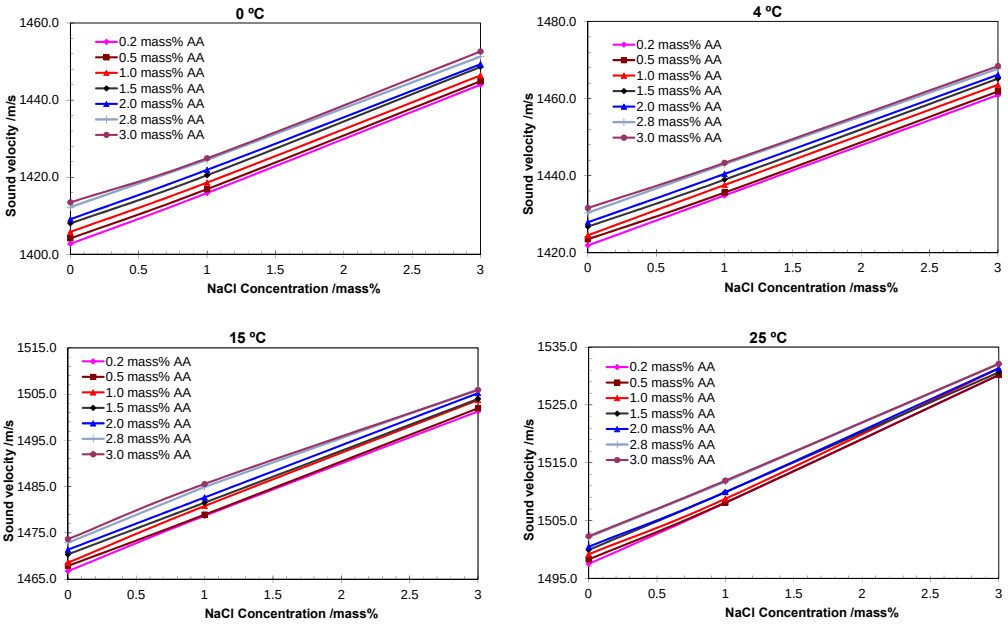

Figure 2.28 Effect of NaCl on sound velocity in the aqueous water-soluble AA solutions.

2.6.2.3. ANN Development for Water-Soluble AA Systems

After analysing and interpolating the data over full temperature range, different ANN structures were tried and tested. Since the changes in the water-soluble AA concentration do not result in significant changes in sound velocity and conductivity, networks with five neurons in their hidden layer didn't have satisfied performance for this AA systems. The best performance was obtained with seven neurons in the hidden layer. The network structure used in this ANN is similar to the one described in Figure 2.19. The trained ANN correlation was evaluated with independent data measured separately over a full temperature range (0 to 25 °C) for solutions containing NaCl and water-soluble AA concentration of (NaCl=0.5,AA=1.25), (NaCl=1.5,AA=0.75), (NaCl=2,AA=2.5),(NaCl=2.5,AA=2)mass %.

Figure 2.29 and Figure 2.30 shows the results of the ANN. The ANN results fairly gives a good output over the temperature range and the results are very close to their actual values.

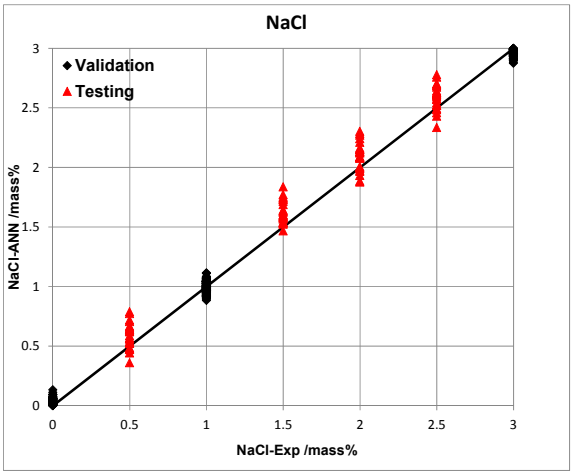

Figure 2.29 Performance of the trained ANN for determining NaCl concentration

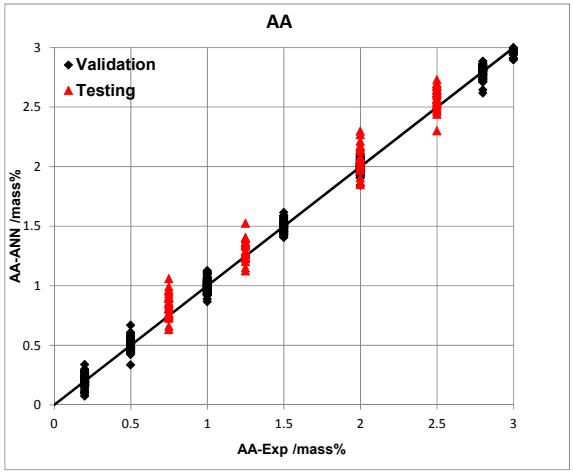

Figure 2.30 Performance of the trained ANN for determining the oil-soluble AA concentration

The validating data shows a slightly better agreement with their actual values compared with the independent data (the triangles in the figure). The maximum deviation observed from this ANN for NaCl testing data was 0.33 mass % over 0 to 3 NaCl mass%. This deviation for the tested water-soluble AA was 0.3 mass% over 0 to 3 mass% AA. Table 2.7 and Table 2.8 summarises the testing results.

Table 2.7 ANN testing results for independent data, mass%

NaCl	Exp	0.5	1.5	2	2.5
	Max	0.78	1.83	2.30	2.77
	Avg	0.55	1.62	2.10	2.58
AA	Exp	1.25	0.75	2.5	2
	Max	1.52	1.05	2.72	2.29
	Avg	1.29	0.83	2.57	2.06

Table 2.8 ANN deviation for the tested water-soluble AA and NaCl for testing and validation data, mass%

	Maximum AD	Average AD
NaCl	0.33	0.05
AA	0.30	0.04

The results from the tested oil-soluble AA and water-soluble AA showed that C-V method could be used for determining the concentrations of salt and AA

simultaneously. However, it should be considered that precipitation of AA/some AA components will strongly affect the results. High concentration of salt will reduce the solubility of AA in the solution. This precipitation causes ANN confusion. Therefore, in order to use this method with a desired accuracy for measuring AA and salt in high salinity systems, it is strongly recommended to dilute the samples before measurements. In this case the ANN can be trained for lower concentrations. Based on this idea, a dilution feature has been successfully designed and tested in developing the C-V prototype, which is presented in chapter 6.

2.6.3. Ethanol Systems with Salt

Ethanol has been used for hydrate inhibition purposes in many fields especially in Brazil (Anderson et al., 2008). Following successful development of the C-V prototype for other common thermodynamic hydrate inhibitors, i.e. methanol and mono ethylene glycol and their successful filed trials which will be explained in chapter 6, it was decided to extend the capability of this method to ethanol systems. The selected concentration range for ANN training was 0 to 10 mass% for NaCl and 0 to 50 mass% for ethanol which covers the typical concentration range used in oil and gas industry (Bonyad et al., 2011). For concentrations higher than these ranges, a dilution factor can be used. The measurements and ANN training were conducted at 20 °C instead of the previous temperature range of 0 to 25 °C. Generating a large database of conductivity and sound velocity over a temperature range from 0 to 25 °C is very time consuming. To cover a full temperature range we need to interpolate the data between the measurement temperatures, which could cause additional errors in some cases although the errors may be very small and negligible. The advantage of the constant-temperature method is easy to be developed and relatively high accuracy. In the single temperature method, a measurement cell with a cooling jacket was used to control and maintain the temperature constant while conducting measurements. In the case of developing ANN for full temperature range, the jacketed measurement cell is only required for generating the database for ANN correlation, which makes the C-V device very robust and user friendly for offshore field applications. This will be detailed in developing the prototype and automation in Chapter 6.

2.6.3.1. Conductivity Measurements

Table 2.9 summarises the measured conductivity values for aqueous ethanol and salt (NaCl) solutions at 20 °C for 0 to 10 mass% of NaCl and 0 to 50 mass% of ethanol. As it was mentioned before, electrical conductivity is a function of ion concentration in the solution. Considering the fact that there are nearly no electrolytes in ethanol, it is expected the conductivity of the ethanol solution to be almost zero in the absence of NaCl, as shown in Table 2.9, in order of μS/cm. Therefore, the conductivity value for these solutions without salt was assumed to be zero.

Table 2.9 The measured conductivity of the aqueous ethanol and NaCl solutions at 20 °C, in mS/cm

T	NaCl	ethanol, mass%					
°C	Mass%	0	10	20	25	30	50
20	0	0.0019	0.0013	0.004	0.003	0.001	0.0023
	1	15.86	10.21	6.64	5.44	4.56	2.347
	5	69.40	44.00	28.73	23.60	19.65	9.65
	10	125.10	80.00	51.90	42.90	35.71	17.02

Figure 2.31 illustrates the measured electrical conductivities versus ethanol concentration at 20 °C for constant NaCl concentrations. The conductivity decreases as ethanol concentration increases in the solution. The slope of the conductivity-ethanol concentration curves increases by increasing NaCl concentration. The conductivity is changing monotonically with ethanol concentration; therefore, good performance of trained ANN was expected.

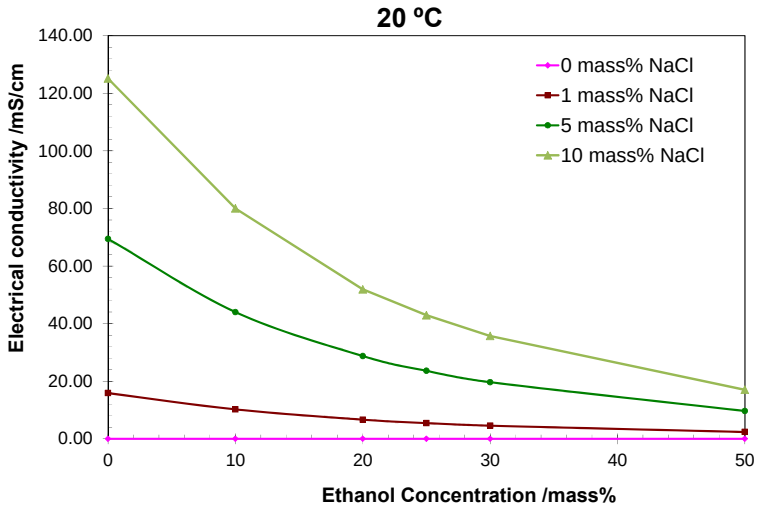

Figure 2.31 Measured electrical conductivity versus ethanol concentration

Figure 2.32 shows the electrical conductivity versus NaCl concentration at 20 °C for different ethanol concentrations. The conductivity is increased linearly by increasing salt concentration due to the effect of salt on conductivity. The slops of the lines decreases significantly by increasing ethanol concentration.

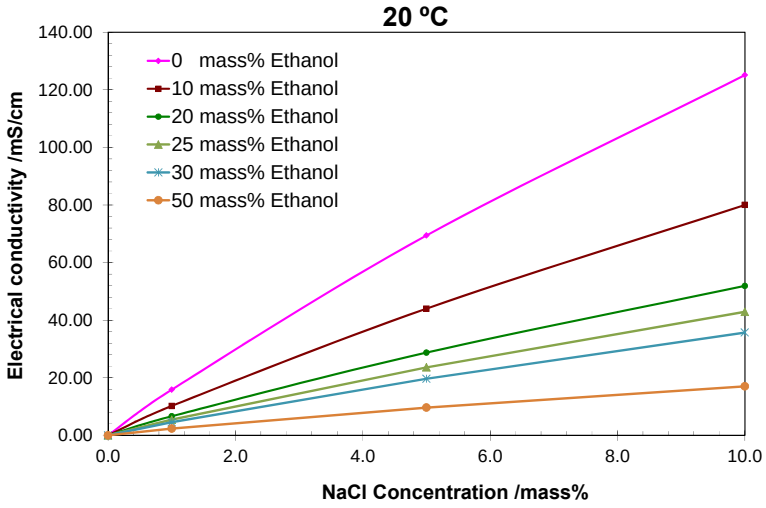

Figure 2.32 Measured electrical conductivity versus NaCl concentrations

2.6.3.2. Sound velocity Measurements

Sound velocity as the second parameter used in the ANN training were measured over NaCl concentration from 0 to 10 mass % and ethanol concentration from 0 to 50 mass%. In this series of measurements a non-monotonic behaviour were observed. The sound velocity increased by increasing ethanol concentration up to about 20 mass% but by further increase in ethanol concentration up to 50 mass%, the sound velocity decreased. Figure 2.33 shows this behaviour for a solution with 5 mass% NaCl as an example.

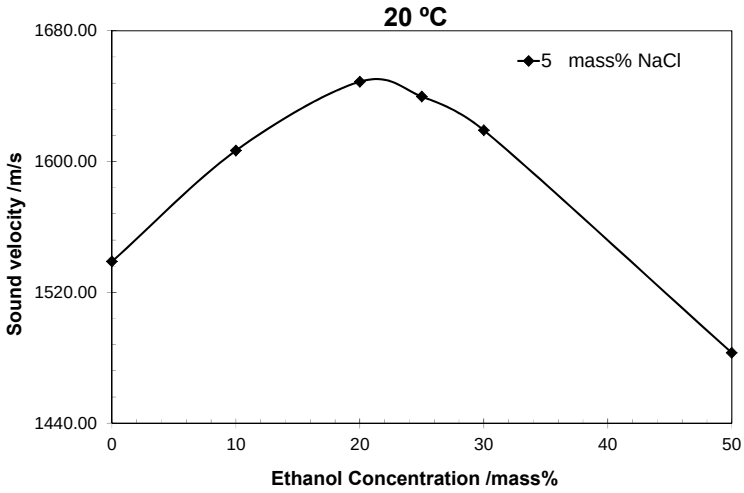

Figure 2.33 Measured sound velocity versus ethanol concentrations for a solution with 5 mass % NaCl

This phenomenon could be explained by specific volume (V) for ethanol-water mixture which is the volume occupied by certain amount of mass which is inverse of the density. The curve for specific volume shows a minimum at about 25 mass% ethanol (Parke and Brich, 1999). This phenomenon was also observed by Kappatos et al. (1996) and Franks and Ives (1996). The initial fall in V at lower concentrations is common to hydrophobic solutes. It is best explained using the Frank & Evans (1945) model of the formation of icebergs around hydrophobic solute molecules in water. When ethanol molecules are introduced to water, the water molecules around the hydrophobic end of the ethanol undergo a structural rearrangement in such a way that strong water-water hydrogen bonds are formed. It is very likely that such an arrangement may be long range (in analogy to Jeffrey's (1993) polarize-ability power

of hydrogen bonds), so that it can be assumed that the cage-like structures normally encountered in bulk water are stabilised in the process, enabling solutes to pack within the interstitial spaces formed within them. Those icebergs, therefore, have a relatively open structure. At the minimum (25% ethanol) in the V curve, all the available interstitial spaces presumably become saturated with either ethanol or water molecules, so that addition of excess ethanol only increases the apparent volume. Apparent specific volume increases rapidly as ethanol-water interactions are replaced by ethanol-ethanol hydrophobic interactions. It will cause an increase in the packing efficiency of the ethanol molecules in water which results in a maximum in the sound velocity curve; this tallies with the idea of hydrophobic packing and iceberg formation. However, at concentrations higher than 25%, ethanol molecules pack less efficiently among water molecules and hence the speed of sound in water falls.

Due to this phenomenon it was not possible to train a single network to determine ethanol and salt concentration for the whole ranges because it was likely to have two concentrations for one sound velocity which will cause confusion in ANN and result in the ANN failure. To overcome this problem the sound velocity measurements were divided into two sections, the first section, from 0 to 20 mass% and the second one from 30 to 50 mass% ethanol in the solution. Table 2.10 shows the results for these measurements. By dividing the data into two sections, sound velocity data were plotted versus ethanol concentrations from 0 to 20 mass% and from 30 to 50 mass % of ethanol for different NaCl concentrations. These sound velocity data were also plotted versus NaCl concentration for different ethanol concentrations Figure 2.34 and Figure 2.35 show these plots.

Table 2.10 The measured sound velocity of aqueous ethanol solutions, in m/s

T	NaCl	Ethanol/ mass%					
°C	Mass%	0	10	20	25	30	50
20	0	1481.99	1561.80	1620.69	1646.62	1624.00	1493.61
	1	1493.61	1571.56	1625.93	1603.41	1622.95	1490.96
	5	1538.86	1606.71	1648.85	1639.71	1619.12	1483.04
	10	1595.60	1653.19	1669.65	1650.48	1616.52	1468.75

In Figure 2.34, for the concentration of ethanol below 20 mass%, the sound velocity is increased by increasing ethanol concentration at a constant NaCl concentration. Sound velocity is also increased by increasing salt concentration.

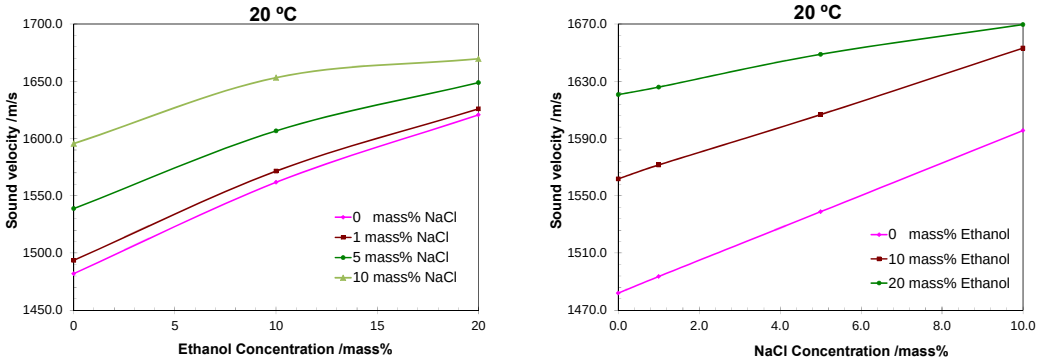

Figure 2.34 Effect of ethanol and NaCl on sound velocity for 0 to 20 mass% ethanol

In the second set of data (30 to 50 mass% ethanol), sound velocity decreases as the concentration of ethanol increases (Figure 2.35). This behaviour could also be due to the packing effect that is altered by the presence of salt.

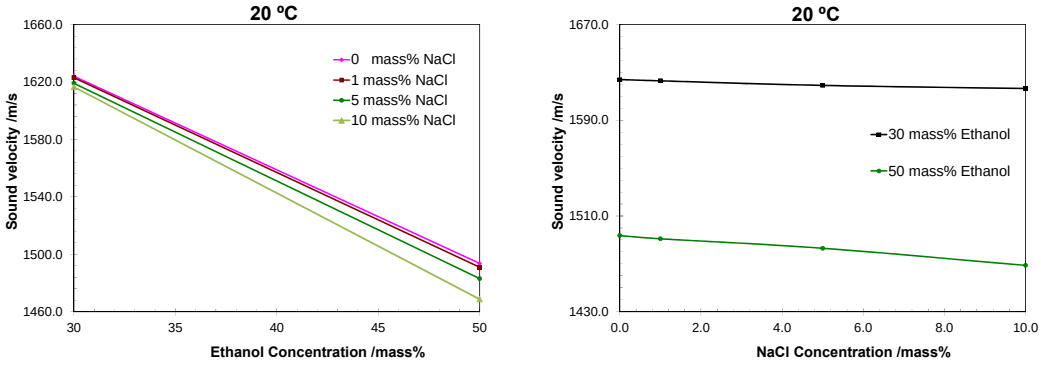

Figure 2.35 Effect of ethanol and NaCl on sound velocity for ethanol concentrations from 30 to 50 mass%

2.6.3.3. ANN Development for Ethanol-NaCl Systems

As it was discussed in the previous section, the data was divided into two groups, first one for 0 to 20 mass% ethanol and the second one for 30 to 50 mass% ethanol. In both cases, the NaCl concentration was from 0 to 10 mass%. Based on this data analysis, two ANNs have been trained for determining ethanol and salt concentrations. The network structure for training was similar to the one explained in the Figure 2.19. The differences are the number of inputs was reduced to two due to a constant temperature (20 °C) and the number of neurons in the hidden layer was reduced to 5 because of the smaller set of data. After trying different ANNs, two of them with the highest performance were selected. The first ANN for the data from 0 to 20 mass% ethanol and the second one for 30 to 50 mass% ethanol. To evaluate the trained networks, two independent data were measured separately with 2.5 mass% NaCl & 14.5 mass% ethanol and 7 mass% NaCl & 39 mass% ethanol. The trained ANNs were evaluated with validating and testing results. Figure 2.29 and Figure 2.30 show the results for both ANNs (0 to 20 and 30 to 50 mass% ethanol).

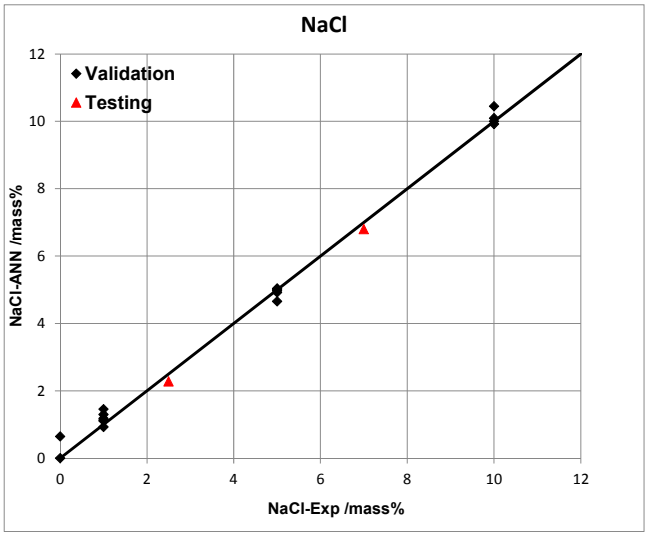

Figure 2.36 Performance of the trained ANN in determining NaCl concentration

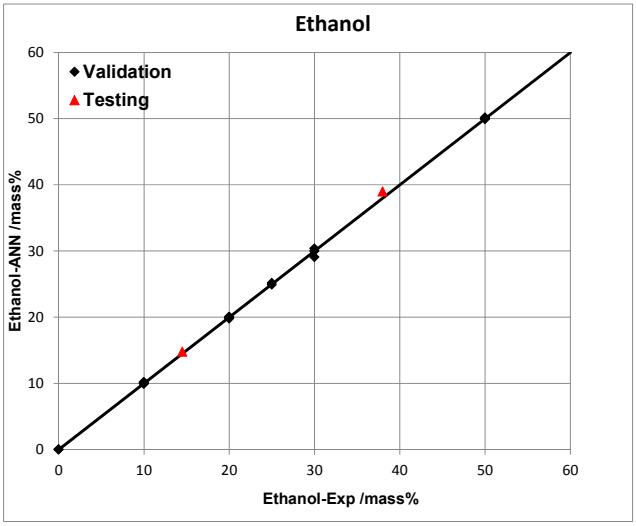

Figure 2.37 Performance of the trained ANN in determining ethanol concentration

As it was expected from the data analysis, ANN for 0 to 20 mass% ethanol shows better results for both testing and validation data. The maximum and average errors for both ANNs are reported in Table 2.11.

Table 2.11 ANN results for determining ethanol and NaCl concentrations

Hydrate inhibitors	Deviation in training		Deviation in testing	
	Average	Maximum	Average	Maximum
Ethanol (0 – 20 mass %)	0.08	0.20	0.10	0.45
NaCl	0.06	0.13	0.09	0.2
Ethanol (30 – 50 mass %)	0.23	0.9	0.11	1.0
NaCl	0.33	0.6	0.2	0.2

According to this table, for ethanol concentration from 0 to 20 mass%, the average error in ethanol concentration is 0.08 mass% however, the maximum error is 0.45 mass% among the independent data. Determining NaCl concentration shows a better accuracy and the average values for NaCl error is 0.06 mass% while the maximum error is 0.2 mass %. For the higher concentration range of ethanol, the error was increased. The average and maximum error for ethanol in the upper ethanol concentration range was 0.23 mass% and 1 mass%, while for NaCl concentration the average error was increased to 0.33 mass% and the maximum was 0.6 mass%. Therefore, the potential error for NaCl measurements for higher concentration of

ethanol was increased. However, using the ANN for 0-20 mass% ethanol, a better accuracy could be achieved by diluting the higher concentrations.

2.6.3.4. Evaluation of the ANNs

The ultimate goal of this work is to develop a method which can monitor hydrate safety margin for optimising inhibitor injection. To evaluate the accuracy and reliability of the C-V method in terms of hydrate phase boundary, the worst case, i.e., the determined ethanol and salt concentrations with maximum errors were used to predict the hydrate phase boundary using our in-house thermodynamic model. Figure 2.38 shows that, in the worst case, the deviation of the determined hydrate phase boundary with C-V method from the one for actual concentrations with typical natural gas composition (Table A.72) is negligible (less than ±0.3 °C), suggesting the high accuracy of C-V method for hydrate monitoring purpose.

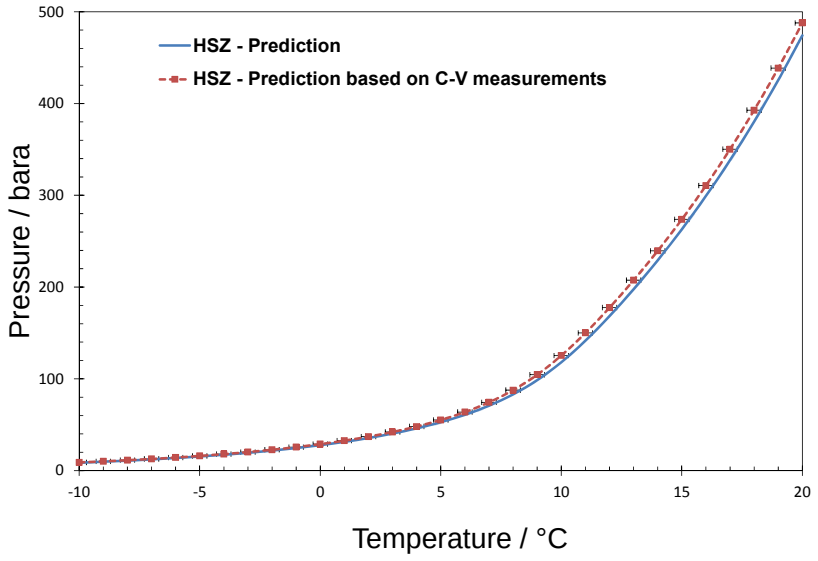

Figure 2.38 Evaluation of the C-V method by predicting the hydrate phase boundary for a NaCl-ethanol solution (20 mass% ethanol and 5.0 mass% NaCl). The error bars shown in this graph is ±0.3 °C.

2.6.4. Kinetic Hydrate Inhibitor (KHI)-NaCl Systems

Application of kinetic hydrate inhibitors (KHI) are growing very fast in the oil and gas industry. The objective of this section is to investigate the ability of C-V method for determining concentrations of KHI and salt in aqueous solutions. KHIs are usually injected at very low concentrations. The commercial KHI investigated in this work has a recommended dosage of 0.5 to 1 mass% based on aqueous phase. A large database of conductivity and sound velocity data for different concentrations of NaCl and KHI were generated. It covers 0 to 2 mass% KHI and 0 to 5 mass% NaCl. The measurements were conducted at 25 ºC. The reason for choosing this temperature was that this ANN was designed for a field application in South Africa with a ambient temperature close to 25 °C.

2.6.4.1. Conductivity Measurements

Table 2.12 shows the measured electrical conductivities for different concentrations of KHI (0 to 2 mass%) and NaCl (0 to 5 mass%) at 25 °C.

Table 2.12 The measured conductivity of aqueous KHI-NaCl solutions at 25 °C, in mS/cm

T	NaCl	KHI, mass%				
ºC	Mass%	0	0.2	0.5	1	2
25	0	0.05	0.05	0.05	0.05	0.05
	1	17.57	17.51	17.46	17.26	16.87
	3	48.30	48.10	47.90	47.40	46.30
	5	76.70	76.30	75.90	75.00	73.40

It can be seen that the KHI didn't affect the electrical conductivity noticeably when there was no salt in the system and the measured values were in order of μS/cm. Therefore, the conductivity value for the solutions without salt has been assumed to be 0.05 mS/cm (typical electrical conductivity of tap water). Figure 2.39 and Figure 2.40 show the measured results.

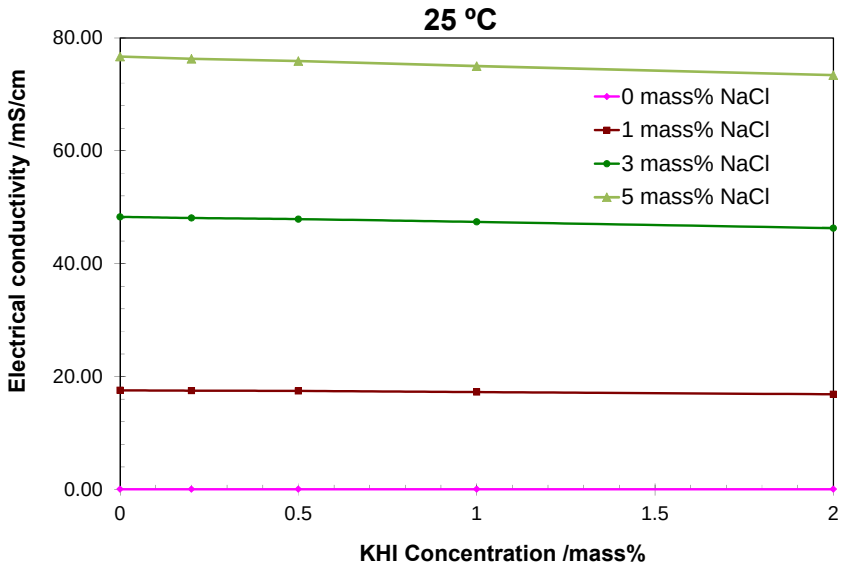

Figure 2.39 Measured electrical conductivity vs. KHI concentrations

In the system with 1 mass% NaCl, by increasing the KHI concentration, the conductivity value decreases slightly. By increase in NaCl concentrations to 3 and 5 mass%, the same trend was observed but the slope of decrease in conductivity due to increase in KHI concentration increases at higher salt concentrations.

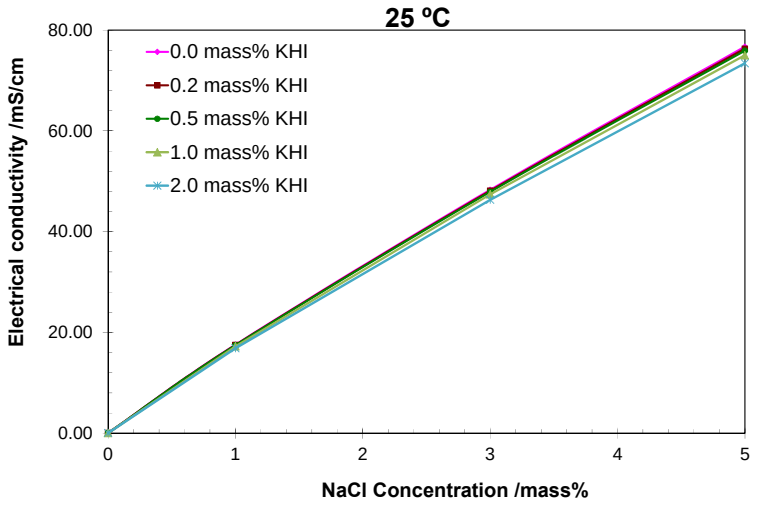

Figure 2.40 Measured electrical conductivity versus NaCl concentrations

In Figure 2.40 the electrical conductivity was significantly increased by increasing NaCl concentration at different KHI concentrations. These increases were very

smooth and monotonic. Although these curves are close to each other due to small effect of KHI on conductivity, there is an enough difference between them and easily can be differed by the conductivity meter. As a result, the measured electrical conductivity can be used for developing an ANN for the KHI-salt systems.

2.6.4.2. Sound Velocity Measurements

Table 2.13 shows the results of the sound velocity measurements for KHI-NaCl solutions at 25 °C.

Table 2.13 The measured sound velocity of the aqueous KHI solutions at 25 °C, in m/s

T	NaCl	KHI/ mass%				
°C	Mass%	0	0.2	0.5	1	2
25	0	1494.20	1495.24	1495.98	1497.31	1500.44
	1	1504.94	1505.84	1507.19	1508.10	1511.27
	3	1526.89	1527.35	1528.28	1530.14	1532.94
	5	1549.01	1549.49	1550.44	1551.40	1554.28

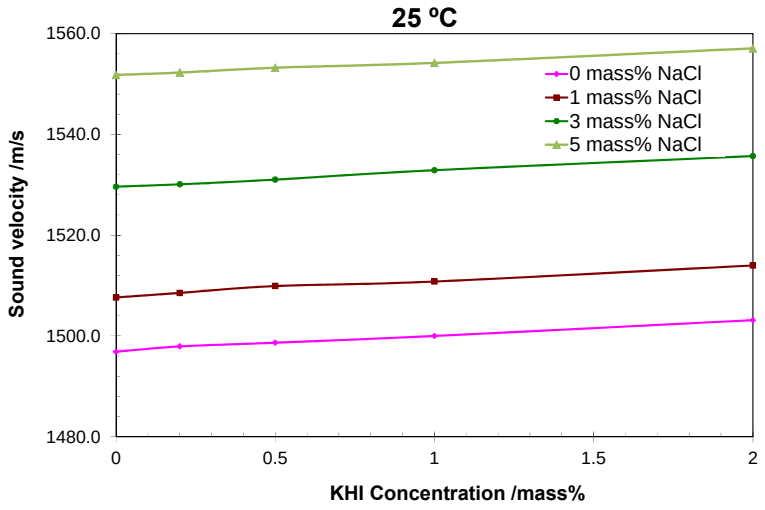

Figure 2.41 Measured sound velocity versus KHI concentration at 25 °C

Figure 2.41 shows that the sound velocity increases with increase in the KHI concentration when the salt concentration is constant. This increase is very monotonic and nearly linear. Similar behaviour can be observed by increasing salt concentrations,

as shown in Figure 2.42. Increasing NaCl concentration causes an increase in sound velocity. The magnitude of the changes in sound velocity due to increase in NaCl concentration is higher than those due to the increase in the KHI concentration. It means that the ANN correlation will be more sensitive to NaCl concentration. These figures also shows that there is a liner relationship between sound velocity-NaCl concentration and sound velocity-KHI concentration. These monotonic behaviours for sound velocity and electrical conductivity ensures high performance of the ANN.

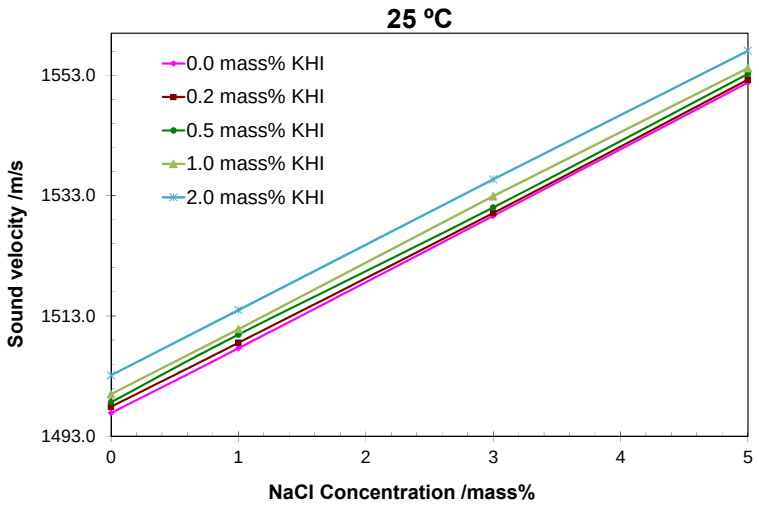

Figure 2.42 Measured sound velocity versus NaCl concentrations at 25 °C

2.6.4.3. ANN Development for KHI-NaCl Systems

An ANN was designed with the same structure illustrated in Figure 2.19 but with 2 inputs (conductivity and velocity) and two outputs. Five neurons were used in the hidden layer due to the observed sensitive response of sound velocity and electrical conductivity to the KHI and salt concentrations. To evaluate the trained network, five independent solutions with (NaCl=2.5, KHI=0.5), (NaCl=2.5, KHI=0.8), (NaCl=4.5, KHI=0.5), (NaCl=4.5, KHI=1.2) and (NaCl=0.52, KHI=0.12) mass % were measured. The results are plotted in Figure 2.43 and Figure 2.44. These results show that both validation and testing data are closely matching their actual values. Due to stronger effect of salt on both conductivity and sound velocity values compared to that of KHI,

slightly better accuracy was observed in NaCl results. However the results for KHI were also accurate with the maximum error of less than 0.1 mass%.

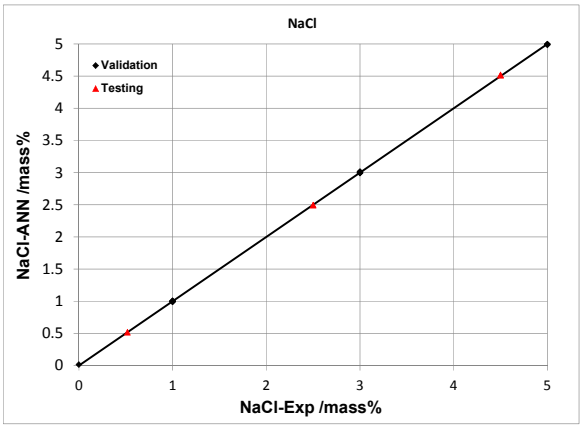

Figure 2.43 Performance of the trained ANN in determining NaCl concentration

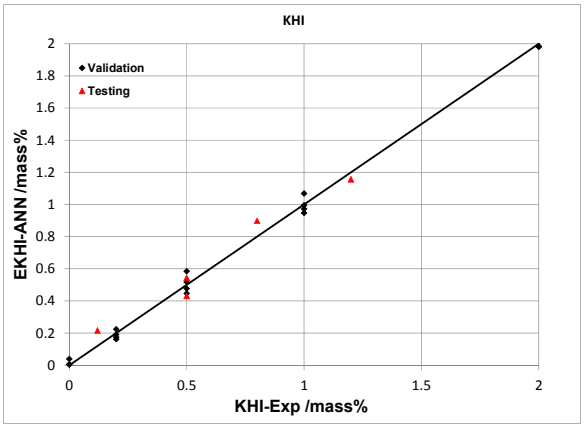

Figure 2.44 Performance of trained ANN in determining KHI concentration

Table 2.14 shows the summarised results of validation and testing for the ANN. The maximum error of the ANN for NaCl was 0.02 mass% while the average error was almost zero in both testing and validation. The maximum error in KHI determination was 0.1 mass%.

Table 2.14 ANN results for determining KHI and NaCl concentrations at 25 °C

Hydrate inhibitors	Deviation in validation		Deviation in testing	
	Average	Maximum	Average	Maximum
KHI (0 – 2 mass %)	0.02	0.08	0.07	0.1
NaCl (0 – 5 mass %)	0.006	0.01	0.02	0.02

2.6.5. KHI-MEG Systems with Salt

In the recent years, application of LDHIs especially KHI has been increased extensively and quickly and a number of operators are thinking of replacing the traditional thermodynamic hydrate inhibitors like MEG, methanol and ethanol with different types of LDHIs. In the replacement process, in most cases there is a transient period within which both thermodynamic and kinetic inhibitors are being injected. After injecting both inhibitors for a certain period, the concentration of thermodynamic inhibitors will gradually be reduced. During the transient period both LDHI and thermodynamic inhibitor will be coexist in the system. Moreover, it is known that KHIs can only work under a certain degree of subcooling. Excessive subcooling could cause the KHI failure to delay hydrate nucleation and formation. Therefore, combination of a thermodynamic inhibitor with a KHI is increasingly accepted as an alternative option. Considering the fact that produced water is saline in nature, in total there will be three parameters (LDHI, thermodynamic inhibitor and salt) to be measured. The two parameter conductivity-velocity method as explained before is able to measure only two parameters so that it will be useful only after the transient period not during transition process. As it was explained in Section 2.2.3, by introducing a third parameter, it might be possible to determine the third unknown parameter if the third measured property is independent from the other two. The third property as was introduced in Section 2.2.3 could be either slope of sound velocity-temperature curves (thermal coefficient of sound velocity) or the slope of electrical conductivity-temperature curves (thermal coefficient of electrical conductivity). These two parameters have been found to be dependent on the solution property and behave independently from the sound velocity and electrical conductivity. To investigate this method KHI-MEG-NaCl system was selected as one of the most common systems. To generate the necessary database for training an ANN a concentration range from 0 to 1 mass% KHI, 0 to 40 mass% MEG and 0 to 5 mass% NaCl was selected. To be able to determine the thermal coefficients of velocity and conductivity, the conductivity and velocity were measured at two temperatures, i.e. 15 and 25 °C. After data analysis, an ANN was trained and evaluated with independent data. The following sections detail the results of this method.

2.6.5.1. Conductivity and its Thermal Coefficient Measurement

The electrical conductivity was measured for different concentration of KHI-MEG-NaCl solutions over the previously mentioned concentration ranges. To be able to calculate the thermal coefficient, all the concentrations were measured at two temperatures 15 and 25 °C. There were two reasons for selecting these two temperatures, based on our experience. In the selected temperature range the thermal coefficients showed high sensitivity to changes of the inhibitor and salt concentrations. The second reason was to shorten test time. The selected temperatures are more close to the ambient and more energy and time can be saved for cooling and heating. The measured data are tabulated in Table 2.15.

Table 2.15 Measured electrical conductivity for NaCl-KHI-MEG systems, in mS/cm

T	NaCl	KHI	MEG /mass%				
°C	mass%	mass%	0	10.0	20.0	30.0	40.0
15.0	0	0	0.05	0.05	0.05	0.05	0.05
		0.5	0.05	0.05	0.05	0.05	0.05
		1.0	0.05	0.05	0.05	0.05	0.05
	1.0	0	13.88	10.32	7.47	5.23	3.58
		0.5	13.8	10.18	7.195	5.14	3.51
		1.0	13.72	10.07	6.92	5.05	3.42
	3.0	0	38.24	28.36	20.53	14.41	9.78
		0.5	37.55	28.01	20.13	13.81	9.54
		1.0	37.35	27.11	19.74	13.21	9.30
	5.0	0	60.92	45.00	32.49	22.70	15.39
		0.5	58.45	43.36	30.68	21.77	14.34
		1.0	55.98	41.73	28.87	20.84	13.29
25.0	0	0	0.05	0.05	0.05	0.05	0.05
		0.5	0.05	0.05	0.05	0.05	0.05
		1.0	0.05	0.05	0.05	0.05	0.05
	1.0	0	17.28	13.03	9.61	6.83	4.76
		0.5	17.18	12.85	9.25	6.71	4.66
		1.0	17.08	12.71	8.90	6.59	4.54
	3.0	0	47.35	35.73	26.31	18.75	12.98
		0.5	44.81	34.16	25.32	17.44	12.03
		1.0	43.96	34.01	24.82	17.19	11.82
	5.0	0	75.38	56.60	41.46	29.56	20.37
		0.5	70.71	53.43	38.63	26.97	18.96
		1.0	69.6	52.63	37.84	25.95	17.72

As KHI and MEG are not electrolytes, their conductivity is very close to the values for deionised water. Therefore, the conductivity was set to 0.05 mS/cm for solutions containing MEG and KHI without salt. This was to avoid any confusion for the ANN.

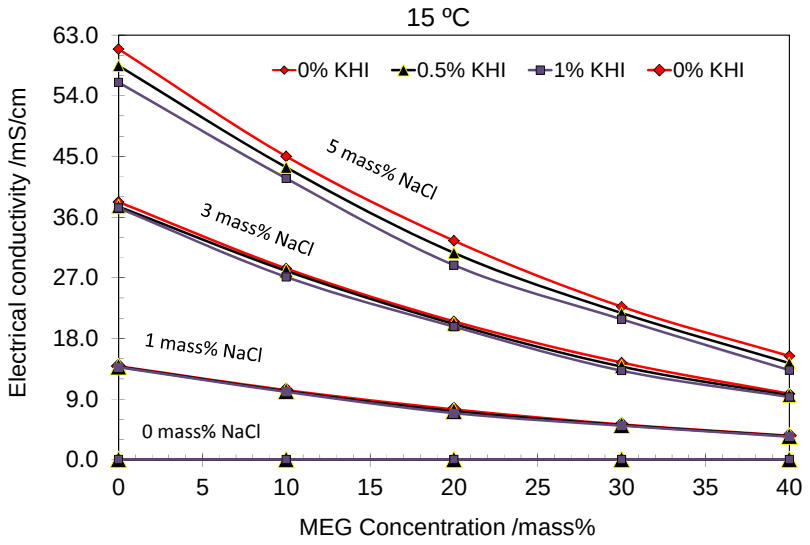

Figure 2.45 Measured electrical conductivity versus MEG concentration at 15ºC

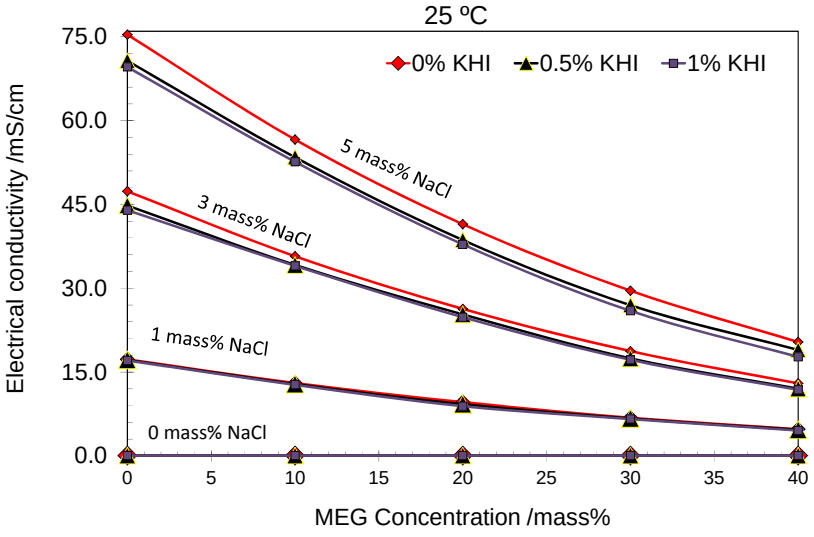

Figure 2.46 Measured electrical conductivity versus MEG concentration at 25°C

As can be seen in Figure 2.45 and Figure 2.46, conductivity is increased significantly by increasing salt concentration, while increasing MEG concentration causes a non-linear decrease in conductivity. This decrease gets more pronounced by increasing salt concentration in the solutions. By increasing salt concentration, the conductivity changes also get more pronounced due to the change in KHI concentration. For example, in the case of 1 mass% NaCl, the graphs with constant KHI concentrations are more close to each other compared to the graphs with 5 mass% NaCl and constant KHI concentrations.

Similar behaviour to 15 °C was observed in the results at 25 °C. Increase in temperature caused a general increase in electrical conductivity values as it was expected. The general trends for all concentrations are the same as those at 15 °C; both KHI and MEG cause reduction in conductivity values when the NaCl is constant.

After data processing and improving the results by numerical analysis, Equation 2.9 was used to calculate the conductivity thermal coefficients. The calculated conductivity thermal coefficients are plotted in Figure 2.47.

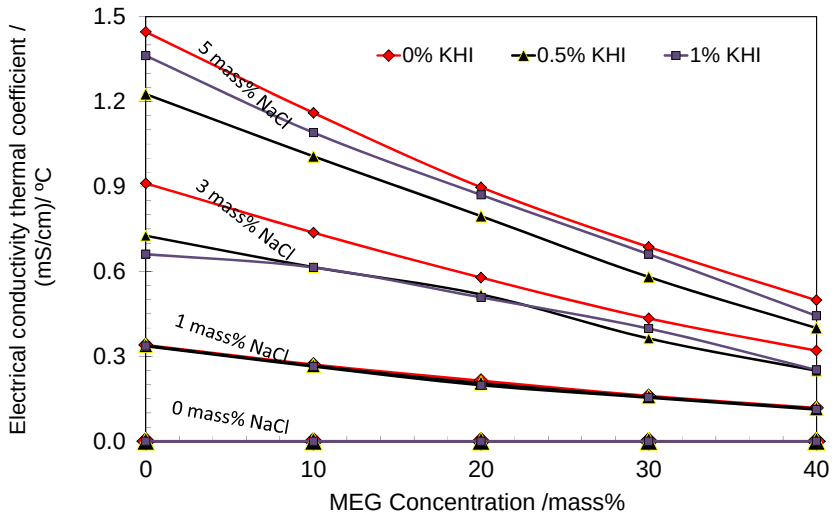

Figure 2.47 Conductivity thermal coefficient versus MEG concentration

Similarly, conductivity thermal coefficient is decreased by increasing MEG concentration but the decrease is not very smooth. For the systems with 1 mass% NaCl, the thermal coefficients for constant KHI curves are very close to each other and it is difficult to differ them. At higher salt concentrations, the curves with constant

KHI concentration, crosses each other at some points. This behaviour is due to the small effect of KHI on conductivity which makes the conductivity thermal coefficient insensitive to KHI concentration.

2.6.5.2. Sound Velocity and its Thermal Coefficient Measurements

Sound velocity as the second parameter for training the ANN was measured over the mentioned concentration range at two temperatures of 15 and 25 °C. Sound velocity thermal coefficient as a third potential parameter was calculated for developing three-parameter C-V method. Table 2.16 shows the results of these measurements.

Table 2.16 Measured sound velocities for NaCl-KHI-MEG system, in m/s

T /°C	NaCl /mass%	KHI /mass%	MEG /mass%				
			0	10	20	30	40
15	0	0	1465.65	1518.58	1571.04	1621.49	1665.00
		0.5	1467.58	1520.42	1573.50	1623.32	1666.11
		1.0	1469.72	1522.72	1575.72	1625.42	1666.94
	1.0	0	1477.72	1529.21	1580.93	1630.43	1672.76
		0.5	1479.46	1531.31	1583.42	1632.55	1674.44
		1.0	1481.42	1533.41	1585.92	1634.41	1675.55
	3.0	0	1500.89	1550.92	1600.57	1646.46	1685.95
		0.5	1502.69	1552.60	1602.61	1648.08	1686.80
		1.0	1504.49	1554.76	1604.15	1649.97	1688.22
	5.0	0	1528.28	1575.23	1621.75	1664.73	1699.93
		0.5	1526.65	1574.00	1620.96	1664.73	1699.93
		1.0	1528.28	1575.72	1622.53	1665.28	1700.21
25	0	0	1496.87	1541.41	1585.17	1627.00	1662.25
		0.5	1498.88	1543.06	1587.17	1629.90	1663.35
		1.0	1500.00	1544.72	1588.93	1629.90	1665.28
	1.0	0	1507.87	1551.4	1595.49	1634.41	1669.99
		0.5	1509.46	1554.97	1596.50	1637.07	1671.10
		1.0	1511.05	1555.00	1598.53	1638.4	1672.21
	3.0	0	1528.05	1571.54	1612.38	1650.78	1682.28
		0.5	1531.07	1572.76	1614.19	1651.87	1683.13
		1.0	1532.47	1574.49	1615.75	1653.23	1683.98
	5.0	0	1554.52	1593.72	1632.55	1667.21	1695.63
		0.5	1552.84	1592.70	1631.49	1667.21	1695.05
		1.0	1554.28	1593.97	1632.81	1667.49	1695.63

Sound velocity data were plotted versus MEG concentrations to analyse sound velocity behaviour in response to the concentration changes. Figure 2.48 shows plots of sound velocity versus MEG concentration for different KHI concentrations at 15 °C. As can be seen in this figure, sound velocity is increased non-linearly by increasing MEG concentration. Increase in salt concentration also increases the sound velocity and shifts the graphs to higher values. Increasing KHI concentrations causes an increase in sound velocity as well. However, the change in sound velocity due to the changes in KHI concentration is not as strong as the changes due to the MEG and NaCl concentration. At lower KHI and NaCl concentrations, the effect of KHI on sound velocity is more pronounced. In total, there is a good repeatable trend in all these graphs.

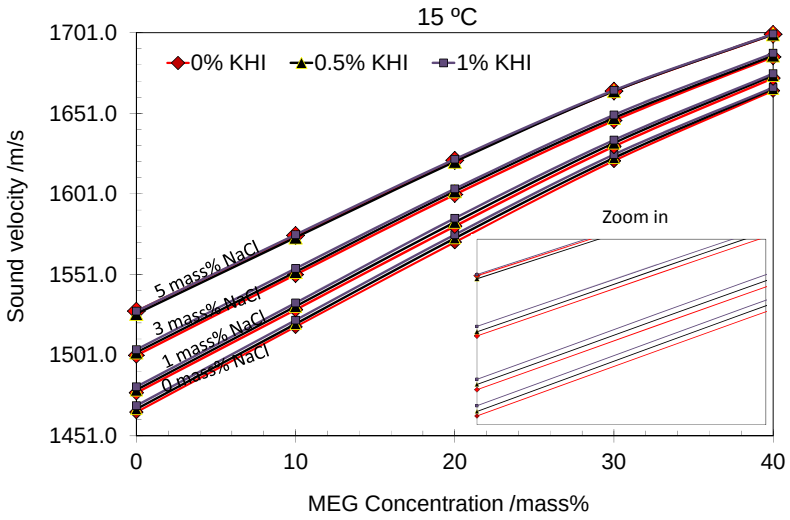

Figure 2.48 Sound velocity versus MEG concentration at 15 °C for different NaCl and KHI concentrations.

Figure 2.49, similar behaviour was observed when the temperature was increased to 25 °C. However, the curves with a constant concentration (0 and 1 mass% NaCl) and different KHI concentrations cross each other at some points.

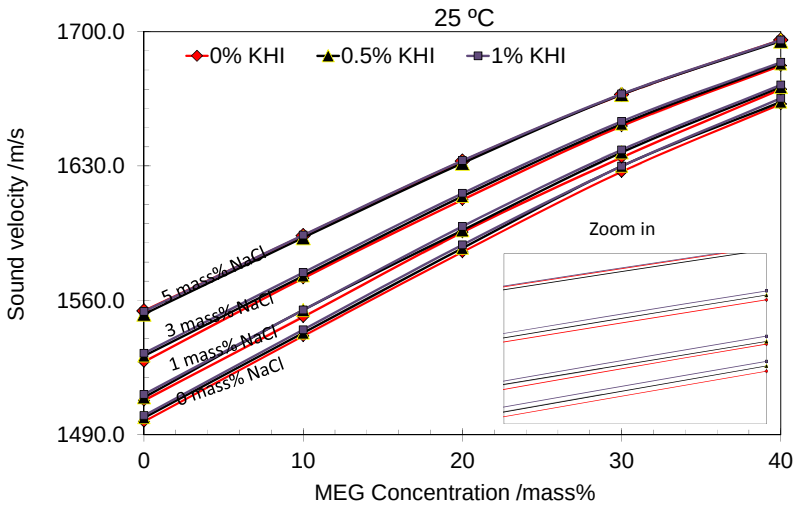

Figure 2.49 Sound velocity versus MEG concentration at 25 ºC for different NaCl and KHI concentrations.

Sound velocity thermal coefficient is calculated according to the Equation 2.8. Figure 2.50 illustrates plots of sound velocity thermal coefficient against MEG concentration for different KHI and NaCl concentrations.

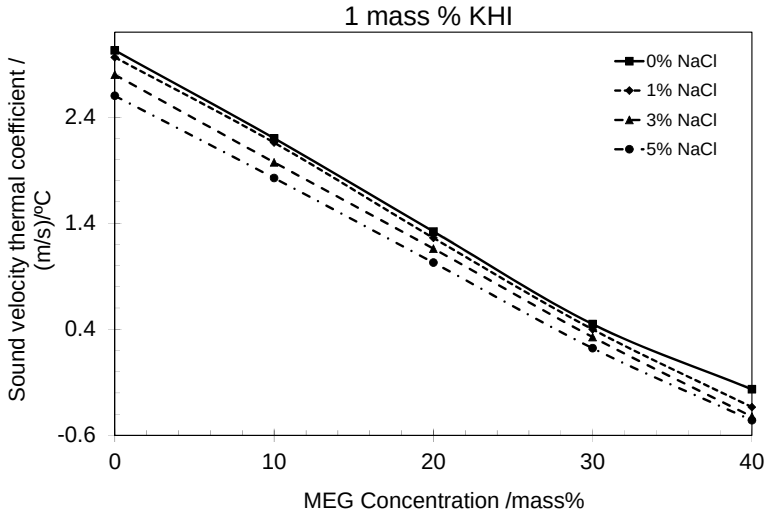

Figure 2.50 Thermal coefficient of sound velocity versus MEG concentration for different NaCl and 1 mass % KHI concentrations

Generally, thermal coefficient of sound velocity decreases with increasing MEG concentration as well as increasing NaCl concentration. Increase in KHI concentration decreases this coefficient at 3 and 5 mass% NaCl concentrations. However, stable behaviour was not observed at lower NaCl concentration (0 and 1 mass% NaCl) for different KHI concentrations. This suggests that the sound velocity coefficient is not sensitive to the KHI concentration. It can be anticipated that training a high performance ANN based on this coefficient will be challenging and there may be large error in determined concentrations compared to the two-parameter C-V method.

2.6.5.3. Developing ANN for KHI-NaCl-MEG Systems

Two set of data were prepared for developing ANN. In both sets of data, conductivity and velocity at 25 °C were used as two parameters out of three ones required. In the first set, conductivity thermal coefficient was used as the third parameter while in the second set the sound velocity thermal coefficient was used in order to investigate which coefficient results in a better performance of the ANN correlation.

To train the ANN, a network structure with 3 inputs and 3 outputs was defined. After a few trials, 7 neurons were used in the hidden layer. To evaluate the performance of the trained ANN six independent mixtures of NaCl, MEG and KHI were prepared and measured. The concentrations of NaCl, KHI and MEG were: (NaCl, KHI, MEG) = (2.5,0.5,21), (0.5,1,15), (0.5,0.8,39), (2.5,0.4,8.7), (4.5,0.1,15), (4.5,0.8,25) in mass%. Figure 2.51 shows the results for validation and testing using conductivity thermal coefficient as the third parameter.

As one can see in this figure the ANN results for NaCl and MEG is in agreement with their actual concentrations. The average error for NaCl concentration was 0.11 mass% while the maximum was 0.6 mass%. The ANN average and maximum errors were 0.73 and 1.13 mass% in determining the concentration of MEG, respectively. The maximum and average errors for KHI concentration were 0.71 and 0.17 mass%, respectively. The errors are too large in comparison to the KHI range from 0 to 1 mass%. As shown in Figures 3.45 to 3.47, insensitivity of the conductivity to the KHI could be the main reason for the ANN failure to accurately determine the KHI concentrations. Table 2.17 summarises the results.

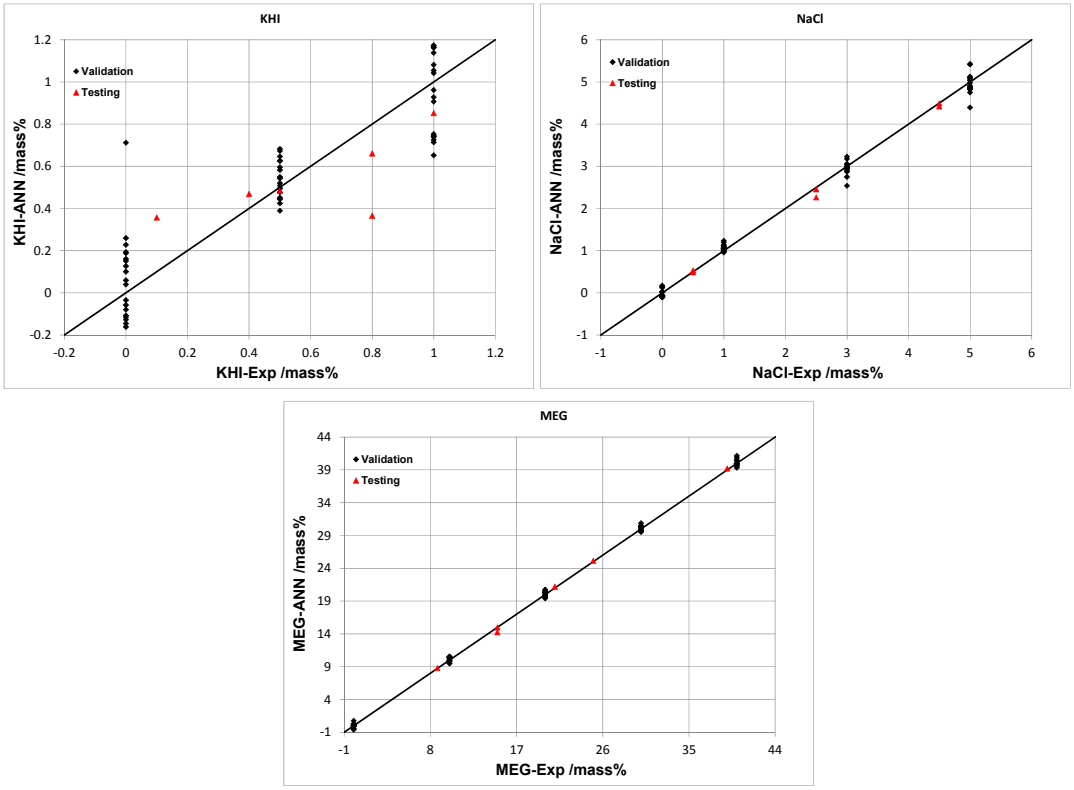

Figure 2.51 Performance of conductivity thermal coefficient-based ANN in determining NaCl, MEG and KHI concentrations

Table 2.17 ANN results for determining KHI, NaCl and MEG concentrations using conductivity thermal coefficient as the third parameter, in mass%

Hydrate inhibitors	Deviation in validation		Deviation in testing	
	Average	Maximum	Average	Maximum
KHI (0 – 1 mass %)	0.15	0.71	0.17	0.43
NaCl (0 – 5 mass %)	0.11	0.60	0.07	0.23
MEG (0 – 40 mass %)	0.32	1.13	0.22	0.73

To investigate the applicability of the thermal coefficient of sound velocity as the third parameter in determining unknown concentrations (NaCl, MEG and KHI), another ANN was trained based on the data processed in the previous section Figure 2.52 Figure 3.52 shows the ANN performance in determining the concentrations for validation and independent testing data. Table 2.18 summarises the errors for these systems.

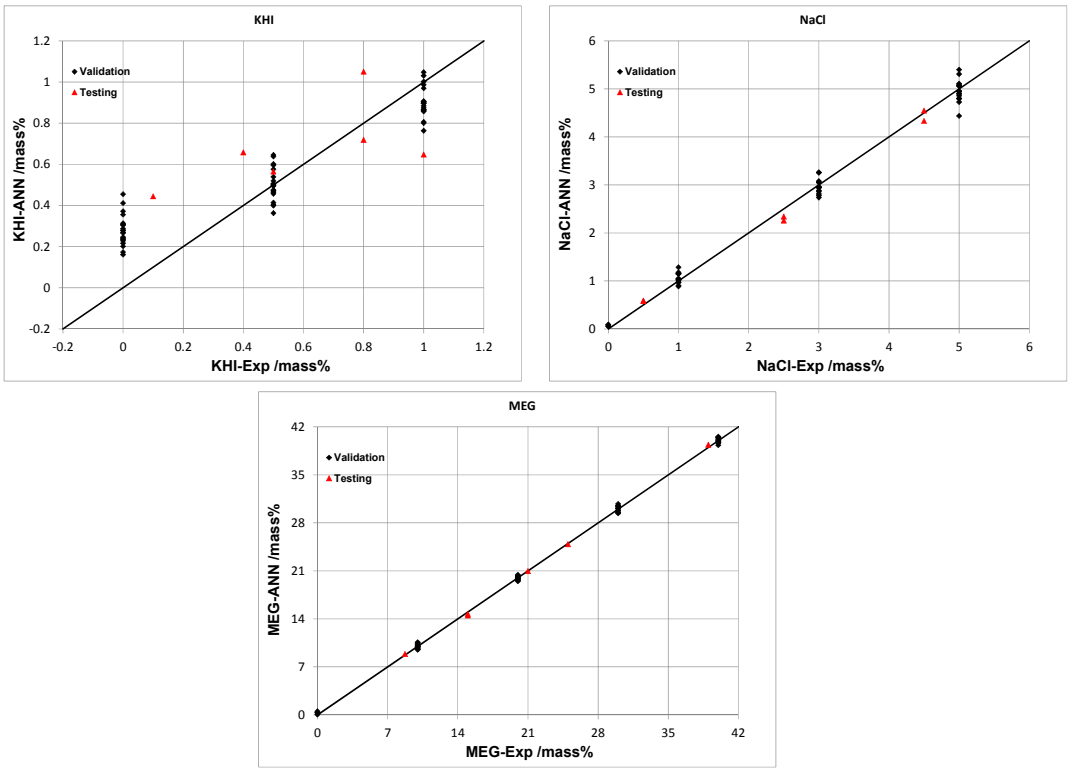

Figure 2.52 performance of the sound velocity thermal coefficient-based ANN in determining NaCl MEG and KHI concentrations

The ANN results for determining NaCl were in good agreement with their actual values. The maximum error observed for training data was 0.56 mass% although it was decreased to 0.24 mass% for independent data. The maximum error in determining MEG concentration in validating and testing were 0.74 and 0.52 mass% respectively. The maximum ANN error for determining KHI concentration was 0.45 mass% in validating which is large considering the narrow window for the KHI concentration.

Table 2.18 Conductivity thermal coefficient-based ANN results for determining KHI, NaCl and MEG concentrations, in mass%

Hydrate inhibitors	Deviation in validation		Deviation in testing	
	Average	Maximum	Average	Maximum
KHI (0 – 1 mass %)	0.15	0.45	0.22	0.35
NaCl (0 – 5 mass %)	0.12	0.56	0.13	0.24
MEG (0 – 40 mass %)	0.30	0.74	0.24	0.51

If we compare the conductivity thermal coefficient-based ANN with the velocity thermal coefficient-based ANN, both give similar accuracy. From these results it can be concluded, the conductivity-velocity-thermal coefficient method could be applied for determining the concentration of 3 unknown concentrations in a system; however, the error in this method is larger than conductivity-velocity method for determining two concentrations. Using this method for determining low concentrations of an inhibitor (0 to 1 mass% KHI in our work) could result in large errors for this inhibitor. Therefore, it is recommended to use the three-parameter method for systems that do not contain very low concentration (few mass%) of inhibitors.

2.7. CONCLUSIONS AND FUTURE WORK

In this work the C-V method was further developed for a number of inhibition systems: a) AA systems (including water-soluble AA and oil-soluble AA in the presence of salt, b) ethanol systems with salt, c) KHI-salt systems d) KHI-MEG-salt systems. In addition to these new systems, the C-V method was tested for a new commercial KHI systems with salt. In each system, a large database of electrical conductivity, sound velocity and thermal coefficients of sound velocity and electrical conductivity where required was created over a wide range of concentrations and temperatures. ANN correlations were trained, validated, and tested for these systems mentioned.

In the AA-salt system (0-3 mass% AA concentration), the performance of the method was acceptable in general. However, high concentration of salt caused the tested AA comes out of solution. This precipitation of AA can cause confusion for the trained ANN and reduce its performance. Precipitation of the tested water-soluble AA was less than the tested oil-soluble AA. It recommended to dilute the samples and consider a dilution factor before measurements to avoid the precipitation problem. This will be detailed in developing the prototype in Chapter 6.

The measured range of the ethanol and salt concentrations in ethanol-salt systems were 0 to 50 mass% and 0 to 10 mass%, respectively. Due to packing effect of ethanol in

water, two ANN was trained in this system; one for 0 to 20 mass% ethanol and the second one for 30 to 50 mass% ethanol. The results show that conductivity-velocity method can be successfully used for determining ethanol concentration in the presence of salt. Moreover, the conductivity-velocity method was evaluated by comparing its measured ethanol concentrations with our in-house thermodynamic model prediction. The hydrate phase boundaries predicted using the C-V method-determined ethanol and salt concentrations was in good agreement with those predicted by the model. This agreement suggests that the C-V method can be used for monitoring hydrate safety margin.

The results for the new KHI-salt system shows good agreement between the ANN outputs and the experimental data, further confirming the applicability of the C-V method for KHI systems.

Results for three parameter method show that the developed three-parameter ANNs can accurately determine concentrations of MEG and NaCl and that the errors could be obviously large for very low concentration of KHI (0 to 1 mass %). However, this method could potentially be used for some specific cases: (1) the ratio of KHI to MEG is known, (2) high concentration (e.g., higher than 3 mass%) KHI is used, (3) the accuracy of the KHI concentration is not essential.

CHAPTER 3. WATER ACTIVITY AND WATER CONTENT TECHNIQUES

3.1. INTRODUCTION

This chapter presents various efficient methods for monitoring and optimising thermodynamic hydrate inhibitors dosage in fluid systems. These methods can be categorised as water activity and water content measurement methods and are based on predicting the hydrate stability zone of fluid by measuring physical properties of aqueous or vapour phases. As the names indicate, the water activity method is based on predicting the hydrate suppression temperature of a fluid from the measured water activity of the downstream aqueous phase, while the water content methods are based on online vapour phase water content measurement and using an in-house thermodynamic model to relate this water content measurement to an equivalent hydrate safety margin. The later method is particularly useful for pipelines where a limited amount of aqueous samples is available.

3.2. WATER ACTIVITY METHOD

Water activity of an aqueous phase at constant temperature depends on the concentration of thermodynamic inhibitors and salt present in the system, therefore monitoring of this parameter can provide an indication of how far the system is from the hydrate phase boundary. These inhibitors and salts are able to bind to water molecules through intermolecular bonds, thus preventing bound water molecules from forming hydrogen bonds with each other and with the remaining free water. More specifically, these compounds reduce the free-water concentration, which is considered as water activity in the system. The water activity method correlates the measured water activity of the downstream aqueous phase to the hydrate suppression temperature of fluid and determines the inhibition characteristics of an aqueous system. It therefore, defines the hydrate stability zone of the fluid containing unknown amount of salt and/or thermodynamic inhibitors.

Water activity of the aqueous phase in this work is measured using a commercial device (LabMaster-a_w water activity meter), which is much easier than measuring hydrate dissociation point and can significantly reduce the time and cost of the experiments. A general correlation has been developed to relate the measured water activities values to the hydrate suppression temperate by generating pseudo-experimental data using a well-proven thermodynamic model (Avlonitis, 1994, Van der Waals,1959). Using pseudo-experimental data instead of real experimental data in developing the correlation makes it possible to generate a large database of different concentrations of salt and alcohols (methanol and MEG) solutions over a wide range of concentrations at shorter time and lower cost. Over 200 aqueous solutions were used in developing this correlation. The correlation has been experimentally established with a high degree of certainty. To validate the correlation and also to examine the reliability of the model in predicting water activity, a large amount of water activity were measured in a wide range of salt and alcohols concentrations. Additionally, different real and synthetic produced water systems have been tested for the same purpose.

3.2.1. Existing Hydrate Phase Equilibrium Correlations/Methods

Despite the development of sophisticated hydrate phase equilibrium calculation models that are both most accurate and most comprehensive, such as the vapour–solid equilibrium ratio (Ki value) method (Carson and Katz, 1942; Wilcox et al., 1941) or the solid solution theory of van der Waals and Platteeuw (1959), hydrate phase equilibria correlations have kept their popularity among engineers in the petroleum industry. The main advantage of these techniques is the availability of input data and the simplicity of the calculation, which can be performed by using charts or hand-held calculators.

Since 1945, the gas gravity method given by Katz (1945) has been an indispensable and simple tool for predicting the gas hydrate stability zone. It only requires the specific gravity of the mixture, i.e., the molecular mass of the gas mixture divided by that of air. The original gas gravity method is only applicable to dry gas systems. However, the development of offshore/arctic oil and gas-condensate fields necessitated a robust and simple method for predicting the hydrate stability zone for these systems. Østergaard et al. (2000) developed a method similar to the gas gravity method, applicable to all reservoir fluids, in the presence of distilled water, from natural gas to black oil, which only requires information on the specific gravity and the concentration of the hydrate forming components in the system. The method can take into account the effect of non-hydrocarbon gases (i.e., CO_2 and N_2) in the petroleum fluid. There also exist simple tools for estimating the hydrate inhibition effect of salts and organic inhibitors. The most famous one is the Hammerschmidt (1934) equation, but also equations by Nielsen and Bucklin (1983) and Yousif and Young (1993) are available. These equations calculate the suppression of the hydrate dissociation temperature, ΔT, compared to that of distilled water (i.e., the hydrate phase boundary in the presence of distilled water should be determined separately). Inherently, they have the following simplifying assumptions, reducing their accuracy; ΔT is independent of the system pressure, ΔT is independent of gas/oil composition and hydrate structure. ΔT is independent of the inhibitor. Østergaard et al. (2005) developed a correlation for predicting the hydrate stability zone of reservoir and drilling fluid in presence of thermodynamic inhibitors (i.e., electrolytes and organic inhibitors). This correlation

requires inhibitor concentration, pressure of the system and if known the dissociation pressure of hydrocarbon fluid in the presence of distilled water at 273.12K.

Mohammadi and Richon (2006) studied the possibility of estimating hydrate stability zone based on reflective index data of aqueous solution containing salt or organic inhibitor using an artificial neural network method. The correlation considers the changes in index of refraction with respect to refractive index of pure water for a given aqueous solution. In a very similar work, Mohammadi et al. (2006). have looked at the possibility of estimating hydrate stability zone from electrical conductivity data of salt aqueous solutions. This correlation cannot predict the effect of presence of thermodynamic inhibitor. Both of these correlations have been validated using only limited literature data.

Recently, our research group (The centre for Gas Hydrate Research at Heriot-Watt University) has developed a correlation based on freezing point depression which determines the hydrate safety zone (HSZ) by measuring the freezing point of the downstream water samples (Tohidi et al, 2009). A prototype has also been developed for this method which has its own limitation, particularly for high inhibitor concentration. To measure freezing point of an aqueous sample the method need to freeze the sample. For high concentrations e.g., 50 mass% of MEG the system needs to be cooled to around -50^{o}C to freeze the sample. The minimum temperature which the current prototype can reach is about -40 $^{\circ}$C. The second limitation is that, in such high concentration limited amount of ice will form, hence accuracy is hindered. This method has also a limited potential for on-line application

So far, to our knowledge the mentioned methods and correlations are the main approaches for predicting hydrate stability zone using correlations. However, it is possible that different companies have developed their own internal methods for specific applications which are not available in the open literature. The above methods have their own limitations as discussed; but their main common drawback is, none of them have offered an integrated system for monitoring purpose.

In this part of work the aim is to develop an integrated system to directly correlate the measured water activity of an aqueous solution to its hydrate suppression temperature and validate this developed method.

3.2.2. Water Activity Correlation Development

A general correlation has been developed to relate the measured water activities of salt and alcohol aqueous solutions to the hydrate suppression temperature by using a phase equilibrium model based on the uniformity of component fugacities in all phases. A brief description of the thermodynamic model will be presented in this section and detailed information can be found elsewhere (Avlonatis et al., 1994).

Water Activity: Water activity is derived from fundamental principles of thermodynamics and physical chemistry

In the equilibrium state:

$$\mu = \mu_0 + RT \ln\left(\frac{f}{f_0}\right) \qquad \text{Equation 3.1}$$

where: μ (J mol^{-1}) is the chemical potential of the system i.e. thermodynamic activity or energy per mole of substance at T and P; μ_o is the chemical potential of the pure material in the reference state (T_0, P_0); R is the gas constant (8.314 J mol^{-1} K^{-1}); f is the fugacity or the escaping tendency of a substance; and f_0 is escaping tendency at reference state (van den Berg and Bruin, 1981). The activity of a species is defined as $a = f/f_0$.

Water activity from its thermodynamic concept is defined as the ratio of fugacities:

$$a_w = \left(\frac{f}{f_0}\right) \qquad \text{Equation 3.2}$$

where water activity (a_w) is the activity of water or the escaping tendency of water in the system (f) divided by the escaping tendency of pure water with no radius of curvature (f_0). The water activity of a system is closely equivalent to the vapour pressure (RVP) of water over that system, although it is not identical to it in theory.

$$a_w = \frac{f}{f_0} \approx \frac{P}{P_0} \qquad \text{Equation 3.3}$$

where P is vapour pressure of water in a solution and P_0 is the vapour pressure of pure water at the same temperature. Van den Berg (1986) reported from other authors that the numerical difference between water activity and RVP at ambient conditions (below

50 °C, at pressure of 1 bar) is less than 0.2%. This difference may be neglected for practical purposes, and justifies what is often stated: that water activity equals vapour pressure. Masoudi et al. (2005) correlated the water fugacity and the water vapour/partial pressure for various systems. They concluded that the values of water fugacity and vapour pressure in the system are very close even at high pressure, temperature and salt and/or organic inhibitor concentrations. As an example, Figure 3.1 presents the water fugacity and the water vapour pressure for various concentrations of sodium chloride in aqueous solutions.

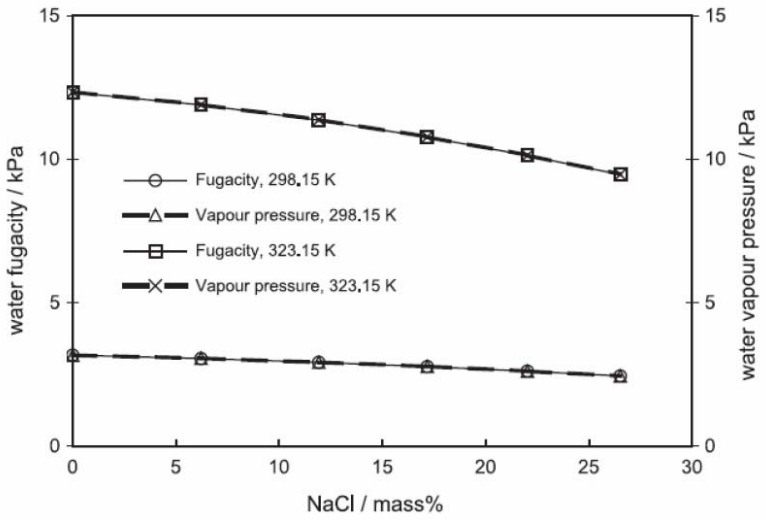

Figure 3.1 Water fugacity and vapour pressure in sodium chloride aqueous solution (Masoudi et al., 2005)

Thermodynamic Model: In summary, the statistical thermodynamics model uses the Valderrama modification of the Patel and Teja equation of state (Valderrama, 1990) and the non-density-dependent (NDD) (Avlonatis et al., 1994) mixing rules for fugacity calculations in all fluid phases. The hydrate phase is modelled using the solid solution theory of van der Waals and Platteeuw (van der Waals and Platteeuw, 1959), as developed by Parrish and Prausnitz (Parrish and Prausnitz, 1972). The equation recommended by Holder et al. (Holder et al., 1982) is used to calculate the heat capacity difference between the empty hydrate lattice and pure liquid water. The Kihara model for spherical molecules is applied to calculate the potential function for compounds forming hydrate phases (Kihara, 1953). The VPT – EoS (Valderrama, 1990) is given by:

$$P = \frac{RT}{v-b} - \frac{a}{v(v+b)+c(v-b)} \qquad \text{Equation 3.4}$$

With:

$$a = \overline{a}.\alpha(T_r) \qquad \text{Equation 3.5}$$

$$\overline{a} = \frac{\Omega_a R^2 T_c^2}{P_c} \qquad \text{Equation 3.6}$$

$$b = \frac{\Omega_b R T_c}{P_c} \qquad \text{Equation 3.7}$$

$$c = \frac{\Omega_{c^*} R T_c}{P_c} \qquad \text{Equation 3.8}$$

$$\alpha(T_r) = \left[1 + F\left(1 - T_r^{\Psi}\right)\right]^2 \qquad \text{Equation 3.9}$$

where P, R and T refer to pressure, gas constant and temperature, respectively. v, a, $\overline{a}$, b, c and $\alpha(Tr)$ stand for molar volume, attractive parameter, parameter of the equation of state, repulsive parameter, parameter of the equation of state and temperature dependent function, respectively and $\psi = 0.5$. The subscripts c and r denote critical and reduced properties, respectively. The coefficients Ω_a, Ω_b, Ω_c^*, and F are given by:

$$\Omega_a = 0.66121 - 0.76105 Z_c \qquad \text{Equation 3.10}$$

$$\Omega_b = 0.02207 + 0.20868 Z_c \qquad \text{Equation 3.11}$$

$$\Omega_{c*} = 0.57765 - 1.87080 Z_c \qquad \text{Equation 3.12}$$

$$F = 0.46283 + 3.58230(\omega Z_c) + 8.19417(\omega Z_c)^2 \qquad \text{Equation 3.13}$$

where Zc is the critical compressibility factor, and ω is the centric factor.

Tohidi (1995) relaxed the alpha function for water and methanol, $\alpha_w(T_r)$, using experimental vapour pressure data, in order to improve the predicted water fugacity:

$$\alpha_w(T_r) = 2.4968 - 3.0661 T_r + 2.7048 T_r^2 - 1.2219 T_r^3 \qquad \text{Equation 3.14}$$

The NDD mixing rules developed by Avlonitis et al. (1994) are applied to describe mixing in the a-parameter:

$$a = a^C + a^A \qquad \text{Equation 3.15}$$

where a^C is given by the classical quadratic mixing rules as follows:

$$a^C = \sum_i \sum_j x_i x_j a_{ij}$$ Equation 3.16

where x stands for mole fraction and subscripts i and j denote components i and j, respectively. b, c and a_{ij} parameters are expressed by:

$$b = \sum_i x_i b_i$$ Equation 3.17

$$c = \sum_i x_i c_i$$ Equation 3.18

$$a_{ij} = (1 - k_{ij})\sqrt{a_i a_j}$$ Equation 3.19

where k is the BIP.

The term a^A corrects for asymmetric interaction, which cannot be efficiently accounted for by classical mixing rules:

$$a^A = \sum_p x_p^2 \sum_i x_i a_{pi} l_{pi}$$ Equation 3.20

$$a_{pi} = \sqrt{a_p a_i}$$ Equation 3.21

$$l_{pi} = l_{pi}^1 - l_{pi}^2 (T - T_0)$$ Equation 3.22

where p is the index of polar components and l represents the binary interaction parameter for the asymmetric term. Superscripts 1 and 2 refer to non-temperature dependent and temperature dependent terms in NDD mixing rules (Avlonitis et al., 1994), respectively and T0 stands for the reference temperature, 273.15 K.

Using the VPT-EoS (Valderrama, 1990) and the NDD mixing rules (Avlonitis et al., 1994), the fugacity of each component in all fluid phases is calculated from:

$$\phi_i = \frac{1}{RT} \int_{\bar{V}}^{\infty} \left[\left(\frac{\partial P}{\partial n_i} \right)_{T,\bar{V},n_{j \neq i}} - RT/\bar{V} \right] d\bar{V} \text{ ln- ln Z}$$ Equation 3.23

for i= 1, 2, ..., nc

$$f_i = x_i \phi_i P$$ Equation 3.24

Where ϕ, n, Z and f refer to fugacity coefficient, number of moles, compressibility factor and fugacity, respectively. $\bar{V}$ and nc are the total volume and number of components, respectively.

As it was mentioned before, the above explained thermodynamic model was used to relate water activities of aqueous solution of salt and alcohol to the hydrate suppression temperate. All of these aqueous systems were assumed to be in contact with a typical natural gas (Table A.72) and hydrate suppression temperatures for these systems were predicted at 50, 100, 200 and 300 bara to evaluate the effect of pressure on the correlation. Figure 3.2 shows the predicted hydrate suppression temperatures as a function of the Neperian logarithm of the water activity of the aqueous phase containing different concentrations of salts and thermodynamic hydrate inhibitors.

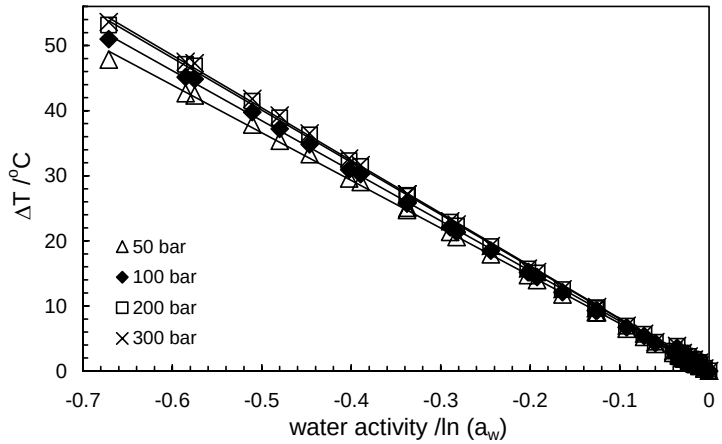

Figure 3.2 Predicted hydrate suppression temperature vs logarithm of the water activity

As can be seen from this figure, all the points closely fit to a line suggesting a linear relation between the hydrate suppression temperature and the Neperian logarithm of water activity of the aqueous phase. To take into account the effect of pressure on the correlation, an equation has also been developed as shown in Figure 3.3.

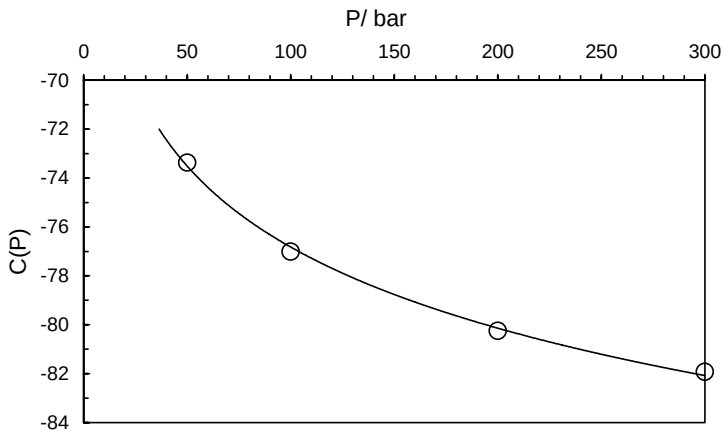

Figure 3.3 Pressure coefficient of the water activity correlation

The water activity correlation is given by the following expressions:

$$\Delta T = T_0 - T = C(P).\ln(a_w) \qquad \text{Equation 3.25}$$

$$C(P) = -4.784\ln(P) - 54.790 \qquad \text{Equation 3.26}$$

where T is the hydrate dissociation temperature in Celsius or Kelvin, T_0 is the hydrate dissociation temperature of the same fluid in the presence of distilled water (without salt and/or inhibitor) in Celsius or Kelvin, a_w is the water activity of the aqueous solution and $C(P)$ is a constant function of the system pressure, P. The developed correlation is simple and enables fast estimation of the hydrate-free zone of various reservoir fluids, in the presence of salts and/or organic inhibitors. The only prerequisite to use the correlation is the hydrate dissociation temperature of the same fluid in the presence of distilled water (T_0), which can be calculated using predictive thermodynamic software capable of predicting hydrate phase boundaries of various reservoir fluids.

3.2.3. Water Activity Measurement Techniques

Techniques developed for measuring water activity of aqueous phase and water content/water dew point of gas phases are very similar in principal to each other. Therefore, this section covers description of commonly used methods for both water activity and water content measurement methods because both of these methods have

been used in this chapter for developing methods for monitoring and optimising thermodynamic hydrate inhibitors dosage in fluid systems. This part is mainly based on those reported by Chapoy (2004), Rossum (1986) and Mohammadi (2004).

The methods can be divided into the following categories:

- Direct methods
- Indirect methods

3.2.3.1. Direct Methods

The direct methods (absolute methods) measure the dew point as temperature (or the water content as mass of water). These methods utilise a direct relationship between the measured quantity and the water activity/water content. In the ideal case, no calibration is necessary. Therefore, these techniques also are called absolute techniques. The following measuring methods belong to the direct methods:

- The dew point mirror (Chilled mirror)
- Karl-Fischer titration
- The gravimetric hygrometer.

The measuring principles are given in the Table 3.1.

Table 3.1 Measurement principles of direct methods

Method	**Measuring principal**
Dew point mirror (Chilled mirror)	Temperature at which water or ice appears on a cooled surface
Karl-Fischer titration	Titration of absorbed water vapour with iodine
Gravimetric hygrometer	Increase in weight by absorption of water

Dew Point Mirror: The observation of dew point via a chilled surface, using either visual observation or instrumental detection of dew formation is a popular technique. For determination of the dew point with a dew point mirror, the gas flows over a chilled metal mirror- a small high polished plate of gold, rhodium, platinum or nickel- in a pressure tight chamber. Historically, the cooling of the surface is accomplished with acetone and dry ice, liquid gases, mechanical refrigeration and, more recently, by thermoelectric heat pumps. During cool down of the mirror, condensate forms on the mirror at the dew point temperature. Condensate is detected by suitable means. The mirror temperature can be measured with a resistance thermometer directly attached to

the backside of the mirror. The mirror method is subject to contamination from heavy hydrocarbons and other components present in the gas. Depending on the kind of set-up, this method can measure dew point temperatures from 200 K to 370 K and accuracy of better than 0.3 K is possible.

Karl-Fischer Titration: This method involves a chemical reaction between water and "Karl Fischer Reagent", which is typically a mixture of sulphur dioxide, iodine, pyridine, and methanol. For many years, this method was limited to laboratory use because of the equipment and chemicals required to carry out the determination. Recently, the newer Karl Fischer methods are faster and more convenient than conventional methods for measuring water in hydrocarbons. The Karl Fischer titration can be divided into two basic analytic groups with respect to dosing or production of iodine, respectively:

- The volumetric titration,
- The coulometric titration.

During volumetric Karl Fischer titration, the water-containing sample is solved in a suitable alcoholic solvent and is titrated with a Karl Fischer solution. The volumetric titration is applied for estimation of larger amounts of water typically in the range of 1 to 100 mg. Compared to that, the coulometric Karl Fischer is a micro method. Iodine is not dosed in form of a solution but is directly used in an iodine containing solution via anodic oxidation. Due to its high analytic accuracy, it is suited for estimation of extremely low amounts of water (10 μg to 50 mg). Therefore, for measuring the water content of gases the coulometric Karl Fischer titration is the preferred choice, compared to the volumetric Karl Fischer titration.

Gravimetric Hygrometer: Gravimetric hygrometer gives absolute water content; since the weight of water absorbed and the precise measurement of gas volume associated with the water determine the absolute water content of incoming gas. Gravimetric methods are of two types: freeze out and adsorption. The freeze out technique can be used for gases containing light components (e.g. methane and ethane), because the condensation temperatures for these hydrocarbons are lower than that of water vapour. For the analysis of systems containing intermediate or heavy hydrocarbons (e.g. propane), the freeze out technique is very difficult because the intermediate or heavy hydrocarbons tend to condense along with water; as a consequence the separation of

condensed phases is required before the amount of water can be determined. The small amounts of water and the loss that would occur on separation of the condensed hydrocarbons from the water rendered such a method of insufficient accuracy.

In the adsorption method, a test gas is pumped from a humidity generator through a drying train and a precision gas volume measuring system contained within a temperature-controlled bath. The precise measurements of the weight of water absorbed from the test gas and the associated volume of gas as measured at closely controlled temperature and pressure, accurately defines the absolute water content of the test gas in units of weight per unit volume. This system has been chosen as the primary standard because the required measurements of weight, temperature, pressure and volume can be made with extreme precision. The gravimetric hygrometer is a rather unwieldy instrument to use, and in the low water content ranges may require up to 30 hours per calibration point. For this reason, the gravimetric hygrometer is not used for normal measurement purposes and would not be useful for industrial measurement or control.

3.2.3.2. Indirect Methods

With the indirect methods as physical property depending on the water content/water activity is measured from which, the dew point or the water content or water activity has to be calculated. The indirect methods, being relative methods, always require calibration. When calibrating the relation between the properties measured (e.g. conductivity, frequency etc.) and the water content / water dew point / water activity is fixed empirically by comparing with a reference method. In other words, these methods can be made useful if the relationship between the water content / water dew point / water activity and the measured quantity can be determined empirically by comparison with a reference method. Such a reference method must be an absolute standard or a derivative of such a standard.

Different categories of indirect methods and measuring principles of the most applicable ones are given in Table 3.2.

Table 3.2 Measurement principles of indirect methods

Method		**Measuring principle**
Spectroscopic	Microwave	The water content is measured by detecting the energy absorption due to the presence of water vapour.
	Infrared	
	Laser	
Gas Chromatography	Detection of water	Size of the peak is proportional to the amount of the analysed sample.
	Conversion to Acetylene	
	Conversion to Hydrogen	
Hydroscopic	Electrolytic	The current due to electrolysis of the absorbed water at known constant gas flow rate is directly proportional to water vapour concentration
	Capacitance	The dielectric constant of aluminium oxide is a function of water vapour concentration
	Change in mass (Quartz Crystal)	Hygroscopic coating adsorbs water; crystal resonant frequency is a function of mass and thus related to water vapour concentration
	Conductivity	Salt / Glycerol solution absorbs water vapour; conductivity is a function of water vapour concentration

Spectroscopic: The spectroscopic methods belong to optical instruments that measure the water content of gases by detecting the energy absorbed to vaporize water. The basic unit consists of an energy source, a detector, an optical system for isolating specific wavelengths, and a measurement system for determining the attenuation of radiant energy caused by the water vapour in the optical path.

These techniques for water content detection generally use radiations ranging from microwave (MW) frequencies to near infrared (NIR). In general, the higher the frequency, the less the depth to which waves penetrates. Therefore, MW tends to be used more for bulk measurements, while NIR would be used for small samples. Because of the large differences in wavelengths, even though all the instruments are measuring the same thing (water content), the mechanics of wave generation and detection differ. MW and NIR spectroscopic water content detectors cover a wide range of water content detectability, typically from 0.01% to over 99 % mol. For many applications, the technologies overlap, and the choice of detector will depend on the size of the sample, process flow, degree of precision, and cost. In contrast with the MW and NIR techniques that are used, Tunable Diode Laser Absorption Spectroscopy (TDLAS) is an extremely sensitive technique used for measuring very low levels—as small as typically 100 parts per trillion (ppt) of water content, or other species, in

gases. In a TDLAS water content analyzer, an infrared laser beam traverses the gas of interest and changes in the intensity due to water absorption are measured. Path lengths are increased by a mirrored cell to bounce the laser light back and forth, thus improving the sensitivity. The gas of interest can be flowing through the chamber, giving real-time monitoring capability. However, these analyzers are expensive and require continual maintenance to care for the optical system. Absorption by gases can also cause severe interference to this method.

Chromatographic: GC is extensively used in various forms for water content determination. Methods vary in complexity from simple injection and separation by GC where the sensitivity is low, to reaction with a reactant in GC where the water is converted into another compound, which exhibits a greater chromatographic response. The chromatographic technique allows analyzing water content on the thermal conductivity detector (TCD), which is a quasi-universal detector. The most difficult part associated with this technique is the calibration of the response of the detector as a function of the number of moles in the sample.

Hygroscopic methods: The hygroscopic methods make use of sensors that respond to the water vapour pressure in the gas. The surface properties of the sensors are important. They will be sensitive to temperature variations, contaminants in the gas, co-adsorption of other gaseous constituents, and past history of exposure.

Electrolytic: The electrolytic method is sometimes considered as being a direct method. This is only true if all of the water vapour flowing through the sensor is completely absorbed. For constant gas flow the amount of charge (current × time) is, by Faraday's law, a direct measure of the water content. In practice, however, instruments based on this method require to be calibrated because of the non-zero background current and because of the difficulty of ensuring that all of the water vapour is absorbed from the gas.

These sensors use a winding coated with a thin film of P_2O_5. As the desiccant absorbs incoming water vapour, an electrical potential is applied to the windings that electrolyses the water to hydrogen and oxygen. The current consumed by the electrolysis determines the mass of water vapour entering the sensor. The flow rate,

and pressure of the incoming sample must be controlled precisely to maintain a standard sample mass flow rate into the sensor. Because the mechanism within the cell is complex, several additional phenomena may affect its operation.

Capacitance: The sensor is fabricated from a thin strip of pure aluminium. The aluminium strip is anodized in sulphuric acid, resulting in a layer of porous aluminium oxide on its surface. A layer of gold or noble metal is evaporated over the aluminium oxide. This sandwich of compounds is essentially a capacitor, with the aluminium oxide layer the dielectric. Water vapour is rapidly transported through the noble metal layer and adsorbs onto the oxide as a function of partial pressure of water surrounding the sensor. The water molecules adsorbed on the oxide will cause a change in the dielectric constant of the sensor. A measure of the sensor impedance is a measure of the sample water partial pressure.

Depending on the water present in the stream, the impedance of the sensor can vary typically from 2 MΩ to 50 kΩ. Thus, the sensor receives a signal from the hygrometer electronics, and returns a signal to the electronics that is proportional to the water content in the measured stream.

These sensors can detect water content levels from as low as 1 part per billion (ppb) to as high as approximately 200,000 parts per million (ppm). It is not, however, designed to measure water vapour at or near saturation conditions. Slugs of liquid condensate, glycol, methanol or water do not destroy it. It is designed for in-process mounting whenever possible, so as to eliminate the additional expense and complexity of sample conditioning. The biggest limitation of the Aluminium Oxide sensor is periodic calibrations against standards are required to determine if its response has changed due to contact with corrosive substances such as strong acids or bases.

Change in mass (Quartz Crystal): This instrument compares the changes in frequency of two hydroscopically coated quartz oscillators. As the mass of the crystal changes due to adsorption of water vapour, its frequency changes correspondingly. The detector crystal is first exposed to the wet sample gas for a fixed period of time and then dried by a known dry reference gas. The difference in frequency between the wet and dry readings is proportional to the amount of water in the sample. In

following this wet- dry cycle, the water partial pressure difference between the sample and detector is kept as great as possible. Thus, the quartz crystal type water content analyzer can inherently respond very rapidly to small changes in water content.

The quartz crystal method is one of the best methods for clean and single component gas; however it can suffer from co-adsorption of other gas constituents by the hygroscopic coating, and degradation of this coating.

This type of instrument is relatively expensive in commercial versions. In addition its flow sensitivity and calibration dependence, make it a difficult instrument to apply in general industrial applications.

Conductivity: The principle of measurement is based on the variation of the electrical conductivity of an unsaturated salt solution at varying gas water content. The saturation vapour pressure over an unsaturated salt solution is lower than over pure water. In this manner, the salt solution can absorb as much water from the surrounding medium until the vapour pressure of salt solution and that of the measuring medium are in equilibrium. The absorption of water in the salt solution causes it to become increasingly more conductive. The process is reversible, that is, with descending gas water content out of the salt solution and this decreases the conductivity. The vapour pressure equilibrium is more quickly achieved; the smaller the supply of salt solution there is and the faster the measuring mediums is transported to the salt solution. At the same time, the temperature of the sensor influences the response speed. In order to make the response speed of the sensor as fast as possible, one would have to construct very small sensors, so that the mass of the salt solution remains small. Because natural gases contain impurities, just a very small impurity would suffice with very little measuring electrolyte to destroy the sensor. The long-term stability of the sensor would not be very large. Conversely, the use of a very large amount of electrolyte in the sensor would make the long-term stability very good, but the response speed would be unreasonably small. A solution to these opposing demands has been found in the construction of sensors today.

A typical sensor consists of two high grade steel plates, which are electrically isolated from each other by a ceramic layer. Small holes are drilled in the layer package, whose inside walls are coated with a very thin film of a salt / glycerol electrolyte.

In this manner a more or less conductive connection between the two steel plates occurs. Several parallel wired single electrodes are created in this way. Because of the parallel wiring of the electrodes, the danger of becoming soiled is much smaller than with just one electrode, while the response speed is the same as for one tiny single electrode.

In normally polluted natural gas the life time of the sensor is typically one year. The measuring accuracy after this time period is still sufficient, but the residue causes the sensors to be slower. For this reason, the sensors are replaced every three months. Afterwards, the sensors can be cleansed and newly coated with electrolyte. It is important in this context that the sensor calibrates itself and this by replacement no adjustment in the analyzing electronics are necessary. The most severe problem in this method is that the salt solution can be washed off in the event of exposure to liquid water.

All of the above mentioned methods can be used for water content measurement; however, for measuring water activity, usually the dew point, capacitance and resistive electrolyte methods are common.

3.2.4. Experimental Set-up Used in This Work for Water Activity Measurement

A LabMaster-a_w water activity meter was used to measure the water activity of aqueous solution at 25 °C. The measuring system of the LabMaster-a_w is a resistive electrolytic humidity sensor. This device analyse static sample (sample volume: 4 cc) at atmospheric pressure. The aqueous phase is equilibrated within the head space of a sealed chamber housing the sensor. Figure 3.4 shows a picture of the LabMaster-a_w.

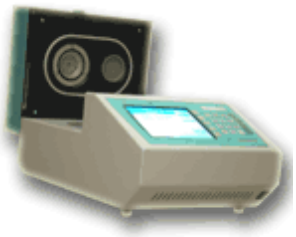

Figure 3.4 A picture of the LabMaster-aw used in this work for measuring water activity of aqueous phase

The resistive-electrolytic measurement method uses the physical principle of the conductivity measurement in a liquid chemical substance. This liquid is very stable and hygroscopic. The water molecules from the surrounding air penetrate in the chemical structure and consequently the conductivity changes. Small air humidity changes induce big conductivity variations. Thus the instruments can precisely detect the environment air humidity. These sensors can detect relative humidity of the air-water mixture from 3% to 100%. The temperature of the cell could be changed from a range of 0 °C to 50 °C. The system allows a high measurement accuracy and repeatability. Observation times for temperature and a_w (time needed for reading becomes stable) were about 5 minutes.

Additional protections are needed to protect the system from chemical assault. In our case, we use a REDOX filter which allows the measurement of all type of solutions, which protects the sensor from most of the alcohol like methanol, ethanol, isopropanol, etc.

Periodic calibrations against standards are required to determine if its response has changed due to contact with corrosive substances such as strong acids or bases. The calibration of the device has been checked by using the standards from the supplier. Table 3.3 presents an example of the calibration results.

Table 3.3 Calibration of LabMaster-a_w device against standards at 25 °C

Standard salt solution	Measured a_w ± 0.003	Standard's a_w ± 0.003
SALT-t / 11	0.113	0.113
SALT-t / 33	0.325	0.328
SALT-t / 53	0.528	0.529
SALT-t / 75	0.754	0.753
SALT-t / 90	0.900	0.901
SALT-t / 97	0.972	0.720
Deionised water	1.000	1.000

After calibration, water activity of different solutions containing salts and alcohols have been measured using the LabMaster-a_w device to validate the result with literature data (ASTM standard). The results have been also compared with the predicted water activity values using in-house thermodynamic model, HWHYD 2.1. All the tests have been performed at 25 °C. Table 3.4 and Figure 3.5 show the results of this comparison.

Table 3.4 Validation of calibrated device with sodium chloride solutions @ 25 °C

Solusion	Measured a_w	ASTM a_w	Predicted a_w
NaCl 10 mass%	0.933	0.935	0.938
NaCl 15 mass%	0.888	0.892	0.899
NaCl 20 mass%	0.837	0.839	0.851
NaCl 25 mass%	0.773	-	0.792

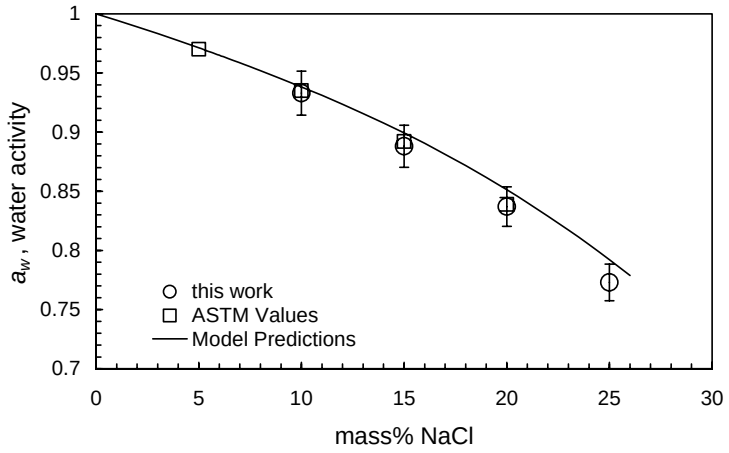

Figure 3.5 Water activity of sodium chloride solutions at 25 °C (Error bars: ± 2%)

The results of water activity measurements have also been validated with aqueous mono ethylene glycol (MEG) solutions without or with sodium chloride. Figure 3.6 and Table 3.5 presents this comparison.

Table 3.5 Validation of calibrated device with ethylene glycol solutions in the presence and absence of sodium chloride at 25 °C

Solution	Measured a_w	Predicted a_w
10 mass% MEG	0.963	0.968
20 mass% MEG	0.927	0.932
30 mass% MEG	0.878	0.889
40 mass% MEG	0.822	0.838
50 mass% MEG	0.756	0.775
3 mass% NaCl, 10 mass% MEG	0.946	0.951
3 mass% NaCl, 20 mass% MEG	0.908	0.910
3 mass% NaCl, 30 mass% MEG	0.859	0.861
3 mass% NaCl, 40 mass% MEG	0.800	0.801
3 mass% NaCl, 50 mass% MEG	0.735	0.729

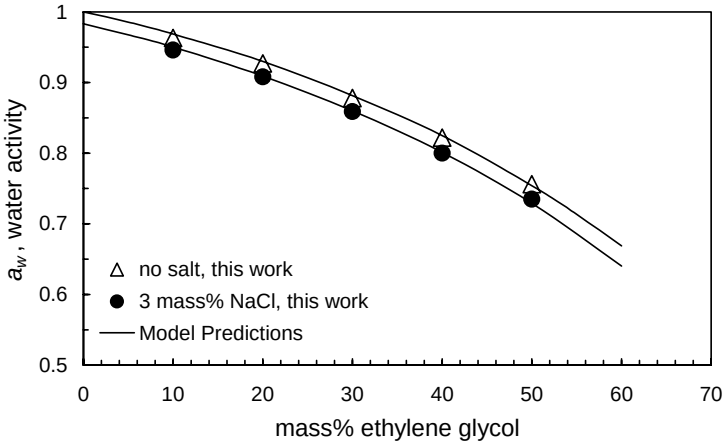

Figure 3.6 Water activity of aqueous ethylene glycol without and with sodium chloride solutions at 25 °C

It can be clearly seen from Table 3.4, Figure 3.5, Table 3.5 and Figure 3.6 that the measured water activity results are in good agreement with the model predictions and the ASTM values suggesting that the device can be accurately used for measuring water activity of aqueous containing different concentrations of salt and ethylene glycol.

3.2.5. Experimental Materials

Materials used in this part of the work were:

- Deionised water
- Thermodynamic inhibitors: methanol and ethylene glycol (MEG) from Sigma-Aldrich with purity of >99.9%
- Salts: NaCl, KCl, Na_2SO_4, $MgCl_2$, $CaCl_2$, $BaCl_2$ and $SrCl_2$ all from Sigma-Aldrich with purity of >99.9%.

3.2.6. Results and Discussion: Water Activity Measurements

A large database of water activity values for different systems, i.e. salts, methanol, ethylene glycol, produced water and combination of these over a wide range of concentration was generated to evaluate the developed correlation. This database was further used to improve the in-house thermodynamic model. This data base has also

been used to examine the capability of the LabMaster-a_w in measuring the water activity in oil industry since this device is mainly used in the food and pharmaceutical industry. The following sub-sections will present the results for each group of systems.

Different Salt Systems:

Different salt systems including NaCl, KCl and $CaCl_2$ as well as combination of these salts were tested over a wide range of concentration. Additionally, different synthetic produced water systems and also a real produced water system were tested in this part.

Table 3.6 and Figure 3.7 present the data for NaCl solution. As it can be seen, water activity of the solution decreases as concentration of salt increases in the system. The measured water activity values are in good agreement with ASTM data and predicted data (using in-house thermodynamic model) before salting out point. For NaCl solution, the salting out point is at about 27 mass% of NaCl at 25 °C.

Table 3.6 Water activity of NaCl aqueous solutions at 25 °C

Solutions	Measured a_w	ASTM a_w	Predicted a_w
5 mass% NaCl	0.965	-	0.971
10 mass% NaCl	0.933	0.935	0.938
15 mass% NaCl	0.888	0.892	0.899
20 mass% NaCl	0.837	0.839	0.851
25 mass% NaCl	0.773	-	0.792
30 mass% NaCl	0.749	-	Salting out

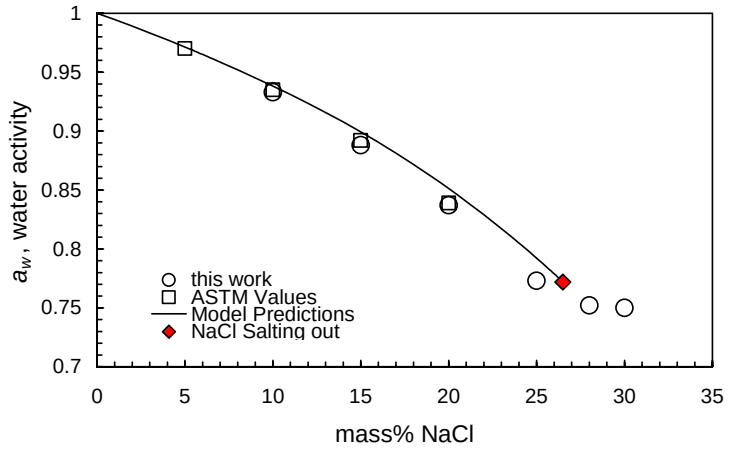

Figure 3.7 Water activity of NaCl aqueous solutions at 25 °C.

Figure 3.8 & Table 3.7 and Figure 3.9 & Table 3.8 show the measured water activity data for KCL and $CaCl_2$ respectively. Again, the measured data are very close to the predicted values. The salting out point of the KCl is about 26 mass% at 25 °C while for the CaCl2, salting out did not happen within our measured range (up to 35 mass%).

Table 3.7 Water activity of KCl aqueous solutions at 25 °C

Solutions	Measured a_w	Predicted a_w
3 mass% KCl	0.986	0.987
5 mass% KCl	0.974	0.978
10 mass% KCl	0.954	0.954
15 mass% KCl	0.925	0.929
20 mass% KCl	0.884	0.898
25 mass% KCl	0.849	-
28 mass% KCl	0.841	Salting out

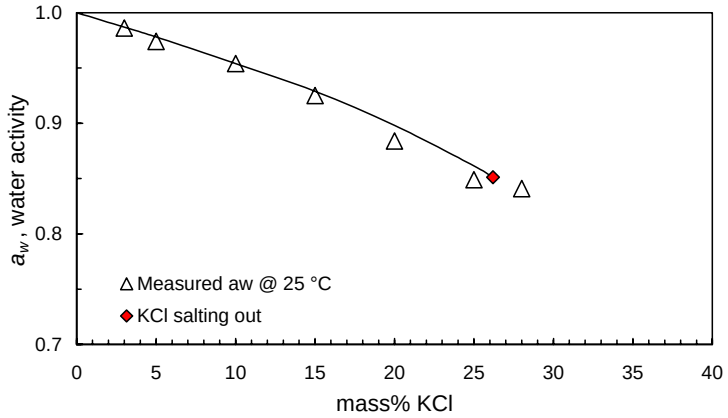

Figure 3.8 Water activity of KCl aqueous solutions at 25 °C (Solid lines: model predictions)

Table 3.8 Water activity of $CaCl_2$ aqueous solutions at 25 °C

Solutions	Measured a_w	Predicted a_w
3 mass% CaCl2	0.983	0.984
5 mass% CaCl2	0.972	0.972
10 mass% CaCl2	0.947	0.941
15 mass% CaCl2	0.901	0.899
20 mass% CaCl2	0.837	0.841
25 mass% CaCl2	0.772	0.762
28 mass% CaCl2	0.717	0.704
30 mass% CaCl2	0.674	0.661
35 mass% CaCl2	0.562	0.567

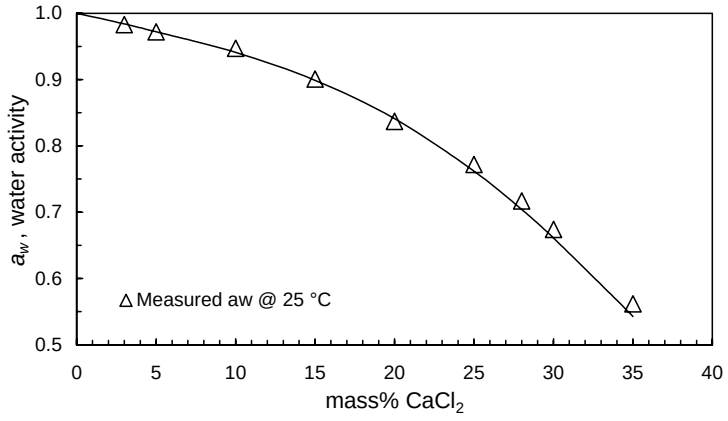

Figure 3.9 Water activity of $CaCl_2$ aqueous solutions at 25 °C (Solid lines: model

predictions)

Results for mixtures of NaCl, KCl and $CaCl_2$ salts have been summarised in Table 3.9.

Table 3.9 Water activity of NaCl+KCl+$CaCl_2$ aqueous solutions at 25 °C

Solutions	Measured a_w	Predicted a_w
3 mass% NaCl+3 mass% KCl	0.963	0.969
5 mass% NaCl+3 mass% KCl	0.953	0.956
3 mass% NaCl+5 mass% KCl	0.941	0.959
5 mass% NaCl+5 mass% KCl	0.956	0.946
3 mass% NaCl+3 mass% CaCl2	0.962	0.965
3 mass% KCl+3 mass% CaCl2	0.964	0.970
3 mass% KCl+3 mass% CaCl2+3 mass% NaCl	0.95	0.951

Four synthetic produced water and one real produced water from BP (salt concentration is equivalent to 5 mass% NaCl) have been also tested in this work. Compositions of the produced waters and the results of the water-activity measurements are given in Table 3.10 and Table 3.11.

Table 3.10 Composition of tested produced water systems

Salt	Produced water			
	Maya	Petronas	Forties	Scale
NaCl	9.000	3.316	6.993	2.231
KCl	0.000	4.468	0.066	0.037
CaCl2	0.800	0.174	0.735	0.133
MgCl2	0.200	0.014	0.186	0.041
Na2SO4	0.000	0.609	0.000	0.000
SrCl2	0.000	0.000	0.099	0.016
BaCl2	0.000	0.000	0.036	0.011
Total Salt	10.000	8.852	8.115	2.469

Table 3.11 Water activity of real and synthetic produced water systems at 25 °C

Produced water systems	Measured a_w	Predicted a_w
BP	0.965	0.971
Maya	0.934	0.938
Petronas	0.959	0.957
Forties	0.951	0.951
Scale	0.982	0.986

Similar to the solution containing only one type of salt, the measured water activity values for mixtures of different salt and real and synthetic produced water systems showed a good agreement with the predicted values.

Mono Ethylene Glycol (MEG) Systems:

Various concentrations of MEG solution in the absence and presence of different salts and produced water were investigated in this part.

Table 3.12 and Figure 3.10 present the results of water activity measurements for aqueous MEG solutions. As with salt systems, the water activity of the solution decreases as MEG concentration increases in the system. The experimental data are very close to the predicted water activity values.

Table 3.12 Water activity of MEG aqueous solutions at 25 °C

Solutions	Measured a_w	Predicted a_w
1.5 mass% MEG	1	0.995
2.5 mass% MEG	0.992	0.992
3 mass% MEG	0.995	0.991
5 mass% MEG	0.982	0.984
10 mass% MEG	0.960	0.967
25 mass% MEG	0.896	0.906
40 mass% MEG	0.821	0.824
50 mass% MEG	0.754	0.754
75 mass% MEG	0.498	0.500
80 mass% MEG	0.428	0.430
90 mass% MEG	0.246	0.256
95 mass% MEG	0.141	0.143
97.5 mass% MEG	0.083	0.076

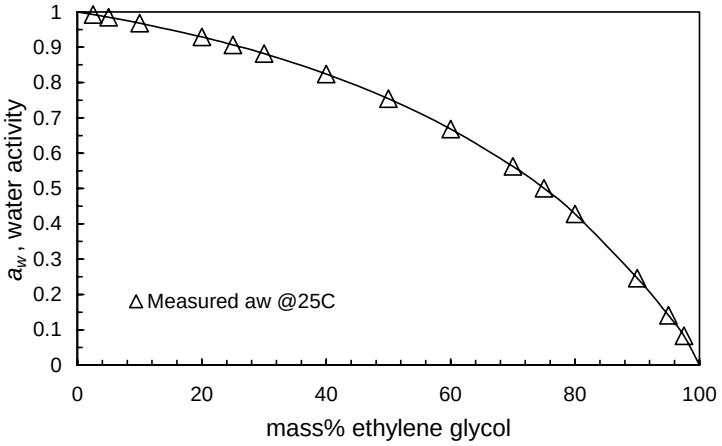

Figure 3.10 Water activity of MEG aqueous solutions at 25 °C (Solid lines: model predictions)

Table 3.13 and Figure 3.11 show the measured and predicted water activities for 5 mass% NaCl solutions with varying MEG concentration.

Table 3.13 Water activity of MEG solutions in presence of 5 mass% NaCl at 25 °C

Solutions	Measured a_w	Predicted a_w
5 mass% NaCl+1.5 mass% MEG	0.962	0.966
5 mass% NaCl+2.5 mass% MEG	0.960	0.963
5 mass% NaCl+5 mass% MEG	0.953	0.954
5 mass% NaCl+10 mass% MEG	0.936	0.937
5 mass% NaCl+50 mass% MEG	0.719	0.711
5 mass% NaCl+80 mass% MEG	0.404	Salting out
5 mass% NaCl+90 mass% MEG	0.225	Salting out
5 mass% NaCl+95 mass% MEG	0.131	Salting out

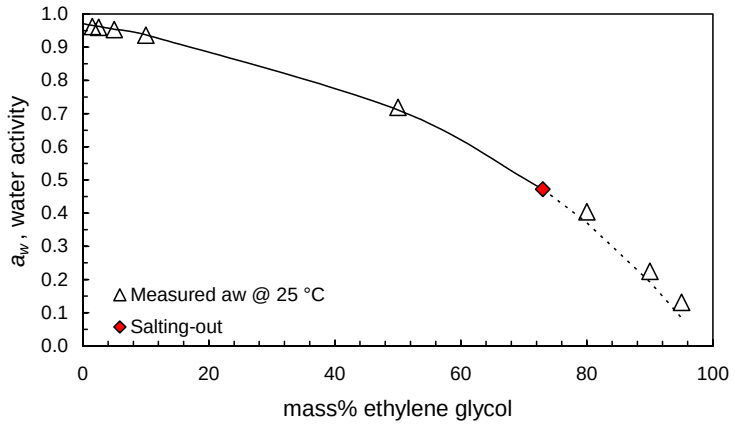

Figure 3.11 Water activity of MEG aqueous solutions in presence of 5 mass% NaCl at 25 °C (Solid lines: model predictions)

Table 3.14 & Figure 3.12, Table 3.15 & Figure 3.13 and Table 3.16 & Figure 3.14 shows the effect of increasing salt concentration on the water activity of 25, 50 and75 mass% of MEG solutions respectively. As can be seen from these tables and graphs, by increasing MEG concentration in the solutions, the salting out point of the systems have been shifted to the lower salt concentrations. The salting out points for 25, 50 and 75 mass% MEG solutions have been observed and predicted at about 26, 15 and 4 mass% of NaCl. The results also suggest that the water activity measurement set-up could be used for determining salting out point of solutions.

Table 3.14 Water activity of varying concentration of NaCl with 25 mass% of MEG at 25 °C

Solutions	Measured a_w	Predicted a_w
25 mass% MEG +5 mass% NaCl	0.863	0.871
25 mass% MEG +10 mass% NaCl	0.828	0.833
25 mass% MEG +15 mass% NaCl	0.786	0.787
25 mass% MEG +20 mass% NaCl	0.735	0.733
25 mass% MEG +25 mass% NaCl	0.682	0.667
25 mass% MEG +30 mass% NaCl	0.667	Salting out

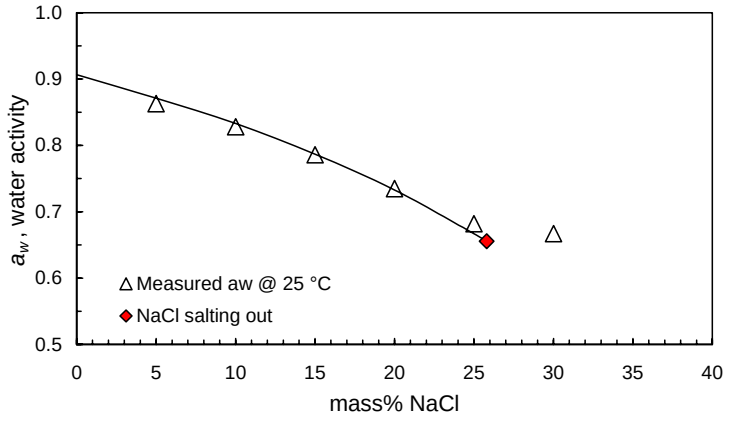

Figure 3.12 Water activity of 25 mass% MEG aqueous solution with varying concentration of NaCl at 25°C (Solid lines: model predictions)

Table 3.15 Water activity of varying concentration of NaCl with 50 mass% of MEG at 25 °C

Solutions	Measured a_w	Predicted a_w
50 mass% MEG +5 mass% NaCl	0.719	0.711
50 mass% MEG +10 mass% NaCl	0.688	0.664
50 mass% MEG +15 mass% NaCl	0.652	Salting out
50 mass% MEG +20 mass% NaCl	0.615	Salting out
50 mass% MEG +25 mass% NaCl	0.573	Salting out
50 mass% MEG +30 mass% NaCl	0.545	Salting out

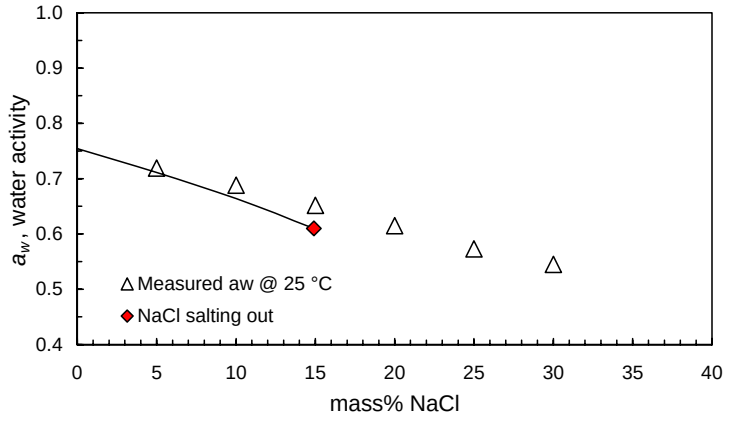

Figure 3.13 Water activity of 50 mass% MEG aqueous solution with varying concentration of NaCl at 25 °C (Solid lines: model predictions)

Table 3.16 Water activity of varying concentration of NaCl with 75 mass% of MEG at 25 °C

Solutions	Measured a_w	Predicted a_w
75 mass% MEG +5 mass% NaCl	0.473	Salting out
75 mass% MEG +10 mass% NaCl	0.451	Salting out
75 mass% MEG +15 mass% NaCl	0.425	Salting out
75 mass% MEG +20 mass% NaCl	0.414	Salting out
75 mass% MEG +25 mass% NaCl	0.383	Salting out
75 mass% MEG +30 mass% NaCl	0.358	Salting out

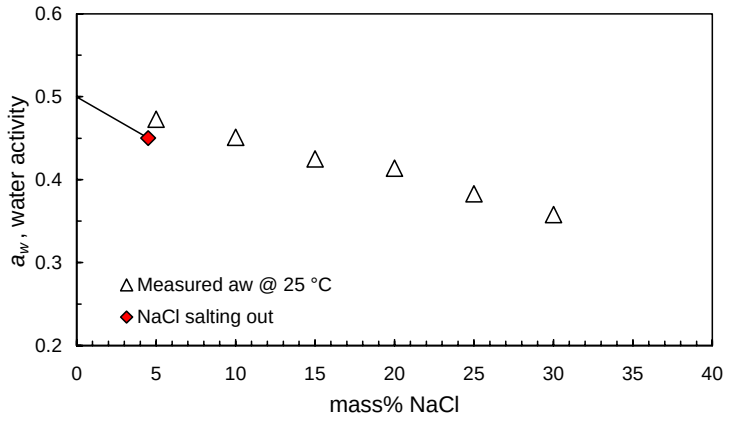

Figure 3.14 Water activity of 75 mass% MEG aqueous solution with varying concentration of NaCl at 25 °C (Solid lines: model predictions)

The water activity measurements were further carried out for MEG systems in the presence of three synthetic and one real produced water systems (compositions of produced water systems are given in Table 3.10. The results are presented in figures from Figure 3.15 to Figure 3.19 and tables from Table 3.17 to Table 3.21. As can be seen from these results, all the experimental data are in very good agreement with the predicted values.

Table 3.17 Water activity of varying concentration of MEG in Maya produced water system at 25 °C

Solutions	Measured a_w	Predicted a_w
Maya 100 mass% + MEG 0 mass%	0.934	0.938
Maya 95 mass% + MEG 5 mass%	0.916	0.921
Maya 90 mass% + MEG 10 mass%	0.900	0.901
Maya 85 mass% + MEG 15 mass%	0.882	0.881

Maya 80 mass% + MEG 20 mass%	0.862	0.858
Maya 70 mass% + MEG 30 mass%	0.812	0.805
Maya 60 mass% + MEG 40 mass%	0.761	0.742
Maya 50 mass% + MEG 50 mass%	0.686	0.665
Maya 40 mass% + MEG 60 mass%	0.613	0.572
Maya 30 mass% + MEG 70 mass%	0.515	Salting out
Maya 20 mass% + MEG 80 mass%	0.402	Salting out
Maya 10 mass% +MEG 90 mass%	0.385	Salting out
Maya 5 mass% + MEG 95 mass%	0.330	Salting out

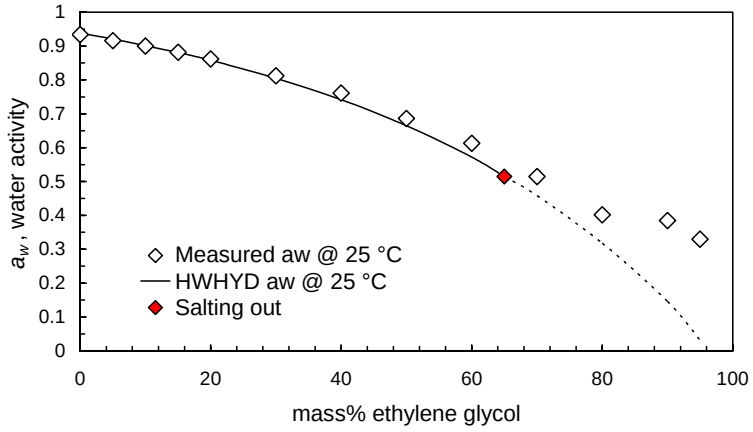

Figure 3.15 Water activity of varying concentration of MEG in the Maya produced water system at 25 °C.

Table 3.18 Water activity of varying concentration of MEG in Petronas produced water system at 25 °C

Solutions	Measured a_w	Predicted a_w
Petronas 100 mass% + MEG 0 mass%	0.959	0.957
Petronas 95 mass% + MEG 5 mass%	0.940	0.940
Petronas 90 mass% + MEG 10 mass%	0.923	0.922
Petronas 85 mass% + MEG 15 mass%	0.899	0.902
Petronas 80 mass% + MEG 20 mass%	0.874	0.879
Petronas 70 mass% + MEG 30 mass%	0.827	0.828
Petronas 60 mass% + MEG 40 mass%	0.768	0.766
Petronas 50 mass% + MEG 50 mass%	0.700	0.691
Petronas 40 mass% + MEG 60 mass%	0.621	0.600
Petronas 30 mass% + MEG 70 mass%	0.519	Salting out
Petronas 20 mass% + MEG 80 mass%	0.458	Salting out
Petronas 10 mass% + MEG 90 mass%	0.245	Salting out
Petronas 5 mass% + MEG 95 mass%	0.256	Salting out

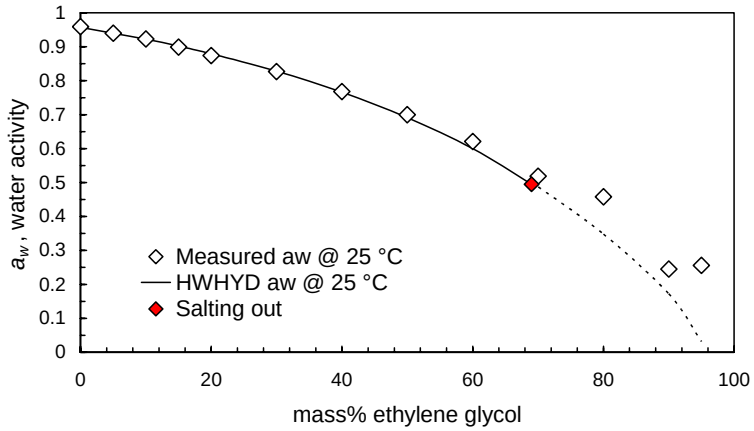

Figure 3.16 Water activity of varying concentration of MEG in Petronas produced water system at 25 °C

Table 3.19 Water activity of varying concentration of MEG in Forties produced water system at 25 °C

Solutions	Measured a_w	Predicted a_w
Forties 100 mass% +MEG 0 mass%	0.951	0.951
Forties 95 mass% + MEG 5 mass%	0.935	0.934
Forties 90 mass% + MEG 10 mass%	0.917	0.916
Forties 85 mass% + MEG 15 mass%	0.897	0.896
Forties 80 mass% + MEG 20 mass%	0.872	0.873
Forties 70 mass% + MEG 30 mass%	0.823	0.821
Forties 60 mass% + MEG 40 mass%	0.766	0.759
Forties 50 mass% + MEG 50 mass%	0.702	0.683
Forties 40 mass% + MEG 60 mass%	0.622	0.591
Forties 30 mass% + MEG 70 mass%	0.52	Salting out
Forties 20 mass% + MEG 80 mass%	0.421	Salting out
Forties 10 mass% + MEG 90 mass%	0.366	Salting out
Forties 5 mass% + MEG 95 mass%	0.309	Salting out

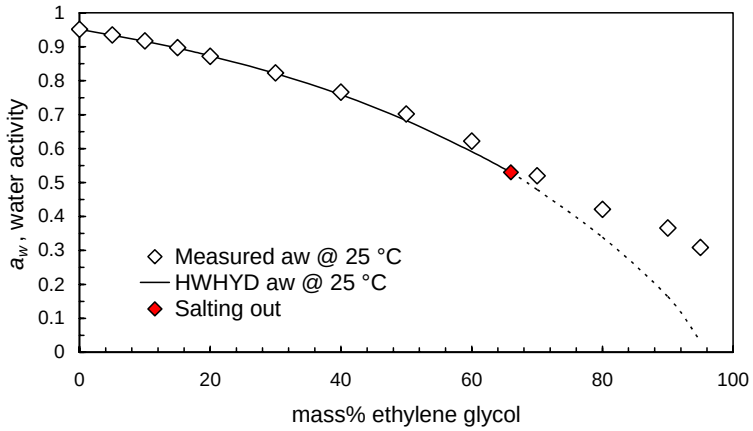

Figure 3.17 Water activity of varying concentration of MEG in Forties produced water system at 25 °C

Table 3.20 Water activity of varying concentration of MEG in Scale produced water system at 25 °C

Solutions	Measured a_w	Predicted a_w
Scale 100 mass% + MEG 0 mass%	0.982	0.986
Scale 95 mass% + MEG 5 mass%	0.970	0.970
Scale 90 mass% + MEG 10 mass%	0.957	0.953
Scale 85 mass% + MEG 15 mass%	0.940	0.934
Scale 80 mass% + MEG 20 mass%	0.917	0.913
Scale 70 mass% + MEG 30 mass%	0.874	0.864
Scale 60 mass% + MEG 40 mass%	0.811	0.805
Scale 50 mass% + MEG 50 mass%	0.744	0.733
Scale 40 mass% + MEG 60 mass%	0.663	0.645
Scale 30 mass% + MEG 70 mass%	0.558	0.536
Scale 20 mass% + MEG 80 mass%	0.437	0.400
Scale 10 mass% + MEG 90 mass%	0.363	0.221
Scale 5 mass% + MEG 95 mass%	0.314	0.032

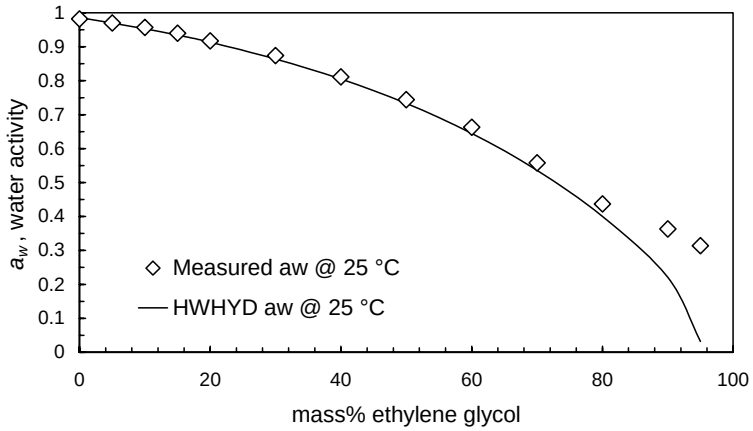

Figure 3.18 Water activity of varying concentration of MEG in Scale produced water system at 25 °C

Table 3.21 Water activity of varying concentration of MEG in the real BP produced water system at 25 °C

Solutions	Measured a_w	Predicted a_w
BP 100 mass% + MEG 0 mass%	0.965	0.971
BP 95 mass% + MEG 5 mass%	0.952	0.954
BP 90 mass% + MEG 10 mass%	0.939	0.937
BP 80 mass% + MEG 20 mass%	0.896	0.895
BP 50 mass% + MEG 50 mass%	0.731	0.711
BP 30 mass% + MEG 70 mass%	0.542	0.510
BP + 5 % MEG + 2 % oil (mass%)	0.949	N/A
BP+5 % MEG + 5 % oil (mass%)	0.952	N/A
BP+5 % MEG + 10 % oil (mass%)	0.949	N/A
BP+10 % MEG + 2 % oil (mass%)	0.89	N/A
BP+10 % MEG + 5 % oil (mass%)	0.89	N/A
BP+10 % MEG + 10 % oil (mass%)	0.886	N/A

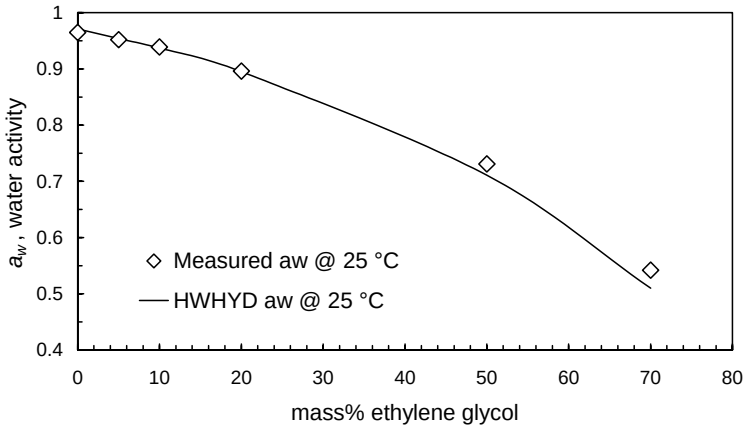

Figure 3.19 Water activity of varying concentration of MEG in the real BP produced water system at 25 °C

In general, results of this subsection suggest that the tested water activity measuring setup can be used for measuring water activity of MEG aqueous solutions in with and without salt(s).

Methanol Systems:

Methanol aqueous solutions with and without salt were also used to test the device. The results are presented in Table 3.22 and Figure 3.20 and Table 3.23 and Figure 3.21 respectively. As can be seen from these results, there are large deviations between the measurements and the predictions. Deviations are observed over the entire methanol range. Based on these results it is concluded that the existing sensor cannot measure the water activity of aqueous solutions containing methanol. The reason for such behaviour was due to the effect of methanol on the measuring sensor. As methanol is very volatile it will be evaporated and goes to the measuring part of the sensor and will affect the measurement results. The problem was reported to the supplier and they are working on the sensor to solve this problem.

Table 3.22 Water activity of varying concentration of methanol solution at 25 °C

Solutions	Measured a_w	Predicted a_w
3 mass% methanol	0.993	0.982
5 mass% methanol	0.99	0.971
6 mass% methanol	0.986	0.965
10 mass% methanol	0.968	0.942
15 mass% methanol	0.971	0.911
20 mass% methanol	0.948	0.88

30 mass% methanol	0.958	0.816
40 mass% methanol	0.959	0.749
50 mass% methanol	0.960	0.677
60 mass% methanol	0.960	0.599

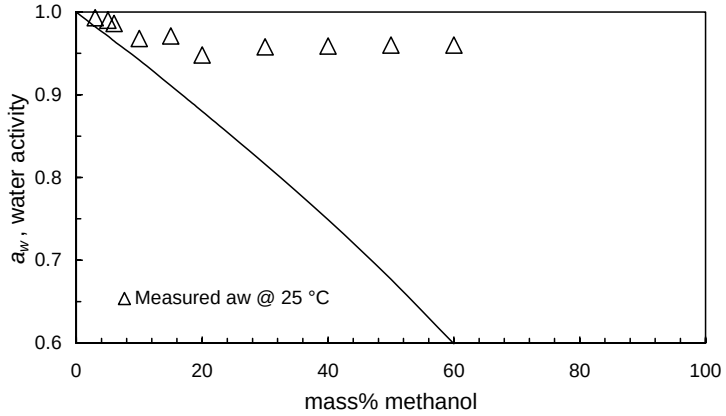

Figure 3.20 Water activity of varying concentration of methanol aqueous solution at 25 °C (Solid lines: model predictions)

Table 3.23 Water activity of varying concentration of methanol aqueous solution in the presence of 3 mass% NaCl at 25 °C

Solutions	Measured a_w	Predicted a_w
3 mass% NaCl+5 mass% methanol	0.970	0.954
3 mass% NaCl+10mass% methanol	0.964	0.924
3 mass% NaCl+15mass% methanol	0.960	0.893
3 mass% NaCl+20mass% methanol	0.959	0.862
3 mass% NaCl+30mass% methanol	0.953	0.796
3 mass% NaCl+40mass% methanol	0.951	0.727

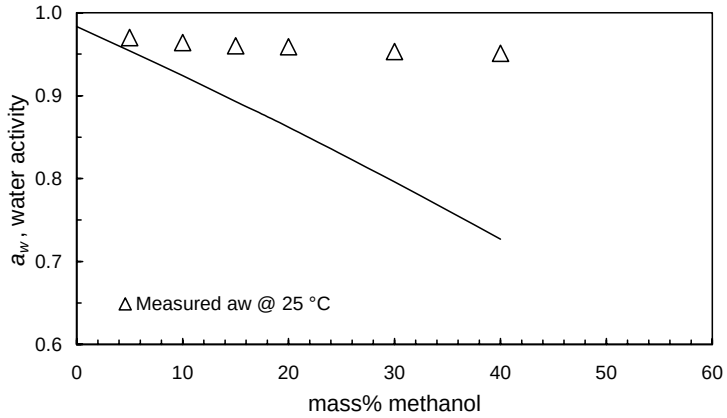

Figure 3.21 Water activity of varying concentration of methanol aqueous solution in the presence of 3 mass% NaCl at 25 °C (Solid lines: model predictions)

3.2.7. Determination of HSZ Using Measured Water Activities and Developed Correlation

The measured water activity data for different systems of salt/produced water and hydrate inhibitors in the previous sections have been used here to predict HSZs by using the developed correlation. First, the potential error of the HSZ predictions in this work which can be caused by the error of the Labmaster a_w setup has been determined based on the declared accuracy of the setup. Then, the developed correlation in this work has been evaluated using the large data base of water activity measurements created in the previous section for a wide range of different salt and inhibitor concentrations. The correlation has been also validated with literature data.

3.2.7.1. Error Analysis of Predicted HSZs Based on Accuracy of the Measured Water Activities

An error analysis has been performed to evaluate the error in predicted HSZs which can be caused by the error in the Labmaster a_w setup. The declared error of this device in its specification sheet is ± 0.003 of absolute reading. The potential equivalent errors in predicted hydrate suppression temperatures have been determined for some selected systems. It has been tried to cover different systems over a wide range of concentrations close to the real systems. Table 3.24 presents results of this evaluation

at 200 bara. The error in the predicted hydrate suppression temperature has been calculated by adding/subtracting 0.003 to/from the water activity values and predicting the corresponding hydrate suppression temperatures for a_w , (a_w +0.003) and (a_w - 0.003) using the developed correlation in this work. The error reported in this table is the difference between the predicted hydrate suppression temperatures for a_w and (a_w ±0.003) values. As can be seen from this table, the maximum error in the predicted suppression temperature is less than 0.3 ºC.

Table 3.24 Effect of the error in Labmaster a_w measurements on the accuracy of hydrate suppuration temperature obtained from the correlation at 200 bara

Solutions	a_w	Error in the suppression temperature / ºC
Deionised water	1	± 0.24
5 mass% NaCl	0.971	± 0.24
25 mass% MEG	0.907	± 0.26
35 mass% MEG	0.855	± 0.28
5 mass% NaCl+35mass% MEG	0.824	± 0.29
7 mass% methanol	0.960	± 0.25
4.5 mass% NaCl+7.5mass% methanol	0.930	± 0.25
5 mass% NaCl+2 mass% KCl+3 mass% $CaCl_2$	0.943	± 0.25
4 mass% NaCl+2 mass% KCl+25 mass% MEG	0.870	± 0.27

It should be mention that, the 0.003 is an absolute error and relative error varies by water activity value. For example, in the 25 mass% MEG solution, the setup error is 0.33% which can result in 0.26 °C error in the hydrate suppression temperature while in 50 mass% MEG solution, the setup error is 0.43% which can results in 0.31 °C error in the hydrate suppression temperature. In other words, the error in hydrate suppression temperature increase as inhibitor concentration increases in the system.

To demonstrate this error over a wide range of pressure the hydrate phase boundaries of some selected systems (Table 3.24) results are plotted in Figure 3.22. As can be seen, effect of the setup error on the hydrate safety zone (HSZ) for different systems in different pressure and temperature is less than 0.3 °C which is negligible.

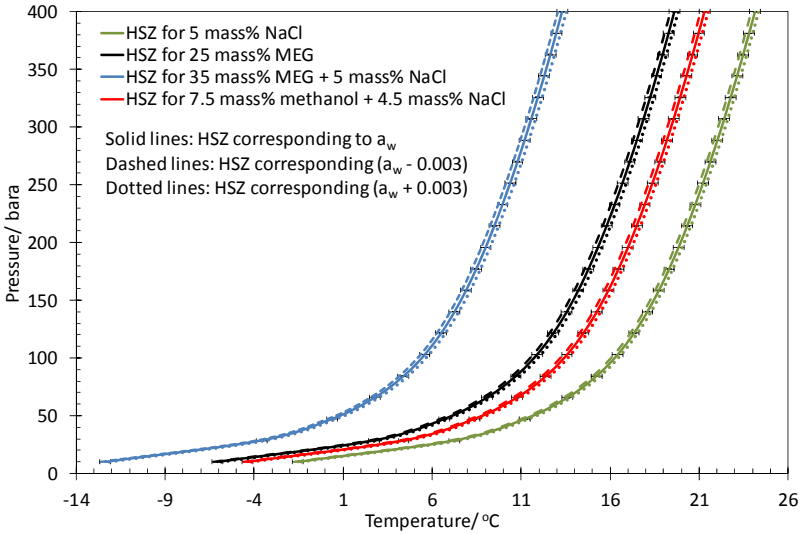

Figure 3.22 Effect of the error of the Labmaster aw setup on the accuracy of hydrate phase boundary using the correlation developed in this work. (Error bars in this graphs are ± 0.3 °C).

3.2.7.2. Evaluation of Water Activity Correlation/Method Using Experimental Water Activity Data

The main objective of this section is to evaluate the accuracy of the developed correlation by comparing the predicted hydrate phase boundaries of different systems using our in-house thermodynamic model with the hydrate phase boundaries of the same systems by measuring their water activities and using the correlation to predict the hydrate suppression temperatures. As it was mentioned before the correlation has been developed by creating a very large data base of pseudo water activities and hydrate suppression temperatures of different systems (more than 300 systems) using our in-house thermodynamic model; here about 40 independent systems (with different combination of salts and hydrate inhibitors) over a wide range of concentrations have been studied to evaluate the correlation. In each system, the water activity has been measured using the Labmaster a_w setup and its corresponding hydrate suppression temperature has been calculated using the developed correlation. Hydrate phase boundary for each system (containing salt and inhibitors) has then been determined based on the calculated hydrate suppression temperature and the hydrate phase boundary in the presence of deionised water for a gas phase with a given composition. The hydrate phase boundary determined with this method for each system has been

compared with the one predicted directly using our in-house thermodynamic model for the same system (containing salt and inhibitors) in the presence of the same gas phase.

In developing the correlation, systems were assumed to be in contact with a standard natural gas (Table A.72); to investigate the effect of composition of gas phase on the correlation, two different gas systems, i.e. methane and a different natural gas from the one used for developing the correlation (Table A.59), has been used to predict hydrate phase boundaries using the developed correlation.

Different combinations and types of salts, e.g. NaCl, KCl and $CaCl_2$, in the presence and absence of hydrate inhibitors over a wide range of concentrations have been tested to evaluate the correlation. Additionally, five different produced water systems (Table 3.10) with different concentrations of hydrate inhibitor have been used for the same purpose. Table 3.25 summarised the studied systems in this section.

Table 3.25 Studied independent systems for evaluating the developed correlation

In the presence of natural gas	
5, 10, 15 and 20 mass% NaCl	3, 5, 10, 15 and 20 mass% KCl
3, 5, 10, 15 and 20 mass% $CaCl_2$	5 mass% NaCl & 3 mass% KCl
5 mass% NaCl & 3 mass% $CaCl_2$	5 mass% NaCl & 5 mass% KCl
BP produced water	Maya produced water
Petronas produced water	Forties produced water
Scale produced water	0 mass% NaCl & 50 mass% MEG
10 mass% NaCl & 25 mass% MEG	5 mass% NaCl & 50 mass% MEG
Maya produced water & 15 mass% MEG	Petronas produced water & 40 mass% MEG
BP produced water & 20 mass% MEG	Scale produced water & 40 mass% MEG
Forties produced water & 50 mass% MEG	
In the presence of methane	
0 mass% NaCl & 40 mass% MEG	10 mass% NaCl & 50 mass% MEG
Maya produced water & 15 mass% MEG	Petronas produced water & 40 mass% MEG
BP produced water & 50 mass% MEG	Scale produced water & 40 mass% MEG

Figure 3.23 shows the results of the evaluation of the developed correlation for 5, 10, 15 and 20 mass% of NaCl solutions. As can be seen, the correlated hydrate phase boundaries are in very good agreement with the predicted ones. The error bars in these graphs are ±0.2, ±0.2, ±0.5 and ±1 °C for 5, 10, 15 and 20 mass% respectively suggesting that the accuracy of the correlation at lower NaCl concentrations, e.g. 5 and 10 mass% is higher than 20 mass% NaCl. In general, it can be concluded that the correlation can be used with high level of confidence for NaCl systems.

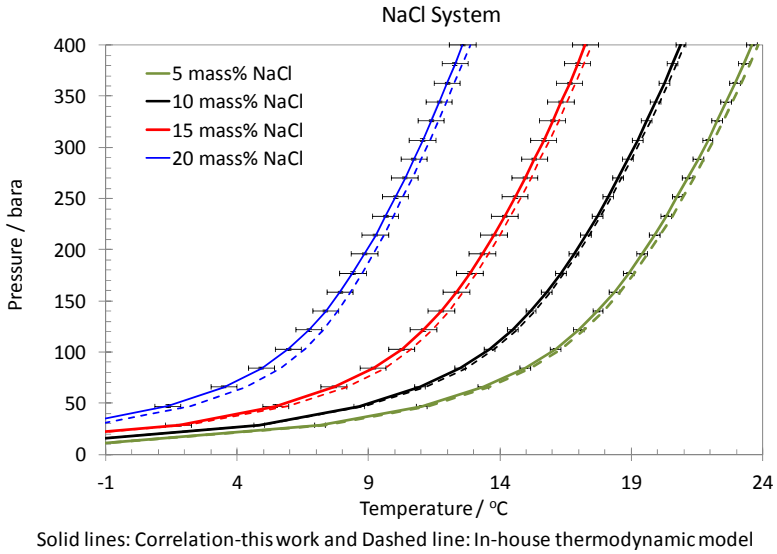

Figure 3.23 Evaluation of the developed correlation for NaCl solutions in presence of natural gas. Error bars in this graphs are ±0.2, ±0.2, ±0.5 and ±1 °C for 5, 10, 15 and 20 mass% respectively.

Although NaCl is the most common electrolyte solute in produced water in different fields, other salts like KCl and $CaCl_2$ can also be found in produced waters. Therefore, the correlation has been evaluated for these systems at 3, 5, 10, 15 and 20 mass%. It should be mentioned that the concentrations of theses salts in the produced water do not usually exceed 10 mass%, however, in this section the evaluation has been performed up to 20 mass% to have an indication of the accuracy of the correlation at very high concentrations as well. The results have been presented in Figure 3.25 and Figure 3.24. Similar trend of accuracy to NaCl solutions were observed for these systems as well. For KCl solutions, the error of the correlation is less than ±0.5 °C up to 10 mass% KCl. In the case of $CaCl_2$ solutions, the error is less than ±0.3 °C up to 15 mass% $CaCl_2$. The higher concentrations of these salts are very unlikely to exist in real produced waters.

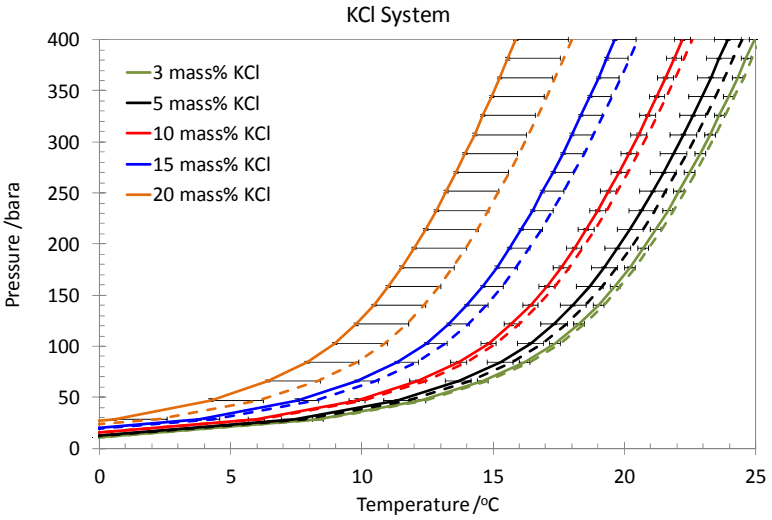

Figure 3.24 Evaluation of the developed correlation for KCl solutions in presence of natural gas. Error bars in this graphs are ±0.3, ±0.5, ±0.2, ±0.8 and ±2.0 °C for 3, 5, 10, 15 and 20 mass% respectively.

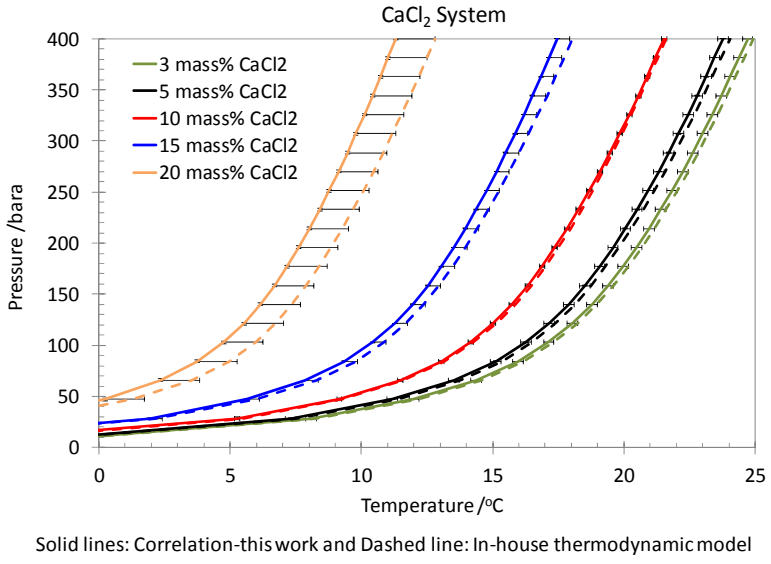

Figure 3.25 Evaluation of the developed correlation for CaCl2 solutions in presence of natural gas. Error bars in this graphs are ±0.2, ±0.3, ±0.1 , ±0.3 and ±1.5 °C for 3, 5, 10, 15 and 20 mass% respectively.

Produced waters are generally a combination of different type of salts rather than a single type of salt. Therefor; it was decided to evaluate the correlation for multi-component solutions of salts and produced waters from different fields. The results show a very good agreement between the correlated and predicted hydrate phase

boundaries. Figure 3.26 is an example of the tested systems. The maximum deviation from the prediction results is 0.4 °C for these systems. Figure 3.27 is the result of evaluation for different produced water systems. The error bars in these graphs are ±0.5 °C. All the results of evaluation of the correlation for tested salts and produced water systems suggest that the developed correlation is in a very good agreement with prediction of our in-house thermodynamic model. It should be mentioned that the BP produced water is a real produced water containing oil, sand and other contaminants which can usually be found in real pipeline and separators suggesting that the accuracy of the water activity measuring setup, Labmaster-a_w, and developed correlation is not affected by the presence of these contaminants at the level present in this sample.

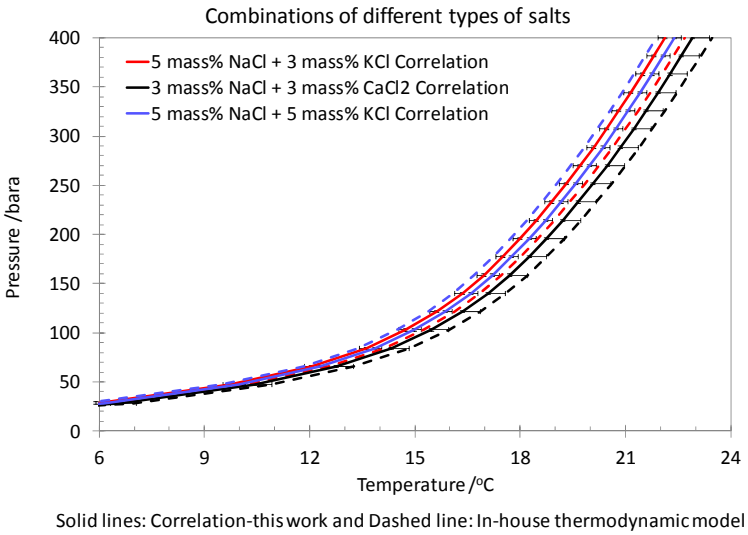

Figure 3.26 Evaluation of the developed correlation for combinations of different types of salts in presence of natural gas. Error bars in these graphs are ±0.4 °C.

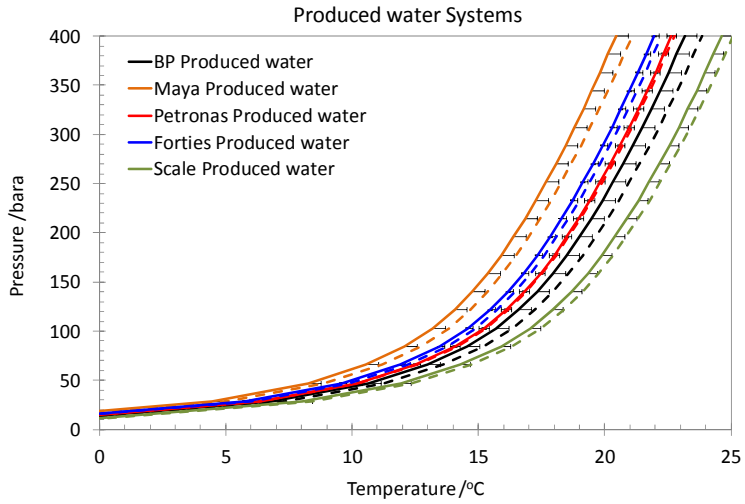

Solid lines: Correlation-this work and Dashed line: In-house thermodynamic model

Figure 3.27 Evaluation of the developed correlation for different produced water systems in presence of natural gas. Error bars in these graphs are ±0.5 °C.

To complete the evaluation of the developed water activity method/correlation for different aqueous systems, selected systems of MEG with salts and MEG with different produced waters were tested. Figure 3.28 shows the results of this part of the evaluation. The maximum deviations of the correlation from the prediction results were ±0.5 °C suggesting very a good agreement between the correlation and the prediction.

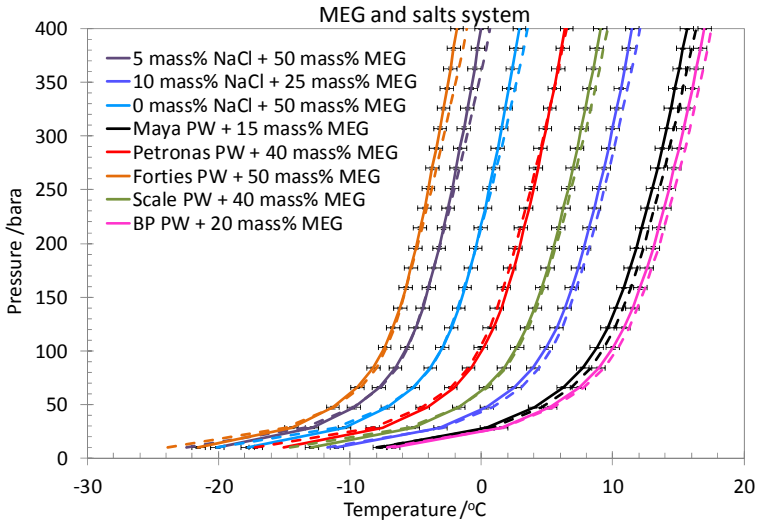

Solid lines: Correlation-this work and Dashed line: In-house thermodynamic model

Figure 3.28 Evaluation of the developed correlation for selected salts with MEG and different produced waters with MEG systems in presence of natural gas. Error bars in these graphs are ±0.5 °C.

Hydrate phase boundaries depends on compositions of both aqueous and gas phases. So far in this section, the water activity method/correlation was evaluated over an extensive range of aqueous phase compositions. The effect of composition of gas phase was also considered in those test because the correlation was evaluated in the presence of a different natural gas than the one used for developing the correlation. The compositions of both natural gases have been provided in Appendix (Table A.72, Table A.59). In order to assess the validity of the correlation/method over large changes in the composition of gas phase, the correlation/method was validated for selected systems in presence of methane as gas phase. The selected systems were very close to the real conditions in the pipelines. As can be seen from these graphs, the hydrate phase boundaries correlated with water activity method are very close to the ones predicted using our in-house thermodynamic method suggesting that the developed method/correlation can be used for different compositions of gas phases.

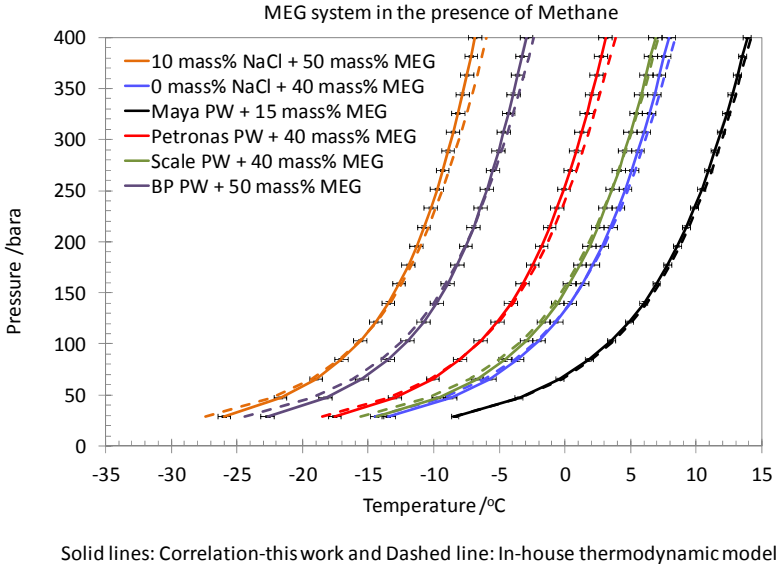

Figure 3.29 Evaluation of the developed correlation for selected salts with MEG and different produced waters with MEG systems in presence of methane. Error bars in these graphs are ±0.5 °C.

3.2.7.3. Evaluation of Water Activity Correlation/Method Against Literature Data

In the previous section the water activity method/correlation was evaluated against our in-house thermodynamic model for a very large amount of systems over wide range of different salts and hydrate inhibitor concentrations. The results show very good agreement between the prediction and correlation. In this section the method/correlation has been evaluated against literature data. In addition, the comparisons have also been performed for the thermodynamic model to validate the previous work, i.e. evaluation of the correlation with the model. The natural gas compositions used in these evaluations were the ones reported for the literature data in each case.

Figure 3.30 shows the results of the comparison for the MEG systems. The results of correlation and prediction for 10 and 30 mass% MEG system match very closely with the experimental data and the maximum deviation of the model and correlation from literature data were ±0.5 °C (gas compositions given in Table A.61 and Table A.62). In the case of very high concentration of MEG, i.e. 50 mass%, the maximum deviation reached ±1.0 °C which is a very good match for hydrate phase boundary determination. The results of correlation were slightly closer to the literature data compared to the predictions.

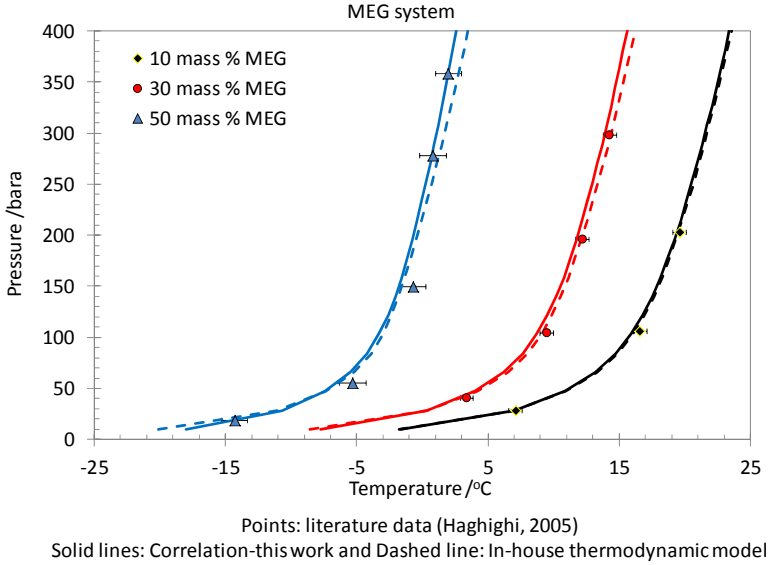

Figure 3.30 Evaluation of water activity method/correlation against literature data for MEG systems. The error bars are ± 0.5 °C for 10 & 30 mass% MEG systems and ±1 °C

for 50 mass% MEG system.

Similar evaluation has been performed for MeOH systems. As it was mentioned before, the Labmaster-a_w setup could not accurately measure the water activity values of the systems containing MeOH; therefore in these tests, instead of experimentally measuring the water activity of the MeOH solutions, these data were generated using our in-house thermodynamic model (gas compositions given in Table A.61 and Table A.62). These pseudo water activity data were used to calculate the hydrate suppression temperature using the correlation. The reason for this evaluation was to prove that the water activity method/correlation can be used for MeOH systems as well if an measurement setup suitable for methanol systems is used.

Figure 3.31 presents the results of evaluation for 10, 40, 50 and 60 mass% MeOH solutions. A very good agreement between the correlation, prediction and literature data can be observed from these figures for MeOH concentration up to 50 mass%. For very high MeOH concentration, i.e. 65 mass%, the maximum error observed was ±2.0 °C. It should be mentioned that although the error increases for very high concentration of methanol, but the correlation gives a more conservative value than the experiments which is a good point from operational view point.

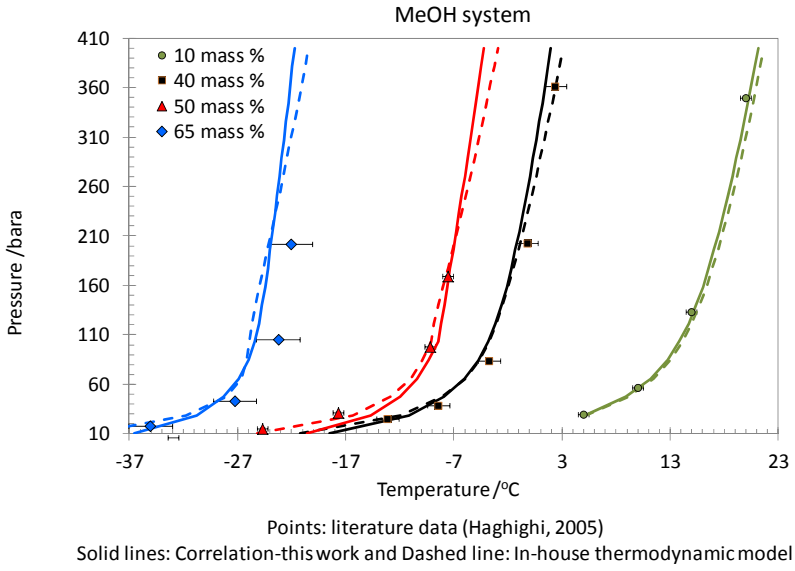

Figure 3.31 Evaluation of water activity method/correlation against literature data for MeOH systems in the presence of natural gas. The error bars are ± 0.5, ±1, ± 0.5 and ±2 °C for 10, 40, 50 and 65 mass% MeOH systems.

3.2.8. Water activity–Pseudo Concentrations Method

As it was detailed in the previous sections, the developed water activity–correlation method is based on measuring water activity of aqueous phase sample and relating the measured value to the hydrate suppression temperature without having any information about the concentrations and type of salts and inhibitors present in the aqueous phase. This method can be further improved by integrating the method with some thermodynamic properties of the aqueous phase. For example, in almost all of the cases, the type of the hydrate inhibitor injected to the system is known; therefore, this information can be used to improve the accuracy of the water activity method. Based on this idea, a new approach, named water activity–pseudo concentration, has been introduced in this work which takes into account the hydrate inhibition characteristics of the inhibitors when predicting hydrate phase boundary. The following section will detail the method.

3.2.8.1. Development of the Water Activity–Pseudo Concentration Method

The basis of this method is to calculate a pseudo inhibitor/salt concentrations based on the measured water activity of the aqueous phase sample. The hydrate phase boundary can then be predicted for the pseudo inhibitor/salt concentrations. A programme has been developed in this work to calculate all the possible combinations of inhibitor/salt concentrations which can result in a given water activity value. To narrow down the possibilities to only the most likely ones, a range of the salinity of the aqueous phase can also be taken into account. In most cases, it is very likely to have a rough estimation of the salinity of the produced water, i.e. 5-15 mass%, therefore, the range of salinity can be consider when calculating the pseudo concentrations. Figure 3.32 illustrates the screen shot of the programme interface. The only required inputs for the programme are the type of thermodynamic inhibitor, i.e. MEG or MeOH, a rough estimation of the salinity range of the aqueous phase equivalent to NaCl and the measured water activity of the aqueous sample. The outputs of the programme are the possible combinations of salt and inhibitor concentrations which in turn have been linked to our in-house thermodynamic model to predict the hydrate phase boundaries based on the selected inhibitor and salt concentrations.

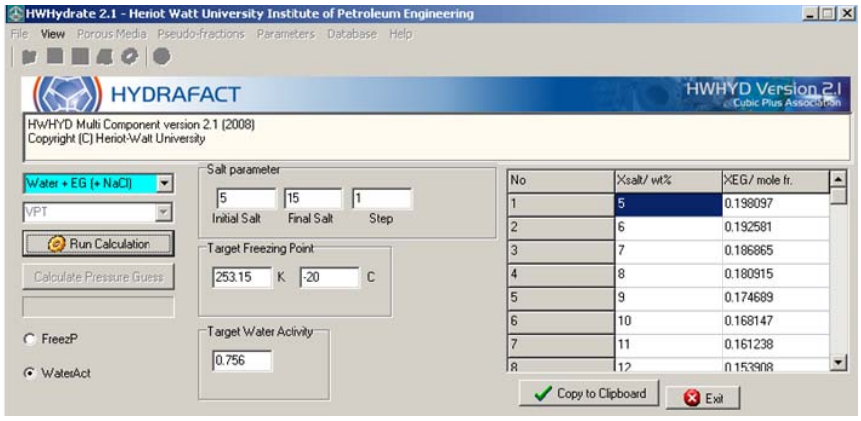

Figure 3.32 Developed programme/software for calculating pseudo concentrations for a measured water activity.

The calculated pseudo concentrations are not necessarily the real ones, but can be used to calculate the hydrate phase boundaries. A feasibility study has been performed to evaluate this method using a large number of systems with different combinations of salt and inhibitors (Table 3.26). The salt range in this table is an estimation of the salinity of the aqueous phase. For example for the 6 mass%, salt concentration it has been assumed that the salt concentration of the field can be varying from 0 to 15 mass%. Based on this assumption and depending on the number of defined steps the programme can calculate salt and inhibitor concentrations combinations which matched the measured water activity for the actual sample. The last column of this table shows the calculated concentrations for the lowest and highest assumed salt concentrations. The hydrate phase boundaries predicted for these systems (gas composition given Table A.56,Table A.57,Table A.58) are plotted in Figure 3.33.

Table 3.26 Some of salt/inhibitor systems tested in feasibility study of the water activity-pseudo concentration method.

Actual concentrations mass%	Salt range mass%	The first (lowest salt concentration) and last (highest salt concentration) pseudo concentrations / mass%
5 NaCl & 10 MEG	3 - 7	3 NaCl & 13.4 MEG - 7 NaCl & 6.4 MEG
6 NaCl & 45 MEG	0 - 15	0 NaCl & 49.8 MEG - 15 NaCl & 33.7 MEG
10 NaCl & 60 MEG	5 - 15	5 NaCl & 62.8 MEG - 15 NaCl & 56.3 MEG

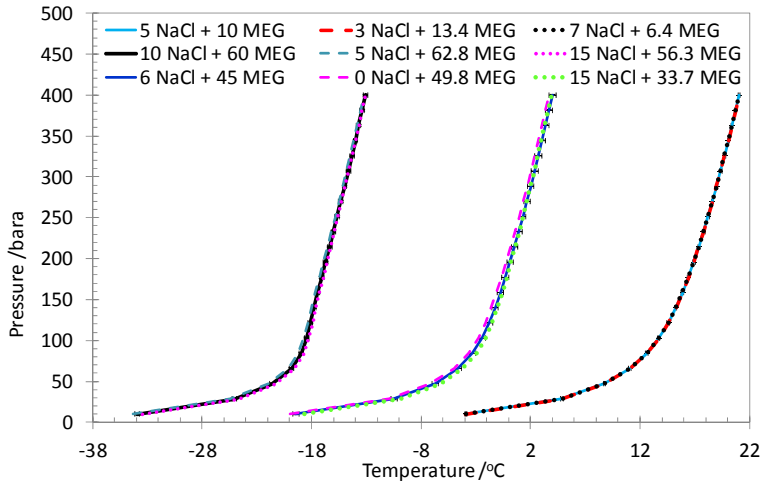

Solid lines: Actual concentration, Dashed lines: Pseudo concentration for the lowest salt concentration, Dotted lines:Pseudo concentration for the highest salt

Figure 3.33 Evaluating of water activity-pseudo concentration method MEG system. Maximum error bar in these graphs is ±0.3 °C.

As an example, feasibility study for the sample with 5 mass% NaCl and 10 mass% MEG has been detailed here. The water activity of this solution is 0.937. The range of the salt concentration has been assumed to be 3-7 mass%. The calculated possible pseudo concentrations using the developed programme for this system have been listed in Table 3.27.

Table 3.27 Calculated pseudo NaCl and MEG concentrations for a water activity value of 0.937

Equivalent concentrations
3.0 mass% NaCl + 13.4 mass% MEG
3.5 mass% NaCl + 12.6 mass% MEG
4.0 mass% NaCl + 11.7 mass% MEG
4.5 mass% NaCl + 10.9 mass% MEG
5.0 mass% NaCl + 10.0 mass% MEG
5.5 mass% NaCl + 9.1 mass% MEG
6.0 mass% NaCl + 8.2 mass% MEG
6.5 mass% NaCl + 7.3 mass% MEG
7.0 mass% NaCl + 6.4 mass% MEG

As can be seen in this table, the concentration of MEG can be varying from 6.4-13.4 mass% for the salt range of 3-7 mass%. It should be mentioned that determining the salt and inhibitor concentration is not the goal of this method and these concentration are acting as an intermediate step to predict the hydrate phase boundary based on the measured water activity. As can be seen from Figure 3.33, the predicted hydrate phase

boundaries for the pseudo concentrations very closely matches the predicted phase boundaries for the actual concentrations. In the case of 5 mass% NaCl and 10 mass% MEG the maximum deviation is ±0.1 °C. For the system with 10 mass% NaCl and 60 mass% MEG and 6 mass% NaCl and 45 mass% MEG, the deviations are ±0.2 and ±0.3 respectively.

These results shows that the water activity-pseudo concentration method is a rigorous method for determining hydrate phase boundaries and the required information are usually available for almost all of the fields.

3.2.8.2. Comparison Between Pseudo Concentration Method and the Correlation

As it was shown before, the developed water activity-correlation method can be used for hydrate phase boundary determination with a good agreement with literature data and our in-house thermodynamic method. However, at very high concentration of inhibitors the error of the method increases up to 1-2 °C. The water activity-pseudo concentration method has been developed to overcome this issue. These two methods have been compared in this section for very high concentrations of salt and inhibitors. As with the previous evaluations, two main hydrate thermodynamic inhibitors, MEG and MeOH have been studied here. A standard natural gas (composition is given in Table A.59) is used in predictions and to keep comparison simple only NaCl has been used as salt. Hydrate phase boundaries have been determined using the water activity-correlation and the water activity-pseudo concentration method. A salt range of ±5 mass% has been used in these comparisons. For example for an actual salt concentration of 10 mass%, the rough estimation of the salinity of the aqueous phase has been considered to be between 5 and 15 mass%. Figure 3.34 and Figure 3.35 shows the results. In the water activity-pseudo concentration method, hydrate phase boundaries have been plotted for the pseudo concentrations with the minimum and maximum salt percentages.

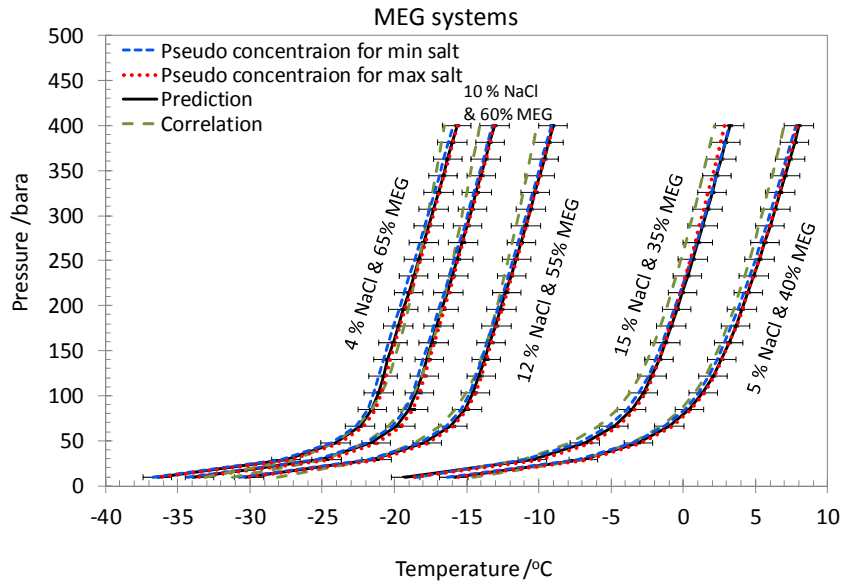

Figure 3.34 Comparison of water activity-correlation and water activity-pseudo concentration methods with our in-house thermodynamic model for the MEG solutions in the presence of natural gas. The error bars are ±1 °C.

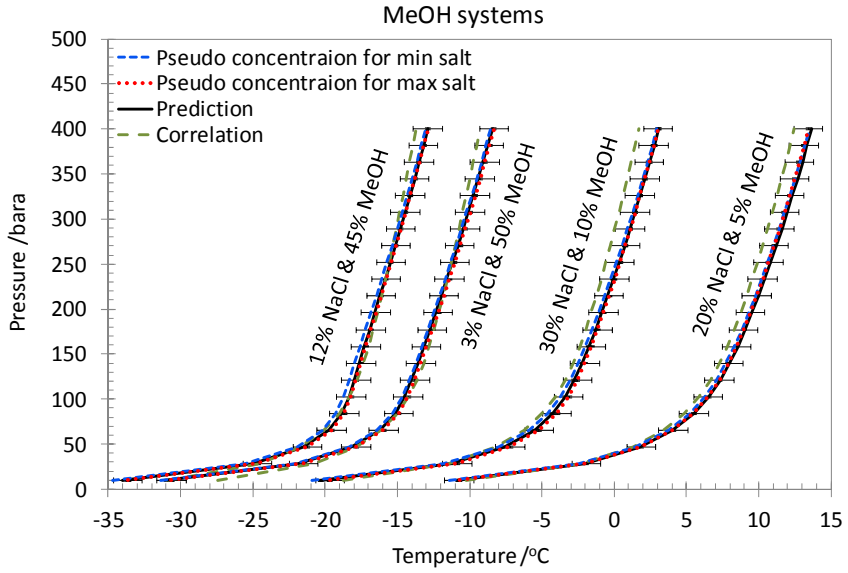

Figure 3.35 Comparison of water activity-correlation and water activity-pseudo concentration methods with our in-house thermodynamic model for the MeOH solutions in the presence of natural gas. The error bars are ±1 °C.

As can be seen from these figures, the deviation between the correlation and prediction slightly increases with salt concentration and pressure. However, this deviation is

about ±1 °C. This deviation has significantly decreased with the pseudo concentration method. The maximum deviation for these systems was ±0.3 °C. An error of ±5 mass% in estimation salinity of aqueous sample did not cause any noticeable change in the results.

Similar comparison has been performed for these systems in the presence of methane to investigate the effect of gas phase composition on the accuracy of the methods. The results in terms of accuracy of the methods were very similar to the ones in the presence of natural gas system. Therefore, to avoid the repetitions, they are not presented here.

3.2.9. Summary

The water activity measurement device, Labmaster-a_w, was extensively evaluated and the reliability of the device for measuring water activity for MEG and/or different types of salts were proven, however methanol systems cannot be analyzed with this device.

Two methods for hydrate monitoring based on water activity of aqueous phase were introduced in this part of the work. The main objective of these methods was to determine hydrate phase boundaries without having salt and inhibitor concentrations in the aqueous phase sample. The introduced water activity methods (correlation and pseudo concentration) were in very good agreement with our in-house thermodynamic method which in turn has been validated with a very large data base of experimental results (Haghighi, 2009). Additionally, the developed correlation's result very closely matched the independent data from literature. A slight deviation ~ ±1 °C between correlation and predictions (using our in-house thermodynamic model) were observed which is quite in acceptance range for industry. However, this method was further improved by taking into account the thermodynamic properties of the inhibitors in the pseudo concentration method. The required information for this method is the type of the injected inhibitor and very rough estimation of the salinity of the aqueous phase. The results showed that the error of ±5 mass% in salinity of aqueous phase do not cause noticeable deviation in the results. The deviation of pseudo concentration

method from our in-house thermodynamic method over a wide range of inhibitor and salt concentrations were less than ±0.3 °C.

A package has been developed in this work which integrates the water activity measurement device and developed water activity methods here with our in-house thermodynamic model. This package can give hydrate phase boundary of the system only with measuring water activity of aqueous phases. The detail of this integration is presented in Chapter 6.

3.3. WATER CONTENT METHOD

The water activity methods presented in the previous section for determining HSZs are based on measuring water activity of aqueous phase samples. However, in some cases sampling from aqueous phase is not applicable due to operational restrictions. Therefore, as part of this work, it was decided to develop an on-line monitoring system as an alternative solution for tackling this restriction. For this purpose, a water content method has been introduced and developed for determining HSZs. This method is based on measuring the water content of vapour phases.

Vapour phase water content is the quantity of water vapour in the gas phase at a given temperature and pressure. Water content in vapour phase decreases with an increase in system pressure and a decrease in system temperature for sweet systems. Existence of any dissolved substance in aqueous phase decreases the vapour phase water content as with liquid phase water activity. For instant, salt and/or hydrate inhibitor (methanol or MEG) in the aqueous phase results in a reduction of the water content. This reduction is proportional to the concentration of the salt and/or inhibitor at the same temperature and pressure. This fact forms the basis of the water content method which relates the measured vapour phase water content to the concentrations of the salt and/or inhibitors in the system and consequently to the HSZ. As with the water activity methods, determining the concentrations of salt and/or inhibitors is not the goal of this method. Equivalent concentrations of inhibitors are calculated in this method to facilitate prediction of HSZs.

Different systems of salt, methanol and MEG without and with salt over a wide range of concentration, temperature and pressure were studied in this part to evaluate the feasibility of the water content method. Two different commercial setups, TDLAS-

SS2000 and VAISALA-HMT360 were used to measure the water content of vapour phases in this work. The following sections detail the feasibility study, error analysis, experimental equipment, procedures and results.

3.3.1. Feasibility Study for Water Content Technique

A feasibility study and an error analysis for the water content method have been performed using our in-house thermodynamic model prior to starting experimental work. To begin with, vapour phase water content of NaCl, MEG, MeOH, MEG plus salt and MeOH plus salt over a wide range of concentration were predicted with the model. Figure 3.36 shows the results for systems with varying concentration of NaCl, MEG and MeOH. MEG and MeOH systems in the presence of 6 mass% NaCl have also been plotted in this figure. It has been assumed that the systems are in equilibrium with natural gas (Table A.72) at 100 bara and 10 °C.

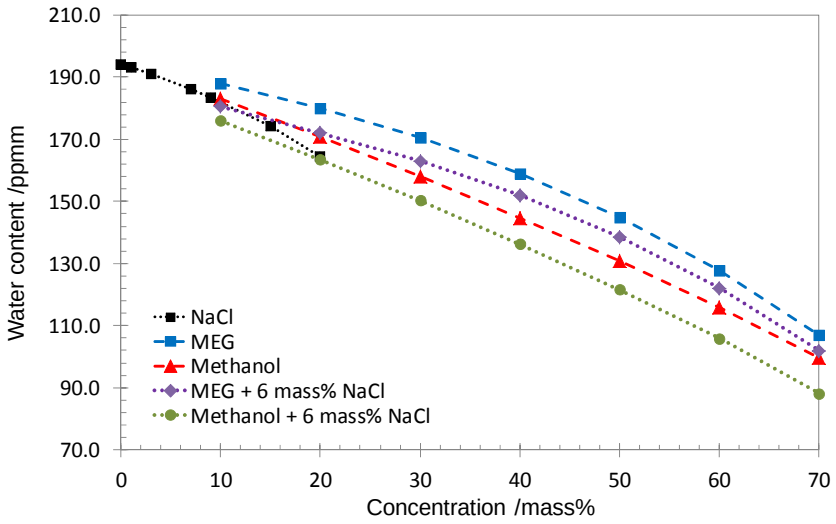

Figure 3.36 Change in water content due to the changes in salt/inhibitor concentrations in the presence of a standard natural gas at 100 bara and 10 °C.

As can be seen in these graphs, water content decreases as salt and/or inhibitor concentration increases in the system. The change of the water content due to the change in salt and/or inhibitor concentrations is not linear and the slopes of the changes for different systems are not similar to each other.

Unlike water activity of aqueous phase, vapour phase water content is not directly related to the hydrate suppression temperature. Two systems with the same water content can have different hydrate suppression temperatures. There are also different parameters which play major roles in water content, i.e. temperature, pressure, composition of gas phase, type and concentration of salt and inhibitors in the aqueous phase. Hence, developing a general correlation based on the vapour phase water content is not helpful in predicting the hydrate phase boundary. Therefore, the developed water content method in this work is based on equivalent concentration of salt or inhibitors in the system at a given temperature and pressure for a certain gas composition.

In systems containing only salt or inhibitor (either MeOH or MEG), it is possible to determine the equivalent salt or inhibitor concentration in the system by measuring the vapour phase water content at a certain temperature and pressure and then matching the measured value using our in-house thermodynamic model at the same temperature and pressure. The hydrate phase boundary can then be predicted for the determined equivalent salt or inhibitor concentration over a wide range of temperature and pressure in the presence of any desirable gas composition using the model. It should be noted that the gas composition being used when determining the equivalent salt or inhibitor concentration (using the model) should be the gas composition of the system of which the experimental water content has been measured.

In systems containing salt and inhibitor (either MeOH or MEG), the salt concentration is assumed to be constant in the system. This assumption is realistic because the salt concentration in the fields is usually constant over a long period of time and the operators usually know the amount of the salt in the system. By knowing the salt concentration and measuring the water content at a certain temperature and pressure, it is possible to determine the equivalent inhibitor concentration using the model and matching the measured and predicted water content. Hydrate phase boundaries can then be predicted by knowing salt and equivalent inhibitor concentrations using the model.

3.3.2. Error Analysis for Water Content Method

An error analysis has been performed for water content method to investigate the effect of error of the water content measurements on the determined equivalent salt and/or inhibitor concentration and consequently on the predicted hydrate phase boundary. Different systems of salt, MEG, MeOH, salt plus MEG and salt plus MeOH over a wide range of concentrations up to 70 mass% were studied for this purpose. Figure 3.37 show the equivalent predicted salt or inhibitor concentrations as an example for some of the tested systems. The idea is to drive an equation for each system at certain temperature and pressures which relates the water content to the concentration of salt or inhibitor in the system. These equations have been used to calculate the error of equivalent concentrations versus different values of errors in water contents. For instant, it is assumed the error in measuring water content to be ±1, ±2, ±5 and ±10 ppm_m; the resulted error in salt or inhibitor concentrations have been estimated by determining the corresponding concentration using the derived equations for different water content values ±1, ±2, ±5 and ±10 ppm_m. It should be mentioned that these equations may also cause some error in estimations; however, the deviation in the concentrations without considering any error in water contents values is not larger 0.5 mass%.

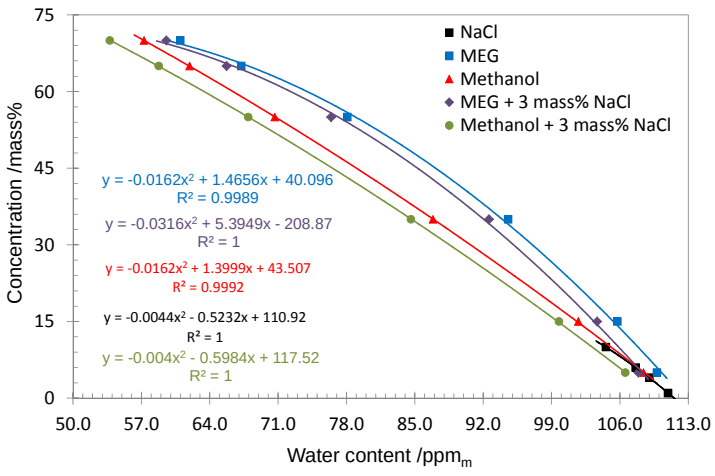

Figure 3.37 Equivalent predicted concentration of salt or inhibitors corresponding to the system water contents in the presence of natural gas 10 (composition given in appendix Table A.72) at 150 bara and 4 °C.

Table 3.28 presents the estimated NaCl concentrations considering ±1, ±2, ±5 and ±10 ppm_m error in water contents for 1, 4, 6 and 10 mass% NaCl systems in the presence of natural gas at 4 °C and 150 bara.

Table 3.28 Equivalent concentration of NaCl calculated based on ±1, ±2, ±5 and ±10 ppm_m error in water contents for 1, 4, 6 and 10 mass% NaCl systems in the presence of natural gas at 4 °C and 150 bara

Actual NaCl Concentration mass%	Water content ppm_m	Water content error ppm_m							
		+1	-1	+2	-2	+5	-5	+10	-10
1	111.0	N/A	2.3	N/A	3.8	N/A	8.0	N/A	13.7
4	109.0	2.2	5.2	0.6	6.6	N/A	10.4	N/A	15.5
6	107.6	4.3	7.1	2.8	8.4	N/A	12.0	N/A	16.6
10	104.6	8.5	10.9	7.2	12.0	2.9	15.0	N/A	18.7

For example, the predicted water content using the equation in Figure 3.37 for NaCl system is 109 ppm_m for 4 mass% NaCl. This table shows the calculated equivalent NaCl concentrations for 109 ±1, 109 ±2, 109 ±5 and 109 ±10 ppm_m water content values. +1 ppm_m error in water content in this system results in 1.8 mass% (4-2.2=1.8) deviation in predicted salt concentration. In the other words, if there is +1 ppm_m error in the water content, salt concentration is predicted to be 2.2 mass% instead of actual 4 mass%. Where the calculation results in negative value for concentrations, it is shown as not applicable (N/A) in the table. As it was expected, the deviation of the predicted concentrations from the actual concentration increase as the error in water content values increases. According to these results, the higher water contents than the actual value causes larger deviations in concentrations compared to the lower water contents than the actual values. Another point to mention is that the same value of water content error causes larger deviation from actual concentration in the lower concentrations compared to the higher concentrations.

It seems that the water content measurements should be fairly accurate in order to accurately calculate the salt concentration in the system. However, as it was mention before, the aim of this method is to determine hydrate phase boundary rather than concentration. Error analysis for hydrate phase boundaries have also been performed which will be presented separately at the end of this section.

Table 3.29 and Table 3.30 present similar error analysis for MEG and MeOH systems over a wide range on concentrations up to 70 mass% in the presence of natural gas and at 4 °C and 150 bara.

Table 3.29 Equivalent concentration of MEG calculated based on ±1, ±2, ±5 and ±10 ppm_m error in water contents for 5, 15, 35, 55, 65 and 70 mass% MEG systems in the presence of natural gas at 4 °C and 150 bara

Actual MEG Concentration mass%	Water content	Water content error ppm_m							
	ppm_m	+1	-1	+2	-2	+5	-5	+10	-10
5	109.8	3.6	7.8	1.4	9.8	N/A	15.7	N/A	25.0
15	105.8	11.9	15.9	9.9	17.8	3.7	23.3	N/A	31.9
35	94.6	32.2	35.4	30.5	37.0	25.4	41.4	16.2	48.2
55	78.1	54.7	56.8	53.6	57.9	50.0	60.7	43.5	64.8
65	67.2	64.7	66.1	63.9	66.8	61.4	68.6	56.7	70.9
70	61.0	68.7	69.7	68.1	70.2	66.3	71.4	62.5	72.7

Table 3.30 Equivalent concentration of MeOH calculated based on ±1, ±2, ±5 and ±10 ppm_m error in water contents for 5, 15, 35, 55, 65 and 70 mass% MeOH systems in the presence of natural gas at 4 °C and 150 bara

Actual methanol Concentration mass%	Water content	Water content error ppm_m							
	ppm_m	+1	-1	+2	-2	+5	-5	+10	-10
5	108.4	4.1	7.0	2.6	8.5	N/A	12.8	N/A	19.9
15	101.8	13.8	16.6	12.4	18.0	8.0	22.2	0.7	28.9
35	86.9	34.0	36.6	32.7	37.9	28.8	41.7	22.0	47.9
55	70.7	54.1	56.4	52.9	57.6	49.3	61.0	43.2	66.5
65	62.0	64.0	66.2	62.9	67.3	59.5	70.5	53.8	75.7
70	57.2	69.1	71.2	68.0	72.2	64.7	75.3	59.1	80.3

Table 3.31 and Table 3.32 present the error analysis for systems containing MEG with salt and MeOH with salt respectively. The salt concentration in these systems is assumed 3 mass%. The results suggest that presence of salt does not have noticeable effect on the error in inhibitor concentrations caused by the error in water contents.

Table 3.31 Equivalent concentration of MEG calculated based on ±1, ±2, ±5 and ±10 ppm_m error in water contents for 5, 15, 35, 55, 65 and 70 mass% MEG with 3 mass% NaCl systems in the presence of natural gas at 4 °C and 150 bara

Actual MEG Concentration mass%	Water content	Water content error ppm_m							
	ppm_m	+1	-1	+2	-2	+5	-5	+10	-10
5	107.9	3.8	8.0	1.7	10.0	N/A	16.0	N/A	25.3
15	103.7	12.5	16.4	10.5	18.3	4.3	23.9	N/A	32.5
35	92.6	32.6	35.8	30.9	37.3	25.8	41.8	16.6	48.6

55	76.4	54.8	56.9	53.6	57.9	50.0	60.8	43.5	65.0
65	65.7	64.8	66.2	64.0	66.9	61.5	68.8	56.6	71.2
70	59.6	68.9	69.9	68.3	70.4	66.4	71.7	62.5	73.1

Table 3.32 Equivalent concentration of MeOH calculated based on ±1, ±2, ±5 and ±10 ppm_m error in water contents for 5, 15, 35, 55, 65 and 70 mass% MeOH with 3 mass% NaCl systems in the presence of natural gas at 4 °C and 150 bara

Actual MEG Concentration mass%	Water content ppm_m	Water content error ppm_m							
		+1	-1	+2	-2	+5	-5	+10	-10
5	106.6	3.7	6.7	2.3	8.1	N/A	12.4	N/A	19.4
15	99.8	13.5	16.3	12.1	17.7	7.8	21.8	0.5	28.5
35	84.6	33.9	36.4	32.6	37.7	28.7	41.4	22.0	47.4
55	67.9	53.9	56.2	52.8	57.3	49.3	60.6	43.4	65.8
65	58.8	63.9	66.0	62.9	67.0	59.7	70.1	54.1	74.9
70	53.8	69.1	71.1	68.1	72.0	65.0	75.0	59.7	79.6

In general, from the error analysis for calculating salt or inhibitor concentrations, it can be concluded that errors larger than 2 ppm_m in measuring water content could result in significant error in calculated salt or inhibitor concentrations.

Figure 3.38 and Figure 3.39 illustrates the error analysis for determining hydrate phase boundaries using water content method for different systems containing salt and/or inhibitors in the presence of natural gas at 4 °C and 150 bara.

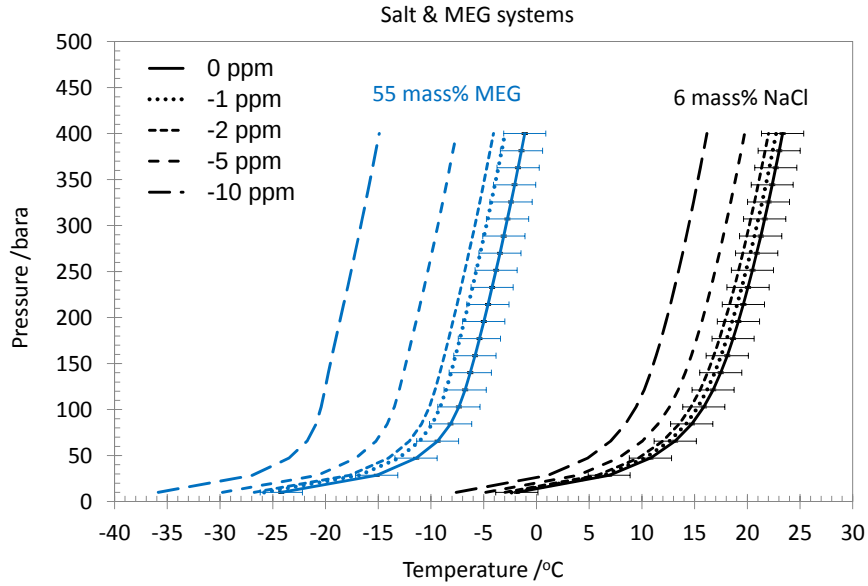

Figure 3.38 Error analysis of hydrate phase boundary based on -1, -2, -5 and -10 ppm_m error in water contents for salt or MEG systems in the presence of natural gas at 4 °C

and 150 bara. The error bars shown in the graph are 2 °C.

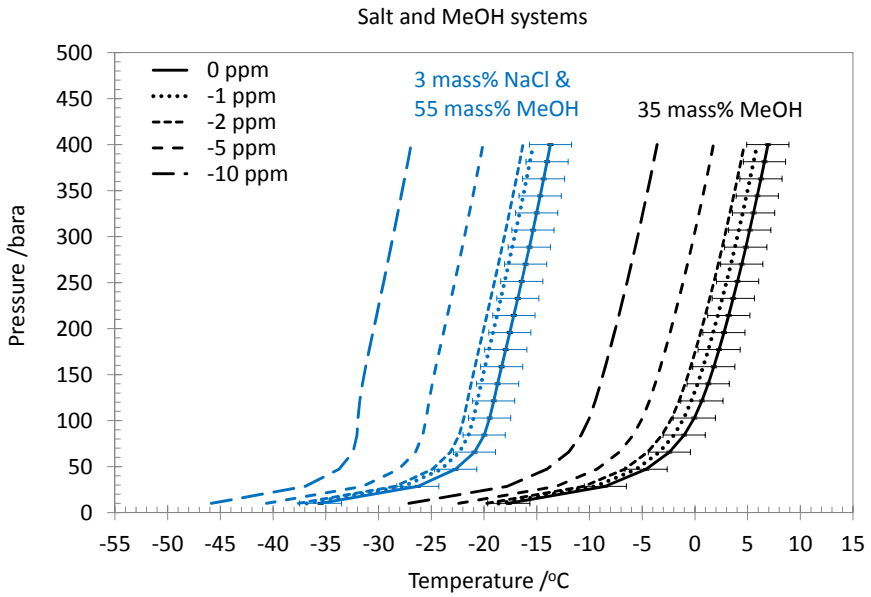

Figure 3.39 Error analysis of hydrate phase boundary based on -1, -2, -5 and -10 ppm_m error in water contents for salt and/or MeOH systems in the presence of natural gas at 4 °C and 150 bara. The error bars shown in the graph are 2 °C.

The error analysis shown in these figures are for the cases in which water contents are less than the actual values, i.e. the error is negative. Therefore, the calculated equivalent salt or inhibitor concentrations are higher than the actual values and consequently the predicted hydrate phase boundaries are shifted to the left (lower temperatures and higher pressures). For the cases in which the water contents are higher than the actual values, predicted hydrate phase boundaries are shifted to the right (not shown in these figures). Hydrate phase boundary errors increase as water content error increases. As can be seen from these figures, the same value of water content error causes larger error in the systems with higher concentrations of salt and/or inhibitors. For instance, in the 6 mass% NaCl system and 35 mass% MeOH system, 2 ppm water content error causes less than 2 ºC deviation in phase boundary while in the 55 mass% MEG system and 55 mass% MeOH and 3 mass% NaCl system, 2 ppm water content error results in deviations larger than 2 °C. Therefore, the error analysis has been shown for the higher concentrations and consequently for the worse cases in this report. In general, water content errors higher than 2 ppm causes

deviations larger than 2 °C in hydrate phase boundaries. Therefore, the accuracy of water content measurement setups for the purpose of this study should not be higher than 2 ppm_m. The following sections present the accuracy of the water content setups used in this study.

3.3.3. Water Content Measurement Setup – TDLAS (Tuneable Diode Laser Absorption Spectroscopy)

SpectraSensor S2000™ is one of the two experimental vapour phase water content measuring setups used in this work to assess their suitability for water content method. TDLAS is a technique for measuring concentration of certain species such as water vapour, methane and many more in a gaseous mixture using a tuneable diode laser and laser absorption spectroscopy. A basic TDLAS setup consists of a tuneable diode laser source, transmitting optics, optically accessible absorbing medium and receiving optics and detector. The wavelength of a diode laser is tuned over a particular absorption line of interest and the intensity of the transmitted radiation is measured. The transmitted intensity can be related to the concentration of the species present by the Beer-Lambert law, which states that when a radiation of wavenumber (v) passes through an absorbing medium, the intensity variation along the path of the beam is given by

$$I(v) = I_0(v)\exp(-\alpha(v)L) = I_0(v)\exp(-\sigma(v)NL) \qquad \text{Equation 3.27}$$

$I(v)$ is the transmitted intensity of the radiation after it has traversed a distance L through the medium, $I_0(v)$is the initial intensity of the radiation, $\alpha(v)$ is the absorbance of the medium, $\sigma(v)$ is the absorption cross-section of the absorbing species, N is the number density of the absorbing species. Figure 3.40 illustrates diagram of Beer–Lambert absorption of a beam of light as it travels through a medium of width L.

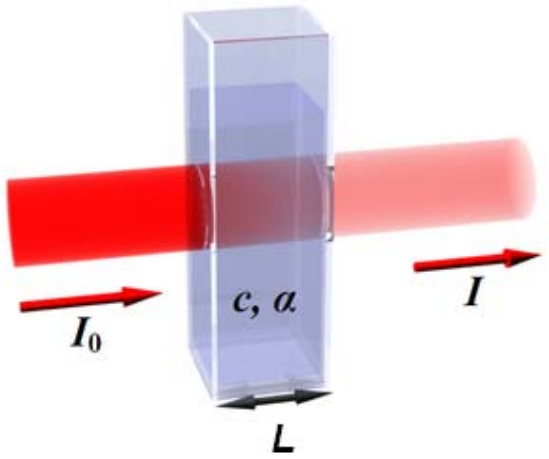

Figure 3.40 Diagram of Beer–Lambert absorption of a beam of light

The main disadvantage of absorption spectrometry (AS) as well as laser absorption spectrometry (LAS) in general is that it relies on a measurement of a small change of a signal on top of a large background. Any noise introduced by the light source or the optical system will deteriorate the detectability of the technique. There are basically two ways to improve on the situation; one is to reduce the noise in the signal, the other is to increase the absorption. The former can be achieved by the use of a modulation technique, whereas the latter can be obtained by placing the gas inside a cavity in which the light passes through the sample several times, thus increasing the interaction length

3.3.3.1. Experimental Setup

The experimental set-up consists of two parts: an equilibrium cell and a tuneable diode laser (TDL) device for measuring the water content in the vapour phase. The system under measurement is equilibrated at desire temperature and pressure condition in the equilibrium cell and the water content of the vapour phase is measured using TDLAS apparatus.

Equilibrium cell

The set-up is comprised of an equilibrium cell, cryostat, and temperature/pressure recording equipment controlled by a PC (Figure 3.41). The equilibrium cell is a piston-type titanium cylindrical pressure vessel with mixing ball, mounted on a

horizontal pivot with associated stand for pneumatic controlled rocking through 180 degrees. Its volume is variable (maximum effective volume of 300 ml). Rocking of the cell, and the subsequent movement of the mixing ball within it, provides mixing of the cell fluids. The outlet from the cell was connected to the gas inlet of a TDL absorption spectroscopy device. To avoid condensation all lines were heated and maintained at 80 °C. The system pressure of the equilibrium cell during the measurement is maintained by injecting water to the piston-side of the cell using a high pressure High Performance Liquid Chromatography (HPLC) pump.

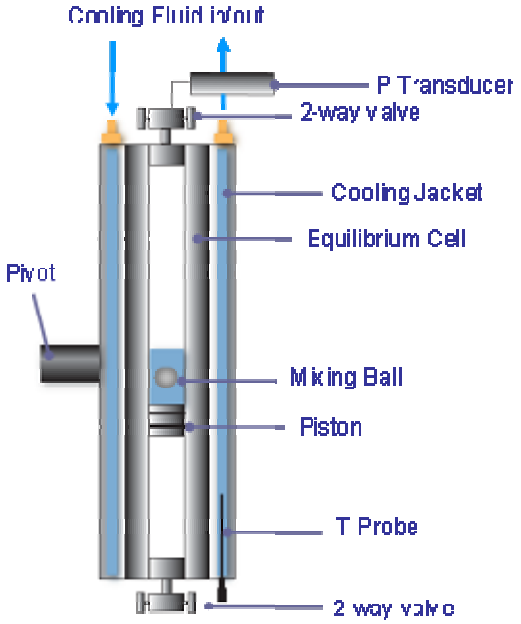

Figure 3.41 Schematic of the Equilibrium Cell

TDLAS Apparatus – SpectraSensorTM S2000

In this work a TDLAS setup from SpectraSensor™ called S2000 has been used. The analyser uses a robust TDL, emits near-IR light that passes through the gas in the sample cell of the analyser. The analyser scans the laser wavelength across the range where H_2O molecules absorb the laser light or energy, reducing the amount of light that passes through to the detector. The ratio of the light absorbed by the water vapour line to the light on the detector when the wavelength is off the water line is proportional to the water vapour concentration. The higher the concentration of H_2O present in the gas sample, the more absorption of light. This ratio is further corrected

for variations in temperature and pressure in the measurement cell. Because the analyser measures the absorption in the volume of the gas, the measurement is more accurate than surface-based sensors that are subject to surface contamination.

This apparatus is able to measure water content from 10 to 422 ppm_v. The accuracy for water content measurement is 2 % of the reading; however it would not exceed ±4 ppm_v.

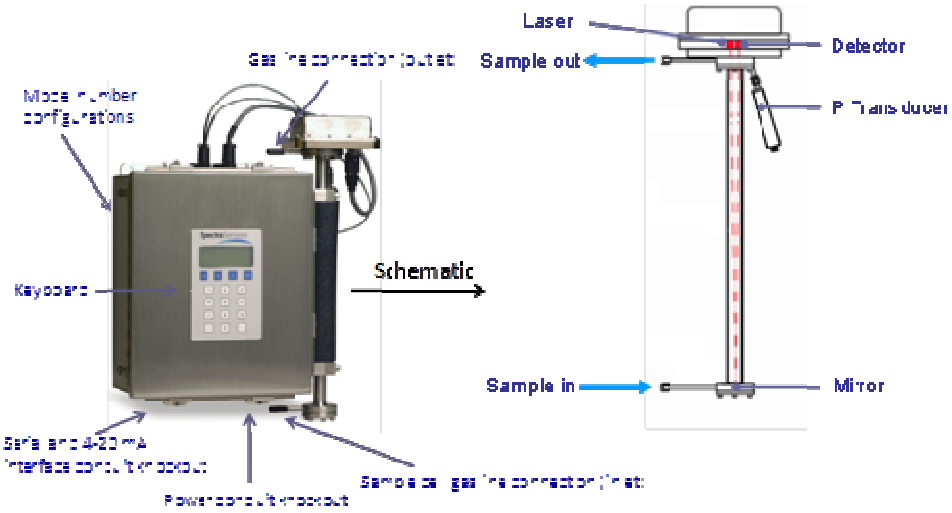

Figure 3.42 Picture and schematic view of SpectraSensor™ S2000

3.3.3.2. Experimental Materials and Procedures

The material used were ultra-high purity grade methane gas (99.95%) and natural gas supplied by BOC, high purity MeOH, MEG and NaCl (99.9 %) supplied by VWR and deionised water.

The cell was vacuumed and the experimental fluid (different salt or MEG or MeOH solutions depending on each experiment) was preloaded to the cell and the cell was then pressurised with methane to reach test pressure at the desired temperature. The system was kept at this condition for sufficient time to establish equilibrium and ensure no leakage. For measuring the vapour phase water content, the outlet of the cell was connected to the inlet of the TDLAS apparatus and by opening the valves the gas was let flowing slowly through the measurement cell. Prior to each measurement TDLAS was purged with dry methane to avoid any possible remains in the cell. To

maintain the cell pressure, water was used to displace the piston and consequently reduce the cell volume. Water was injected into the piston side of the cell using a HPLC (High Performance Liquid Chromatography) pump. To avoid water condensation along the line connecting the cell outlet to the TDLAS inlet, the line was kept at 85 °C using a heat tracing element.

3.3.3.3. Results and Discussions

Methane systems

In this section, three series of experiments were conducted with different concentrations of salt (0, 5, 10 and 15 mass%), MEG (0, 5, 15, 30 and 50 mass%) and methanol (0, 5, 10, 20, 30 and 50 mass%) for methane system. Each measurement was repeated 10 times and the results are averages of all measurements for each system/concentration. In each test, the water content was measured experimentally and also predicted using our in-house thermodynamic model. Using the measured water contents and knowing the system, the equivalent salt/inhibitor concentration was estimated using the model. Therefore, it is possible to predict hydrate dissociation temperature for a given pressure using the models. The deviations between actual and equivalent salt/inhibitor concentration and also deviations between predicted hydrate dissociation temperatures for actual and equivalent salt/inhibitor concentration are presented in Table 3.23 and Figure 3.43. These experiments have been carried out at 103.4 bara and 20 °C. This temperature and pressure condition is close to the first stage separator condition in most of the fields.

Table 3.33 summarises the result for salt system. The first system tested was deionised water without any NaCl. The measured and predicted water contents for this system are 337 and 340.9 ppm_m respectively. The deviation between measured and predicted water content is 3.9 ppm_m which results in 2.1 mass% deviation in equivalent NaCl concentration. Since the aim of this method is determining hydrate phase boundary, the predicted hydrate equilibrium temperatures for the actual and equivalent salt concentration are also compared in this table. These values for the deionised water system is 13.2 and 12.4 °C respectively resulting in 0.8 °C deviation. The deviation between predicted hydrate equilibrium temperature for actual and equivalent concentrations for 5, 10 and 15 mass% NaCl are 0.9, 0.4 and 0.9 °C respectively.

These results suggest that TDLAs apparatus potentially could be used for brine-methane systems in water content method.

Table 3.33 Experimental and calculated results (hydrate dissociation temperature and equivalent concentration) for methane and salt (NaCl) system at 103.4 bara and 20 °C

Actual concentration/ mass%	0	5	10	15
Measured water content/ ppmm	337	335.3	321.8	303.2
Predicted water content using in-house model / ppmm	340.9	331.2	320.0	306.7
Equivalent concentration/ mass%	2.1	3.0	9.3	16.2
Deviation of actual and equivalent concentration/ mass%	2.1	2.0	0.7	1.2
Dissociation temperature for actual concentration/ °C	13.2	11.1	8.5	5.4
Dissociation temperature for equivalent concentration/ °C	12.4	12.0	8.9	4.5
Deviation of dissociation temperature for actual and equivalent concentration/ °C	0.8	0.9	0.4	0.9

Figure 3.43 illustrates extends these evaluation to wider range of pressures from 20 to 400 bara. As can be seen the deviation between the model and water content method using TDLAS set up in salt-methane system is less than 1 °C.

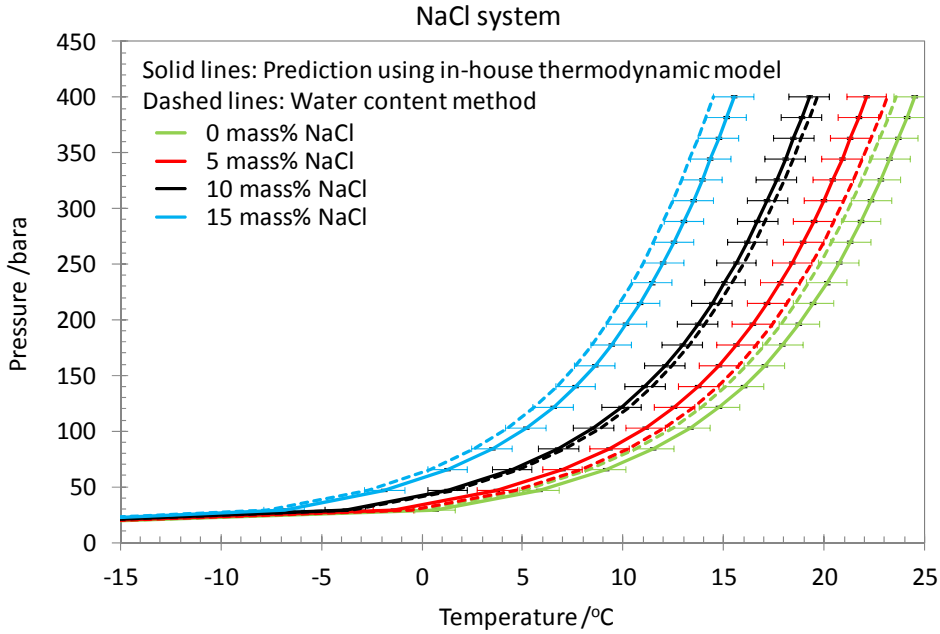

Figure 3.43 Evaluation of hydrate phase boundaries for salt-methane system determined with water content method using TDLAS apparatus. The error bars shown in this graph are 1 °C.

Table 3.34 and Figure 3.44 show the results of evaluating water content method using TDLAS apparatus for different concentrations of MEG systems. As can be seen, there is very good agreement between water content method and the model up to 30 mass% MEG. The deviation between the method and model was less than 0.1 °C for these concentrations. For very high MEG concentration, 50 mass%, the deviation is about 1.9 °C.

Table 3.34 Experimental and calculated results (hydrate dissociation temperature and equivalent concentration) for methane and MEG system at 103.4 bara and 20 °C

Actual concentration/ mass%	5	15	30	50
Measured water content/ ppmm	336	324	300	251
Predicted water content using in-house model/ ppmm	335.6	323.5	300.2	256.2
Equivalent concentration/ mass%	4.7	14.7	30	52
Deviation of actual and equivalent concentration/ mass%	0.3	0.3	0.0	2.0
Dissociation temperature for actual concentration/ °C	12.1	9.3	3.4	-9.5
Dissociation temperature for equivalent concentration/ °C	12.2	9.4	3.4	-11.3
Deviation of dissociation temperature for actual and equivalent concentration/ °C	0.1	0.1	0.0	1.8

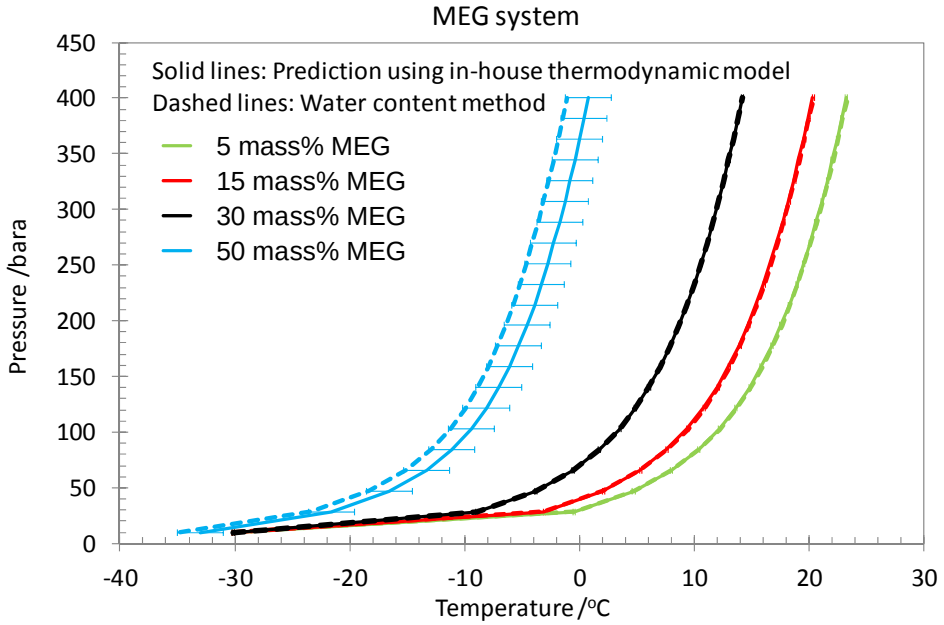

Figure 3.44 Evaluation of hydrate phase boundaries for MEG-methane system determined with water content method using TDLAS apparatus. The error bars shown in this graph for 5, 15 and 30 mass% MEG concentrations are 0.1 °C and for 50 mass% MEG is 2 °C.

The results for 0, 5, 10, 20, 30 and 50 mass% MeOH systems are shown in Table 3.35 and Figure 3.45. As can be seen from the table, the difference between measured and predicted water content values are ~ 5-15 ppm_m. These large differences results in large deviation between actual and equivalent MeOH concentrations and consequently large deviation between hydrate equilibrium temperatures. These results suggest that TDLAS apparatus is not vary suitable for methanol system. The reason could be attributed to the high volatility characteristic of methanol. The presence of considerable amount of methanol in vapour phase could affect the intensity of the light travelling through measuring cell.

Table 3.35 Experimental and calculated results (hydrate dissociation temperature and equivalent concentration) for methane and MeOH system at 103.4 bara and 20 °C

Actual concentration/ mass%	5	10	20	30	50
Measured water content/ ppmm	306.6	315	286	269	238.6
Predicted water content using in-house model/ ppmm	331.5	321.8	301.4	279.7	232.7
Equivalent concentration/ mass%	17.5	13.3	27.0	34.8	47.6
Deviation of actual and equivalent concentration/ mass%	12.5	3.3	7.0	4.8	2.4
Dissociation temperature for actual concentration/ °C	11.1	8.7	3.4	-3.0	-19.4
Dissociation temperature for equivalent concentration/ °C	4.8	7.0	-1.0	-6.4	-17.1
Deviation of dissociation temperature for actual and equivalent concentration/ °C	6.3	1.7	4.4	3.4	2.3

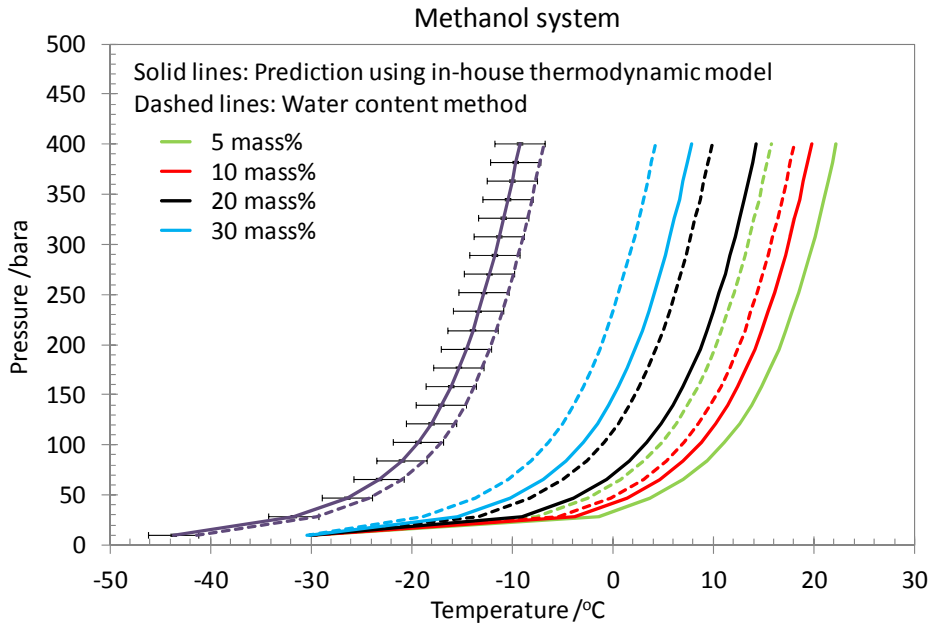

Figure 3.45 Evaluation of hydrate phase boundaries for MeOH-methane system

determined with water content method using TDLAS apparatus. The error bar shown in this graph 2.5 °C.

Natural gas systems

The main objective of this section is to evaluate the accuracy and suitability of the TDLAS setup for being used along with water content method at more realistic conditions, i.e. in presence of natural gas and at different temperatures. The reason for conducting the experiments at different temperatures is to investigate if and how temperature changes along the pipeline can affect the results of water content method. As it was mentioned before, water content depends on temperature; therefore, measurements were carried out at three different temperatures. For each temperature, the equivalent inhibitor concentrations were calculated using our in-house thermodynamic model at that temperature. Two series of experiments were conducted in this section for MEG and methanol systems in presence of synthetic Petronas produced water (Table A.65) and natural gas (Table A.72) at 105.8 bara and 10, 15 and 20 °C. Hydrate inhibitor (MEG or methanol) concentration in these tests were 20 mass% in both cases.

Table 3.36 summarises the results for MEG system. As can be seen from this table, the deviation between prediction using the model and results of water content method using TDLAS setup is not negligible. For instance, in the case of 15 °C, the measured and predicted water content values are 228.1 and 220.8 ppm (ppm mole) respectively. The equivalent MEG concentration is 13.7 mass% which is 6.3 mass% lower than the actual MEG concentration (20 mass%). Deviation between the predicted hydrate equilibrium temperatures for actual and equivalent MEG concentrations is 2.3 °C. This deviation is even larger in the case of measurements at 10 and 20 °C. Figure 3.46 illustrates hydrate phase boundaries for three different temperatures at which water contents were measured. The error bar shown in this graph is 5 °C.

Table 3.36 Experimental and calculated results (hydrate dissociation temperature and equivalent concentration) for natural gas and 20 mass% MEG system in presence of synthetic Petronas produced water at 105.8 bara and different temperatures of 10, 15 and 20 °C

Measurement temperature /ºC	10	15	20
Measured water content /ppmm	172.3	228.1	280.3
Predicted water content using HWHYD2.2 /ppmm	162.5	220.8	296.6
Equivalent concentration /mass%	8	13.7	29.2
Deviation of actual and equivalent concentration /mass%	12	6.3	9.2
Dissociation temperature for actual concentration /ºC	8.2	8.2	8.2
Dissociation point for equivalent concentration /ºC	12.4	10.5	4
Deviation of dissociation temperature for actual and equivalent concentration /ºC	4.2	2.3	4.2

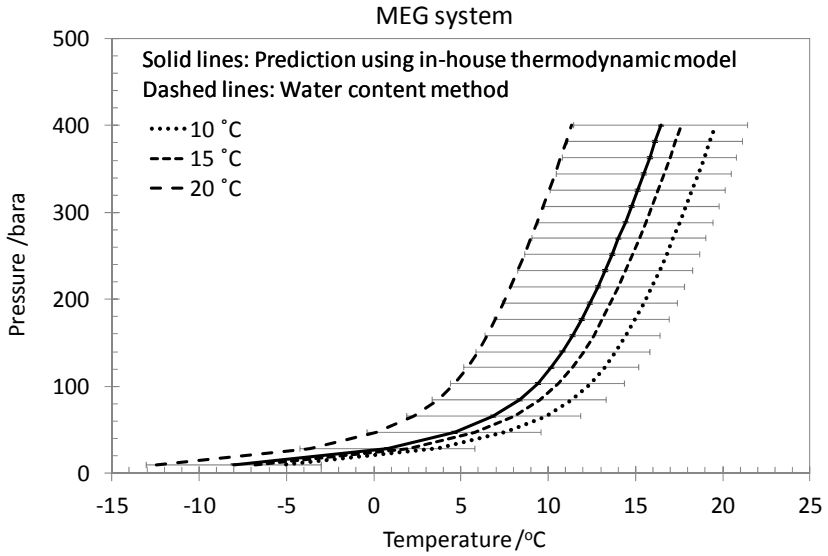

Figure 3.46 Evaluation of hydrate phase boundaries for MEG-natural gas system in the presence of synthetic Petronas produced water determined with water content method using TDLAS apparatus. The error bar shown in this graph 5 °C.

Table 3.37 and Figure 3.47 presents the results for 20 mass% methanol systems in presence of synthetic Petronas produced water and natural gas at 105.8 bara and 10, 15 and 20 °C. The deviation between the predicted hydrate phase boundaries using actual and equivalent inhibitor concentration in methanol system is in average less than MEG system. However, the deviations are not negligible.

Table 3.37 Experimental and calculated results (hydrate dissociation temperature and equivalent concentration) for natural gas and 20 mass% methanol system in presence of synthetic Petronas produced water at 105.8 bara and different temperatures of 10, 15 and 20 °C

Measurement temperature /ºC	10	15	20
Measured water content /ppmm	159.8	219.2	277.4
Predicted water content using HWHYD2.2 /ppmm	154.4	210.1	282.9
Equivalent concentration /mass%	15.7	14.5	22.5
Deviation of actual and equivalent concentration /mass%	4.3	5.5	2.5
Dissociation temperature for actual concentration /ºC	4.3	4.3	4.3
Dissociation point for equivalent concentration /ºC	6.8	7.5	2.7
Deviation of dissociation temperature for actual and equivalent concentration /ºC	2.5	3.2	1.6

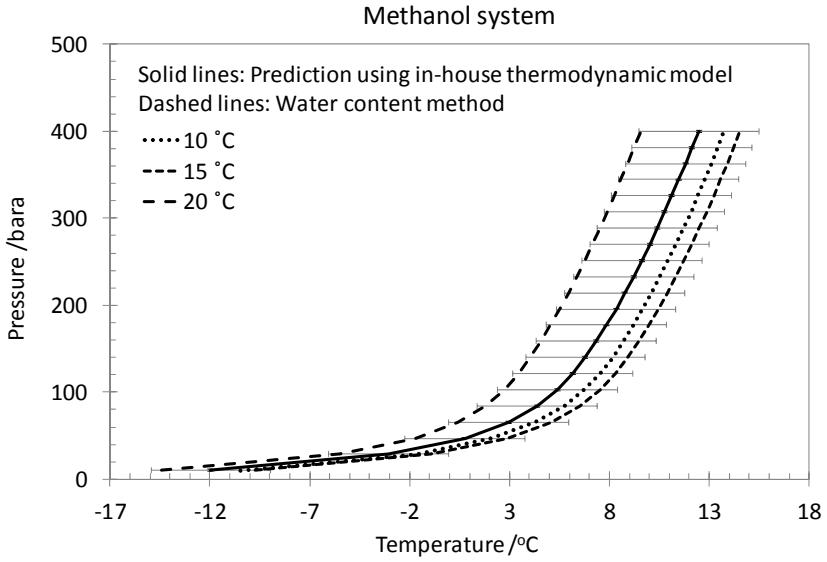

Figure 3.47 Evaluation of hydrate phase boundaries for methanol-natural gas system in the presence of synthetic Petronas produced water determined with water content method using TDLAS apparatus. The error bar shown in this graph 3 °C.

In general, it can be concluded that deviations are larger in natural gas systems in comparison with methane systems. The reason could be that the tested TDLAS SpectraSensor^{TM} S2000 set up is tuned for water molecules in systems which methane is the background gas. It is likely that the presence of other components of natural gas affect the intensity of the light travelling through measuring cell by affecting laser absorption. In the presence of methane, the deviation between results was larger in methanol system compared to MEG system while in the presence of natural gas; this deviation is larger in MEG system in comparison with methanol system. The reason could be attributed to the high volatility characteristic of methanol. Presence of

methanol or natural gas components in vapour phase can affect the water content. It might be possible that coexistence of methanol and natural gas components neutralise or impede the effect.

To summarise the suitability of the tested TDLAS – SpectraSensor^{TM} S2000 set up for water content method, based on the experimental results in this work, it can be concluded that TDLAS system could work fairly for methane system in presence of MEG and/or salt, the accuracy will decrease if MEG is replaced with methanol in methane system. Further investigation showed that the results are being affected in presence of natural gas. TDLAS results for natural gas in presence of MEG and salt showed a less accuracy and bigger deviation in hydrate phase boundary. The result for natural gas and methanol system was slightly better. To reduce the deviation, it could be possible to tune the TDLAS for methanol or natural gas system; however, because the objective of this study was to find a suitable commercial device which can be employed in water content method, therefore, it was decided to test another device which is detailed in the following section.

3.3.4. Water Content Measurement Setup – Vaisala HMT360 humidity

In this work Vaisala HMT360 is used to measure water content. The humidity/water content measurement in this setup is based on capacitance method presented in section 3.2.3. Figure 3.48 shows the structure of the sensor.

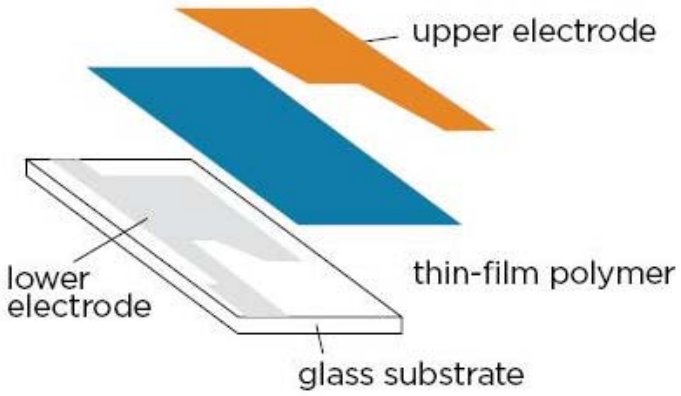

Figure 3.48 Vaisala HMT360 sensor structure

The main part of the sensor is a thin-film polymer capacitance which either absorbs or releases water vapour as the relative humidity of the ambient air rises or drops. The dielectric properties of the polymer film depend on the amount of water contained in it. The dielectric properties of the film change when relative humidity changes and as result, the capacitance of the sensor changes. The electronic parts of the instrument measure the capacitance of the sensor and convert it into equivalent humidity/water content reading. As it is shown in Figure 3.48, thin-film polymer is between two electrodes. The capacitor value of the capacitance is surface value of the electrode multiplied by dielectric of the material between two electrodes (here is the thin-film polymer) divided by electrodes distance from each other. In this sensor, electrodes surface and distance is constant. Thin-film polymer is very sensitive to moisture and consequently the capacitance of the capacitor becomes a function of the moisture. Therefore, by measuring the capacitance values with the electronics and using calibration data, the humidity and water content can be determined.

HMT360 setup is calibrated for natural gas system and this point can be considered as one of its advantages for being used along with the water activity method. Like all capacitance based measurements, volatile components like methanol would significantly affect the measurements and the accuracy, so this could be a negative point for HMT360 because it could not be used for methanol systems. Therefore, in this work, the applicability of HMT360 setup will be investigated in MEG and salt systems.

3.3.4.1. Experimental Setups and Procedures

Two experimental setups were used in this part. The experiments in static condition were carried out in a 300 ml high pressure set-up and the experiments in flowing condition in a 2300 ml high pressure set-up. Details of the experimental setups are given below.

All static condition experiments were conducted in a high-pressure rig specially designed and built by the Centre for Gas Hydrate Research. The rig is cylindrical in shape and made of stainless steel (Figure 3.49). The cell volume is about 300 ml and it can be operated up to 6000 psia between -40 and 50 °C. The equilibrium cell is held in a metallic jacket heated or cooled by a constant–temperature liquid bath. The

temperature of the cell is controlled by circulating coolant from a cryostat within the jacket surrounding the cell. The cryostat is capable of maintaining the cell temperature within 0.05 °C. One platinum resistance probe is placed inside the equilibrium cell and monitors the temperature; the probe is connected directly to a computer for direct acquisition. The calibrated probe has a reported accuracy of ± 0.1 °C. To achieve good temperature stability, the jacket is insulated with polystyrene board and the pipes (which connect it to the cryostat) are covered with plastic foam. The pressure is measured by means of a pressure transducer mounted directly on the cell and connected to the same data acquisition unit. This system allows real time readings and storage of temperatures and pressures throughout the different isothermal runs. Pressure measurement uncertainties are estimated to be within 0.1 bar in the 0-400 bar range. To achieve a faster thermodynamic equilibrium and to provide a good mixing of the fluids, the cell is equipped with a magnetic stirrer with adjustable rotation speed (i.e., rpm) can be used to agitate the test fluids. A HMT360 Vaisala humidity transmitter is directly mounted on the top of the cell. The transmitter can be operated up to 160 bar and from –60 to 20 °C. The calibrated probe has a reported dew point temperature accuracy of ± 1 °C over the temperature range.

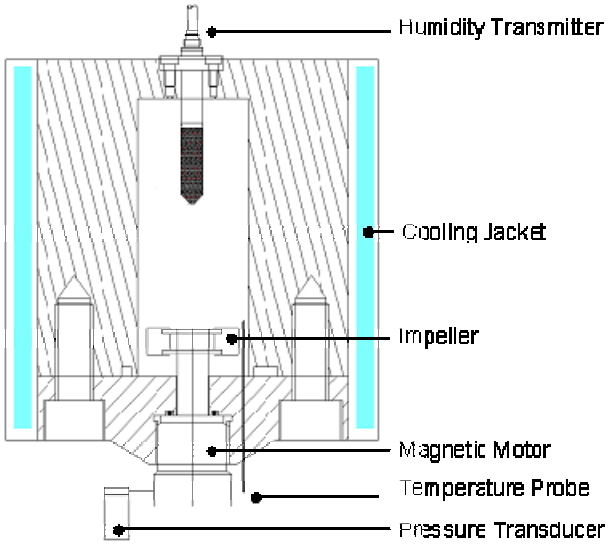

Figure 3.49 Schematic of the water content rig

For flowing condition a 2230ml cell was used to equilibrate samples. A small cell was especially designed to accommodate the HMT360 Vaisala humidity transmitter as

shown in Figure 3.50. The setup is equipped with a high pressure piston cylinder for controlling the flowing condition and maintaining the pressure.

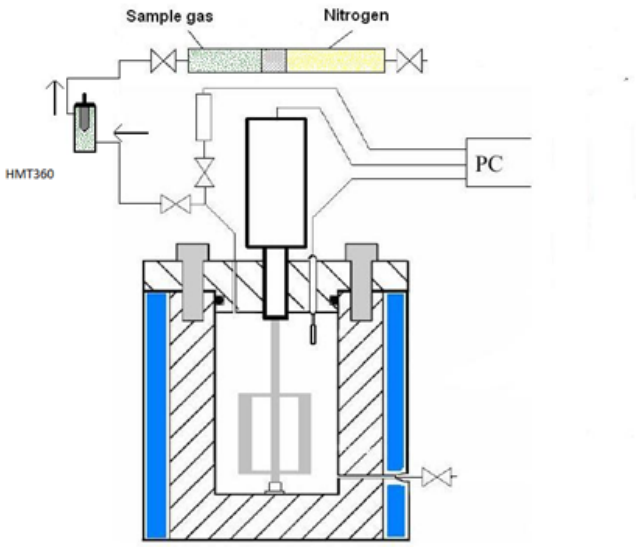

Figure 3.50 Schematic of the water content rig in flowing condition

To conduct each experiment, the equilibrium cell was preloaded with 100 ml of aqueous solution. Following vacuuming the cell, natural gas was injected to the cell to reach the desired pressure. The temperature system was kept at this condition for a day to reach equilibrium. To do the measurements, the valve of the measuring cell was opened gradually to flow the gas through the measuring cell. At the same time the inlet valve for piston cylinder was opened to maintain the system pressure and to avoid considerable change in pressure. The entire measuring path was insulated to reduce temperature changes. Every 2 minutes a reading was taken and the average of all reading was considered as finial reading. The pressure change was very small to avoid change on water content measurements. All the experiments were conducted twice to ensure reliable results.

3.3.4.2. Results and Discussions

Static condition experiments

Two series of experiment were conducted in this part; salt systems with 0, 5, 10 and 15 mass% NaCl and MEG systems with 5, 10, 20, 30 and 50 mass% MEG. Both systems were in the presence of a standard natural gas with composition given in (Table A.55).

Table 3.38 and Figure 3.51 present the result for NaCl systems. As can be seen, there is a very good agreement between the predictions for actual and equivalent concentrations. The maximum deviation between predicted hydrate phase boundaries for actual and equal concentrations is ±0.3 °C.

Table 3.38 Experimental and calculated results (hydrate dissociation temperature and equivalent concentration) for natural gas and varying NaCl concentrations at 103.4 bara and 20 °C.

Actual concentration/ mass%	0	5	10	15
Measured water content/ ppmm	344.9	334.3	323.1	311.2
Predicted water content using in-house model / ppmm	345.4	335.4	323.8	309.7
Equivalent concentration/ mass%	0.2	5.5	10.25	14.6
Deviation of actual and equivalent concentration/ mass%	0.2	0.5	0.25	0.4
Dissociation temperature for actual concentration/ °C	18.7	16.6	14	10.9
Dissociation temperature for equivalent concentration/ °C	18.6	16.4	13.9	11.2
Deviation of dissociation temperature for actual and equivalent concentration/ °C	0.1	0.2	0.1	0.3

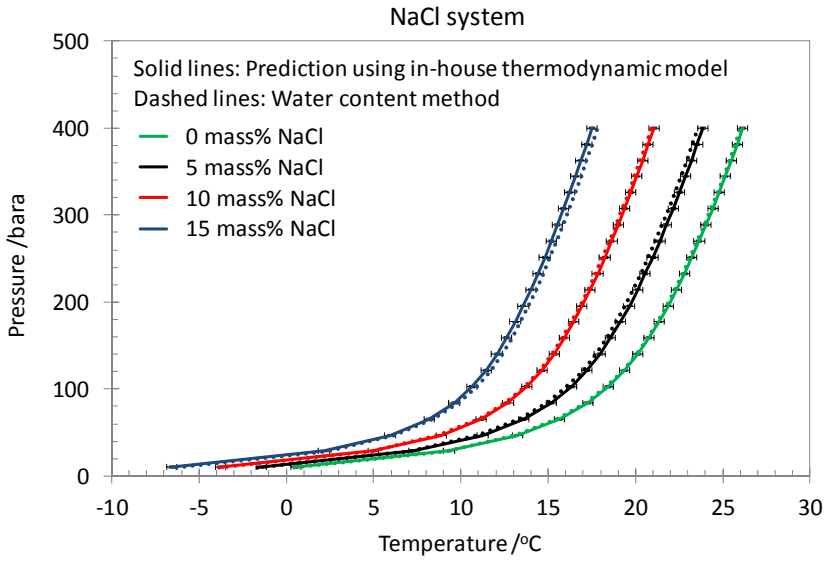

Figure 3.51 Evaluation of hydrate phase boundaries for varying concentrations of NaCl system determined with water content method using HMT360 Vaisala humidity transmitter. The error bar shown in this graph ±0.3 °C.

As with NaCl systems, a very good agreement between predicted hydrate phase boundaries for actual and equal concentrations was observed for MEG systems below 50 mass% concentrations and maximum deviation was ±0.3 °C. For 50 mass% MEG concentration the deviation at 103.4 bara and 20 °C was 1.2 °C and this did not exceed 1.5 °C over a wide range of temperature and pressure. Table 3.39 and Figure 3.52 illustrate the result for MEG systems.

Table 3.39 Experimental and calculated results (hydrate dissociation temperature and equivalent concentration) for natural gas and varying MEG concentration at 103.4 bara and 20 °C.

Actual concentration/ mass%	5	10	20	30	50
Measured water content/ ppmm	339.3	332.6	320.9	303.7	255.5
Predicted water content using in-house model/ ppmm	340.1	334.3	320.7	304.2	259.6
Equivalent concentration/ mass%	5.7	11.3	19.6	30.2	51.5
Deviation of actual and equivalent concentration/ mass%	0.7	1.3	0.4	0.2	1.5
Dissociation temperature for actual concentration/ °C	17.6	16.4	13.3	9.4	-2.7
Dissociation temperature for equivalent concentration/ °C	17.4	16.0	13.4	9.4	-3.9
Deviation of dissociation temperature for actual and equivalent concentration/ °C	0.2	0.4	0.1	0.0	1.2

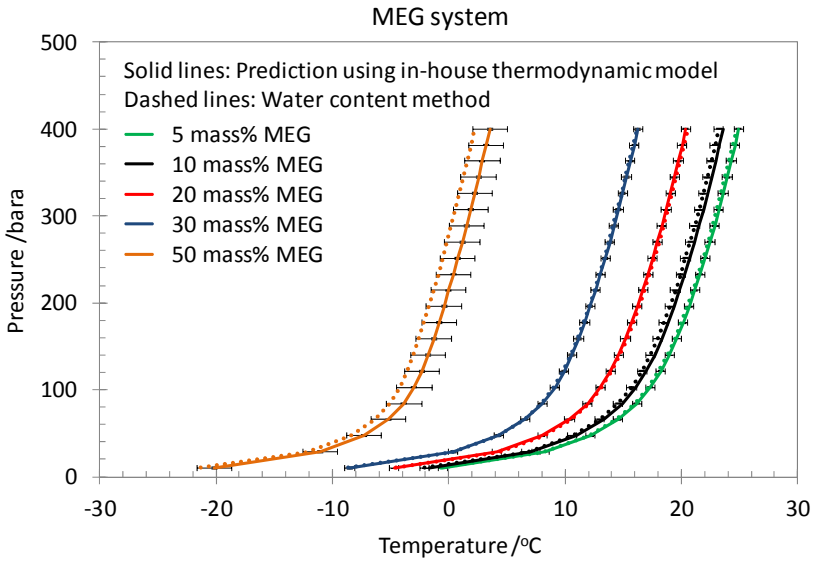

Figure 3.52 Evaluation of hydrate phase boundaries for varying concentrations of MEG system determined with water content method using HMT360 Vaisala humidity transmitter. The error bar shown in this graph for MEG concentrations below 50 mass% is ±0.4 °C and for 50 mass% MEG is ±1.5 °C.

Flowing condition experiments

To further evaluate the performance of the HMT360 Vaisala humidity transmitter closer to real conditions, tests were also carried out in gas flowing condition. 20 mass % of MEG solution was used in presence of the Petronas produced water and natural gas at 103.4 bara and different temperatures, i.e. 10, 15 and 20 °C. Table 3.40 summarises the results. It shows that the equivalent concentrations are very close to the actual ones and consequently the hydrate dissociation temperatures are in very good agreement with the ones obtained from actual concentrations. Figure 3.53 extend the predictions over a wider range of temperature (-10 to 15 °C) and pressure up to 400 bara. In general it can be concluded that the HMT360 Vaisala humidity transmitter is fairly capable for measuring water content in natural gas system in presence of salt and MEG.

Table 3.40 Experimental and calculated results (hydrate dissociation temperature and equivalent concentration) for natural gas and 20 mass% MEG system in presence of synthetic Petronas produced water at 103.4 bara and different temperatures of 10, 15 and 20 °C

Measurement temperature /ºC	10	15	20
Measured water content /ppmm	167.8	227.4	303.3
Predicted water content using HWHYD2.2 /ppmm	166.4	226.2	304.2
Equivalent concentration /mass%	18.5	19.1	20.6
Deviation of actual and equivalent concentration /mass%	1.5	0.9	0.6
Dissociation temperature for actual concentration /ºC	9.5	9.5	9.5
Dissociation point for equivalent concentration /ºC	10.2	9.9	9.3
Deviation of dissociation temperature for actual and equivalent concentration /ºC	0.7	0.4	0.2

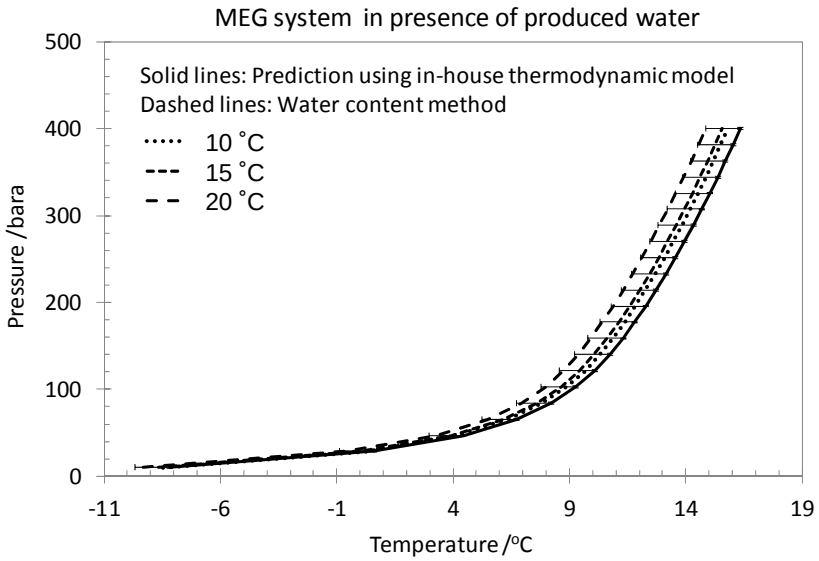

Figure 3.53 Evaluation of hydrate phase boundaries for MEG-natural gas system in the presence of synthetic Petronas produced water determined using with water content method using HMT360 Vaisala humidity transmitter. The error bar shown in this graph is -2 °C.

3.4. CONCLUSIONS

In this chapter the aim was to developed methods for monitoring hydrate phase boundary based on measuring water activity of aqueous phase and water content of vapour phase.

In the water activity section, a general correlation was developed which relates water activity of aqueous phase to hydrate suppuration temperature. The correlation was extensively evaluated with different systems including different methanol or MEG mixtures in presence and absence of different types and concentrations of salts or synthetic/real produced water. Different standard natural gases were also used in this study. The results were compared with our in-house thermodynamic model. The results showed that the correlation can be used for different mixture types and has a very good accuracy (0.5 °C in HSZ). To further validate the correlation and the model, both were compared with literature data and very good agreement was observed. This method was further improved by taking into account the thermodynamic properties of the inhibitors in the pseudo concentration method. The required information for this method is the type of injected inhibitor and a rough estimation of the salinity of the

aqueous phase which should be available in almost all fields. The results showed that this method was significantly improved.

Water content method was introduced as a complementary technique for water activity method for the cases that online monitoring is required or where there is no access to aqueous phase sample. In this method water content in vapour phase was related to an equivalent concentration of inhibitor in aqueous phase by using the in-house model. The equivalent concentrations were used to predict the hydrate phase boundary. Applicability of this method was extensively evaluated in presence of different salt and thermodynamic inhibitors. The results showed that this method could be used for online hydrate phase boundary monitoring. However, the accuracy of water content measurement setups for the purpose of this study should not be higher than 2 ppm_m. Therefore, two different commercial setups (TDLAS - SpectraSensor S2000^{TM} and HMT360 Vaisala humidity transmitter) for measuring vapour phase water content were tested in this study to evaluate their applicability for being used along with water content method. The results showed about 2 ºC deviations in hydrate phase boundary when using TDLAS setup in methane system in presence of MEG and/or salt. This deviation was slightly higher for methane-methanol system. TDLAs setup was not accurate enough for natural gas systems. The second water content measurement setup evaluated in this study was HMT360 Vaisala humidity transmitter. This setup was tested for natural gas systems for which the TDLAS setup was not suitable. The results showed that this setup is very accurate for measuring water content in presence of MEG and salt in natural gas system. The predicted hydrate phase boundaries were in very good agreement with the hydrate phase boundary predicted using actual concentrations. The accuracy achieved by using this device was better than 1 ºC in hydrate phase boundary however at high concentration of MEG the deviation slightly increased. The HMT360device was also tested in flowing condition at different temperatures. Results were fairly acceptable with less than º2 C deviation in phase boundary. The results showed that the HMT360 is very accurate for measuring water content in presence of MEG and salt in natural gas systems. The predicted hydrate phase boundaries with this method were in very good agreement with the ones predicted using actual concentrations. The accuracy achieved by using this device was better than 1 °C in hydrate phase boundary however at high concentration of MEG (50

mass%) the deviation slightly increased. This setup was further evaluated at condition very close to real systems and condition, i.e. for MEG-natural gas system in the presence of synthetic produced water under flowing condition. The results were fairly acceptable with less than 2 °C deviation in phase boundary.

CHAPTER 4. INITIAL HYDRATE FORMATION DETECTION TECHNIQUE BASED ON HYDRATE MEMORY

4.1. INTRODUCTION

Current industrial solution for avoiding hydrate problems are based mainly on injection of thermodynamic hydrate inhibitors and/or low dosage hydrate inhibitors (LDHIs) at upstream without systematic downstream monitoring. In Chapters 2 and 3, two methods were introduced to determine hydrate safety margin. However, these monitoring techniques are based on analysis of downstream samples, therefore, hydrate blockage risks cannot be eliminated completely for particular cases. Moreover, as oil and gas production expands to deeper waters and colder environments, the production facilities will require more security against hydrate problems. As a complementary option, in order to give operators adequate time to take proper action prior to a hydrate blockage formed, techniques were developed for detecting early signs of hydrate formation.

4.1.1. Hydrate Memory

To be able to detect initial signs of hydrate formation, early warning techniques need to pick up the footprints of early hydrate formation. Hydrate memory could be used as such a footprint of hydrate formation. It is well known that, hydrate can form much earlier in a system where gas hydrates were previously formed and dissociated under certain thermodynamic conditions. This is attributed to a phenomenon that is called

hydrate memory. In other words, the presence of hydrate memory can makes hydrates form more easily from gas and water mixture which has been resulted from dissociation of hydrates, compared with the case where hydrate is formed for the first time from fresh water and gas mixture without any previous hydrate experience/history. This effect suggests that hydrate formation can be promoted by multiple dissociation and reformation processes (Sloan and Koh, 2008).

Researchers worldwide have studied hydrate memory effect from different aspects. While some of the reports suggest that this phenomenon is due to dissolved gas remaining in solution after hydrate dissociation (Rodger, 2000), other studies relate this memory to residual structures (i.e., partial hydrate cages or polyhedral clusters) (Lederhos et. al, 1996, Takeya et al., 2000, Ohmura et al., 2003) or persistent fine hydrate crystallites (Buchanana, et al., 2005). According to Bishnoi and co-workers (Parent et al., 1996, Vysniauskas et al., 1983), the induction time for nuclei formation is affected by the history of aqueous phase. Takeya et al. (2000) measured nucleation rates of CO_2 hydrates using water from melted ice and non-frozen water. They observed that the nucleation rate was one order of magnitude larger when formed from melt water, which proposed a freezing-memory effect of water on nucleation. This effect faded when the melt water was heated up to 25 °C and conversely, it was enhanced when saturated with CO_2. Hwang et al. (1990) studied crystallisation and crystal growth of methane hydrates and observed that hydrates only formed when melting ice was present. They concluded that melting ice provides a template for hydrate nucleation and also a heat sink for absorbing hydrate formation heat. Sloan et al. (1998) reported residual structures after hydrate dissociation by measuring apparent viscosity (using a rolling-ball sapphire viscometer) upon hydrate formation and dissociation. Based on this observation, they recommended promptly removing of dissociated hydrate water from pipeline for preventing rapid reformation of hydrates. The memory effect has also been described by Ohmura et al. (2003) by performing a statistical study of hydrate nucleation in a quiescent hydrochloroflurocarbon-in-water system with a memory of previous hydrate formation and dissociation. The authors reported that the rate of nucleation strongly depends on the thermal history of the system. According to their results, this effect tended to decrease by heating the samples and holding them for longer time before reforming hydrates. On molecular-

level, Buchanan et al. (2005) used neutron diffraction with H/D isotope substitution to investigate structure of water before hydrate formation and after hydrate dissociation. In these studies they found that there is a significant change in the water structure of the remaining water at various stages of hydrate formation and dissociation. They concluded that this local change in water structures due to the presence of hydrate crystallites could be responsible for memory effect. In other words, persistent hydrate crystallites in dissociated hydrate water lead to a locally modified water structure which in turn eases hydrate reformation. Although there are different reported hypothesises on the mechanism of the hydrate memory, all of them agree on the existence of the so-called memory effect.

4.1.2. Onset of Hydrate Formation

Despite of whatever hydrates memory is, it was experimentally proven that, if a fluid system has experienced hydrates, it will form hydrate with less degree of sub-cooling and at a faster rate than a fresh sample. If systems with identical hydrate forming gas and aqueous fluid are continuously cooled at a constant cooling rate to form hydrates, the ones that have hydrate memory will start to form hydrate earlier, i.e., the onset of hydrate formation will appear earlier in the system that previously experienced hydrate formation.

4.1.3. Hydrate Initial Detection Technique

It was proposed that it may be possible to develop a novel technique for detecting early signs of hydrate formation by experimental determination of the onset of hydrate formation. The proposed technique could be established based on measuring the required degree of subcooling at which the onset of hydrate formation is detected for a aqueous sample taken from a certain point of a pipeline. For the sample, after completely destroying the water structure (or remove the hydrate memory) by heating, it is expected that gas hydrates can not form until a higher degree of subcooling in comparison to the former one with hydrate memory.

To be able to develop a hydrate early warning system, systematic studies need to be done to investigate the sustainability of hydrate memory, for example, how far outside the hydrate stability zone (HSZ) and how long after hydrate dissociation the memory

effect can be sustained. Furthermore, in terms of practical application, the device should be able to facilitate quick measurements of the onset of hydrate formation, i.e., easy control of the temperature and fast formation of gas hydrate. It is also important for the early warning system to be a simple and portable apparatus which could be used in field conditions.

In this work, the feasibility of using hydrate memory was further investigated as a signal for detecting early signs of hydrate formation. Based on the gained understanding of hydrate memory phenomenon, a device with a mini cell was especially designed for developing a hydrate early warning system. Feasibility of using this cell for detecting the onset of hydrate formation was then experimentally examined. Finally, by means of this min cell, the effect of different parameters were studied, including inhibitor types, durations outside the hydrate stability zone, temperature degrees outside hydrate the stability zone, gas compositions, and effect of depressurisation.

4.2. EXPERIMENTAL SETUP AND PROCEDURE

4.2.1. Experimental Setup

The experimental setup is a purpose-built mini autoclave cell (Figure 4.1) with an effective volume of 3 ml and made of stainless steel. Small volume/mass of the mini cell is to make it possible to use thermoelectric modules for cooling and heating in development of hydrate memory-based early warning device, which could facilitate its application in field conditions. The cell can be operated up to 170 bara between -40 and 60 °C. The cell is immersed in a temperature-controlled liquid bath that maintains the desired temperature. In order to perform accurate temperature measurements in the equilibrium cell, temperature is measured directly inside the cell with uncertainty within ± 0.1 °C. Pressure is measured by means of a Druck pressure transducer with uncertainty within ±0.2 bar in the 0 to 400 bar range. To achieve a fast thermodynamic equilibrium and a good mixing of the fluids, a magnetic stirrer was in the cell and the cell was placed on the magnetic mixing plate which can be operated from 0 to 60 °C in the same cooling bath. A high pressure piston cylinder was used for controlling the pressure when it is desired. A HPLC pump was connected to the piston

side of the cylinder to maintain the desired pressure. Figure 4.1 shows the schematic of the experimental setup and a picture of the mini cell on the right side of the figure.

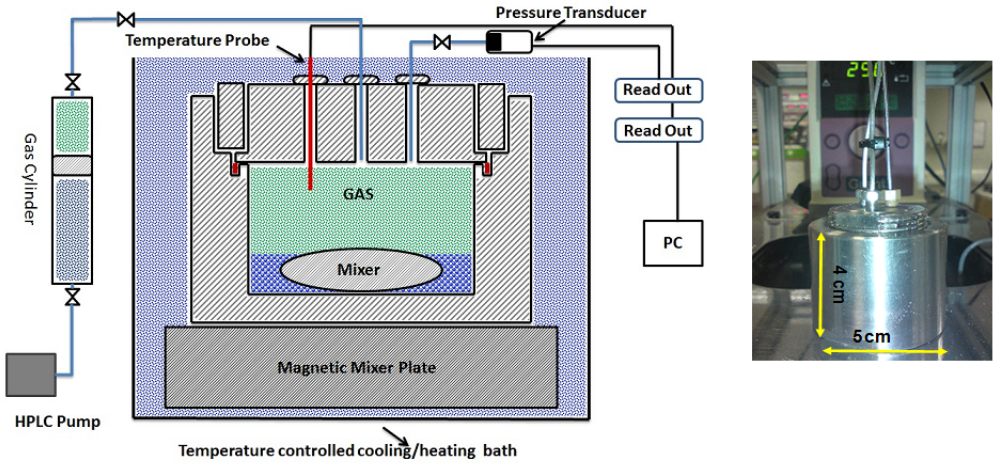

Figure 4.1 Schematic of the experimental setup and a picture of the mini cell

4.2.2. Experimental Materials

Methane gas (99.95% pure) supplied by BOC, natural gas (Table A.57 and Table A.59), produced water (with 5 mass% salts in total, provided by BP), methanol and ethylene glycol (MEG) supplied by VWR(99.9 % pure), deionised water produced with hydrate lab purification system and Luvicap-EG supplied by BASF.

4.2.3. Experimental Procedure

The experimental procedures consist of several steps. In each experiment, the cell was preloaded with 1 ml of the aqueous liquid solution under test (The type of solutions depends on the individual experiments) and vacuumed prior to gas injection. Natural gas (NG) was injected into the cell to achieve the desired equilibrium pressure at 25 °C. The system was then cooled down about 10 to 12 °C inside the hydrate stability zoon at a cooling rate of 0.3 °C/min while a constant mixing rate was set. The subcooling temperature at which hydrate started to form was measured as the onset of hydrate formation and the system was left for 3 hours at that subcooling to have sufficient amount of hydrate. The hydrates were then dissociated by heating up the system to the targeted degree Celsius outside the hydrate stability zone and left for

certain time that depends on the experiment. Then the system was cooled down for the second time to the same subcooling at the same cooling rate and mixing rate. The onsets of hydrate formation that were measured in the first cycle and the second cycle of hydrate formation were compared to understand the effect of the parameters under investigation on hydrate memory.

It should be mentioned, experimental procedure is the part of this hydrate memory detection method, a brief procedure will be explained in each system as the results are depends on the procedure.

4.3. EVALUATION OF THE MINI CELL

The applicability of the mini cell was examined prior to being used for hydrate memory experiments. One experiment was conducted to investigate if gas hydrate can be formed in the mini cell and how long it may take to form hydrates. In this experiment natural gas and deionised water were used for simplicity. The cell was loaded with 1ml of deionised water and 2 ml of natural gas at 172.4 bar and 29.1 °C. Then it was cooled straight to 4 °C. Figure 4.2 shows the results.

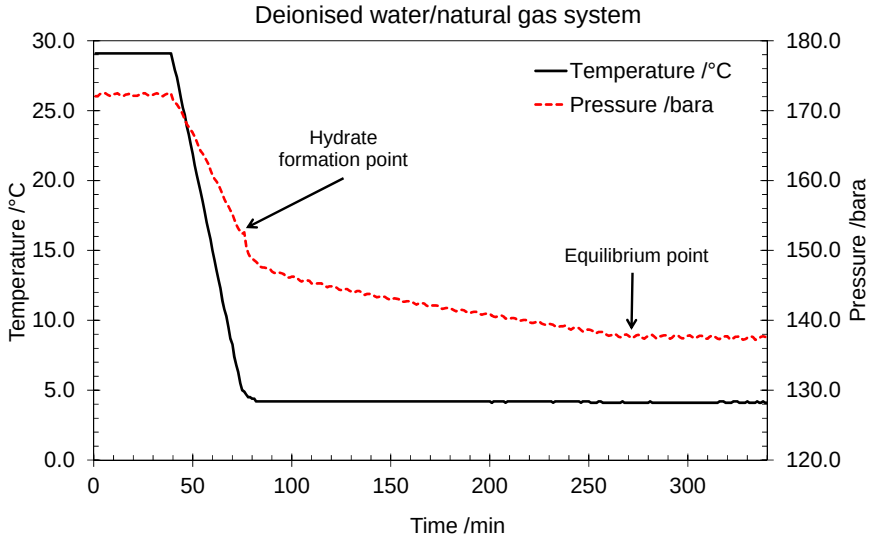

Figure 4.2 Mini cell performance

As can be seen in Figure 4.2, the system temperature reached the target 4 °C from 29.1 °C in about 40 minutes, initial hydrate formation started at 35 minutes after the cooling

process started. It took about 150 minutes after the initial hydrate formation for the NG-distilled water system to reach equilibrium.

To investigate the reliability and accuracy of the mini cell for determining the onset of hydrate formation, hydrate dissociation points were measured at two different pressure for the same NG-water system. The two pressures were chosen as they were close to its working pressure rating (170 bar) and the typical experimental pressure (103.4 bar), respectively. Table 4.1 shows that the measured dissociation temperatures are in good agreement with the thermodynamic model.

Table 4.1 Hydrate dissociation point measurements using mini cell

Pressure /bara	Measured dissociation point	Predicted dissociation point
134.7	19.7	19.9
166.1	20.9	21.0

4.4. RESULTS AND DISCUSSIONS

In this section, hydrate memory phenomena will be investigated for different aqueous systems containing salt, alcohol and kinetic hydrate inhibitors using the mini cell. The aim of these experiments is to evaluate the feasibility of hydrate memory method for detecting early signs of hydrate formation. Meanwhile, the performance of the mini cell was further examined with different systems for hydrate early warning purposes.

4.4.1. Detecting Early Sign of Hydrate Formation for Deionised Water-Natural Gas Systems

In the first series of experiments natural gas (Table A.57) and deionised water were used. According to the procedure described in Section 4.2.3 the cell was loaded with 1 ml of deionised water and pressurised with natural gas to 107 bar at 25 °C. In the first run with fresh water in the absence of hydrate memory, initial hydrate formation was started at 10.7 °C. The system was left at 5 °C for 3 hours to form adequate amount of hydrate for evaluating hydrate memory effect. The hydrate-water system was heated up to 3 °C outside the hydrate phase boundary and left at this point for 3 hours. Then the system was cooled down again to 5 °C following the same procedure. In this run when hydrate memory was exist, the initial hydrate formation was observed at 16.7 °C

and the formation rate was faster than the previous run without hydrate memory. This experiment was repeated for 3 cycles to confirm the validity and reproducibility of the results. It should be mentioned that the determined onsets of hydrate formation were repeatable in 0.2 °C deviation. These results show that the presence of hydrate memory in the repeating cycles leads the onset of hydrate formation appeared about 6 ºC earlier than that in the first cycle without hydrate memory. This results also proves that the mini cell can be used for hydrate early warning for NG-water systems. Figure 4.3 shows a typical run of this experiment.

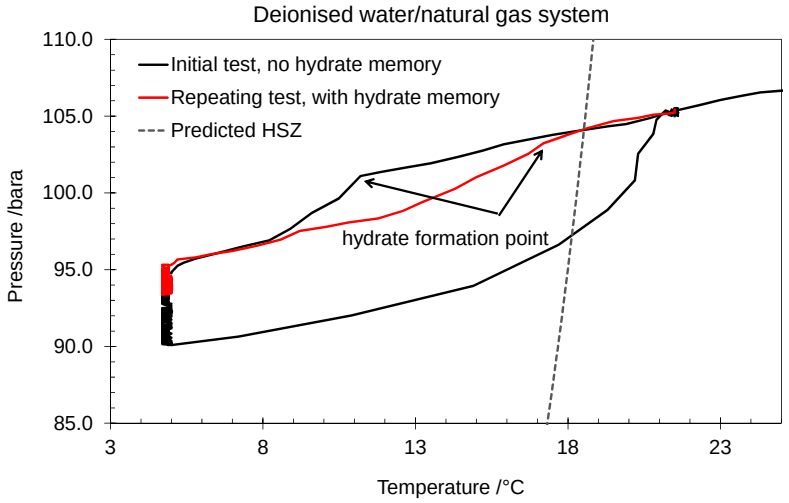

Figure 4.3 Effect of hydrate memory on the initial hydrate formation: deionised water and natural gas system, 3 hours at 3 °C outside the hydrate stability zone.

So far it was shown that hydrate memory is resulting to earlier hydrate formation and mini cell is appropriate for detecting this sign. In practice, hydrates may dissociate somewhere in a pipeline and the water with hydrate memory reaches a platform after hours. Therefore, it is important to investigate the sustainability of hydrate memory, i.e., for how long hydrate memory can still be detectable at a certain temperature outside the stability zone. To investigate these detection limits, experiments with same procedure were conducted at different durations and temperatures outside hydrate stability zone. Each experiment was repeated at least twice and the average degrees of the measured subcooling of initial hydrate formation are reported in Table 4.2. In this table, the temperature outside HSZ represents the temperature difference from the

hydrate stability zone (predicted by our in-house thermodynamic model), at which the system was left for the desired time. Figure 4.4 illuminates the results.

Table 4.2 Subcooling observed for initial hydrate formation for deionised water-natural gas systems

Temperature outside HSZ (°C)	Duration outside HSZ (hour)		
	3	6	12
3	1.3	1.5	5.5
6	4.3	4.9	5.9
9	5.9	6.5	7.0
12	6.0	7.5	7.4

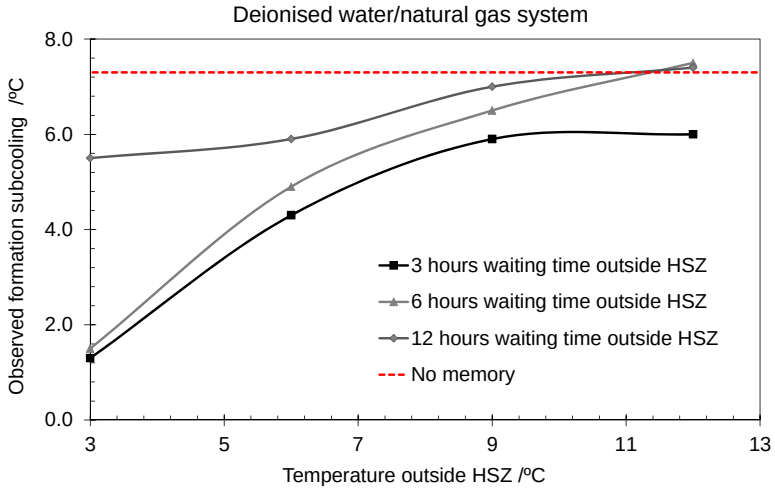

Figure 4.4 Effect of waiting time and temperature outside hydrate stability zone on the delectability of hydrate memory for deionised water-natural gas systems.

In this figure, the red dotted line shows the subcooling temperature when hydrate was formed from fresh water (there was no hydrate memory). It is taken as a reference for hydrate memory disappearance in the deionised water experiments. It should be mentioned that this reference has been determined based on a good number of repetition due to the stochastic nature of hydrate formation. The number of the repetition can vary from one system to another and should be repeated until a good confidence is achieved. Moreover, the worst case, i.e. the lowest subcooling was taken as the reference for no memory case to minimise the effect of stochastic nature of hydrate formation on memory technique. If hydrate forms at the same degree of

subcooling or higher, it means it is not possible to detect the memory effect. In the first series of experiments, as shown in Figure 4.3, after hydrate formation and dissociation, the system was left for 3 hours outside the hydrate stability zone at different temperatures outside the hydrate stability zone. For this series of experiments, hydrate was formed with 1.3 °C subcooling. By increasing TOHSZ (Temperature Outside Hydrate Stability Zone) the required subcooling temperature was increased. For example, when TOHSZ is 6 °C, the observed subcooling of hydrate formation is increased to 4.3 °C. It suggests that by increase in TOHSZ hydrate memory was weakened and a higher degree of subcooling is needed to initiate hydrate formation. For TOHSZ equal to 12 °C the memory effect was at its minimum and the subcooling was close to the one with no memory. It means that for TOHSZ greater than 12 °C hydrae memory became undetectable, and consequently difficult to be used for hydrate early warning system.

Knowing this time is important for practical applications. This method is being developed for filed applications where the operator will take an aqueous sample from a downstream pipeline or separator. The taken sample is not just after hydrate formation or dissociation; of course it is travelled along the pipe line so it might be very short time after dissociation or days, it is very important to select the right point of the sampling. By these experiments, first we try to proof the applicability of the method and then by determining the time outside stability zone and TOHSZ, we could define the limits of the method and based on these limits it is possible to select a right sampling point and also a procedure for this method. In this work different time outside HSZ was examined with the same TOHSZ. As can see in Figure 4.4, by increasing the waiting time outside stability zone, hydrate memory effect is decreased and consequently the required subcooling for initial hydrate formation was increased. The results show that memory existence is highly dependent on the TOHSZ and the waiting time outside stability zone (in practical cases could be related to the sampling point and the fluid travelling time before reaching the sampling point). Based on these results for this specific natural gas and deionised water, it could be said that the detection limits are about 9 degree Celsius outside the hydrate stability zone and 12 hours waiting time outside stability zone, but more reliable results could be observed at TOHSZ equal to 6 °C. The practical interpretation of these results is that this method

is suitable for deionised water and natural gas systems when the taken sample is not heated more than 9 °C outside hydrate stability zone and the travelling time should not be greater than 9 hours. It is important that these results may be fluid system dependent, therefore, further experiments were conducted for other fluid systems, typically, produced water containing different impurities like salt or inhibitors.

4.4.2. Detecting Early Sign of Hydrate Formation for Brine-Natural Gas Systems

Salts have always been seen in produced water in many fields. In this section, effect of salt on hydrate memory will be evaluated and performance of the mini cell will be examined for the systems containing salts. In this experiment an aqueous solution with 6 mass % of NaCl was used with natural gas. In first series of experiments, similar to the previous section, the system was loaded and hydrate was formed with no memory. This measured initial formation point was taken as a reference of memory disappearance. In the second run, at 3 °C outside hydrate stability zone with the waiting time of 3 hours, hydrate was formed far earlier than the time with fresh water. Figure 4.5 shows one of the repeated runs. The time when water was fresh and there was no hydrae memory, the observed subcooling was seen at about 7.5 °C, but in the next run with hydrate memory hydrate was formed at about 1.1 °C subcooling. These experiments were repeated for different waiting times and TOHSZ.

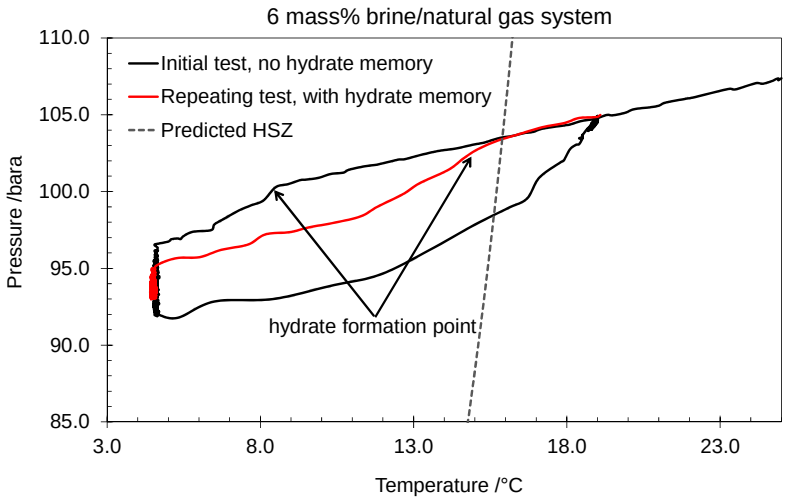

Figure 4.5 Effect of hydrate memory on the initial hydrate formation after 3 hours at 3 °C outside hydrate stability zone for brine with 6 mass% NaCl and natural gas systems.

Table 4.3 summarises the results for different waiting hours and temperatures outside hydrate stability zone. It can be seen that the existence of salt prolongs the memory remaining time so that hydrate memory can remain at increased TOHSZs.

Table 4.3 Subcooling observed for initial hydrate formation for 6 mass% NaCl/natural gas systems

Temperature outside HSZ (°C)	Duration outside HSZ (hour)		
	3h	6h	12h
3	1.1	1.0	2.7
6	3.4	3.5	5.1
9	3.3	3.0	6.6
12	5.0	5.7	7.7
18	7.5	7.3	8.1

It can be seen that, in the presence of 6 mass% salt, the sustainability of hydrate memory was increased. The results shows that for 3 °C outside stability zone, up to 12 hours, memory still existed and hydrate formed obviously earlier than that with the fresh system when there was no hydrate memory. But for the same conditions in the previous experiments with deionised water and natural gas, the memory was less sustainable. By increasing the TOHSZ to 6 °C ,waiting 6 hours outside the hydrate stability zone the memory did not change significantly. Until the waiting time was increased to 12 hours, although the required subcooling was increased, the memory still had detectable effect on the reformation process. By increasing TOHSZ to 9 °C the memory was still detectable, which is comparable to that at 3 °C outside the hydrate stability zone for 6 hours. However, it became significantly weaker and was close to the subcooling with no memory. Increasing the TOHSZ to 12 °C weakened the memory effect significantly but it was still possible to detect up to 6 hours, and disappeared after 12 hours outside stability zone. By increasing the TOHSZ to 18 °C the memory effect was completely disappeared and the average formation subcooling was like that with no hydrate memory. Figure 4.6 illustrate s these results.

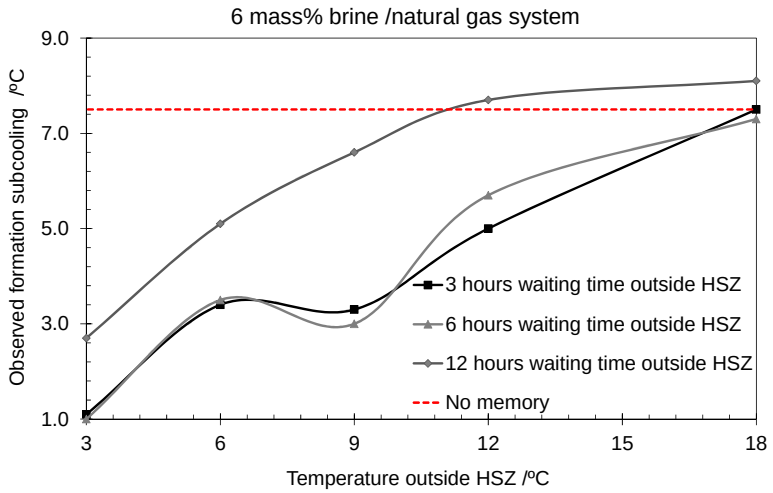

Figure 4.6 Effect of waiting time and temperature outside hydrate stability zone for systems containing brine with 6 mass% NaCl and natural gas.

To further investigate the effect of salt on the sustainability of hydrate memory, 10 mass% NaCl solution was loaded in the cell. The experiments were conducted in the same procedure in the previous ones with 6 mass% NaCl. Table 4.4 shows the results. In the first experiment the average formation subcooling was observed at 8.5 °C for no memory cycle.

Table 4.4 Subcooling observed for initial hydrate formation for 10 mass% NaCl/natural gas systems

Temperature outside HSZ (°C)	Duration outside HSZ (hour)		
	3h	6h	12h
3	1.9	2.5	5.5
6	4.7	5.1	4.5
9	5.3	7.3	7.1
12	6.0	6.5	7.4
18	10	8.8	9.2

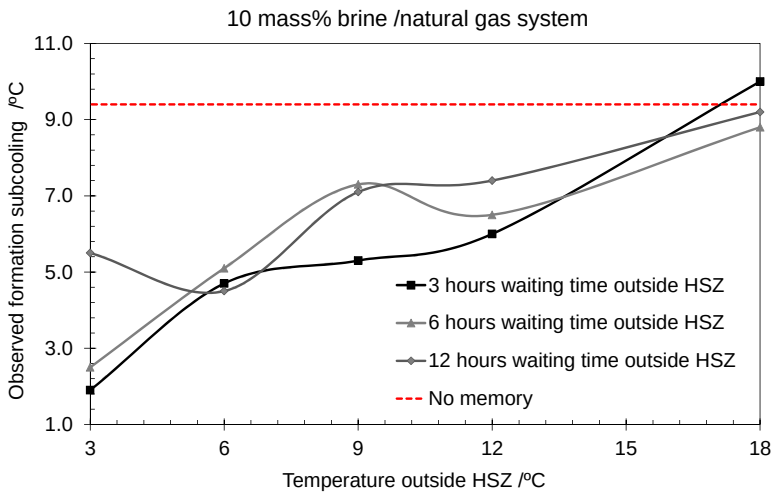

Figure 4.7 Effect of waiting time and temperature outside hydrate stability zone for systems with 10 mass% NaCl and natural gas.

Figure 4.7 illustrates the results. Similarly, at 3 hours waiting time, the memory had strong effect when the TOHSZ was 3 °C, but by increasing TOHSZ, the memory effect gradually became weakened and completely faded at 18 °C. Same behaviour was observed for other waiting times, increase in the waiting time expedited the hydrate memory disappearance, however it was still detectable. But increase in the TOHSZ significantly affected the memory and at 18 °C outside the HSZ the memory was completely destroyed and became undetectable.

Comparing the results from deionised water, 6 mass% and 10 mass % NaCl in the system, It can be seen that existence of salt has improved the memory effect and makes it more sustainable to be detected.

To investigate the applicability of this method for more realistic conditions, real produced water was used. The produced water was from one of the project sponsors production filed. Its salinity was reported approximately 5 mass % NaCl equivalent salts without any chemical additives. According to the experiments procedure, the fresh sample was loaded and hydrate was formed. It shows that memory effect for this produced water is slightly weaker than for higher concentration of NaCl explained in previous section.

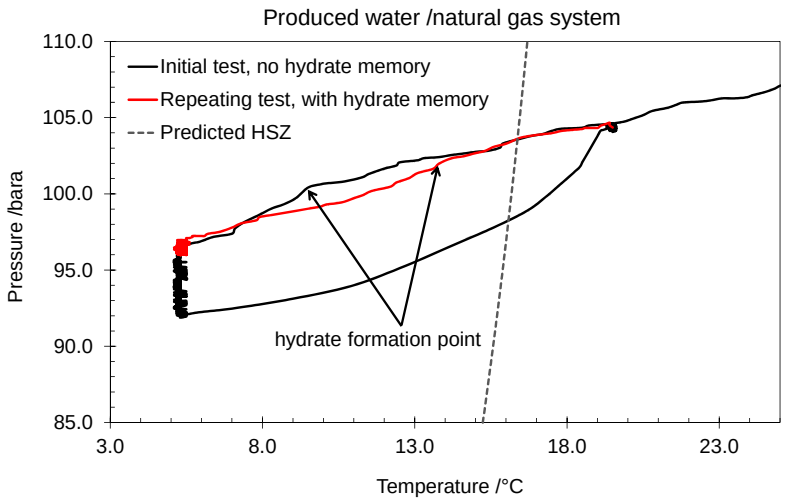

Figure 4.8 Effect of hydrate memory on the initial hydrate formation after 3 hours and 3 °C outside hydrate stability zone for real produced water and natural gas system.

Same experiments were conducted with different TOHSZ and waiting hours and the average results are reported in Table 4.5 and Figure 4.9.

Table 4.5 Subcooling observed for initial hydrate formation for real produced water/natural gas systems

Temperature outside HSZ (°C)	Duration outside HSZ (hour)		
	3h	6h	12h
3	2.7	3.1	3.3
6	2.5	3.7	4.1
9	4.5	4.4	5.2
12	5.1	5.7	6
18	6.1	7.2	7.5

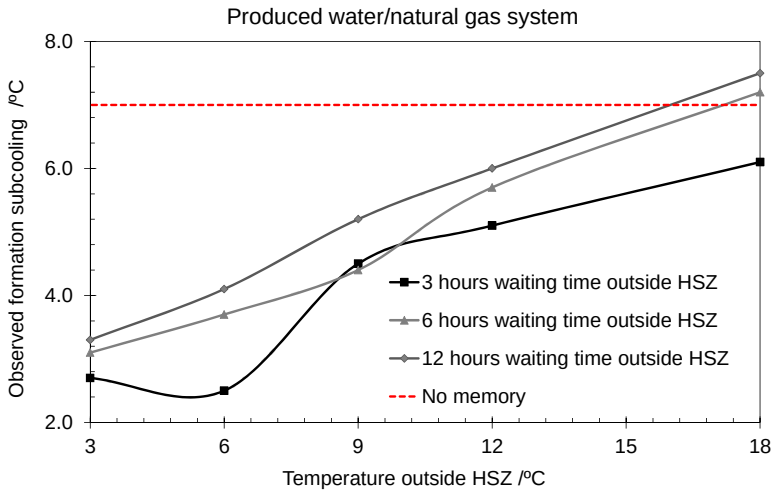

Figure 4.9 Effect of waited time and number of degrees outside hydrate stability zone for produced water and natural gas.

By increase in the waiting hours same trend has been observed, increase in TOHSZ, caused increase in formation subcooling temperature. The trends show that, memory is detectable up to 12 °C outside hydrate stability zones even for the waiting time of 12 hours. But by increase in the temperature to 18 °C the memory was destroyed for these waiting times. Based on these results, one can say that, limits for this specific produced water is 12 °C outside hydrae stability zone with the waiting time of 12 hours.

4.4.3. Effect of Hydrate Inhibitors on the Sustainability of Hydrate Memory

4.4.3.1. Methanol-Produced Water-Natural Gas Systems

To evaluate the applicability of the hydrate memory method and the mini cell in the presence of methanol, an aqueous sample was prepared containing 5 mass% of methanol with the real produced water to more closely simulate pipeline conditions. Following the same procedure explained before, the system was loaded with an aqueous solution that was prepared with the produced water, 5 mass% methanol and natural gas. Then hydrate was formed to determine the subcooling temperature when there was no hydrate memory. Figure 4.10 shows an example cycle of these experiments. After initial formation and defining the subcooling, test was started at 3

°C outside hydrate stability zone with a waiting time of 3 hours as shown in Figure 4.10.

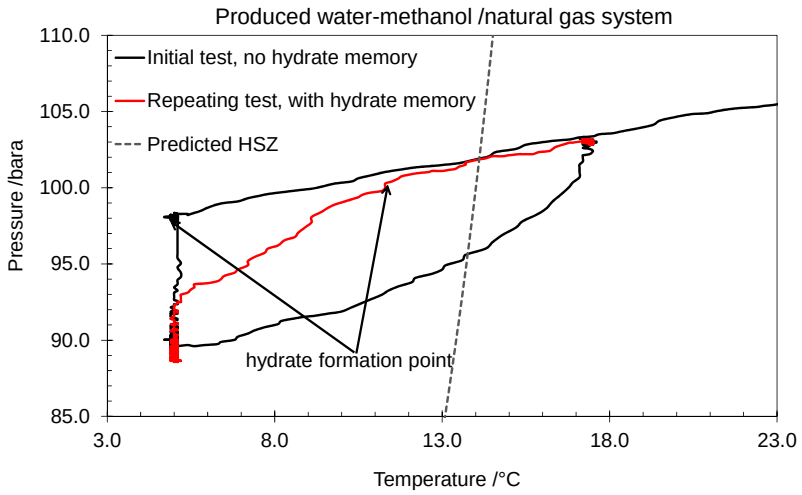

Figure 4.10 Effect of hydrate memory on the initial hydrate formation at 3 ºC outside hydrate stability zone after 3 hours for a system containing real produced water, 5 mass% of methanol in presence of natural gas.

Table 4.6 shows these average results for different waiting times and temperatures outside hydrate stability zone. For the TOHSZ to 6 °C, the hydrate memory was significantly weakened and hydrate was formed 5.1 °C subcooling which is almost twice as the one at 3 °C TOHSZ. By increasing the temperature to 9 °C the observed subcooling was further increased. Regarding to previous experiments the increase was expected, but the amount of increase was much bigger than the time without methanol, especially for 3 hours waiting time which memory always showed a very strong effect. Increasing the TOHSZ to 12 °C caused a big increase in observed subcooling and it was almost same as the observed value in the initial formation without memory. Increasing TOSHZ to 18 °C completely destroyed the hydrate memory and the observed formation subcooling was same as what was seen in the no memory cycle. It should be added, when there is no memory or memory is completely destroyed, hydrate formation took longer time at higher subcooling in comparison to the previous experiments without methanol in the systems. Same experiments were continued for longer waiting time outside hydrate stability zone. Results show that with 6 hours waiting time, memory was almost destroyed for above 6 °C TOHSZ..

Table 4.6 Subcooling observed for initial hydrate formation for real produced water- 5 mass% methanol and natural gas systems

Temperature outside HSZ (°C)	Duration outside HSZ (hour)		
	3h	6h	12h
3	2.8	4.5	6.7
6	5.1	6.3	7.2
9	7.4	9.0	9.0
12	8.1	9.0	9.0
18	9.0	9.0	9.0

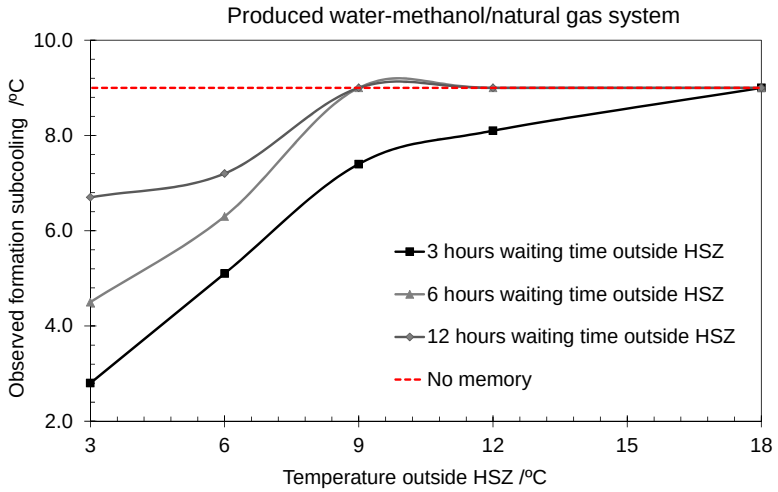

Figure 4.11 Effect of waiting time and temperature outside hydrate stability zone for systems containing produced water, 5 mass% of methanol, and natural gas.

Figure 4.11 shows that memory will weakened by increasing waiting time or TOHSZ likewise what was seen in previous experiments. However, this plot also shows that for 3 hours waiting time, memory was detectable up to TOHSZ equal to 12 °C. Same behaviour can be seen for longer waiting times, longer waiting caused memory effect disappear much earlier. For example for 6 and 12 hours waiting time at TOHSZ equal to 9°C, memory was completely destroyed. Based on these experiments, one can say the presence of methanol reduced the memory effect and detecting the hydrate memory become more difficult for systems containing methanol. To be able to practically use this method for systems containing methanol, it is suggested, the sampling point should be very close to the area which there is hydrate formation risk and the fluid travel time from the point of the risk should not be more than 6 hours or the TOHSZ

should be smaller than 9 °C. Also it should be mentioned these results are for evaluating the applicability of the hydrate memory method and for practical systems, the specific system should be tested according to the explained procedure to define the limits for that specific system. Also for practical uses it is strongly suggested to incorporate this method with one of the monitoring systems like water activity or C-V method to define the actual phase boundary; it will help to improve the accuracy of the measurements and also it could be used to define the right sampling point by considering the pipe line flow rate and aqueous phase travel time.

4.4.3.2. MEG-Produced Water-Natural Gas Systems

This method was further investigated for systems containing MEG and produced water. The produced water with 5 mass% of MEG was tested according to the explained procedure. After initial formation and defining the subcooling, test was started at 3 °C outside hydrate stability zone with a waiting time of 3 hours as shown in Figure 4.10. Table 4.7 and Figure 4.13 show the average results for different waiting times and temperatures outside hydrate stability zone.

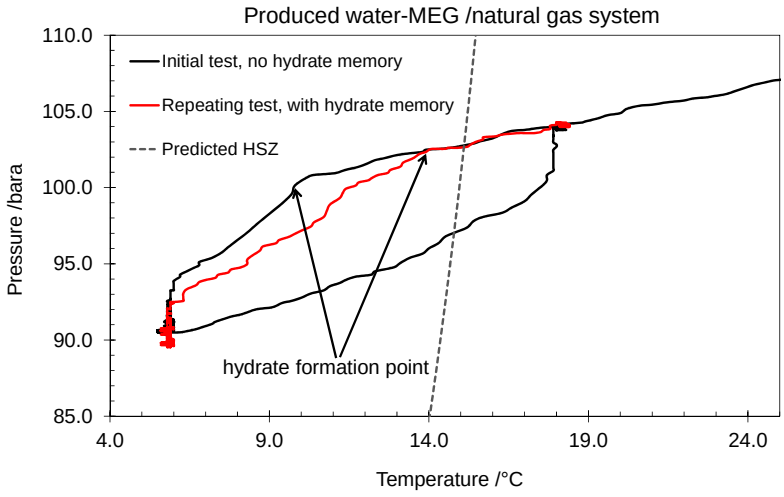

Figure 4.12 Effect of hydrate memory on the initial hydrate formation after 3 hours at 3 °C outside hydrate stability zone for systems containing real produced water, 5 mass% MEG and natural gas.

Table 4.7 Subcooling observed for initial hydrate formation for systems containing real produced water, 5 mass% MEG and natural gas

Temperature outside HSZ (°C)	Duration outside HSZ (hour)		
	3h	6h	12h
3	1	1.1	1
6	1.6	1.8	2.1
9	2.3	2.7	2.6
12	3.7	4	3.9
18	6.1	7.9	7.4

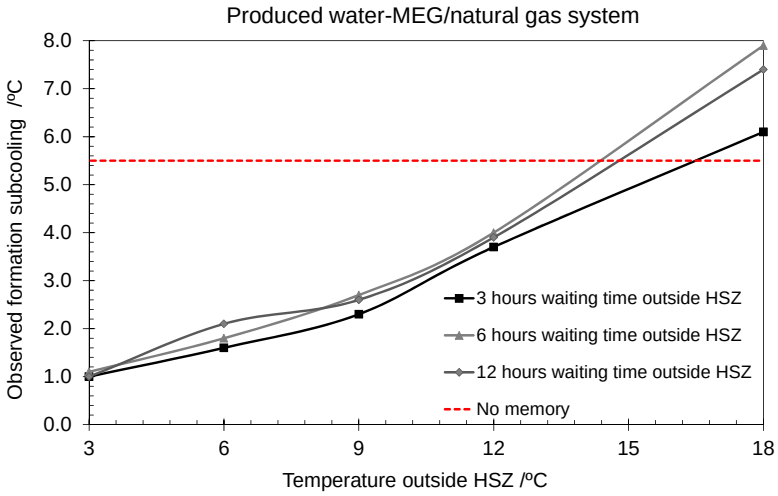

Figure 4.13 Effect of waiting time and temperature outside hydrate stability zone for systems containing produced water, 5 mass% MEG and natural gas.

The initial formation happened at about 5.5 °C in average. It means that, it might be more difficult to determine the hydrate memory as initial formation range is narrowed to a smaller subcooling and consequently if the formation occurs at bigger values it will be difficult to be used. The figure shows that, initial hydrate formation with system containing memory is forming much earlier than that initial formation point without memory. It means memory detection by using this method is possible in that narrowed range. For 3 hours waiting outside hydrate stability zone with 3 °C TOHSZ, the average initial formation subcooling defined about 1 °C. By increasing the TOHSZ, the subcooling was increased. Up to 12 °C TOHSZ, the memory was clearly detectable, by heating the system to 18 °C outside hydrate stability zone, the initial formation subcooling was very close to the one for system without memory. So it was

difficult to say if the memory exist or not and it is considered as memory is destroyed at this temperature. Similar results were observed for 6 and 12 hours waiting outside hydrate stability zone. The memory was detectable up to 12 °C TOHSZ but not clear for 18 °C. Other point can be obtained in this figure is that, the average formation subcooling values are very close to each other for same TOHSZ while the memory exist. It means waiting time has less effect on the memory for system containing MEG. In general, one can say from these results, detecting hydrate memory is possible for MEG system by using the memory method and the mini cell. The method might me more sensitive and more difficult to define the waiting time outside hydrate stability zone which was useful for determining the sampling point. In summery one can say, for 12 hours waiting outside hydrate stability zone for TOHSZ up to 12 °C this method and setup could detect the hydrae memory and could be used for early warning purposes.

4.4.3.3. Luvicap EG-Produced Water-Natural Gas Systems

In the recent years use of kinetic hydrate inhibitors (KHIs) are increased in oil and gas industry. These hydrate inhibitors prolong hydrate induction time and delay hydrate formation. It means that the degree of subcooling for initiating hydrae formation will increase in the presence of KHIs. To evaluate the water memory method and the mini cell in the presence of kinetic hydrate inhibitors, a commercial Luvicap EG was used. 2.5 mass % of this inhibitor was loaded in the cell. For the first cycle with the fresh solution, hydrate could not form at 5 °C after a long time waiting (more than 16 hours), which could be due to the inhibition effect of this inhibitor. In the heating cycle hydrate was not dissociated for 3 hours and 3 degree outside hydrae stability zone. The system was left for 6 and 12 hours and very small progress was observed and hydrate was still exist in the system. It was found that the reason is, when KHI exist in the system, the hydrate dissociation will be divided into two different regions, slow dissociation and fast dissociation (Anderson et al., 2011). It seems that for this specific KHI, 3 °C TOHSZ is inside slow dissociation region and it might take days to dissociate hydrate.

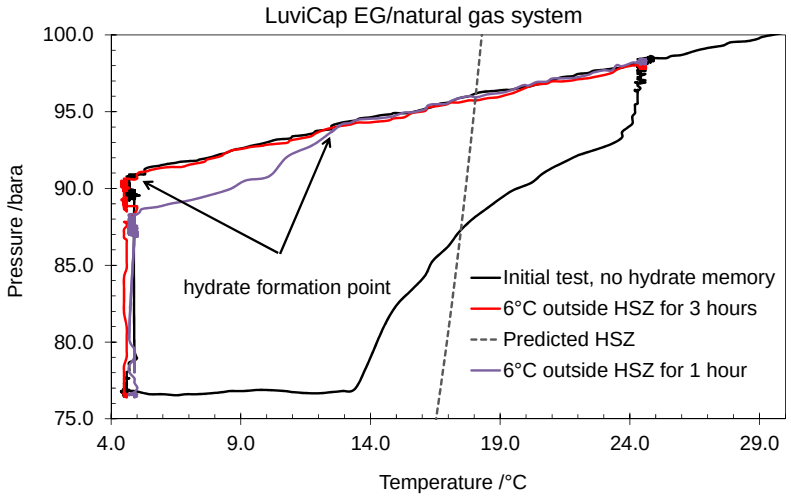

Figure 4.14 Effect of hydrate memory on the initial hydrate formation at 6 °C outside hydrate stability zone after 1 and 3 hours and for systems containing 2.5 mass% Luvicap EG and natural gas.

To be able to dissociate hydrate for our purpose, the temperature was increased to 5, 6 and 12 °C outside hydrate stability zone for waiting 1, 3, 6 and 12 hours. Figure 4.14 shows an example cycle when hydrate was dissociated at 6 °C TOHSZ for 6 hours and 1 hour. As one can see in this figure, after 3 hours waiting outside hydrate stability zone hydrate reformation was happened at same condition as the first time, which means that the memory was destroyed by waiting for 3 hours. But waiting just one hour shows that the initial formation subcooling was slightly smaller than the time with no memory. It shows that waiting 1 hour outside hydrate stability zone didn't kill the memory. However, it may be a very short time to determine hydrate memory in practical applications. The results of these experiments are tabulated in Table 4.8.

Table 4.8 Subcooling observed for initial hydrate formation for systems containing 2.5 mass% Luvicap, MEG, and natural gas

Temperature outside HSZ (°C)	Duration outside HSZ (hour)			
	1h	3h	6h	12h
3	N/A	N/A	N/A	N/A
5	4.5	6.1	13	13
6	5.2	13	13	13
12	13	13	13	13

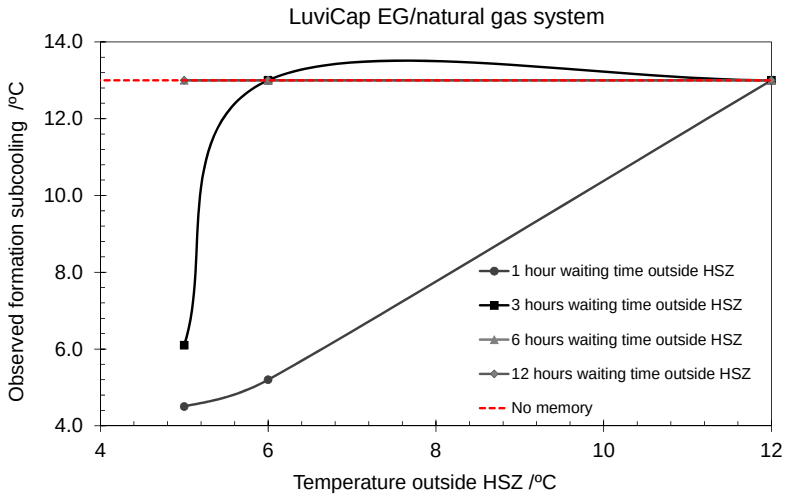

Figure 4.15 Effect of waiting time and temperature outside hydrate stability zone for systems containing produced water, Luvicap EG and natural gas.

In Figure 4.15 it can be seen that for this specific KHI, the memory is detectable for maximum of 6 °C outside hydrate stability zone however the waiting time is very small and practically it is really difficult to be used. For 5 °C outside the hydrate stability zone, it seems that the memory remained up to 6 hours. In conclusion, existence of KHI makes memory detection technique more limited.

4.4.4. Effect of Depressurisation on Hydrate Memory

In the previous sections we have investigated the effect of waiting time, temperature outside hydrate stability zone for salt and hydrate inhibitors. All experiments were conducted under pressure in a closed system. The crucial part of this method is the first sample taken from a pipeline, which is used as a reference of memory existence. It would be easier and simpler for field application if it is possible to take the aqueous samples at atmospheric or lower pressure. However, does the sample have to be taken under pressure or could it be a depressurised sample? To answer this question a series of experiments were conducted for 3 mass% NaCl in a methane system. Selecting a brine solution was to make more close to pipeline fluids and also it was to use the advantage that NaCl could slightly prolong the hydrate memory, making the study easier. To avoid any compositional effect in this experiment, methane was used instead of natural gas. Like the procedure for all the previous experiments, initially

hydrate was formed and then dissociated (at 3 °C outside hydrate stability zone for 3 hours in this tests). The system was depressurized to different pressures for one minute and then re-pressurised to the exactly same pressure before depressurization. Hydrate was formed again by cooling the system down. Figure 4.16 shows the sample and simplified results of these experiments.

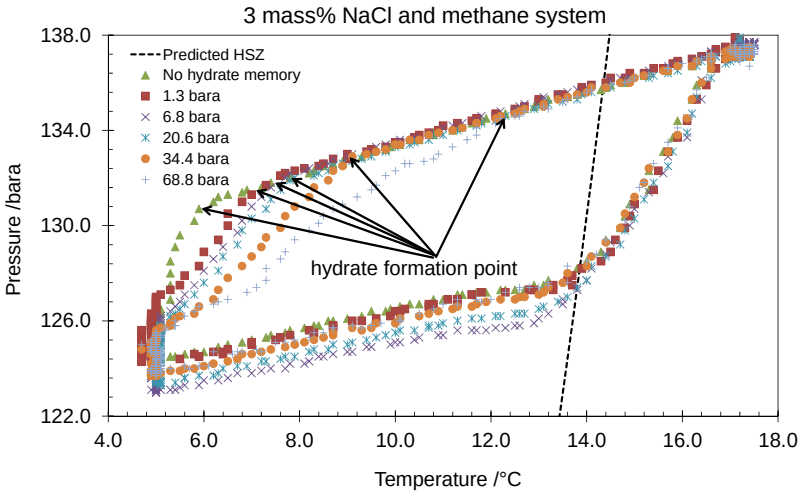

Figure 4.16 Effect of depressurization on hydrate memory after 3 hours and 3 °C outside hydrate stability zone for 3 mass% NaCl and methane system.

This figure shows that depressurisation weakens the hydrate memory effect even when depressurised for a very short period of time. Depressurisation to very low pressure close to atmosphere caused a sever damage to the hydrate memory and the observed formation subcooling was very close to the one when there is no hydrate memory. By depressurising the system to higher pressures, the memory showed a stronger effect and the observed formation subcoolings were decreased. These behaviour is shown in Figure 4.17. As can be seen in this figure, when the system is depressurised to 68.8 bara, the observed formation subcooling was very close to the system which was not depressurised; meaning that in the system can be depressurised to this pressure without effecting hydrate memory. However, the observed formation subcooling when the system was depressurised to 34.4 bara can be acceptable for the purpose of this technique.

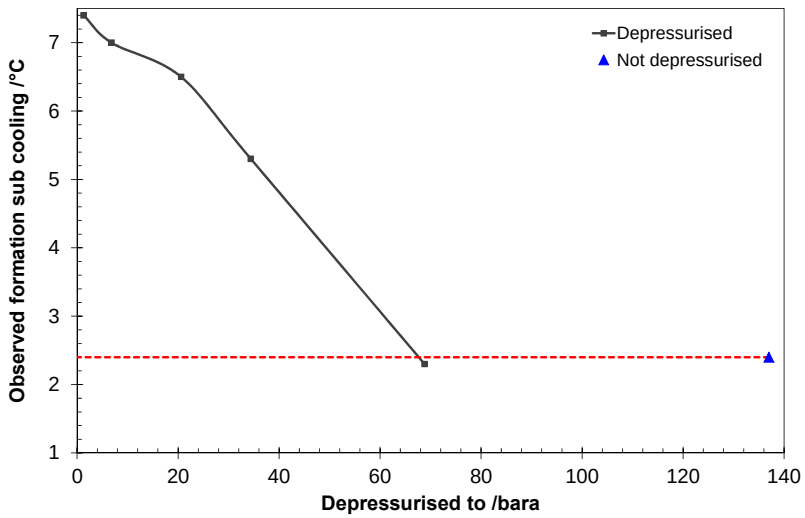

Figure 4.17 Depressurisation effect on hydrae memory for the brine (3 mass% NaCl) and methane system

Based on these results it can be said that, depressurization to very low pressure will cause a severe damage to the hydrate memory and it is strongly suggested to take the sample close to its actual pipeline pressure to avoid any damage to the hydrate memory.

4.4.5. Effect of Gas Composition on Hydrate Memory

These experiments were conducted to study the feasibility of simplifying the test procedure by replacing the produced natural gas with a simple gas or gas mixture like methane or lab-held natural gas with different composition. It was attempted to make the test easier as we don't have to use the original produced gas sample. In these experiments the same produced water was used. Initially, the system was loaded with the typical natural gas (Table A.57) and cooled down to form hydrate. After hydrate formation the system was heated up to 3 °C outside phase boundary for 3 hours.

There were two options to replace the formation gas with methane. The first one was to completely release the gas and re-pressurise it with methane. In this case, as expected according to the results described in Section 4.4.4, the memory was completely destroyed due to depressurisation, and even hydrate was not formed after leaving the system at 4 °C for a long time. The second option was to gradually displace the natural gas with methane by gradually releasing the gas and replacing with

methane in seven steps. The results show that hydrate was not formed earlier than the first time. These results show that replacing the initial formation gas with methane was not a successful option.

One more experiment was conducted to investigate if it is possible to use a slightly different gas mixture instead of the initial one used in the formation cycle. In this test, after heating the system to 3 °C outside hydrate stability zone and waiting for 3 hours, 10 % of the gas was gradually released and replaced with methane and the system was cooled down to form hydrate. This time the observed initial formation temperature was about 7 °C, showing that small changes in the composition would not destroy the memory. Figure 4.18 shows the simplified heating cooling process for methane replacement and changed composition gas.

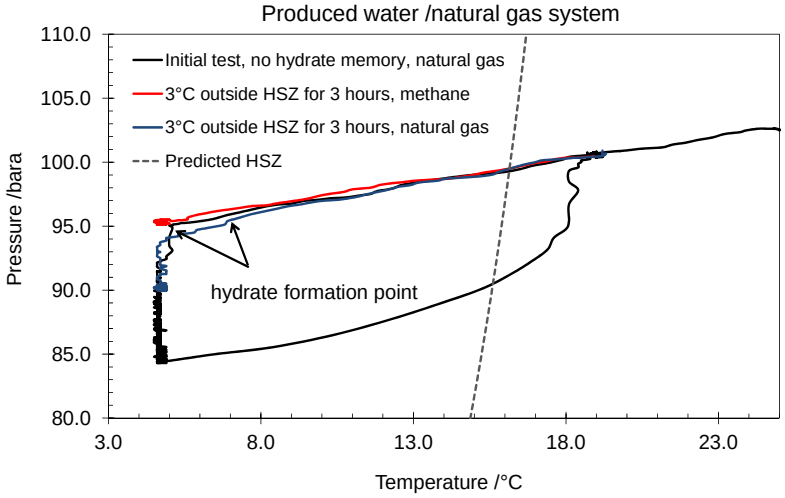

Figure 4.18 Effect of gas composition on hydrate memory in real produced water and natural gas system.

Based on these results, it is strongly recommended to use same gas composition from the same pipeline or a gas mixture with a composition similar to the original natural gas.

4.5. SUGGESTED APPROACH OF USING HYDRAE MEMORY METHOD

To facilitate field applications of the hydrate memory technique for detecting initial hydrate formation, an approach has been suggested. Figure 4.19 shows the different

steps in this algorithm. To start hydrate memory evaluation, aqueous and gas samples should be taken from pipeline under pressure and should be loaded into the cell. Depressurisation and temperature increase that may destroy hydrate memory should be avoided this temperature and pressure can vary from one system to another as it was shown earlier in this chapter). By using water activity or C-V technique hydrate phase boundary should be determined. To form hydrates system should be cooled about 10 degree inside hydrate stability zone. The hydrate formation subcooling (ΔT_m) should be recorded. The memory should be destroyed by heating the system to a high temperature e.g. 20 °C outside hydrate stability zone for determining the reference line. To achieve a high level of confidence it is suggested to repeat the reference test and take the smallest subcooling as no memory reference, ΔT_r. If the ΔT_m is greater than ΔT_r it means possibly there is no risk of hydrate formation. If ΔT_m is less than ΔTr, there is risk of hydrate formation. Since these tests are dependent on time, temperature and pressure, it is recommended to conduct these tests at the same condition of sampling and avoid damage to the possible memory in the sample (the system should not be exposed to high temperature and low pressure). If hydrate memory exists in the system, potentially it could be possible to define the time of hydrate formation by defining different retain time and temperature outside hydrae stability zone (TOHSZ) and comparing the results with ΔT_m. The location of hydrate formation could be defined by having hydrate formation time and flow rate. It should be mentioned that due to stochastic nature of hydrate formation this time and location should be considered with large error margin.

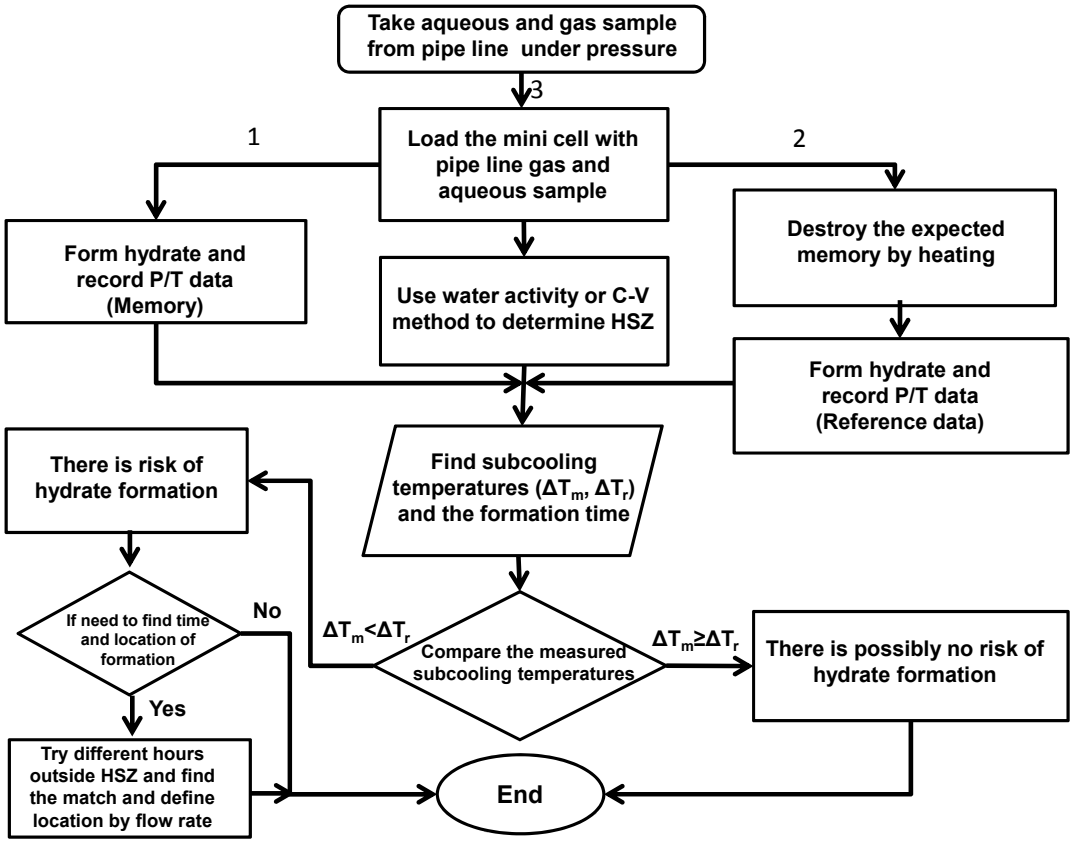

Figure 4.19 algorithm of using hydrate memory method and mini cell for hydrate early warning.

4.6. CONCLUSIONS

In this work hydrate memory was investigated for developing a hydrate early warning system. A mini cell was designed and manufactured especially for this purpose. Small volume and fast equilibrium was the main advantage of this cell. Its performance was experimentally examined by measuring hydrate dissociation points and the accuracy was confirmed by comparing the measure dissociation temperatures with the well proven in-house thermodynamic model. Sustainability of hydrate memory was investigated using the mini cell for various systems, including deionised water, NaCl, produced water, MEG, methanol and LuviCap EG. Effect of the temperature outside hydrate stability zone and the waiting time was evaluated for these systems. The results show that this method could possibly be used for all above mentioned systems with one exception. That is the presence of LuviCap EG significantly weakens the

sustainability of hydrate memory, short the waiting time small tolerance to the temperature outside the hydrate stability zone.

In this work the effect of depressurisation on hydrate memory was also studied. The results show that, if the depressurization is higher than 35 bara (for methane and 3 mass% NaCl), the memory will remain in the system for 3 hours at 3 °C outside the hydrate stability zone, while depressurisation to very low pressure will destroy the memory. Moreover, the effect of changing composition on hydrate memory was investigated. It seems that replacing the formation gas with methane may destroy the memory and make it undetectable. Replacing the original gas with a close composition to the original one will not damage the memory so that the memory is still detectable. However it is suggested ideally to use the original gas sample from the pipeline.

An approach has been suggested for facilitate the hydrate memory technique for hydrate early warning. To test the applicability of this method in real conditions, a field trial is planned in one of the sponsors filed.

CHAPTER 5. HYDRATE INITIAL DETECTION TECHNIQUE BASED ON COMPOSITIONAL CHANGE

5.1. INTRODUCTION

In chapter 4, a hydrate early warning method was introduced based on the effect of hydrate memory on onset of hydrate reformation. This method mainly was introduced for lab based tests or offline sampling for detecting early sign of hydrate formation in field applications. Following the successful results of this method, development of an online method was suggested as a complementary technique beside hydrate memory method.

As it was explained in chapter 1, gas hydrates are ice-like crystalline structures formed by hydrogen bonded water molecules and stabilised by the presence of guest molecules within the lattice cavities. Gas hydrates usually prefer large round molecules like (ethane, propane, isobutane…) in their structure. In oil and gas industry the molecules commonly found in natural gas that occupy the cavities are light alkanes (C1-C4), carbon dioxide, and nitrogen and hydrogen sulphide. Hydrate sII is the main structure usually forming in a pipeline depending on the gas composition and line conditions however sI can form as well. Different research groups have worked on evolution of gas composition in hydrate phase and vapour phase for different purposes like gas hydrate storage or transportation. The results of these studies show that composition of gas in both hydrate and gas phases significantly changes due to hydrate formation. Kawasaki et al. (2002) have studied gas mixture of methane, ethane, propane and isobutane. According to their results, methane content in the gas phase increased in comparison with original composition but the concentrations of ethane, propane and isobutane decreased significantly. The compositional changes in the hydrate phase were opposite; the concentration of methane was lower while the concentrations of the other components were higher than the original gas composition. In another work,

Kondo et al. (2010) studied the evolution of the gas composition in a methane-ethane-propane mixture (90, 7 and 3 mole% respectively). Their results showed that during the formation, concentration of methane continuously increased until the system reached equilibrium and hydrate formation stopped. At the same time the concentration of ethane and propane continuously increased. These results showed that propane was almost all consumed and a very small amount of it remained. Kobayashi et al. (2007) also have studied a mixture of methane, ethane and propane for hydrate rate controlling purposes in presence of water and methylcyclohexane. Their results also showed increase in methane concentration in gas phase while the ethane and propane concentration was decreasing significantly. Seo et al. (2009) studied the composition and structure of natural gas hydrates using NMR spectroscopy. In their work, the composition of the gas retrieved from hydrate at different formation temperatures showed that the concentration of methane was much lower than the feed composition and the concentration of heavier components were increased significantly. Similar results were observed in literature for changes in concentration of methane, ethane and propane. All these results confirm that formation of hydrate structure II will results an increase in concentration of methane and decrease in concentration of heavier components like ethane and propane in the gas phase and opposite results could be observed in the hydrate and aqueous phases.

The aim of this work is to use these phenomena and define methods able to pick up these changes and use them as online hydrate initial formation detection. As it was explained, this property will affect both aqueous phase and gas phase but in opposite way. To be able to develop a more robust method, feasibility of using both aqueous and gas phase has been studied with different means. This work has been divided into two parts, one is to study the effect of hydrate formation on the gas phase and the other one is to study the extracted gas from aqueous phase after hydrate dissociation which is related to the residual gas after hydrate dissociation.

5.2. COMPOSITIONAL CHANGE IN VAPOUR PHASE

5.2.1. Feasibility Study

To investigate the feasibility of using composition change monitoring for early warning systems, numerical and experimental modelling were conducted for various scenarios. Simulation study to investigate the feasibility of this technique was completed using a well-proven thermodynamic model (Avlonitis, 1992; Tohidi et al., 1993). The main objective is to predict the variation in the composition of a simultaneously fluids by total conversion of 1 bbl water in MMscf of gas into hydrates. The gas composition is given in Table 5.1. Propane is the component selected as reference because of higher variation in case of simulated conversion of 1 barrel of water into hydrates. Propane concentration variations in the gas phase are shown in Figure 5.1. Simulation studies for this specific scenario show that propane concentration in gas phase varies in the sensitivity range measurable by a flame ionization detector (FID) of a gas chromatograph.

Table 5.1 Natural gas composition

Component	Mole (%)
N_2	0.82
C_1	88.52
CO_2	1.44
C_2	6.76
C_3	1.76
iC_4	0.21
nC_4	0.34
iC_5	0.08
nC_5	0.08
TOTAL	100.00

The apparatus used in this work to validate the modelling study is shown in Figure 5.2 and is based on a static-analytic method with fluid phase sampling. The phase equilibrium is achieved in a cylindrical cell made of hastelloy, the cell volume is about 80 ml and it can be operated up to 400 bar between -40 and 100 °C. The cell is immersed in a constant–temperature liquid bath that controls and maintains the desired temperature. In order to perform accurate temperature measurements in the equilibrium cell, temperature is measured directly inside the cell with uncertainty within ± 0.05 °C. Pressure is measured by means of a Druck pressure transducer. The

pressure transducer was calibrated against a dead weights pressure balance and measurement uncertainties are estimated to be within ± 0.1 bar in 2 to 400 bar range. The analytical work was carried out using a GC (VARIAN model CP-3800) equipped with a Flame Ionisation Detector (FID) and a Thermal Conductivity Detector. The FID was used to detect hydrocarbon concentrations and the TCD to detect nitrogen and carbon dioxide. The sampling is carried out using a capillary sampler. A capillary sampler-injector is connected to the top of the cell through a 0.1 mm internal diameter capillary tube. The withdrawn samples are swept to the Varian 3800 gas chromatograph for analysis. The composition of the natural gas used in this work is given in Table 5.1.

The online analysis of vapour phase was made during hydrate dissociation. The main purpose was to simulate on-line measurements. The analysis was done at high pressure (100 bar). Based on the results shown in Figure 5.1, it was observed that there is a direct relation between the composition of propane in the vapour phase and the ratio of the mole of water converted to hydrate per total mole of gas in the system. Concentration variations of propane in the natural gas for the previous modelling study and of the experimental work are shown in Figure 5.1. As it can be seen the results are in good agreement. The variation in the composition of propane is a strong function of the amount of hydrate formed. In laboratory conditions, hydrate formation is detectable in the case of one barrel or higher content of water converted into hydrates per one million cubic feet of gas.

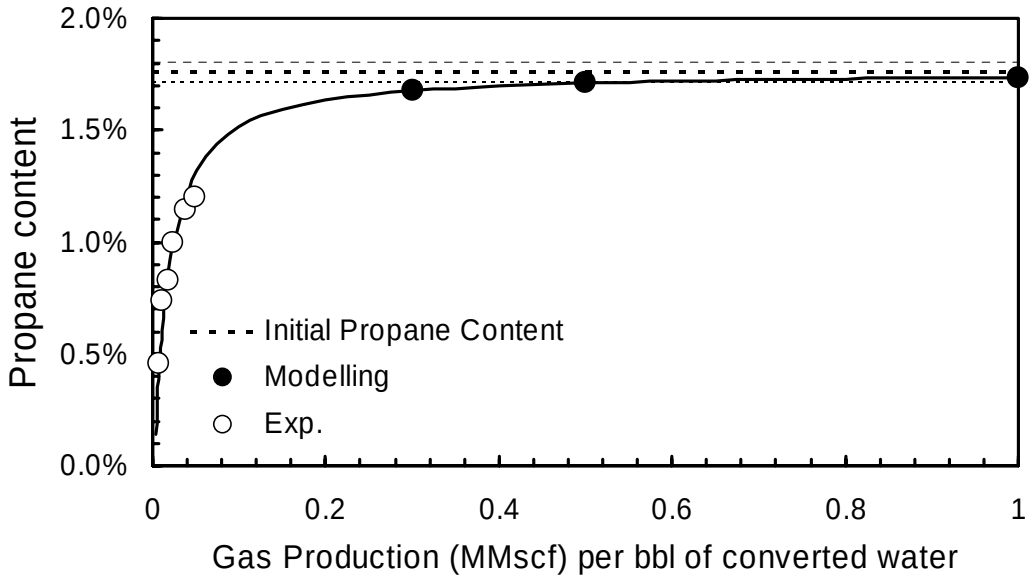

Figure 5.1 Compositional monitoring of propane in the vapour phase in function of the gas production per barrel of water converted to hydrate.

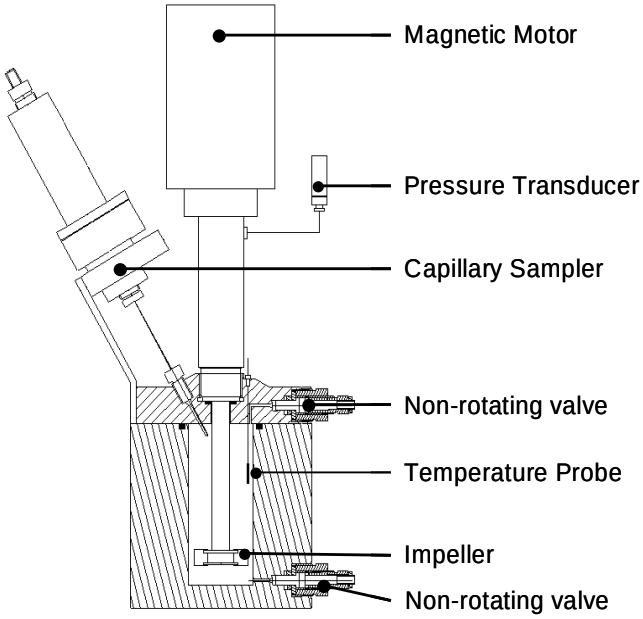

Figure 5.2 Schematic of gas phase monitoring equilibrium cell.

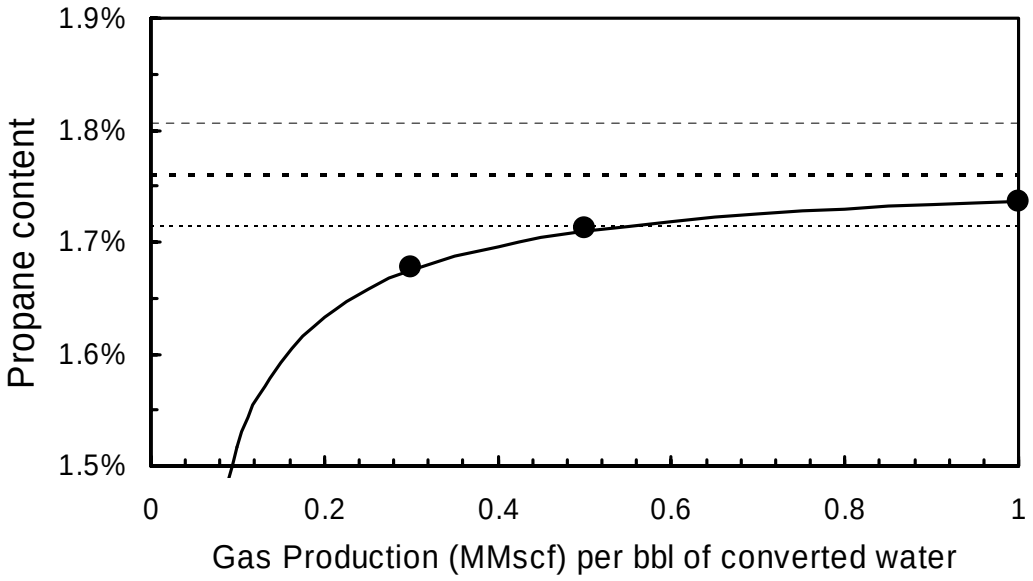

Figure 5.3 Compositional monitoring of propane in the vapour phase in function of the gas production per barrel of water converted to hydrate (the grey zone is the typical propane variation over a month of one of the sponsor field).

A seen in Figure 5.3, hydrate formation could be hidden by natural variation in the propane content and is the main weak point of this technique. The variation of the propane content of a natural gas field has been analysed over a two year period. Typically, the propane variation in the gas content for this example over one month is ± 0.1%, this could potentially hamper the sensitivity of this method (Figure 5.1 and Figure 5.3). However a continuous online device monitoring the C_1 and C_3 content of the gas phase could overcome this issue. The potential techniques that will be investigated in this chapter will be:

-Monitoring compositional change using Ultrasound

-Monitoring compositional change using Gas property measurement apparatus (GasPT)

5.2.2. Monitoring Compositional Change Using Ultrasound

In this section feasibility of using ultrasound for monitoring compositional change was investigated. To study the effect of compositional change on speed of sound an experimental cell with ultrasound transducer and visual windows has been used.

Volume of the cell was 1750ml. A specially designed mixer was used to avoid blocking the wave path. The cell was surrounded by a cooling jacket connected to a cooling/heating bath for temperature control purposes. To measure the pressure a Druck pressure transducer were used with the accuracy of ±0.3 bar. Temperature measurement was done by using a PRT temperature probe with the accuracy of ±0.1 °C. To measure speed of sound a parametric pulser/receiver has been used to agitate a 5 MHz ultrasound transducer, the ultrasound receiver was connected to a 500MHz DSO (digital oscilloscope) for data analysis (the measurement method has been explained in chapter 3). A PC was used to record all the data during the experiment. This cell could operate up to 415 bar. Figure 5.4 shows the schematic of the experimental setup.

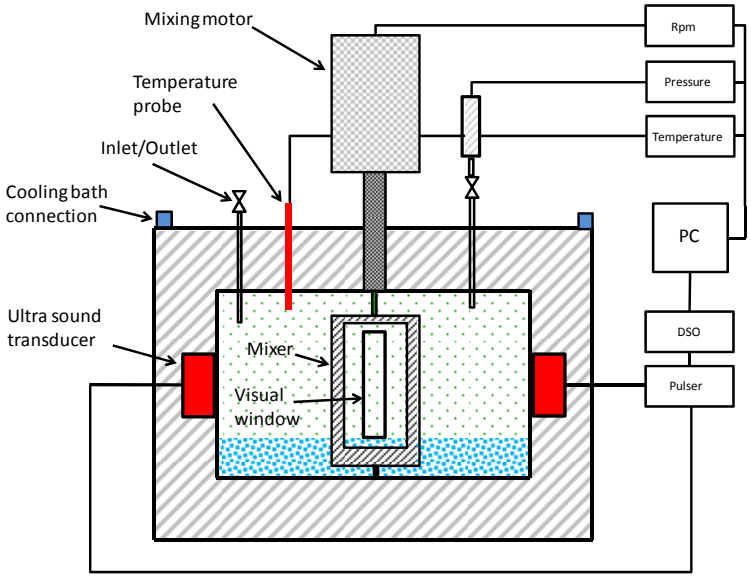

Figure 5.4 Schematic of the high pressure ultrasound cell

To perform these experiments deionised water was injected with an equivalent amount of 1bbl/MMscf and after vacuuming the system was pressurised with natural gas (Table A.56). Because of the small amount of water, to be able to form hydrate, the cell was cooled down to freeze the water and then heated up to the desired equilibrium temperature to form hydrate. After hydrate formation (confirmed with visual observation) and determining the equilibrium point, sound velocity was measured. At the same equilibrium point but without hydrate the speed of sound was measured for

comparison. Figure 5.5 demonstrates the difference for system with and without hydrate.

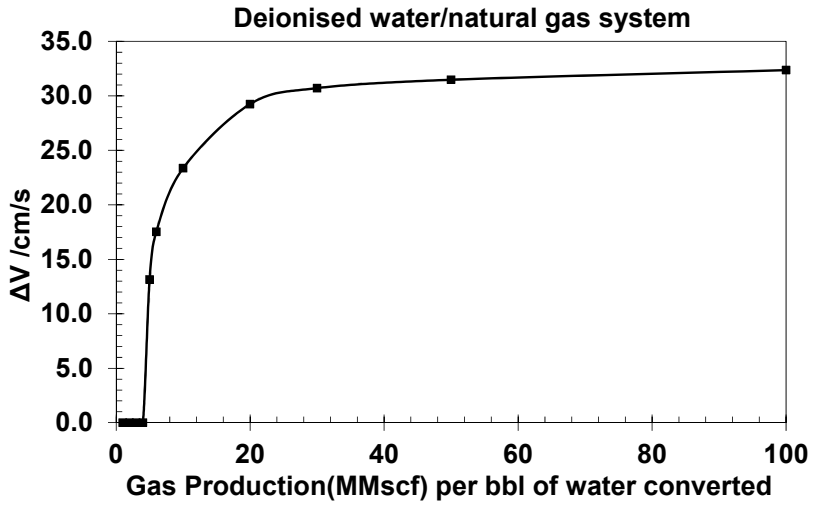

Figure 5.5 Monitoring changes in speed of sound between system containing hydrate and without hydrate at same pressure and temperature.

As one can see in this figure, changes in the gas composition cannot be detected up to 5 bbl of water converted to hydrate. By increasing the amount of water converted to hydrate above 5 bbl, changes in composition caused an increase in the speed of sound. At 30 bbl, the speed of sound increased but the slope of this increase is significantly decreased. For higher amount of water converted to hydrate the changes are not significant. The investigation showed that it could be due to formation of hydrate structure I. To clarify this effect the related hydrate phase boundaries are plotted in Figure 5.6.

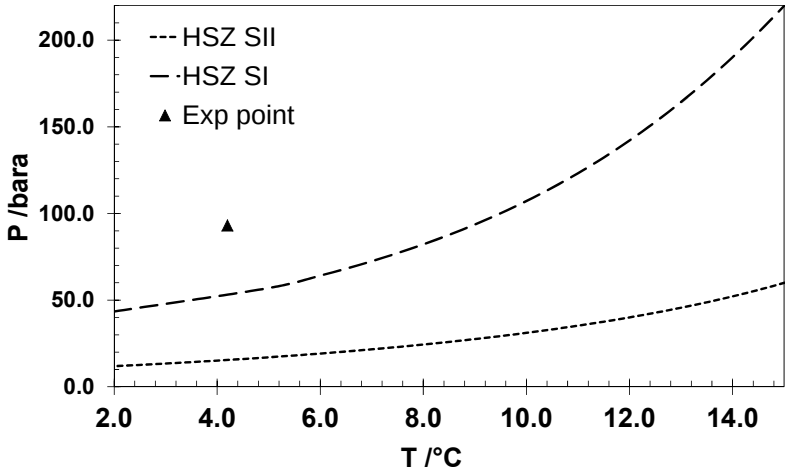

Figure 5.6 Phase boundary for hydrate structure I and hydrate structure II and the experimental conditions.

As can be seen in this figure the measurement point is far inside hydrate structure I stability zone and after initial formation of hydrate structure II, hydrate structure I has formed in the system due to consumption of heavier components. To avoid this issue the following series of experiments were designed to form hydrate outside the hydrate sI stability zone but inside the hydrate sII stability zone. Figure 5.7 shows the results of these experiments. As one can see in this figure, from 5 bbl of water converted to hydrate the change in speed of sound become detectable but the important finding here is, by increasing the amount of water converted to hydrate (sII) the speed of sound is increasing continuously. So based on these results it can be concluded that using speed of sound measurements in gas phase could be used as a method for monitoring hydrate form in the pipeline however it should be mentioned the detection level is after 5 bbl of water converted to hydrate per MMscf. Finding a more sensitive speed of sound measurements could improve the sensitivity level.

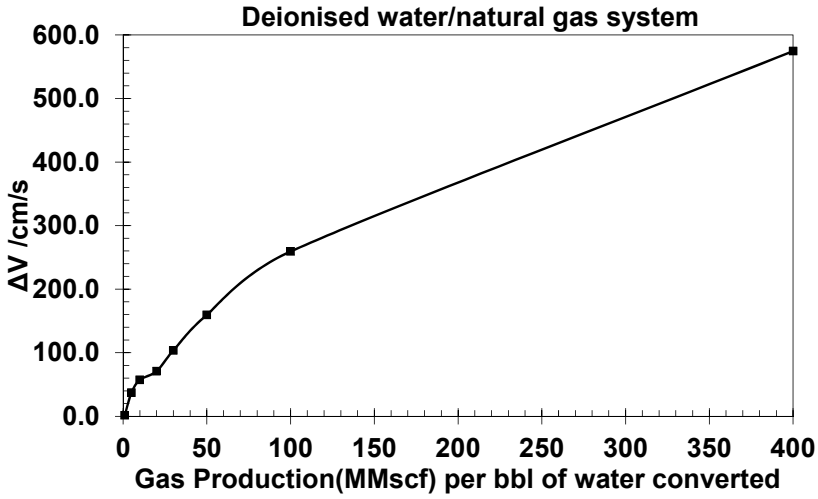

Figure 5.7 Monitoring changes in speed of sound between systems containing hydrate sII and without hydrate at same pressure and temperature.

The non-intrusive property of speed of sound measurement is a very positive point for this method. Because of the non-intrusive property this method could be a perfect apparatus for monitoring changes in speed of sound due to hydrate formation compositional change. However to use this method it should be calibrated for a specific pipeline and gas and non-hydrate related fluctuations in composition should be considered. The main drawback for this method is hydrate sI formation. As it was shown, if hydrate sI forms, changes in speed of sound would not be significant enough to be clearly detected and sharp decision be made and it might be effected by pipeline gas composition variation condition however in pipeline condition main structure will be sII which is easily detectable by this method but this possible effect should be considered in the calibrations. As it was mentioned before this issue is due to sensitivity of speed of sound to changes in all composition and not being sensitive to one component so any changes in total composition could change the speed of sound and will affect the method sensitivity. To overcome this challenge a new commercialised device was used to focus on some specific components. The next section will describe this apparatus, related experiments and results.

5.2.3. Monitoring Vapour Phase Compositional Change Using GasPT

To be able to monitor composition changes while hydrate is forming, it was decided to use a commercial device called GasPT (gas property measurement) using the same procedure as done for speed of sound measurements.

GasPT sensor can measure pseudo gas composition of methane, propane, carbon dioxide and nitrogen. It is not like a calorimeter, which measures the calorific value directly or a gas chromatograph, which measures the concentration of each component within the gas. Instead it measures speed of sound, thermal conductivity at two points, temperature and pressure. From these measured properties and considering the total concentration of all components as 100, it infers an effective gas mixture comprising the mentioned four components. To be able to use this device, the gas should be flown through the inlet of the equipment and be released to atmosphere; to have continues supply with maintained pressure, a 9 litre piston/cylinder cell was used to conduct the experiments. Figure 5.8 shows the experimental setup used for these measurements.

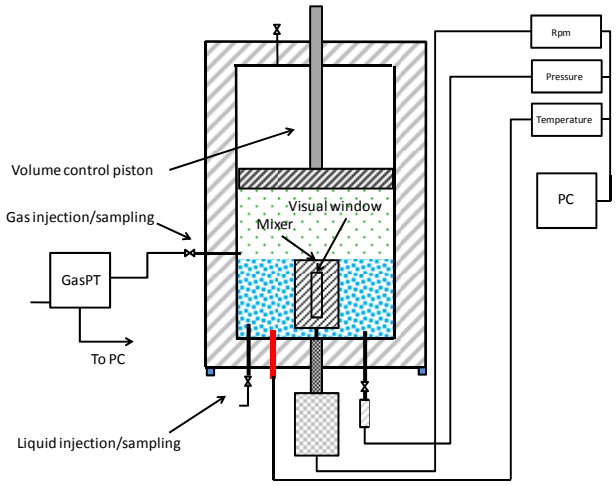

Figure 5.8 Schematic of GasPT measurement setup and the 9 litters piston/cylinder cell

Like the speed of sound measurements procedures, hydrates were formed based on 1 bbl of converted water in MMscf of gas. In these experiments hydrate was formed once inside sI hydrate stability zone and in another series outside sI and inside sII. All the measurements were also confirmed with gas chromatograph analysis. Figure 5.9 and Figure 5.10 show the results of these measurements. As one can see in Figure 5.9 when the system is inside sI hydrate stability zone, initially when hydrate forms and

the amount of water converted to hydrate is small (below 30 bbl/MMscf) the propane to methane ratio start to decrease and it means that propane has been consumed during hydrate formation which is a sign of sII hydrate formation this change start to be detected from 5 bbl of water converted to hydrate in MMscf of gas. After increase in the amount of water converted to hydrate the curve starts to increase slightly and at higher amount converted water the propane to methane ratio is almost constant and difficult to detect with this method.

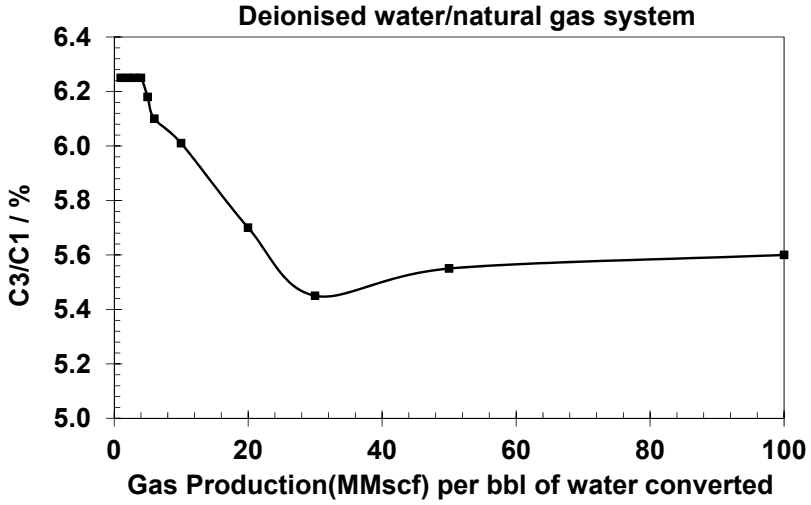

Figure 5.9 Monitoring changes in equivalent propane to equivalent methane by using GasPT and confirmed with GC.

In the next set of experiments, same procedure was followed but the equilibrium point was changed to avoid hydrate sI. As one can see in Figure 5.10 the propane to methane ratio is continuously decreasing. These results also show, changes due to hydrate formation is significant enough to be detected with GasPT. GasPT could clearly detect the changes due to hydrate formation. As it is already commercialised it can be used for monitoring compositional changes along pipeline due to hydrate formation with slight modification.

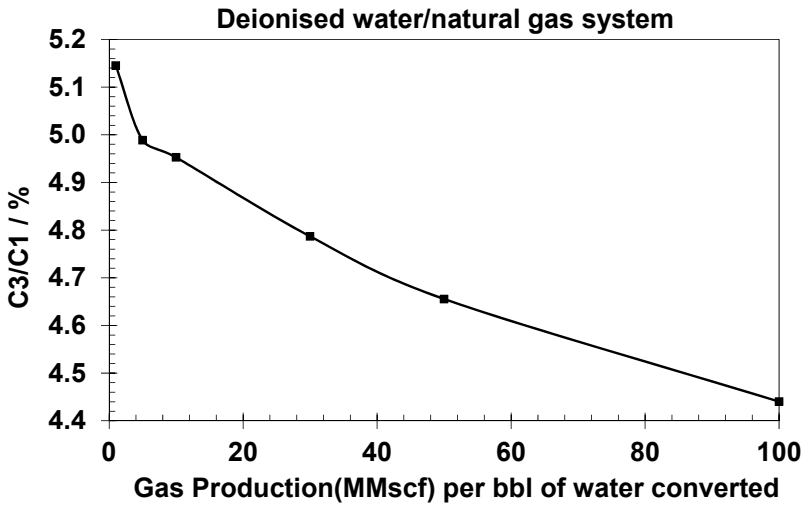

Figure 5.10 Monitoring changes in equivalent propane to equivalent methane by using GasPT and confirmed with GC when system is outside sI and inside sII hydrate stability. Zone.

The main advantage of using GasPT in pipeline condition in comparison to speed of sound method is it could give the changes in equivalent propane and methane concentration, it will help to define the hydrate structure formed so the operators could detect while it is difficult for speed of sound method to detect the changes due to hydrate formation. Other benefit of this method is that, it will be less sensitive to background noises, hence making this method more robust. However this device is only designed to work at low pressure and the gas must be released to the system very slowly and should not exceed the pressure limit (3 bar) also it is sensitive to water as well. It means to be able to use this device a pre-conditioning system is required for field applications to clean the gas and reduce the pressure to the limit range. Also during the measurements more stable reading will be obtained if the flow is kept constant. Periodic calibration check for specific gas and maintenance will keep the setup more reliable.

5.2.4. Monitoring Extracted Gas from Aqueous Phase

Using the speed of sound and GasPT in gas phase was suitable while the amount of hydrate was small (if large amount of hydrate forms it is too late for early warning system) but at same time the hydrate must exist in the system to be able to see the change in composition. In some cases hydrates will form in pipeline at some point but

may dissociate later at the point of monitoring. To be able to detect this formation for early warning purposes a memory based method was suggested and the feasibility was investigated in chapter 4. In this section a compositional change method has been investigated as a complementary to hydrate memory technique.

To be able to conduct these tests, two experimental setup were designed, one setup was used the GasPT apparatus (Figure 5.8), in this work different amounts of hydrate were formed and dissociated in different runs. In each test, after dissociating the hydrate, the piston was pushed toward the product side to reduce the size of the cell and consequently remove the free gas from the system. The piston was then pulled back to expand the cell volume and consequently release the dissolved gas from the aqueous phase. This released gas was then flown through to the GasPT at a constant flow rate.

In the second setup hydrates were formed in a 2400 ml cell. In this cell PRT temperature was used for temperature measurements and a Druck pressure transmitter was used for pressure measurement purposes. The measurement accuracy for temperature was ±0.1 °C and for pressure was ±0.3 bar. Figure 5.11 shows the schematic of this setup.

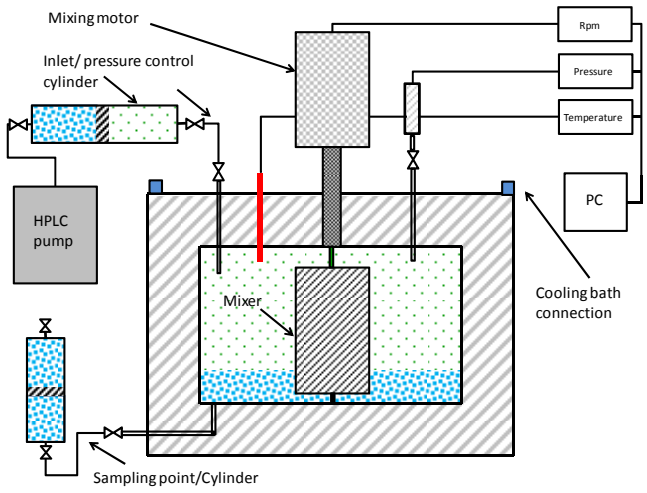

Figure 5.11 Schematic of high pressure cell for monitoring gas composition released from aqueous phase.

As a general procedure for all of these experiments, 1000ml of aqueous phase was loaded in the cell and after vacuuming, the cell was pressurised with a typical natural gas to the desired pressure. The system was cooled down to form hydrate and after

certain amount of hydrate was formed, the cell was heated up to dissociate hydrate. After hydrate dissociation and certain waiting time, to simulate the separator condition, the pressure was dropped to 20 bar and the temperature was set to ambient. At this equilibrium point, a sample of the aqueous phase was taken from the bottom of the cell and transferred to a piston cylinder. By expanding the piston side of the cylinder, the released gas was analysised with GC. In this work like in previous section the experiments were conducted for two equilibrium points, one inside the hydrate sI stability zone and the second point was outside sI stability zone but inside the sII stability zone.

5.2.4.1. Results

Deionised water and natural gas system

In this test hydrates were formed in presence of natural gas and deionised water. According to the explained procedure inside hydrate sI and sII, 9 mass% of water was converted to hydrate. After hydrate formation, the system was heated to 3 °C outside hydrate stability zone and left at this point for 3 hours. The released gas from aqueous phase was taken at separator condition (20 bara and ambient temperature), the gas sample was analysed with GC and GasPT (GasPT results was used to confirm the trends not for absolute comparison). Figure 5.12 shows the results of these experiments. As one can see in this figure, in the test without hydrate formation the concentration of methane is considerably higher than for the system with hydrate. The opposite results could be seen for heavier components, for example, in the system with hydrate history, the propane content is twice the value of the system without hydrate history. The same can be observed for ethane and butane, the reason for selecting propane as the indication in this work is propane is a hydrate structure II former and its concentration is usually significant enough in natural gas for detection. This experiment was repeated 3 times to confirm the repeatability of the results, almost the same trends were also observed in same experiment in the other cell analysed with GasPT.

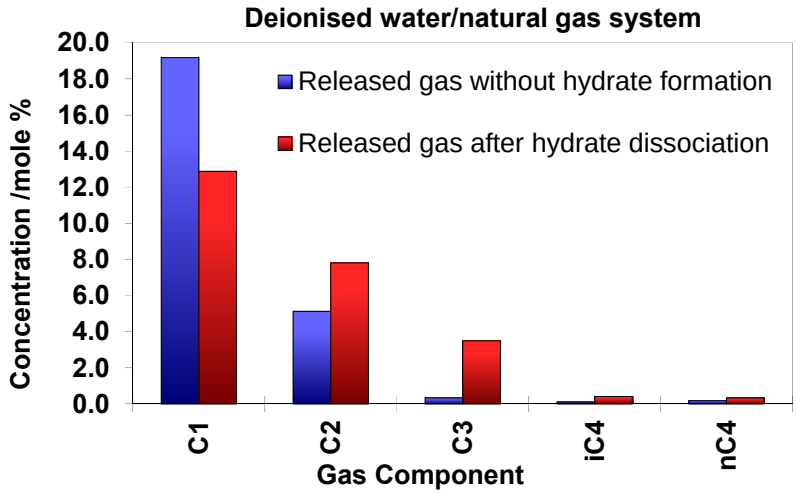

Figure 5.12 Released gas composition comparison for system with hydrate and system after hydrate dissociation (methane composition was subtracted with 75 to have better illustration for heavier components).

The effect of amount of hydrate

To study effect of amount of hydrate on the extracted gas from aqueous phase different amounts of hydrate were formed and the concentrations of the components were measured by GC and GasPT. Figure 5.13 shows the results of these measurements. As one can see in this figure, when the system did not experience hydrate in its history the value is shown as zero, at this point propane to methane ratio is very small, when the system has experienced 3 mass % hydrates (water converted to hydrate) in its history, the propane to methane ratio will increase significantly. This increase was expected as hydrate prefers large round molecules in its structure so reduction of heavier components will have opposite effect in the aqueous phase. The propane to methane ratio was still significantly bigger than for the system which never faced hydrate formation but the trend shows that by increase in the amount of hydrate, propane to methane ratio are decreasing in comparison to the lower amount hydrate. These results could be due to hydrate structure I formation as observed in the previous section.

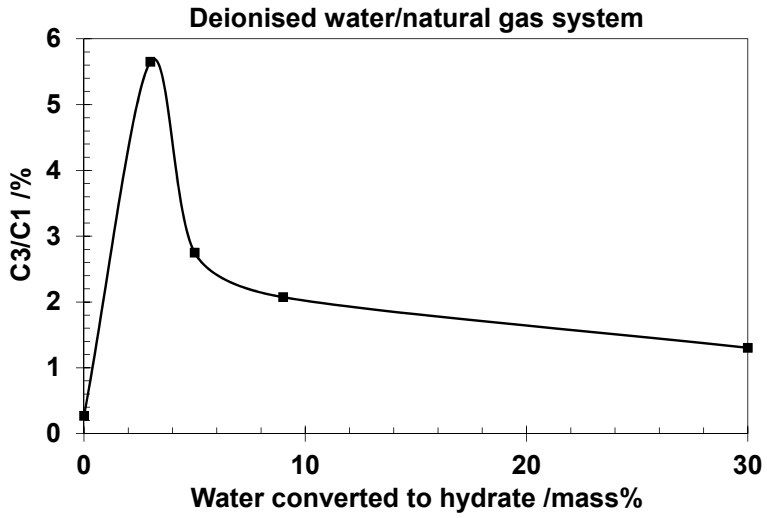

Figure 5.13 Propane to methane ratio for different amount of water converted to hydrate.

Another series of experiments were designed outside structure I and inside structure II stability zone to avoid any risk of hydrate structure I formation. Figure 5.14 shows the results of these experiments. As one can see by increasing the amount of water converted to hydrate, the propane to methane content (C3/C1) is significantly increased. Based on these results it can be concluded that when the system is far inside hydrate structure I stability zone for small amount of hydrate the dissolved propane to methane ratio will be increased, by increase in the amount of hydrate this value become smaller due to hydrate sI formation as more methane will be consumed although these values are always greater than the initial values (no hydrate history). Based on these results, the formation of hydrate in the system (mainly sII) will increase the propane to methane content. It means that if hydrate forms in a natural gas system, a while after (for these experiments three hours after) if an aqueous sample is taken at the separator and the gas is extracted from this sample; the propane to methane ratio will be more than the time if system never experienced hydrate. This property could be used for hydrate early warning system by using a base test experiment and comparing the results with the pipeline propane to methane ratio. If the propane to methane ratio is significantly greater than the baseline test, it is a sign of hydrate risk along the pipeline and the operator should take action against the risk by

optimising the inhibitor injection rate (using water activity method or C-V device) or changing the pipeline condition.

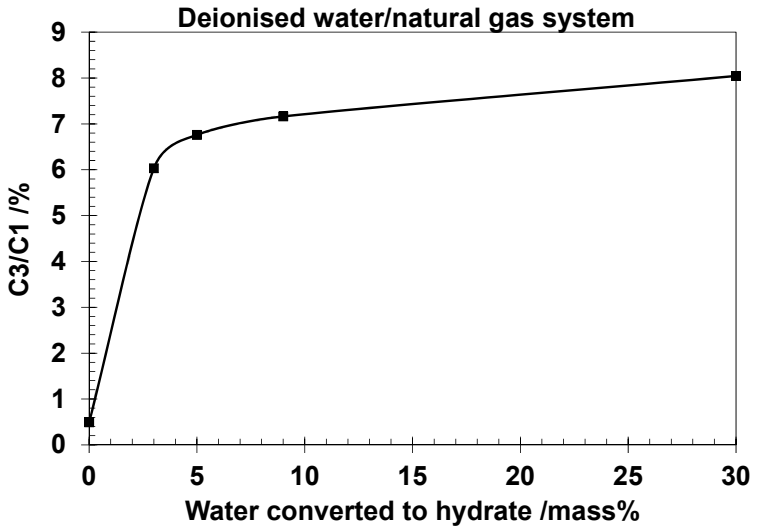

Figure 5.14 Propane to methane ratio for different amount of water converted to hydrate.

Based on the results obtained in these series of experiments all the experiments after, are conducted outside sI and inside sII hydrate stability zone to avoid any effect caused by sI formation.

Effect of time outside hydrate stability zone

In this series of experiments the aim is to study the effect of waiting time outside the hydrate stability zone. In this work, 9 mass% of water was converted to hydrate. After hydrate formation, the system was heated to 3°C outside the hydrate stability zone and the sample time was varied to study the effect of time. The sample was taken at separator condition (ambient temperature and about 20 bara). The gas sample was analysed with GC and. Figure 5.15 shows the results of these experiments.

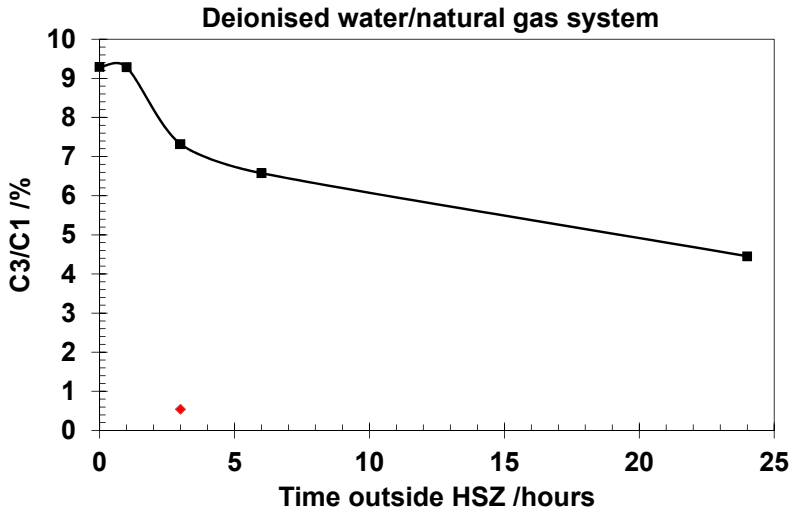

Figure 5.15 Propane to methane ratio for different time outside hydrate stability zone.

The red point in the figure shows the propane to methane ratio for the blank test when there is no hydrate in the system. In the first measurement, sample was taken just after hydrate dissociation. As one can see C3/C1 value is significantly high showing the high concentration of the propane due to hydrate formation. By increasing the time before sampling the aqueous phase to 1 hour this value is not changing significantly. For 3 hours waiting time the ratio was reduced and this trend continued for longer waiting time. The C3/C1 ratio after 24 hours was still much higher than for the system without hydrate. Based on these observations it can be said that waiting time will reduce the C3/C1 ratio. In a practical point of view the longer time passed after hydrate dissociation might weaken this effect and the propane to methane content will become smaller and consequently more difficult to differentiate from the base test. So it can be concluded that this method could be used at least 24 hours after hydrate dissociation.

Effect of oil as impurity in the system

Aim of this experiment is to evaluate the effect of oil (Table A.16) as an impurity in the aqueous phase. Because gas is highly soluble in oil and this method is very dependent on the solubility of gas components in the aqueous phase it was decided to evaluate this method in presence of oil and study how the results will be affected. To

conduct these experiments 300 ml of black oil was added to the system and a similar procedure was followed for sampling. Figure 5.16 shows the results of this work.

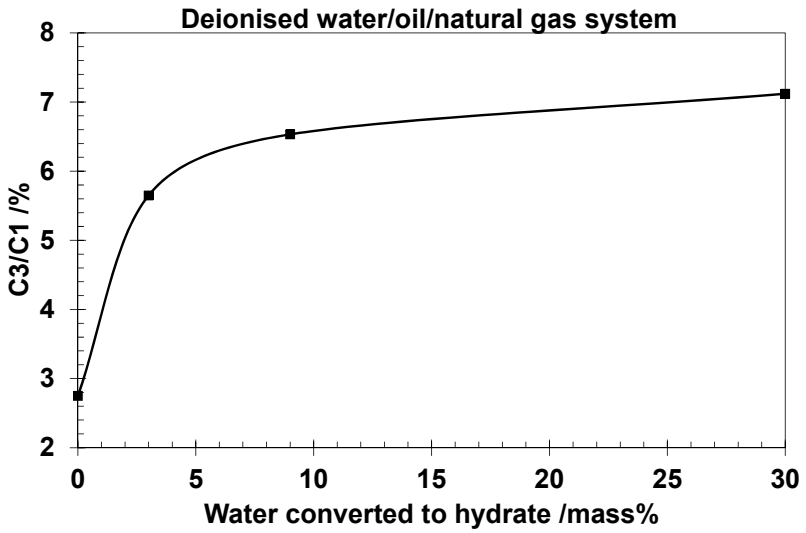

Figure 5.16 Propane to methane ratio for different mount of water converted to hydrate in deionised water, oil and natural gas system.

This results show that in the blank test (no hydrate) the C3/C1 ratio is significantly increased in comparison to the one without oil. When system experience hydrate, like the system without oil the C3/C1 ratio increases and by increasing the amount of hydrate this ratio will increase. Presence of oil in the system has mainly effected the blank test and increased C3/C1 however this value is still much smaller than the time when there is hydrate so the results show when oil is present it might slightly affect the results but this method is still applicable. For field applications it might be good to have a conditioning system prior to taking the sample if there is oil.

Effect of hydrate inhibitors and salt on the method

In this section the C3/C1 ratio was investigated in presence of MEG, methanol, NaCl and KHI. In these series of experiments, 10 mass% MEG, 10 mass% methanol, 5 mass% NaCl and 1 mass% KHI was used to form hydrate in presence of natural gas. The system was heated up to 3 °C outside hydrate stability zone after about 15 mass% of water was converted to hydrate. For different waiting time outside hydrate stability zone, aqueous samples were analysed. Figure 5.17 shows the results of these tests. The red point in the figure shows the blank test. As one can see the C3/C1 ratio is

significantly increased in comparison to the time when there is no hydrate history. The C3/C1 ratio decreased with time but this decrease is still significantly higher than the blank test.

In general, these experiments showed that hydrate history in systems containing MEG. Methanol, salt and KHI caused a significant increase in propane content and C3/C1 ratio for the gas released from aqueous phase in comparison with the same system without hydrate history. However for system containing methanol this effect will disappear much earlier than the other systems. These results also showed that this method could efficiently be used for MEG and salt system and with less waiting time could be used for KHI system as well.

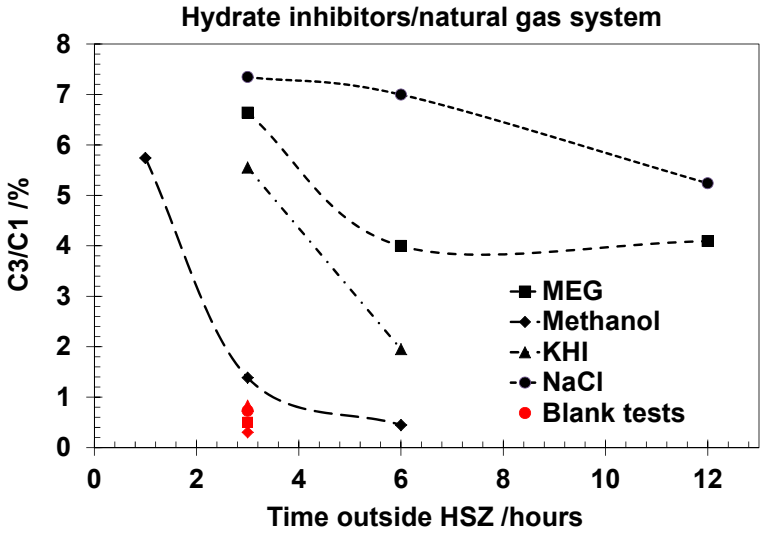

Figure 5.17 Propane to methane ratio for different systems and different time outside hydrate stability zone.

Simulating pipeline condition

In the previous experiments hydrates were formed in a closed system to investigate effect of hydrate formation on the released gas from aqueous phase. When hydrate forms in a system, heavier components will go to hydrate phase and therefore after consumption of heavier components hydrate formation will stop. In these series of experiments the aim was to simulate the pipeline condition by continuous injection of fresh gas from the bottom of the cell and release with the same rate from top of the cell to replace the gas with lower amount of heavy components. In this work 7 mass% of

NaCl and 25 mass% of MEG were tested individually as well as deionised water system. In these experiments approximately 30 mass% of water was converted to hydrate before dissociation. These experiments were repeated for different waiting time. Figure 5.18 shows the results of these experiments. As before blank test were measured for system containing same gas and aqueous phase without hydrate formation. These measurements are shown with the red points in the figure. For MEG system, after hydrate dissociation and 3 hours waiting time, the propane content significantly increased. With time, the C3/C1 monotonously decreased but the value was still significantly higher than in the blank test after 12 hours. The same behaviour was seen for 7 mass% of NaCl and deionised water confirming that this method may have better performance in real pipeline condition because the gas will continuously be replaced with fresh gas.

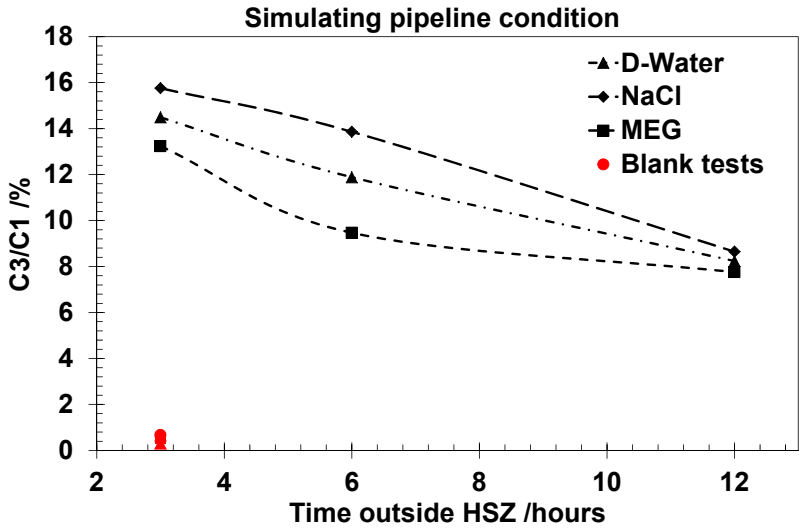

Figure 5.18 Propane to methane ratio for different systems and different time outside hydrate stability zone in flowing condition.

5.3. CONCLUSIONS AND FUTURE WORK

In this chapter, two methods have been suggested to be used for initial hydrate formation detection technique based on the effect of hydrate formation on the gas composition in vapour phase and extracted gas from aqueous phase. The effect of hydrate formation was studied in gas phase to see for low amount of hydrate formation how the propane content will change; also these data were compared with a filed data

provided with one of the project sponsors to study the variation range of gas composition over a time period. The results showed that formation of small amount of hydrate could interfere with gas composition variation however for higher amount of hydrate formation; these variations would not affect the results. The measurement results were also compared with an in-house thermodynamic model, the results were in a very good agreement. To use this method two series of experiments were designed, one was focused on the gas phase and the second to monitor the extracted gas from aqueous phase after hydrate dissociation. To monitor the changes due to hydrate formation in gas phase, sound velocity measurement and a commercialised device called GasPT were used. Various concentrations of Hydrates were formed based on 1 bbl/MMscf and after each formation sound velocity was measured and compared with the related blank test and same procedure repeated for GasPT. Results showed that this method could detect hydrate formation for more than 5 bbl/MMscf of water converted to hydrate for both sound velocity and GasPT, it was found that for large amount of hydrate formation, structure I will stabilise in the system and for above 20 bbl/MMscf it is very difficult to detect the changes. These results were confirmed by forming hydrate outside structure I stability zone and inside structure II stability zone. This method could be used for pipeline condition as the main structure is II.

Extracted gas from aqueous phase was used to determine hydrate history. It was found that propane concentration was significantly increased in the gas released from aqueous phase in comparison with the same system without any hydrate history. These test were conducted in presence of deionised water, MEG, methanol, NaCl, KHI in natural gas system for different waiting times outside hydrate stability zone and different amount of water converted to hydrate. The gas sample was analysed with GC and also same experiments were conducted in another cell and measured by GasPT (to confirm the trend and validating the GasPT results). In all tested systems it was seen that hydrate history caused a significant increase in C3/C1 ratio in comparison to the related blank test. Because of high dependency of the system to gas solubility in aqueous phase, black oil was used to investigate distortion of results due to presence of oil in the system. Results showed that propane to methane ratio was still high in comparison to the blank test however this time the ratio was much bigger for the blank test. These results showed that for different amount of hydrae this method can easily

be used to detect hydrate history. To further simulate the pipeline condition a continues fresh gas flow was applied in another series of experiments for deionised water, NaCl and MEG system and the results showed a much bigger difference between the blank test and the sample from water with hydrate history. These results confirmed that this method could possibly give better results in pipeline condition.

In general from these results we can say compositional change due to hydrate formation in gas phase and from the extracted gas after hydrate history could be a robust method for detecting early sign of hydrae formation and can be a very powerful complementary method for other hydrate monitoring and initial hydrate formation detection techniques developed in this thesis. A patent was also successfully filed for this method for commercialised applications.

It was suggested to organise a field trail at one of the sponsor's facilities to evaluate the feasibility of this method for real applications.

CHAPTER 6. PROTOTYPES DEVELOPMENT AND FIELD TRIALS

6.1. INTRODUCTION

Several novel techniques, i.e. conductivity-velocity, water activity, water content, compositional change, onset of hydrate formation (memory effect), based on downstream and online measurements have been successfully developed in this work and detailed in Chapter 2 – 5. For some of these methods which have the potential to be applied in industry and could have very crucial effect in optimising hydrate inhibitor injection rates, prototype devices were developed for monitoring the actual degree of hydrate inhibition in oil and gas transport pipelines, hence hydrate safety margin. This chapter details these prototypes and related field trials

6.2. CONDUCTIVITY-VELOCITY (C-V) PROTOTYPE DEVELOPMENT

One of the main developed methods in this work is the integrated conductivity-velocity (C-V) device. By using this method one can measure alcohol and salt concentrations, or KHI and salt concentrations, or AA and salt concentrations in aqueous phase, and determines the hydrate stability zone (HSZ) hence the degree of hydrate inhibition. This method can also be used to determine the amount of impurity in high concentration of MEG solutions up to 100% for monitoring MEG regeneration process. The main aim of measuring inhibitor and salt concentrations is to determine the degree of hydrate inhibition, or safety margin, by determining the hydrate stability zone (HSZ). The first step of this part was to develop a prototype which is able to measure the salt and inhibitors concentrations. After successful development of the first step, the second step was to integrate this prototype with our in house thermodynamic model for determining hydrate phase boundary. And the final goal

was moving toward online applications. Figure 6.1 shows the principle of this development.

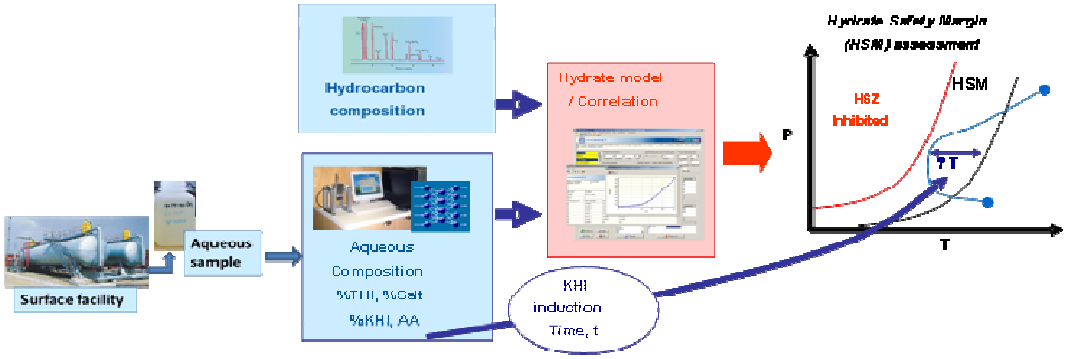

Figure 6.1 Principal of integrated conductivity-velocity (C-V) prototype.

6.2.1. Hardware Development

To be able to develop the prototype, raw data should be measured for electrical conductivity and sound velocity. A microcontroller based CMD230 wave generator was used including a built in 16 bit AD convertor which measures the induced voltage for translating to electrical conductivity. Temperature was also measured by using an 8 bit AD convertor integrated with the system. The measured data were transferred to computer over RS232 serial port.

To measure sound velocity, a pair of 1 MHz, Panametric V104 ultrasound transducer was used for transmitting sound wave and receiving the data through the sample inside the cell. A generic ultrasound pulse generator from paramedic (PR5072) was used to generate -100 volts pulse to agitate the ultrasound transducer. This pulser was set to 1 MHz to meet the ultrasound sound transducer specification. To acquire the ultrasound wave a very high frequency data acquisition board from Linkinstruments® based on ultrafast 8bit Atmel ADC and Xilinx Spartan FPGA (Field Programmable Gate Array) was used. The large amount of captured raw data was transferred to the PC over Universal Serial Bus (USB2.0). To power up all these electronic circuits a power supply was designed to meet all power requirements.

6.2.2. Software Development

To output salt and inhibitor concentration and predict hydrate phase boundary, a programme must be developed to meet the following requirements:

- Transfer captured ultra sound waveform from data acquisition board
- Transfer the captured data from conductivity measurement board
- Analyse the transferred data
- Feed the conductivity, sound velocity and temperature data to processing unit
- Process feed data by using a suitable pre-trained ANN network to output salt and inhibitor concentrations
- Use the salt and thermodynamic inhibitor concentrations to output hydrate stability zone using integrated in-house thermodynamic model

Addressing each of these requirements has been detailed in the following sections.

6.2.2.1. Capturing and Analysing Ultrasound Waveform

To communicate and initialise the FPGA (Field Programmable Gate Array) a dynamic link library (DLL) was developed. This library was then used to capture data on 100 MSPS (Mega Sample per Second) and transfer the data to a PC over USB port. To process the raw data and measure the speed of sound two methods were used: averaging method and autocorrelation method.

Averaging method:

In this method a real time averaging subroutine was developed to reduce the noise by low-pass filtering and averaging the raw data. Principle of the averaging has been presented in chapter 2. To calculate the speed of sound it is necessary to find the time in which the wave travels from the transmitter surface and arrives at the receiver side. The time delay for the cell wall should be considered when determining the travel time. To determine this time delay, the wave first arrival and second arrival should be found and the travel time could be calculated using the equation explained in chapter 2. Figure 6.2 illustrate this method.

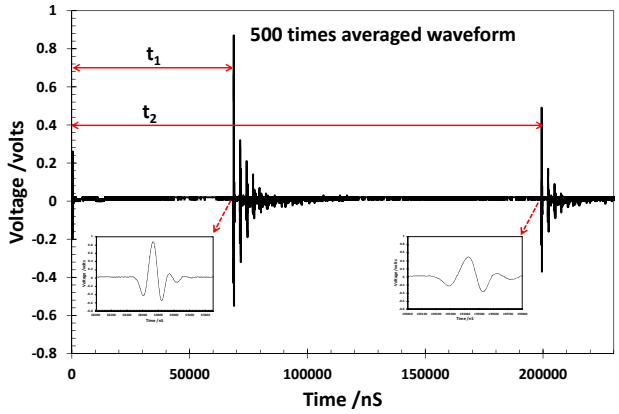

Figure 6.2 Determining travel time using averaging method

A subroutine programme was developed to fit a curve on the received waveform and calculate first and second arrival times by crossing this fitted curve with the average base line. The speed of sound can be accurately calculated by knowing the distance between the two walls of the cell (obtained from calibration package). This method for determining the travel time is accurate enough for our purpose; however there are two drawbacks for this method. First, at measurement temperature above 24°C the waveform can get distorted and therefore determining the first and second arrival may not be possible and consequently the subroutine could not find the speed of sound. Second, the huge amount of calculation and data capturing take about two minutes to be completed which may not be desirable for operators. To overcome the first problem, a protection subroutine was developed to adjust the curve fitting point until it finds the perfect match. To reduce the 2 minute processing time, it is possible to reduce the number of averaging from 500 wave sample to smaller numbers (10, 100, 300, and 400) but it can result in about 2 % reduction in measurement accuracy.

To further improve the accuracy and reduce the processing time of sound velocity measurement, a new approach was introduced which solves both problems simultaneously. The new method is called autocorrelation.

Autocorrelation method:

This method is used to process the waveform and find the travel time directly instead of finding first arrival and second arrival times. Ultra sound waveform is a combination of periodic waves with attenuated amplitude. Autocorrelation is a

mathematical tool for finding periodic patterns such as the presence of a period signal which is buried under noise. In our case by autocorrelating the waveform, the periodic pattern will appears in the peak points of the autocorrelated waveform. By defining the distance between any two sequential peaks the travel time can be calculated directly. The main advantage of autocorrelation is that there is no need to average the waveform for removing the noise because autocorrelation will remove the noise effect. Another advantage of autocorrelation is that any distortion in the waveform (like the one sometimes observed at temperatures above 24 °C) would not affect the results. Further advantage of using autocorrelation is that human measurement error while generating data required for training ANN will be removed and more precise results will be achieved. Equation 6.1 and Equation 6.2 show the related equations for auto correlation:

$$Y_j = \sum_{k=0}^{N-1} X_k^{\bullet} \times X_{j+k} \qquad \text{Equation 6.1}$$

$$R_{XXi} = Y_{i-(N-i)} \qquad \text{Equation 6.2}$$

For i= 0, 1, 2, …, (2N-2) and for j= -(N-1), -(N-2), …, -1, 0, 1, …,(N-2), (N-1)
where X is the discrete signal, $X^{\bullet}$ is complex conjugate of the signal X, N is the number of elements, Y represents sequence indexing and R_{XX} represents the autocorrelation of the discrete signal.

Figure 6.3 is a real example of the autocorrelated waveform generated in this work.

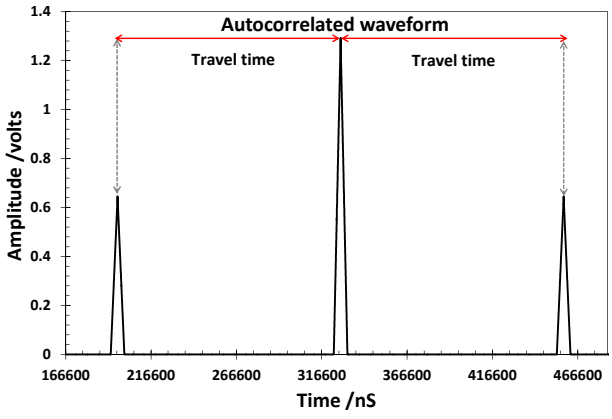

Figure 6.3 Determining the travel time using autocorrelation method

As one can see all the noise effect has been removed and only by selecting the peak points the travel time could be defined very precisely. This method also improved the processing time to less than 10 seconds. A program subroutine was developed to determine the travel time based on autocorrelation signal processing method.

6.2.2.2. Capturing and Analysing Conductivity and Temperature

To be able to determine electrical conductivity and temperature, a subroutine was developed to communicate with the microcontroller board. This subroutine initialises communication parameters for the conductivity measurement board and loads the calibration data. The captured temperature and conductivity data will be then transferred to the processing subroutine for determining the salt and inhibitor concentrations. In this subroutine, a stabilisation check has been also designed to avoid unstable readings error.

6.2.2.3. Determining Salt and Inhibitor Concentrations

After hardware integration and developing the capturing and calculation subroutines in previous sections, a Graphical User Interface (GUI) is required to interface between the operator and the hardware. The GUI is comprises of five main modules: a) capturing and analysing temperature, conductivity and sound velocity data, b) determining salt and inhibitor concentrations, c) predicting hydrate phase boundary, d) calibrating sound velocity measuring cell and e) calibrating electrical conductivity and temperature. A dilution factor has been designed in the main GUI for the time when measuring actual concentration of solution is not possible e.g. the concentration is not in training range or precipitation happens for high concentration of salt. By diluting the sample with same weight present of deionised water and setting the dilution factor to the right number of dilution the software will output the actual concentration by considering the dilution effect automatically. Figure 6.4 illustrates snapshots of these modules. Figure 6.5 shows a simplified flowchart and structure of developed C-V prototype software.

(a) & (b)

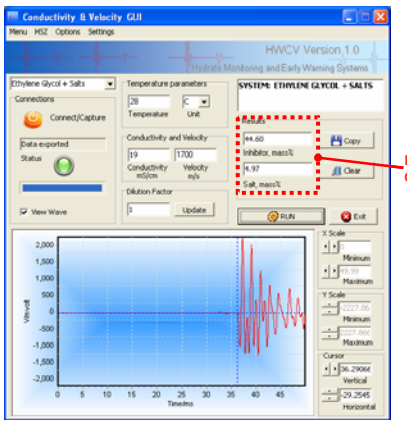

(c)

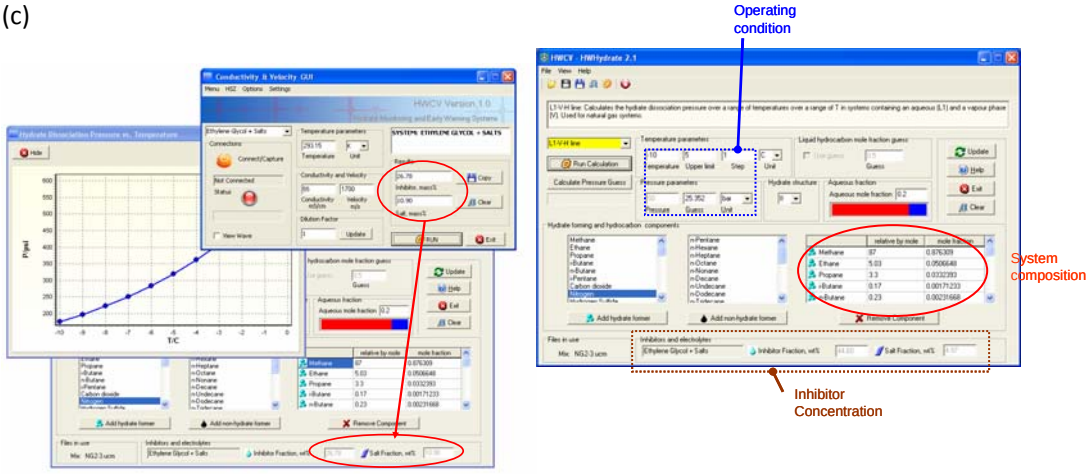

(d)

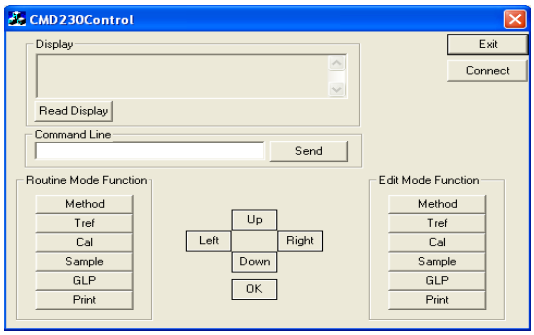

(e)

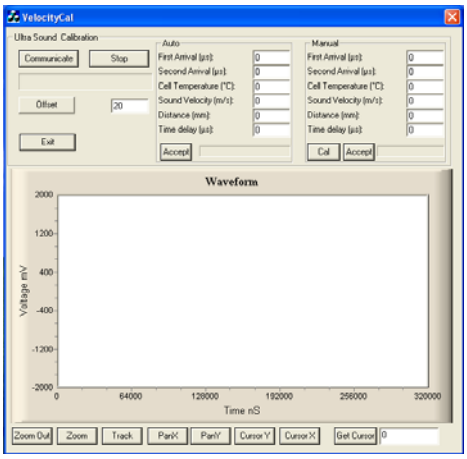

Figure 6.4 Developed C-V prototype GUI

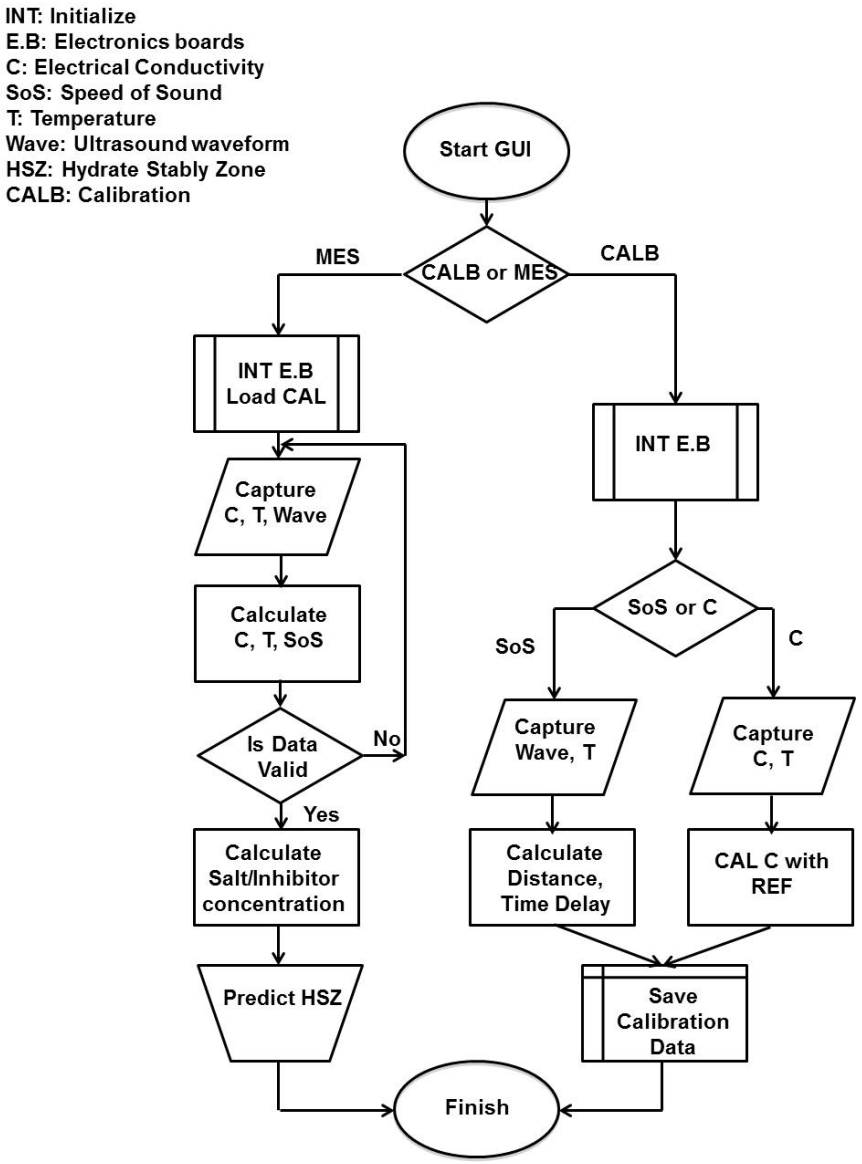

Figure 6.5 Simplified flowchart and structure of developed C-V prototype.

6.2.3. Developed C-V Prototype

Figure 6.6 and Figure 6.7 show two versions of the developed C-V prototype: stand-alone and temperature controlled prototype. The stand-alone version has a metal cell without temperature control which can be used for routine measurements, e.g. two parameters salt and inhibitor systems. The temperature controlled version which is equipped with a temperature controlled jacket can be used for ANN training data

generation and special applications like three-parameters measurements or constant temperature measurements.

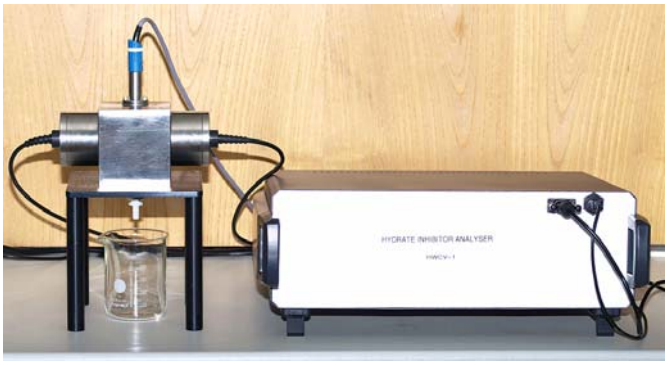

Figure 6.6 Stand-alone CV device.

Figure 6.7 Jacketed CV cell.

6.2.4. On-line C-V Prototype

The developed prototypes were designed for batch sampling. However, the C-V device has shown great potential for online application which could have a major impact in reducing the time required for sample handling and testing. Furthermore, online measurements would reduce the response time as devices could be installed subsea and nearer to the hydrate formation region.

Two avenues were explored to develop an online system:

- Direct online application at high pressure

- Indirect with a high pressure batch sampling system and pressure reduction to atmospheric pressure

Direct online application:

For this option, there are several challenges, including; 1) operating under pipeline pressure and temperature conditions, 2) sample collection, isolation, and discard, 3) some of out-sourced devices (e.g., high-pressure conductivity probes) are not designed for working at high pressure. To overcome these challenges we have designed a new C-V cell (Figure 6.8) and imbedded cooling channels to maintain a homogenous temperature in the cell and a medium pressure conductivity measurement probe from Kemetron. Data were generated for MEG-salt and MeOH-salt systems at high pressure (not reported in this thesis); the effect of pressure has been implemented in the C-V GUI for these systems as shown in Figure 6.9. In parallel an in-house high pressure (250 bara) conductivity probe was designed and constructed in our laboratory and workshop. Figure 6.10 shows the in-house conductivity measurement probe. This probe was tested under pressure and the results are in very good agreement with the low pressure commercialised one, however performance of this probe was affected by the presence of salt due to corrosion over time.

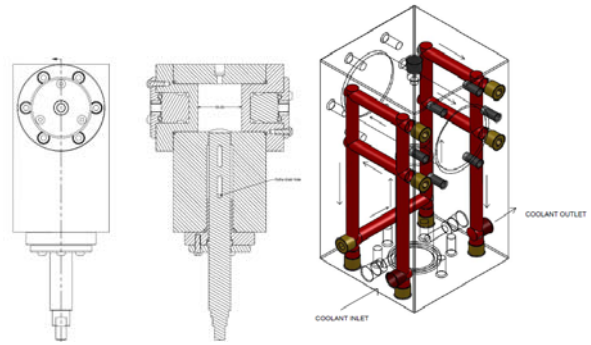

Figure 6.8 C-V high pressure cell.

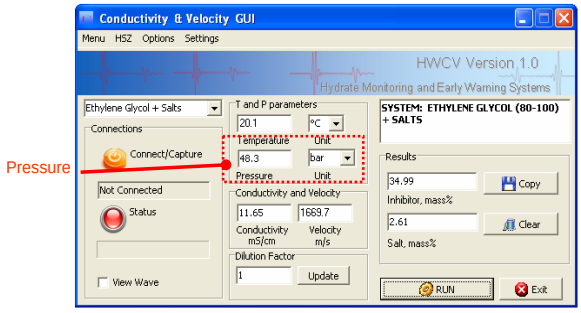

Figure 6.9 GUI of the C-V with pressure effect.

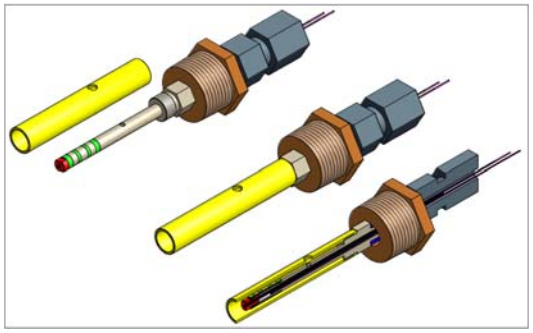

Figure 6.10 Drawing of the high-pressure conductivity probe

Indirect online sampling:

The second option is to sample the fluid (e.g. in the separator) under pressure and reduce its pressure to atmospheric pressure with an adequate sampling system. In corporation with a high pressure sampling expert company a flow diagram and P&ID (process and instrumentation diagram) was developed for offline sampling for the C-V prototype. The aim of this design is to improve the C-V prototype to an industrial standard for high pressure sampling and working in hazardous area as well as communicating with ITR (instruments technical room). As a brief description of this sampling system, the sample is coming from a high pressure sampling point, then the sample is filtered and the pressure is progressively reduced. Following pressure reduction, the sample is heated to limit the impact of oil contamination. The sample is then cooled down and placed in the C-V cell for analysis. The results can be then directly available in the control room. The fluid sample after analysis is sent to a storage drum, which can be emptied back to the process when full. Figure 6.11 shows the arrangement diagram of the indirect online C-V system.

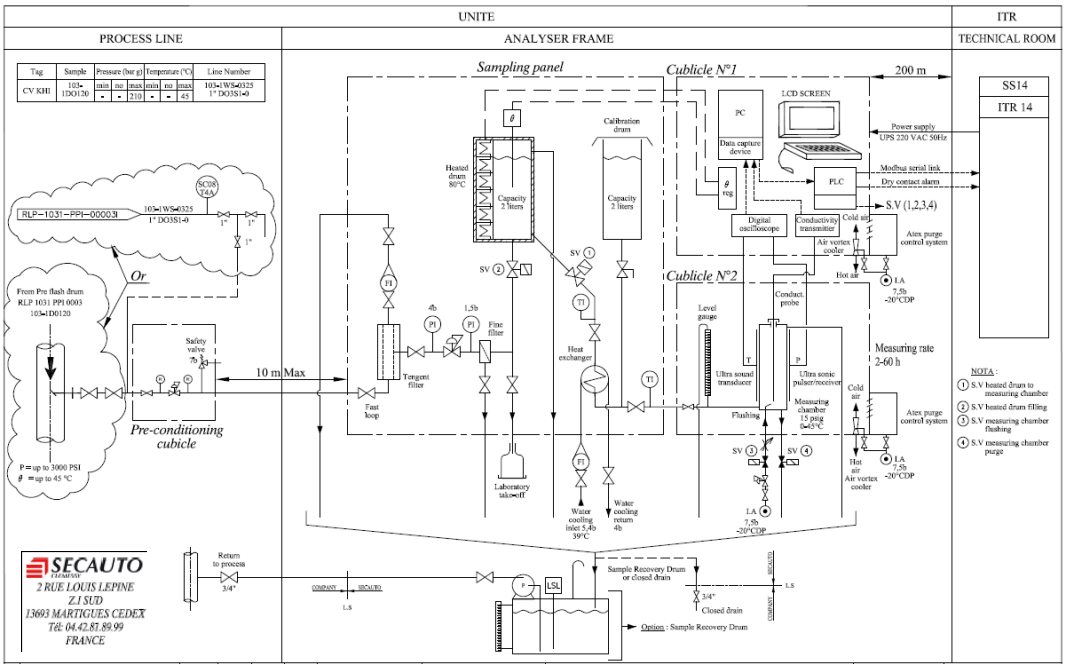

Figure 6.11 Online indirect C-V measurement P&ID developed in corporation with SECAUTO.

6.2.5. Improvement of Calibration for KHI System

For each new KHI system, the device needs to be recalibrated and this calibration depends on the concentrations and temperature ranges and sometimes may take 1 month to be developed. For some KHIs, we have developed and tested a new quicker calibration procedure because there was large interest in using C-V method in oil and gas industry for KHI systems.

For a salt system, we have:

$$v = f(T, x_{salt}) \qquad \text{Equation 6.3}$$

$$\sigma = h(T, x_{salt}) \qquad \text{Equation 6.4}$$

Where v and σ are the velocity and conductivity of the solution, respectively. T is the temperature of the sample and x_{salt} is the concentration of salt. For KHI systems, we have found out that the conductivity can be simply expressed as:

$$\sigma = 1 + g(T, x_{KHI}) \times f(T, x_{salt}) \qquad \text{Equation 6.5}$$

$$g(T, x_{KHI}) = (a_0^{KHI} + a_1^{KHI} \times T) \times x_{KHI} + a_2^{KHI} \times x^2{}_{KHI} \qquad \text{Equation 6.6}$$

Where x_{KHI} is the concentration of KHI in the sample and a_i are constants, which need to be determined for each system.

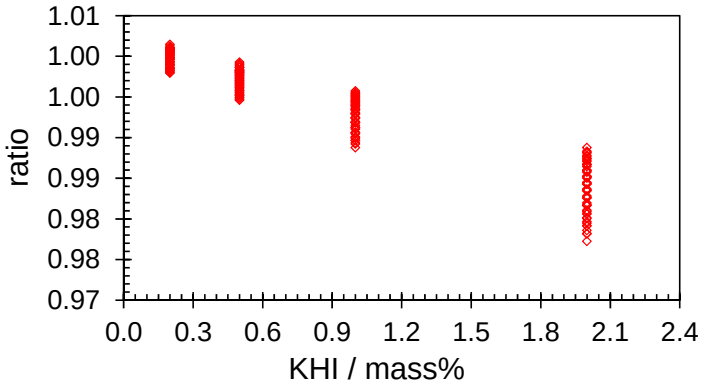

Figure 6.12 Ratio of the measured KHI/salt conductivity with the KHI free conductivity vs. KHI concentration.

Where x_{KHI} is the concentration of KHI in the sample and a_i are constants, which need to be determined for each system.

For velocity, we have similarly:

$$v = 1 + h(T, x_{KHI}, x_{salt}) \times f(T, x_{salt}) \qquad \text{Equation 6.7}$$

$$h(T, x_{KHI}) = (b_0^{KHI} + b_1^{KHI} \times T) \times x_{KHI} + b_2^{KHI} \times x_{KHI}^2 + b_3^{KHI} x_{KHI} x_{salt} \qquad \text{Equation 6.8}$$

Because of the nature of these equations, calibration data are only necessary for 2 temperatures and for a limited number of KHI concentrations.

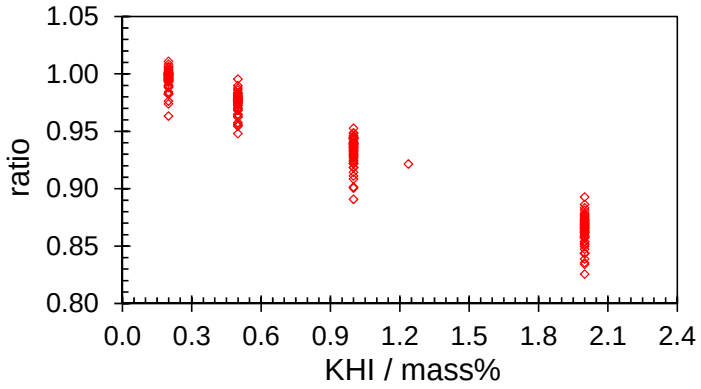

Figure 6.13 Ratio of the measured KHI/salt velocity with the KHI free velocity vs. KHI concentration.

6.2.6. CV Prototype Evaluation – Laboratory Results

In this section the developed prototype has been evaluated for different solutions containing salt, thermodynamic inhibitors, low dosage hydrate inhibitors (different KHI's and AA). The results have been presented in Table 6.1. The results showed that the developed prototype has a very good accuracy as well as good repeatability in different concentration at different temperatures.

Table 6.1 Laboratory evaluation of the developed prototype

Inhibition system	NaCl, mass%			Inhibitor, mass%		
	Exp.	C-V	AD	Exp.	C-V	AD
Deionised water	0.00	0.03	0.03	0.00	0.05	0.05
MEG-NaCl	3.50	3.49	-0.01	25.00	24.88	-0.12
MEG-NaCl	6.00	5.80	-0.20	35.00	34.76	-0.24
MeOH-NaCl	2.50	2.62	0.12	18.00	18.20	0.20
MeOH-NaCl	8.00	8.08	0.08	15.00	15.03	0.03
MeOH-NaCl	4.00	3.13	-0.87	24.00	23.32	-0.68
Ethanol-NaCl	7.00	7.06	0.06	15.00	15.09	0.09
Ethanol-NaCl	3.00	3.04	0.04	20.00	20.11	0.11
Ethanol-NaCl	5.00	5.14	0.14	45.00	45.27	0.27
LuvicapEG-NaCl	4.50	4.48	-0.02	0.80	0.87	0.07
LuvicapEG-NaCl	4.00	3.94	-0.06	1.50	1.53	0.03
KHI-NaCl	1.00	1.03	0.03	1.50	1.64	0.14
KHI-NaCl	1.50	1.54	0.04	2.20	2.38	0.18
AA(a*)-NaCl	1.00	1.26	0.26	0.80	0.91	0.11
AA(a*)-NaCl	0.50	0.47	0.03	1.50	1.23	0.27
AA(b*)-NaCl	2.00	2.14	0.14	2.50	2.61	0.11
AA(b*)-NaCl	1.00	1.17	0.17	1.0	1.19	0.19

a* stands for water soluble AA and b stands for oil soluble AA.

These lab tests showed that the fully automated developed prototype could successfully measure different concentration of salt and hydrate inhibitors (AA, KHI or thermodynamic inhibitors) in presence of salt with a very good repeatability and accuracy.

6.2.7. C-V Prototype Field Trials

The developed prototype was also evaluated in field laboratories by some of the oil and gas companies such as Total in Pau/France; Statoil in Trondheim/Norway; Dolphin Energy (Total) in Qatar; Petronas in Nouakchott/Mauritania; NIGC (National Iranian Gas Company) in South Pars Gas Complex (SPGC) fields/Iran and Champion Technology, Aberdeen/UK. In this section some of these field trials are briefly reported.

6.2.7.1. C-V Field Trial in South Pars Complex

South Pars is a giant gas condensate field in the Persian Gulf shared between Iran and Qatar (known as North Dome in Qatar). The field is the World largest gas field, with an estimated 50 trillion cubic meters of in-situ gas and around 50 billion barrels of condensate. In the Iranian part, the gas condensate field is connected with 110 km pipelines to various phases to onshore facilities in Assaluyeh for processing. Gas hydrates is a serious flow assurance problem during winter seasons. The design basis for most phases in the Iranian part is based on injection of MEG and MEG regeneration with KHI as back up. The produced water consists of condensed water and formation water. The produced gas contains H_2S and various techniques, including pH control and inhibitor injection are being used for corrosion control.

It is important to constantly monitor the concentration salts and MEG to prevent gas hydrate formation and pipeline blockage. Monitoring the concentration of lean and rich MEG in the MEG regeneration units are also being monitored continuously. The conventional techniques are based on densitometry, GC and a combination of the above.

Measuring MEG concentration using densitometer

There is a linear correlation between MEG concentration and density. Therefore, it is possible to generate a calibration curve based on MEG concentration and density for systems with known concentration of MEG. The calibration curve can then be used for measuring the un-known concentration of MEG by measuring density of the system. It should be noted that, both calibration tests and concentration measurement tests should be conducted at the same temperature, e.g. 20 °C.

This technique works well only in the early life of the field when the salt concentration is not varying. But after a while, it is no longer reliable due to changes in the concentration of salts in the system. The technique is not also applicable for measuring MEG concentration within the range of less than 10 mass %.

Using Gas Chromatography System

This method can produce accurate results for calculation of MEG concentration. The device can be used over all range of MEG concentrations from low value to 100%. However, salt deposition in the GC is a major problem and limits the application of this technique.

Combination of densitometer and GC Methods

The third method is a combination of the two methods mentioned above. It is currently being used in SPGC Phases 4 & 5 laboratory. Since the daily injection of samples into the GC depreciates the device and induces column break down, therefore, it used only once a week. Thus, the calibration curve generated for densitometry technique is being modified and verified by the results obtained from the GC on a weekly basis and new modified calibration curve is being used for calculating the concentration of the MEG samples.

In this field trial the aim was to investigate the feasibility of using C-V prototype in determining the concentration of salt and MEG. To conduct this evaluation the C-V prototype was used in the SPGC lab for their daily measurements routine beside the conventional methods.

The MEG Regeneration Unit of Phases 4&5 of SPGS has six packages named P1 to P6. Samples taken from each package are shown with the name of the package, i.e.

P1, etc. Samples from Unit (No. 102) are from inlet of the MEG regeneration unit. Samples collected from units 100ph4 or 100ph5 are those gathered from the slug catcher unit in the refinery and are the inlet MEG flows from the platform.

As a daily routine, the described samples are tested with the densitometer. The C-V device was used in parallel with both GC and densitometer on daily basis and results were compared to investigate its applicability and robustness. The first series of results are summarized in Table 6.2.

Table 6.2 Field evaluation of the C-V device – Series 1 (values are in mass %)

UNIT	GC	Density	CV		Δ(C-V & GC)	Δ(C-V & Density)
			MEG	Salt		
SC01-L. MEG	56.2	53.5	57.1	5.1	0.9	3.6
SC06-R. MEG	27.7	27.1	31.2	2.0	3.5	4.1
102/3	58.0	56.2	59.0	5.6	1.0	2.8
102/5	55.4	50.5	54.9	4.6	0.5	4.4
102/6	56.6	57.6	59.5	5.6	2.9	1.9
100/1	46.4	44.8	46.7	3.4	0.3	1.9
100/2	47.1	44.1	47.6	3.6	0.5	3.5

As one can see in this table the GC and densitometry results can only provide concentration of MEG but C-V could measure both salt and MEG concentration in one measurement. As the SPGC lab was not certain about the results of densitometry the main reference for the accuracy of the C-V was the results of GC measurements. It should be mentioned due to presence of salt in the sample SPCG lab mentioned that in some cases the GC measurements might not be accurate enough however it was the main reference in their measurements. As one can see in the table GC and C-V measurements are always very close to each other and the densitometer shows some deviation with both methods. Based on these first series of the tests, SPGC lab decided to stop the densitometry measurements due to low accuracy. Figure 6.14 shows the comparison of the GC and C-V measurements reported in the Table 6.2. This plot shows that GC and C-V are in very good agreements. Due to simplicity and

accuracy of the method SPGC lab was very much interested to continue the evaluation for a longer period of time for all their units.

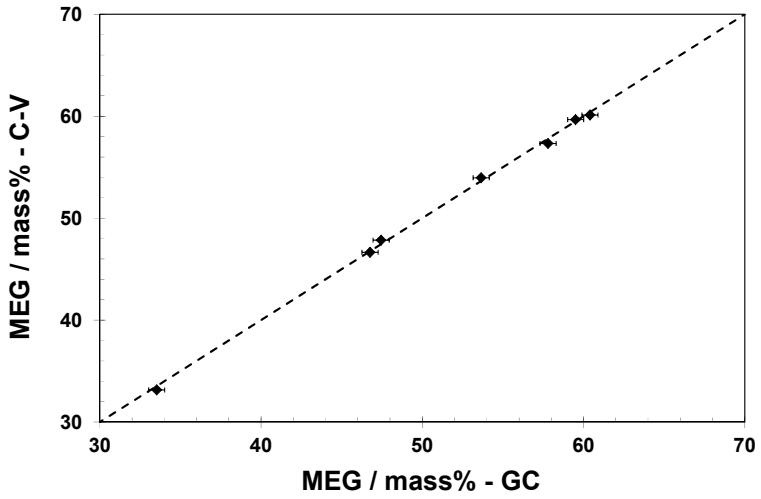

Figure 6.14 Comparison of C-V and GC measurements in the first series of tests (error bar is 0.5 mass %).

This evaluation was then continued for a period of three month however in this period GC and densitometer measurements were replaced with C-V prototype and GC was used every few often to confirm the C-V measurements. Figure 6.15 shows some part of comparison for C-V and GC measurements. As one can see in this figure GC and C-V are in very good agreement and the deviation is less than 0.5 mass%. It should be mentioned in some cases the deviation between the measurements were higher (not more than 2 mass %). No specific reasons were found for such deviation but in some cases the SPGC lab reported that due to presence of salt the GC gave wrong readings.

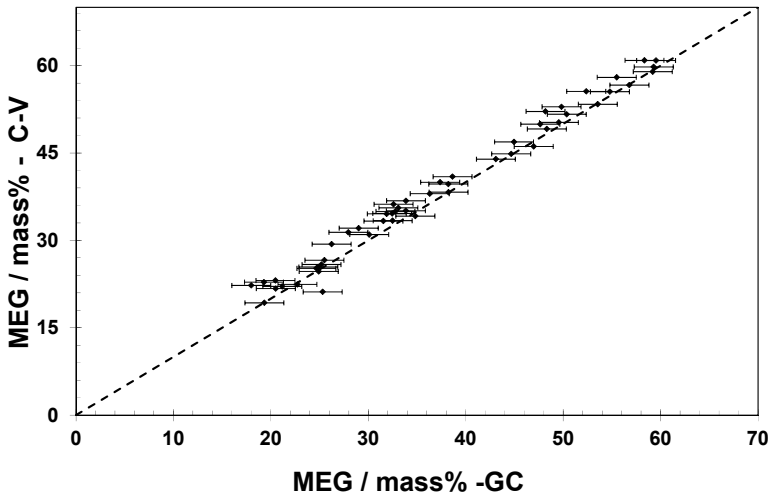

Figure 6.15 Comparison of C-V and GC measurements during the evaluation time (error bar is 2 mass %).

Following their evaluation, the South Pars Gas Complex (SPGC) decided to replace the GC and densitometry method with the C-V prototype. They have suggested some modification in the operation of the device as below:

- Designing a conductivity probe holder while cell is being loaded and the top lid should stay aside to protect the probe.
- At high temperatures sometimes the apparatus could not measure speed of sound and consequently could not output salt and inhibitor concentrations.
- Improving the sample draining connection after measurements.
- Automatically saving the measured data with time and date stamp in excel format.
- Improving the sample transfer procedure to avoid propagation of the sample smell (the SPGC samples contained sulphur compounds).
- Reducing the processing time (it was about two minutes at that time).
- Making the system more flexible to be used with the existing lab computers (at that time it has its built-in computer).

According to SPGC comments a standalone C-V prototype was designed. This new design was a flexible hardware which could be connected to any computer as well as laptop over a single USB port. The software was modified which automatically save the measured data with time and date stamp. The signal processing was completely changed. Averaging and curve fitting method were replaced with the autocorrelation method as described in the previous sections. This improves the measurement

accuracy and speed (processing time reduced to 25 seconds) and the wave is not affected by higher temperature (above 24 °C). A conductivity probe holder also was designed to hold the probe while loading the sample. The draining valve was replaced with a quick connection for convenience.

This field trial was a big step for the C-V prototype toward commercialisation and proving that this apparatus could be wildly used for hydrate monitoring purposes. The fast, accurate and robust property of the prototype beside its simple operation could cause a big saving in CAPEX and APEX in oil and gas industry.

6.2.7.2. C-V Field Trial in Dolphin Energy Qatar

Dolphin is a sour gas/condensate field located offshore Qatar about 70 km from shore in 55 m water depth. Two 36 inches production sea lines route the untreated fluids to the on-shore treatment plant. The maximum operating temperature and pressure are 90 °C and 125 bar, respectively. The hydrate risk exists only during winter times, either in the sealine but also at the slug-catcher reception. Regarding hydrate mitigation strategy, Dolphin Energy Ltd. has opted for a KHI continuous injection. A first injection is performed offshore in order to cover the risk of hydrate formation in the two 36" sealines. Because the hydrate risk occurs to be occasionally much higher at the level of the on-shore slug-catcher, a complementary second KHI injection is directly performed onshore when required at the slug-catcher inlet. This hydrate mitigation strategy has been implemented on the field since its start-up in 2007 without any major incident and is still going-on. Dolphin Energy Limited (DEL) decided to acquire one C-V device equipment to monitor the KHI concentration in produced waters and compare it with the usual chemical assay used since the field start-up.

Manual colorimetric method

This method is laborious and analyst should take care at all steps including the reagent preparation, sample dilution, and time period of colour generation. To do one single measurement the below steps should be followed:

- Sample preparation: in order to get rid of any excess hydrocarbon, take about 300 mL of produced water sample in a clean 500 mL separating funnel. Allow the sample 3 min for gravity separation. Draw 200 mL from the bottom as sample. Sample measurement:

- Primary dilution: Weigh 10.0 g of sample and add 90.0 g of deionised water. Note weight to 0.1mg. Mix well. Secondary dilution and measurement:
- Prepare duplicate test samples by taking 1.0 g from primary dilution and add 18.0 g of deionised water
- Weight should not exceed 19.0 g and note the weight. Weigh out 19.0 g of blank stock solution and run concurrently with samples.
- Add 5.0 g of Acetic Acid buffer solution. Note the weight.
- Add 1.0 g of freshly prepared Potassium tri-iodide solution. Note the weight. Start time measurement.
- Select Absorbance at 500 nm and after 15 min note down the blank absorbance.
- Measure the absorbance of the duplicate test samples.
- Extrapolate % KHI from prepared seven point calibration graph.

Results

To start the field trial, series of pre known standard samples were tested with both calorimetric method and C-V to evaluate the applicability and repeatability of C-V prototype for the field trial. Table 6.3 shows the results of these experiments

Table 6.3 KHI Standard Solutions checked by both calorimetric and C-V methods

S.N°	**Sample ID**	**Results (mass %)**	
		Calorimetric	**C-V**
1	2 % KHI Std sol	1.85	2.13
2	2 % KHI Std sol	2.05	2.03
3	2 % KHI Std sol	2.03	2.11
4	2 % KHI Std sol	1.62	2.12
5	2 % KHI Std sol	1.81	1.9
6	2 % KHI Std sol	1.8	2.08
7	2 % KHI Std sol	1.86	2.15
8	2 % KHI Std sol	1.82	1.95
9	2 % KHI Std sol	2.02	1.89
10	2 % KHI Std sol	2.07	2.11
11	4 % KHI Std sol	3.43	4.12
12	4 % KHI Std sol	4.06	4.01
13	4 % KHI Std sol	4.28	4.18
14	4 % KHI Std sol	4.4	3.85
15	4 % KHI Std sol	3.63	4.05
16	4 % KHI Std sol	3.86	3.9
17	4 % KHI Std sol	3.86	4.03
18	4 % KHI Std sol	3.92	4.11
19	4 % KHI Std sol	4.14	4.03
20	4 % KHI Std sol	4.54	3.88

This pre-evaluation showed a very good agreement between the standard known sample and the results were repeatable. As one can see from this table, C-V measurements in most of the cases show better accuracy in comparison to the colorimetric method. After confirming the repeatability and accuracy of C-V prototype with standard samples, produced water samples were measured. Table 6.4 shows the results.

Table 6.4 KHI Solution spiked in winter production water sample and checked by both manual and automatic methods.

S.N°	Sample ID	Results (mass %)	
		Calorimetric	C-V
1	Preflash drum	0.92	0.98
2	Preflash drum	0.92	1.05
3	Preflash drum	1.04	1.2
4	Preflash drum	1.08	1.11
5	Preflash drum	1.03	1.08
6	Preflash drum	0.99	0.88
7	Preflash drum	1.22	1.16
8	Preflash drum	1.05	1.19
9	Preflash drum	1.08	1.12
10	Preflash drum	0.93	1.06
11	1 % KHI Spiked Preflash drum	2.02	2.16
12	1 % KHI Spiked Preflash drum	1.96	2.15
13	1 % KHI Spiked Preflash drum	2.07	2.25
14	1 % KHI Spiked Preflash drum	1.98	2.24
15	1 % KHI Spiked Preflash drum	2.17	2.14
16	1 % KHI Spiked Preflash drum	2.23	2.1
17	1 % KHI Spiked Preflash drum	2.45	2.02
18	1 % KHI Spiked Preflash drum	2.03	2.06
19	1 % KHI Spiked Preflash drum	2.05	2.1
20	1 % KHI Spiked in 103 SC08 Preflash drum	2.18	2.01
21	3 % KHI Spiked Preflash drum	4.25	4.09
22	3 % KHI Spiked Preflash drum	3.93	4.31
23	3 % KHI Spiked Preflash drum	3.95	4.22
24	3 % KHI Spiked Preflash drum	4.22	4.05
25	3 % KHI Spiked Preflash drum	3.88	3.94
26	3 % KHI Spiked Preflash drum	4.3	4.15
27	3 % KHI Spiked Preflash drum	3.86	4.16
28	3 % KHI Spiked Preflash drum	3.97	4.22
29	3 % KHI Spiked Preflash drum	4.2	3.85
30	3 % KHI Spiked Preflash drum	3.92	4.12

These results showed that the C-V and calorimetric measurements in most cases are in very close agreement with each other. Considering the high accuracy of the C-V prototype in the results of the known solution tests explained earlier, the C-V measurements in this part can be also used with high level of confidence.

As a summary of this field trial, both calorimetric and C-V techniques were used and compared for the measurement of KHI concentration in different water solutions including real produced waters taken at the Dolphin slug-catcher outlet. Results show that both methods are almost equally accurate. The C-V prototype is incomparably faster compared to the manual method. This automated C-V technique has allowed Dolphin to rapidly monitor the KHI present in the waters at reception facilities and in its own manner has then contributed to the success of the KHI deployment on this field.

6.2.7.3. C-V prototype Field Trial in Total- Alwyn Field/UK

The Alwyn Area lies in the UK sector of the North Sea 160 kilometres east of the Shetland Islands and 440 kilometres north-east of Aberdeen. It comprises five fields – Alwyn North, Dunbar, Ellon, Grant and Nuggets. Collectively the fields produce some 150,000 barrels of oil equivalent a day. In these fields methanol are being injected at the upstream for hydrate inhibition. Produced water samples from the downstream reception facility has been analysed to determine concentration of methanol in the formation water for monitoring purposes. The concentration of methanol was being determined in these fields using the conventional method Karl Fischer titration and salt concentration with ionic analysis on irregular basis. However, these methods are time consuming and not accurate enough for hydrate monitoring purpose. Therefore, a field trial for C-V prototype was requested by Total/UK.

C-V prototype was initially tested in our laboratory for two different samples of field produced water. The results were also confirmed using gravity method and FTIR (Fourier Transform Infra-Red). Results (concentration of salt and methanol) of both methods were in very good agreement (better than 0.2 mass %) with the C-V method. Therefore the prototype was sent to Nuggets platform for field evaluation. During this period, the C-V prototype had been used in daily basis beside the conventional method. Figure 6.16 shows an example of the results of these measurements. As one

can see in this figure, there is almost constant deviation between methanol concentrations measured using KF (Karl-Fischer) and C-V method which has been shown with Δ(KF-CV) in this graph. Our investigation showed that this deviation is due to KF measurement method which shows total concentration of salt plus methanol instead of only methanol concentration. The comparison between salt concentration and Δ(KF-CV) confirmed this conclusion.

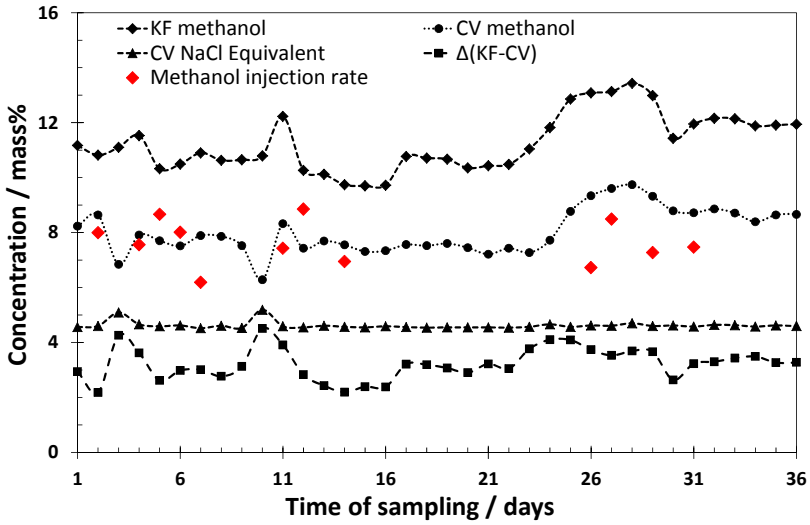

Figure 6.16 Comparison of C-V and Karl-Fischer measurements during the evaluation time.

Based on these results and the field provided data (Table A.11 and Table A.14, pressure and temperature profile), the C-V prototype has been used to predicted the hydrate phase boundary. Figure 6.17 shows the predicted hydrate phase boundary.

In this figure four hydrate phase boundaries have been plotted. The red dotted plot represents hydrate phase boundary for deionised water. The black points are the pipeline temperature and pressure operation conditions. As can be seen, the system is in hydrate risk zone in the absence of methanol and salt.

The orange dashed curve shows the actual hydrate phase boundary for the system determined using C-V prototype. This curve shows that the system with their current methanol injection rate is in the hydrate safe zone. The blue solid curve in this figure is the phase boundary predicted based on the concentrations determined using KF method. As it was expected, this hydrate phase boundary has been shifted to lower temperatures (left side) due to the error in methanol concentration measurements with

KF. In the other word, this system mistakenly shows that the system is safer than what it actually is. For example if the operating temperature falls to 2 °C or below, the system will be inside hydrate risk zone while the KF method shows it is in the safe zone. As can be seen from this figure, the operation condition is about 4 °C outside hydrate phase boundary with the current methanol injection rate meaning that the system is over inhibited. It was suggested to reduce the methanol injection rate. The green dashed curve in this graph shows the new phase boundary with the proposed optimised injection rate.

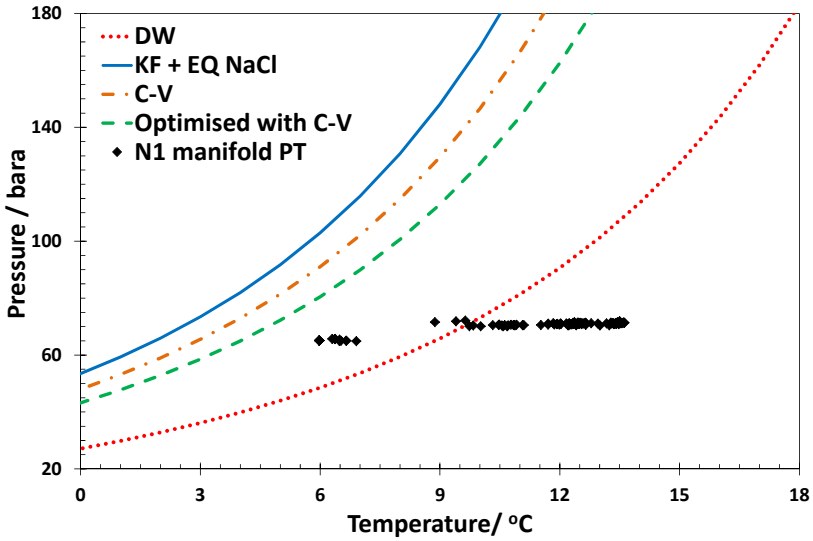

Figure 6.17 Comparison of C-V and Karl-Fischer measurements during the evaluation time.

6.2.7.4. Other Field Trials for C-V Prototype

In addition to the field trials explained in previous sections, five further field trials have been conducted for the developed C-V prototype; however due to confidentiality only a brief description of these field trials will be presented here.

Champion technologies

Champion technologies, as a global supplier of oilfield speciality chemicals, extensively tested the applicability of C-V prototype for measuring concentration of a commercial KHI in presence of salt and corrosion inhibitors. The comparison of actual and measured data shows a good agreement for the tested KHI concentrations of 0.4, 1, 2 and 5 mass%. However, the results of CV measurements were not quite as

accurate for concentrations lower than 0.4 mass% KHI (0.15 and 0.2 mass%) due to the 0.1 mass% uncertainty in CV prototype measurements for the tested KHI system. In the presence of salt in the system this uncertainty was reduced.

In continuation of this trials, effect of different impurities, e.g. presence of hydrocarbon, corrosion inhibitors and heavy aromatic naphtha, on the measurements were investigated. In presence of n-heptane the measured concentrations were dropped compared to actual concentrations and the data showed some variation over time period of the test. The 1 mass % samples showed a steady upward trend from 0.6% to 1.1% while the 2% samples remained almost constant. In presence of heavy aromatic naphtha, the results showed a similar pattern to that observed in presence of n-heptane. The measured concentrations were significantly dropped upon addition of naphtha but the readings appeared to be almost stable over time. These changes and variations in KHI concentration readings are attributed to the effect of n-heptane and aromatic naphtha on solubility and partitioning of KHI in aqueous phase.

Also in this field trial different combination of some commercial chemical has been investigated to study the partitioning of the KHI in presence of these chemicals as well.

In general, they have concluded that the C-V prototype works in the broad sense of the word. The instrument will measure the concentration of a KHI formulation in a brine solution, or when partitioned with organic solvents, either straight chain or heavy aromatic naphtha. The generated data is broadly accurate and is reliable in terms of reproducibility.

In another field trial Personas has investigated the prototype in the Chinguetti field, Berge Helene FPSO, Mauritania. In this field, methanol is being used as hydrate inhibitor. The aim of this field trial was to evaluate the applicability of the C-V prototype for optimising inhibitor injection rate. Two series of tests were conducted with formation water taken from the separator. The results of these measurements were also compared with their in-house measurement method in the laboratory. The first series of the tests showed a very good agreement between C-V measurements and their in-house method for both salt and methanol concentrations. In the next series of the test there was a fluctuation in C-V readings and the results showed a very large deviation between the C-V measurements and the lab measurements. Further

investigations showed that a crack had happened on the glass part of the conductivity probe and therefore the readings were not valid.

In a field trial conducted in South Africa, temperature controlled C-V prototype was used to evaluate the three parameter method. The aim was to investigate applicability of the C-V prototype in determining MEG, NaCl and KHI concentrations in aqueous phase. Results of these evaluation showed that C-V prototype could measure the concentration of salt and MEG fairly accurate however the concentration of KHI was not accurate enough. In addition it should be mentioned that the injected KHI at upstream was 1 mass%. As this field trial was for a short period of time (less than a week) there was no way to troubleshoot the reported problem. On the return of the device to our lab, it was found that the ultrasound transducers were loosens (might be caused due to transportation) and it was caused a slight shift in sound velocity results. Because salt and MEG concentration were high enough this shift did not significantly caused error in their measurement but for KHI the situation was different. Because of very small amount of KHI (less than 1 mass %) this deviation in sound velocity caused the ANN to optimise the error and as this value was below 1 mass %, so the output was converged to a number around 0.5 mass%. Also it was concluded using the 3 parameter method for concentration below 1 mass % in not accurate enough as it was reported that the average error could be a number around 0.4 mass%. This average error could be acceptable for higher concentration above 1 mass %.

In another field trial Total has used the jacketed C-V prototype in Pau, France for their research centre to develop ANN for specific chemicals. They have reported successful development of different ANN for their specific chemicals.

Statoil in Trondheim has also conducted a field trial for C-V prototype and their report showed the successful results for MEG system.

Regarding to the successful development and field trials of the prototype, this prototype has been commercialised through a university spin-out company Hydrafact Ltd. The C-V prototype name now has been changed to HydraCHEK™ and more than 5 of them are in operation in different oil and gas field helping to improve hydrate monitoring and inhibitor optimisation.

6.3. WATER ACTIVITY PROTOTYPE

As described in chapter 3, a correlation was developed which directly relates water activity to hydrate suppression temperature. A water activity measurement device, the Labmaster-aw, was used to measure water activity of solutions under examination. It was shown that Labmaster-aw works well for MEG and salt solutions. To facilitate this water activity method for hydrate monitoring, a software programme has been developed. The programme controls Labmaster-aw and automatically measure water activity and then determines the hydrate suppression temperature by using the developed water activity correlation in this research (detailed in chapter 3). The developed prototype is also linked to the in-house thermodynamic model and determines hydrate phase boundary hence hydrate safety margin and the degree of inhibition as well. Figure 6.18 shows the GUI of the water activity software programme and Figure 6.19 shows the water activity measurement window. Figure 6.20 is an example of predicted hydrate phase boundary using this prototype.

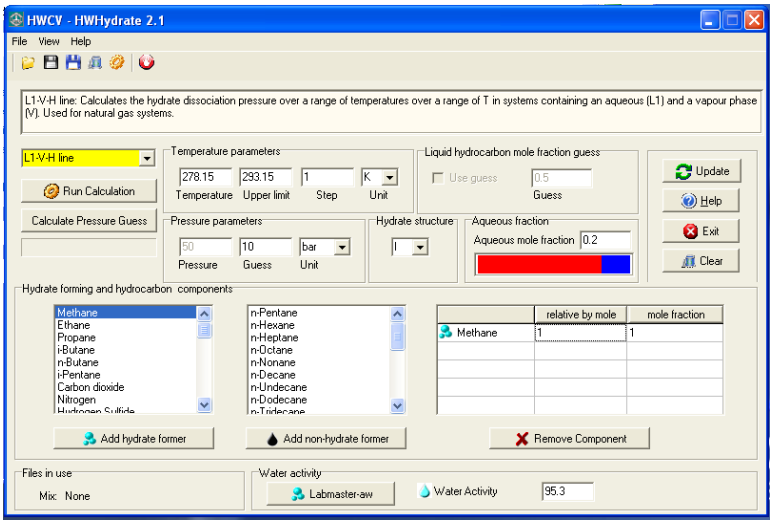

Figure 6.18 GUI of the water activity software programme.

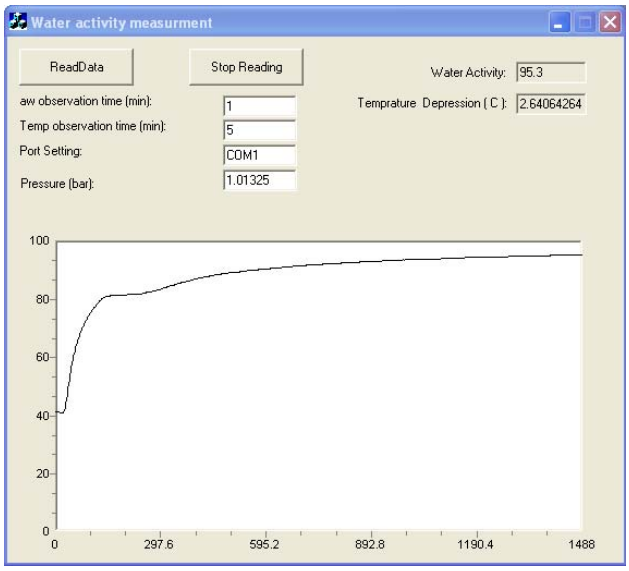

Figure 6.19 Water activity measurement window.

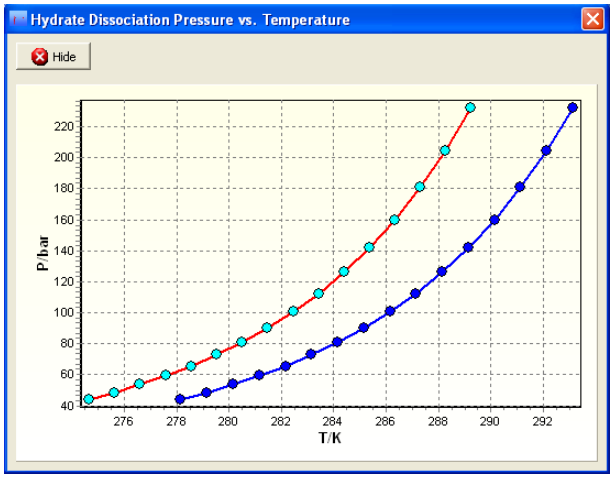

Figure 6.20 Example of predicted hydrate phase boundary using using water activity prototype.

CHAPTER 7. CONCLUSIONS AND RECOMMENDATIONS FOR FUTURE

7.1. CONCLUSIONS

Gas hydrate formation poses high risks to oil and gas transport pipelines. Currently, hydrate inhibitor injection is the most common measure to prevent hydrate blockages. However, lack of any hydrate monitoring and warning techniques results in barriers to improve the reliability of flow assurance operation and unnecessarily more cost and severer impact to the environment. In this thesis, a number of novel techniques have been developed for monitoring hydrate inhibition and detecting early signs of hydrate formation based on downstream sample analysis and online measurements. The main achievements of this study can be categorised as follow.

7.1.1. Hydrate Inhibition Monitoring Techniques

The aim of hydrate inhibition monitoring techniques is to provide an accurate and timely data of the degree of hydrate inhibition in the pipeline or processing facilities, i.e., how far away the operating conditions are from the HSZ. The techniques perform measurements of physical parameters of produced fluids, which are then used to either

directly calculate hydrate phase boundary or indirectly determine the hydrate safety margin using the measured inhibitors concentrations. Three techniques, i.e. conductivity-velocity (C-V) technique, water activity technique and water content technique, were developed for determining the hydrate risk free zones and optimising inhibitor injection rates.

In C-V technique, it was found that the conductivity and velocity monotonically response to the concentration changes in salt and hydrate inhibitors and their concentrations in certain ranges. This technique was developed for a number of two-parameter inhibition systems: a) water-soluble AA-salt systems, b) oil-soluble AA-salt systems, c) ethanol-salt systems and d) KHI-salt systems as well as a three-parameter systems: KHI-MEG-salt systems. For AA-salt systems (0-3 mass% AA concentration), the performance of the technique was good. However, higher concentration of salt (3 mass%) resulted in precipitation of the tested AAs, which in turn caused confusion for the trained ANN and affected performance of the technique. Therefore, it was recommended to dilute the samples before measurements to avoid the precipitation problem. This dilution function was also implemented later in the developed prototype of the C-V device. The ethanol-salt system covered the concentration range of 0 to 50 mass% for ethanol and 0 to 10 mass% for salt. Due to packing effect of ethanol in water, two separate ANN was trained: one for 0 to 20 mass% ethanol concentration and the second one for 30 to 50 mass%. The results show that the C-V technique can be successfully used for determining ethanol concentration in the presence of salt. The results for the KHI-salt system also showed good agreement between the ANN outputs and the experimental data, further confirming the applicability of the C-V method for KHI systems. Moreover, the conductivity-velocity method was further evaluated by comparing the hydrate phase boundaries predicted for the actual inhibitor concentrations with the ones for the concentrations measured using the C-V technique. These phase boundaries were in good agreement with each other, demonstrating that the C-V method can be used for monitoring hydrate safety margin with high level of confidence. Results for the three-parameter method show that the developed three-parameter ANNs can accurately determine concentrations of MEG and NaCl and that the errors could be obviously larger for the low concentration range of KHI (0 to 1 mass %). However, this method could still potentially be used for some specific cases: (1) the ratio of KHI to

MEG is known, (2) high concentration (e.g., higher than 3 mass%) KHI is used, (3) the accuracy of the KHI concentration is not essential.

In water activity/content techniques, it was found that the suppression of hydrate dissociation temperature due to the presence of salts and hydrate inhibitors can be determined by measuring the water activity of a liquid phase or the water content in the vapour phase of a sample without the need to know the specific type of the salts and thermodynamic inhibitors. Thermodynamic modelling was also performed to predict the water activity and water content for the experimentally tested inhibition systems, which showed good agreement with the experimental measurements. In the water activity technique, a general correlation was developed which relates the water activity of aqueous phase to hydrate suppuration temperature. The correlation was intensively evaluated with different systems, e.g. different MEG mixtures in the presence and absence of different concentrations and types of salts (NaCl, KCl, CaCl2 and MgCl2) or synthetic/real produced water. The results were compared with our in-house thermodynamic model. The results showed that the correlation can be used for different mixtures and has a very good accuracy (0.5 °C in HSZ). Moreover to validate the correlation, both correlation and the model were compared with literature data and very good agreement was observed. The water activity technique was further improved by taking into account the thermodynamic properties of the inhibitors in the pseudo concentration method. The required information for this method is the type of injected inhibitor and a rough estimation of the salinity of the aqueous phase. The results showed that using pseudo concentrations significantly improved the accuracy of the water activity technique.

Water content technique was introduced as a complementary technique for water activity method for the cases that online monitoring is required or where there is no access to aqueous phase samples. In this technique water content in vapour phase was related to an equivalent concentration of a hydrate inhibitor in the aqueous phase. The equivalent concentrations were used to predict the hydrate phase boundary using the in-house model. Accuracy of the technique was intensively evaluated for the systems containing different concentrations and types of thermodynamic inhibitors (MEG and methanol from 0 to 50 mass%) and salt (0 to 15 mass%). The results showed that this method could be used for online monitoring of hydrate inhibition. The error analysis

showed that the error of the water content measurement setups should not be higher than 2 ppm to have desired accuracy for the determined hydrate phase boundaries. Therefore, two different commercial water content setups (TDLAS - SpectraSensor S2000TM and HMT360 Vaisala humidity transmitter) were tested to evaluate their applicability for facilitating the water content technique.

TDLAS setup was tested for salt, MEG, methanol, synthetic produced water-methanol and synthetic produced water-MEG systems in the presence of methane or natural gas under flowing conditions. The results showed that this setup is suitable for methane systems but its error in the presence of natural gas is not in the acceptable range for water content technique. The result for systems containing methanol inhibitor was not good enough, either. Vaisala humidity transmitter was tested for salt only systems and MEG-salt systems under static measurement conditions. The results showed that this setup is accurate for measuring water content in the presence of natural gas. The predicted hydrate phase boundaries were in very good agreement with those predicted using actual concentrations. The accuracy achieved by using this device was better than 1 °C in the hydrate phase boundary, though the deviation slightly increased at high concentrations of MEG. This setup was further evaluated at conditions very close to real systems and the results were fairly acceptable with less than 2 °C deviation in the phase boundaries.

7.1.2. Initial Hydrate Formation Detection Techniques

The main objective of detecting early signs of hydrate formation is to give the operators adequate time to prevent hydrate plug formation and start remediation actions if it is required. Two techniques including the onset of hydrate formation (hydrate memory) and compositional change were developed for detecting initial hydrate formation.

Onset of hydrate formation technique is based on detecting hydrate memory. The principle of the technique is that hydrate forms more easily, i.e. at less degree of subcooling, from a solution with hydrate memory than from a freshly prepared gas-water mixture. An experimental setup named mini cell was especially designed and built for facilitating the initial hydrate formation detection method. Feasibility of this

purpose-built setup for detecting the onset of hydrate formation was experimentally examined. In evaluation of the feasibility of hydrate memory technique, the effect of hydrate memory on the onset of hydrate formation was investigated for different systems, i.e. salt, methanol, MEG, KHI and produced water systems. In each system, the dependence of hydrate memory on the retaining time (3, 6, 12 and 18 h) and the temperature outside the hydrate stability zone (3, 6, 9, 12 and 18 °C) was tested. In general, increasing retaining time and temperature outside hydrate stability zone (TOHSZ) expedited the hydrate memory disappearance. The results suggested that for each system at a given TOHSZ, how long the hydrate memory can be effective or vice versa for a given retaining time; how far outside the hydrate stability zone the system can be to remain the hydrate memory detectable. From practical view point, this information is very important and useful in selecting the right point of the sampling (e.g. downstream pipeline or separator). The results were promising for the deionised water system, different brine systems (different concentration of salt solution as well as a real produced water system), MEG and real produced water systems and methanol and real produced water systems. The results for the other systems also suggested that the presence of salts and MEG in the system prolonged the hydrate memory effect, while the presence of methanol reduced the sustainability of the hydrate memory. In the systems treated with KHI (LuviCap EG), the retaining time at 5 °C TOHSZ was shortened to maximum 3 hours. It was found that the memory was disappeared at higher TOHSZs and at lower TOHSZs (e.g. 3 °C) hydrate didn't dissociate even after one day, which was due to the effect of the KHI on kinetic of formation and dissociation of hydrate. Therefore, KHI treated systems needs more investigations, which is beyond of the scope of this work.

To further examine the applicability of the technique, sampling conditions and procedures were also examined in this study. The effect of depressurisation after hydrate formation/dissociation was investigated to see if it is possible to take samples at atmospheric conditions for hydrate memory detection. The results showed that depressurising to very low pressures destroys the hydrate memory. For the tested system (brine-natural gas system), minimum pressure of about 35 bara is required to sustain the hydrate memory effect. In continuation of the work, the possibility of simplifying the test procedure was also examined by replacing the produced natural gas

with a simple gas or gas mixture like methane or lab-held natural gas with different compositions. The results recommended conducting the test with original gas samples from the same system (pipeline or surface facility) rather than replacing with another gas.

Compositional change technique relies on the fact that composition of gas in both free gas and dissolved gas significantly changes due to hydrate formation. In this technique, the changes in the composition of gas phase and gas released from aqueous phase were investigated for detecting hydrate history. In investigating the compositional change in gas phase, two methods were used for detecting hydrate history: Ultrasound (studying the effect of compositional change on speed of sound in gas phase) and GasPT (this sensor can measure pseudo gas composition of methane, propane, carbon dioxide and nitrogen). The results of both methods showed that gas phase compositional change technique could detect hydrate formation for more than 5 bbl/MMscf of water converted to hydrate. In investigating compositional change in extracted gas from aqueous phase, it was found that propane concentration was significantly increased in the gas released from aqueous phase resulted from hydrate dissociation in comparison with the same system without any hydrate history. The effects of different parameters on the gas compositional change were experimentally tested, such as hydrate saturation, retaining time, temperature outside the hydrate stability zone, and the presence of different inhibitors (MEG, methanol and KHI) and salts. In each system, the gas released from aqueous phase resulted from dissociation of hydrate was analysed with GC and GasPT. For each test, the gas released from aqueous phase when no hydrate was formed was also analysed and compared with the one with hydrate experience. In all the tested systems it was seen that hydrate history caused a significant increase in C3/C1 ratio in comparison to the corresponding blank test. Because of high dependency of the system to gas solubility in aqueous phase, black oil was used to investigate distortion of results due to the presence of oil in the system. Results showed that propane to methane ratio was still high in comparison to the blank test. To further simulate the pipeline condition a continues fresh gas flow was applied in another series of experiments and the results showed a much bigger difference between the blank test and the sample from water with hydrate history. These results confirmed that this method could possibly give better results in pipeline conditions. In general, it was demonstrated that the compositional

change in gas phase and the extracted gas could be a robust method for detecting early sign of hydrae formation therefore can be a very powerful complementary method for other hydrate monitoring and initial hydrate formation detection techniques developed in this thesis. A patent of this method has been successfully filed for commercialised applications in future. A field trail at one of the sponsor's facilities has been planned to evaluate the feasibility of this method for real applications.

7.1.3. Development of Prototypes

Following the above fundamental studies, prototypes of the C-V and water activity techniques have been developed. The developed C-V prototype can determine salt and hydrate inhibitor concentrations simultaneously by an artificial neural network (ANN) correlation using the measured conductivity and velocity, and can also predict the hydrate stability zone with an integrated in-house thermodynamic model using the determined salt and inhibitor concentrations given that the hydrocarbon composition is known. The autocorrelation approach was applied to improve the accuracy and reliability of the C-V prototype. The C-V prototype has been commercialised after intensive evaluation in our lab and under field conditions by some oil and service companies. A water activity correlation was developed to determine the suppression of hydrate dissociation temperature using the measured water activity over a wide range of temperature and pressure for salt systems and salt-MEG systems. Pseudo salt and inhibitor concentrations were introduced to improve the accuracy of water activity technique. The developed water activity prototype can determine hydrate suppression temperature and stability zone using the measured water activity by integration with our in-house thermodynamic model and a commercial water activity meter.

The developments of hydrate inhibition monitoring and initial hydrate formation detection techniques open a novel flow assurance approach for the oil and gas industry. The developed hydrate monitoring techniques like the C-V technique, water activity and content techniques can be used to optimise hydrate inhibitor injection hence reducing their economic cost and impact on the environment. In the near future, further development of the investigated early hydrate formation detection techniques like gas

compositional change technique could provide an effective measure to minimise the risk of hydrate blockage.

7.2. RECOMMENDATIONS FOR ADDITIONAL RESEARCH

This thesis serves as an important step for other researchers who wish to further investigate and develop novel techniques for hydrate inhibition monitoring and initial hydrate formation detection. Following issues are recommended for further studies.

1. Following on very successful development of the C-V technique/prototype and its commercialisation (under HydraCHEK trademark) and considering the high demand for its on-line version, it is recommended to expand its applicability for online measurement. For this purpose, in this study as it was mention in Chapter 6, a high pressure conductivity probe has been designed, built and tested. However, the probe failed after a short while due to corrosion. Modifying this high pressure conductivity probe will be able to facilitate online version of this technique.
2. In the current version of the C-V prototype, sound velocity is measured using two transducers (transmitter and receiver).The size of the setup can be reduced by using a transducer based on reflection. Applicability of reflection method needs to be evaluated for this purpose.
3. The C-V technique for three parameters systems were developed for MEG-KHI-salt system. It would be useful to expand the three parameter method for other systems like MEG-AA-salt, methanol-KHI-salt, etc.
4. Although the results of water activity technique showed that it is very viable technique, the existing sensor cannot measure the water activity of aqueous solutions containing methanol due to the effect of methanol on the measuring sensor. As methanol is very volatile it will be evaporated and goes to the measuring part of the sensor and will affect the measurement results. The problem was reported to the supplier and they are working on the sensor to solve this problem. Having a sensor which can be used in the presence of volatile components can further extend the application of this technique.

5. In developing the water content technique, the results of evaluating TDLAS apparatus showed that this apparatus is not suitable for natural gas system. To overcome this limitation, it is recommended to tune TDLAS for natural gas system. Similar tuning can be also performed for methanol as well.
6. When developing the onset of hydrate formation (hydrate memory) technique for KHI systems, it was found that the memory behaviour of KHI inhibited systems became much more complicated due to the interfering of KHIs on kinetics of hydrate formation and dissociation, which was beyond the scope of this thesis. This can be systematically investigated in the future works.
7. During development of the onset of hydrate formation (hydrate memory) technique, sampling conditions and procedures were also examined and addressed in this work. In continuation of this work, it is recommended to design a sampling device to match the suggested sampling condition and procedure.
8. A Mini cell was designed and evaluated in this study for facilitating the onset of hydrate formation (hydrate memory) technique and the results showed that it can be effectively used for this purpose. However, the external mixing system of this setup had limitation for sub-zero conditions. The mixing design of this setup can be improved to extend its applicability to sub-zero condition and consequently to higher inhibitor and salt concentrations. The cooling and heating system of this system can also be changed to thermoelectric devices which will make the technique more user friendly for field application.
9. The gas analysing system in developing the gas compositional change technique was based on manual sampling or sampling on flow condition at reduced pressures. It would be very useful to use an online gas analyser, e.g., online GC or any other available online gas analyser, which can be used under pipeline pressures.
10. Field trials for the developed techniques (water activity and water content, hydrate memory, and compositional change) in this work are highly recommended in order to provide a high level of confidence for their performance at real fields.

References

Anderson, R., Chapoy, A., Tanchawanich, J., Haghighi, H., Lachwa-Langa, J. and Tohidi, B., 2008. Binary Ethanol-Methane Clathrate Hydrate Formation in the System CH4-C2H5OH-H2O: Experimental Data and Thermodynamic Modelling. *6th International Conference on Gas Hydrates,* Vancouver, British Columbia, CANADA, 6-10 July 2008.

Anderson, R., Mozafar H. and Tohidi B., 2011. Development of A Crystal Growth Inhibition Based Method for the Evaluation of Kinetic Hydrate Inhibitors. *7th International Conference on Gas Hydrates*., Edinburgh, Scotland, United Kingdom, July 17-21, 2011.

Argo C.B., Blain R.A., Osborne C.G., Priestley I.D. Commercial deployment of low-dosage hydrate inhibitors in a Southern North Sea 69 km wet-gas subsea pipeline. *SPE Production & Facilities*, 2000; **15**: 130-134.

Avlonitis D. A. 1992. Thermodynamics of gas hydrate equilibria. PhD dissertation, Heriot-Watt U., Edinburgh, United Kingdom.

Avlonitis D., Danesh,A., Todd A.C., 1994, Prediction of VL and VLL Equilibria of Mixtures Containing Petroleum Reservoir Fluids and Methanol with a Cubic EoS. *Fluid Phase Equilibra*., **94**, 181-216.

Barker J.W., Gomez R.K., 1989. Formation of hydrates during deepwater drilling operations. *Journal of Petroleum Technology* **41**, 297-301.

Bonyad, H., Zare, M., Mosayyebi, M. R., Mazloum, S., Tohidi, B., 2011. Field Evaluation of A Hydrate Inhibition Monitoring System, *Offshore Mediterranean Conference*, Ravenna, Italy, 2011.

Brustad S., LØken K.-P., Waalmann J.G. Hydrate prevention using MEG instead of MeOH: Impact of experience from major Norwegian developments on technology selection for injection and recovery of MEG. *OTC 17355, Offshore Technology Conference*, Huston, Texas, USA, 2-5 May, 2005.

Buchanana, P., Soper, A.K., Thompson, H., Westacott, R.E., Creek, JL, Hobson, G, Koh, CA. 2005.Search for memory effects in methane hydrate: Structure of water before hydrate formation and after hydrate decomposition. *J Chem Phys*; **123**(16): 4507.

Carson, D.B. and Katz, D.L.: *Natural Gas Hydrates*. Trans., AIME ~1942:146, 150

Chapoy, A.: Phase Behaviour in Water/Hydrocarbon Mixtures Involved in Gas Production Systems, Ph.D. Thesis, Paris School of Mine, 2004.

Clay C.S., Medwin H., 1977. *Acoustic Oceanography: Principles and Application*, New York, Wiley.

Corrigan, A.; Duncan, S.; Edwards, A. R.; Osborne, C. G. *In Proceedings of the SPE 70th Annual Technical Conference*, Dallas, TX, October 1995; SPE 30696

Cowie J., Bollavaram P., Erdogmus M., Johnson T., Shero W. 2005. Optimal hydrate management and new challenges in GoM deepwater using "Best in Class" technologies. OTC 17328, *Offshore Technology Conference*, Huston, Texas, USA, 2-5 May, 2005.

Frank, H. S., & Evans, M. W. (1945). Free volume and entropy in condensed systems III. Entropy in binary liquid mixtures; partial molar entropy in dilute solutions; structure and thermodynamics in aqueous electrolytes. *J. Chem. Phys*., **13**, 507-532.

Franks, F. & Ives, D. J. G. (1966). The structural properties of alcohol-water mixtures. Quarterly Reviews, 1-44.

Fu B., Neff, S., Mathur A., Bakeev K. 2002.Application of low-dosage hydrate inhibitors in deepwater operations. *SPE Production & Facilities*; **17**: 133-137.

Goodenough T.I.J., Rajendram V.S., Meyer S., Pretre D., 2005. Detection and qualification of insoluble particles by ultrasound spectroscopy, *Ultrasonics*, **43**, 231-235.

Hammerschmidt, E.G. 1934. *Gas Hydrate Formations*, **15**, No. 5, 30, 94.

Henning, B., Daur, P.C., Prange, S., Dierks, K., Hauptmann, P., 2000. *Ultrasonics*, 388, 799-803.

Holder G.D., Corbin G., Papadopoulos K.D., 1980, Thermodynamic and molecular properties of gas hydrate from mixtures containing methane, argon and krypton, Ind. *Eng. Chem. Fundamental*., **19**, 282-286

Hoppe, R., Martin, R. L., Pakulski, M.K. and Schaffer, T. D., 2006. Corrosion Mitigation with Gas Hydrate Inhibitors. *SPE Gas Technology Symposium.* Calgary, Alberta, Canada, 15-17 May 2006.

Hwang MJ, Wright DA, Kapur A, Holder GD. 1990. An experimental study of crystallization and crystal growth of methane hydrates from melting ice. *Journal of Inclusion Phenomena and Macrocyclic Chemistry*; **8**:103-116

Jeffrey, G. A. (1993). Hydrogen bonding with sugars and the role of hydrogen bonding in molecular recognition. In J. A.Kanters. M. Mathlouthi, & (Eds.) G.G. Birch, Sweet-taste Chemoreception (pp. 1-10). Essex: Elsevier Science Publishers Ltd.

Jerie K., Baranowski A., Przybylski J, Glinski J., 2004. Electrolytic solutions in ethylene glycol: ultrasonic and positron annihilation studies, *Physics Letters* A, 323, 148-153.

Kappatos, T., Gordon, M. H., & Birch, G. G. (1996). Solution properties of vanillin and diacetyl in aqueous-ethanol solutions. *Food Chemistry*, **57**(2), 275-282.

Katz, D.L.: 1945.*Prediction of Conditions for Hydrate Formation in Natural Gases*. Trans., AIME 160, 140.

Kawasaki T, Kikuchi K,Terasaki D, Toshiharu Okui, Miyata K, Hirayama H, Ihara Masaru. 2002. Composition of Guests in Hydrates from Gas Mixture, *Proceedings of the Fourth International Conference on Gas Hydrates*, Yokohama, 2002.

Kelland M.A. History of the development of low dosage hydrate inhibitors. *Energy & Fuels*, 2006; **20**: 825-847.

Kihara T., 1953, Virial coefficient and models of molecules in gases, Rev. *Modern Phys*., **25**(4), 831– 843

Kobayashi T., Imura N., Ohmura R. and Mori H. 2007. Clathrate Hydrate Formation by Water Spraying in a Methane + Ethane + Propane Gas Mixture: Search for the Rate-Controlling Mechanism of Hydrate Formation in the Presence of Methylcyclohexane. *Enargy &Fuels*,. **21**, 545-553

Kondo W., Ogawa H., Ohmura R. and Mori H. 2010. Clathrate Hydrate Formation from a Hydrocarbon Gas Mixture:Evolution of Gas-Phase Composition in a Hydrate-Forming Reactor. *Enargy Fuels*,. **24**, 6375-6383

Lederhos J P, Long JP, Sum A, Christiansen RL, Sloan ED. Effective kinetic inhibitors for natural gas hydrates. *Chemical Engineering Science* 1996; **51**(8):1221-1229.

Lederhos J.P., Long J.P., Sum A., Christiansen R.L., Sloan E.D. Effective kinetic inhibitors for natural gas hydrates. *Chemical Engineering Science*, 1996; 51: 1221-1229.

Levenberg K., 1944. A method for the solution of certain non-linear problems in least squares, *Quarterly Journal of Applied Mathematics*, 2,164-168.

Malcolm J. W. Povey, 1997. *Ultrasonic techniques for fluids characterization*. California: Academic Press

Marquardt D.W., 1963. An algorithm for least squares estimation of non-linear parameters, *Journal of the Society of Industrial and Applied Mathematics*, **11**, 431-441.

Masoudi, R., Tohidi, B.: "Estimating the Hydrate Stability Zone in the Presence of Salts and/or Organic Inhibitors Using Water Partial Pressure", *Journal of Petroleum Science and Engineering*, **46**, 23-36, 2005.

Mitchell G.F., Talley L.D. Application of kinetic hydrate inhibitor in black-oil flowlines. SPE 56770, SPE Annual Technique Conference and Exhibition, Houston, Texas, USA, 3-6 October. 1999.

Mohammadi, A.H., and Richon, D. Estimating the Hydrate Safety Margin in the Presence of Salt or Organic Inhibitor Using Refractive Index Data of Aqueous Solution. Ind. *Eng. Chem*. *Res*. 2006, **45**, 8207-8212.

Mohammadi, A.H., martinez-Lopez, J.F., Richon, D., 2007. Determination of hydrate stability zone using electrical conductivity data of salt aqueous solution, *Fluid Phase Equilibria*, **253**, 36-41.

Mokhatab, S., Wilkens, R. J. and Leontaritis, K. J., 2007. A Review of Strategies for Solving Gas Hydrate Problems in Subsea Pipelines. *Energy Source,* 29(Part A), pp.39-45.

National Physical Laboratory, 2000. Underwater Acoustics: Speed of Sound in Pure Water, NPL, UK

Nielsen, R.B. and Bucklin, R.W.: ''Why Not Use Methanol for Hydrate Control, Hydrocarbon Process. April 1983 71.

Notz P.K., Bumgardner S.B., Schaneman B.D., Todd J.L. Application of kinetic inhibitors to gas hydrate problems. *SPE Production & Facilities*, 1996; **11**: 256-260.

Ohmura R, Ogawa M, Yasuoka K, Mori YH. Statistical Study of Clathrate-Hydrate Nucleation in a Water/Hydrochlorofluorocarbon System: Search for the Nature of the "Memory Effect. *J Chem Phys*. B 2003; 107:5289-5293

Ostergaard, K. K., Masoudi, R., Tohidi, B, Danesh, A.,. Todd, A.C. 2005. general correlation for predicting the suppression of hydrate dissociation temperature in the presence of thermodynamic inhibitors. *Journal of Petroleum Science and Engineering* Volume 48, Issues 1–2, 30 July 2005, Pages 70–80.

Ostergaard, K.K., B. Tohidi, Danesh A., Todd A.C, , and Burgass R.W. 2000. A General Correlation for Predicting the Hydrate-Free Zone of Reservoir Fluids. SPE Prod. & Facilities, Vol. 15, No. 4,

Ostergaard, K.K., Masoudi, R., Tohidi, B., Burgass, R.W., Danesh, A., Todd, A.C., 2005. A general correlation for predicting the suppression of hydrate dissociation temperature in the presence of thermodynamic inhibitors, *Journal of Petroleum Science & Engineering*, **48**, 70-80.

Padmini, P. R. K. L.; Ramachandra Rao, 1961. Molar Sound Velocity in Molten Hydrated Salts. *Nature* **191** (4789): 694 - 695.

Parent JS, Bishnoi PR. Investigations Into the Nucleation Behaviour of Natural Gas Hydrates. *Chem Eny Comm* 1996; 144:51-64

Parrish W.R., Prausnitz J.M., 1972, Dissociation pressures of gas hydrates formed by gas mixtures, *Ind. Eng. Chem. Process Des. Dev*., **11**(1), 26–35

Radiometer analytical SAS, 2004. *Conductivity Theory and Practice*.

Ripmeester J.A., Tse J.S., Ratcliffe C.I. and Powell B.M. (1987) A new clathrate hydrate structure, *Nature*. **325**, pp. 135–136.

Rodger PM. Methane Hydrate Melting and Memory Annals of the New York Academy of Sciences 2000; 912:474-482.

Sandengen, K.,and Kaas, B., 2006. Estimation of Monoethylene glycol (MEG) content in water-MEG-NaCl+NaHCO3 solutions*, Journal of Chemical Engineering Data*, 51, 443-447.

Seo Y, Kang S, Jang W. Structure and Composition Analysis of Natural Gas Hydrates: C NMR Spectroscopic and Gas Uptake Measurements of Mixed Gas Hydrates. J Phys Chem A 2009;113:9641–9649.

Sloan E.D. A changing hydrate paradigm-from apprehension to avoidance to risk management. *Fluid Phase Equilibria*, 2005; 228-229: 67-74.

Sloan E.D., 2000. Hydrate engineering. Edited by Bloys J.B., Richardson, Texas: Society of Petroleum Engineers Inc.

Sloan E.D., Koh C.A. Clathrate *Hydrates of Natural Gas*, Third ed. Boca Raton, U.S.A.: CRC Press, 2008.

Sloan ED, Subramanian S, Matthews PN, Lederhos JP, Khokhar AA. Quantifying Hydrate Formation and Kinetic Inhibition. *Ind Eng Chem Res* 1998; 37:3124-3132

Smith J P, Clancy J. Understanding AGA Reprot NO. 10, Speed Of Sound in Natural Gas and Other Related Hydrocarbons Gases, Report no. 10 American Gas Association January, 2003

Sneha A. Parke, Gordon G. Birch, 1999. Solution properties of ethanol in water. *Food Chemistry* **67** (1999) 241-246

Takeya S, Hori A, Hondoh T, Uchida T. Freezing-Memory Effect of Water on Nucleation of CO2 Hydrate Crystals. *J. Phys. Chem*. B 2000; 104:4164-4168

Tohidi B., Burgass R. W., Danesh A. and Todd A. C. (1993). Hydrate Inhibition Effect of Produced Water, Part-1. Ethane and Propane Simple Gas Hydrates. Paper SPE 26701 presented at the SPE *Offshore European Conference, Aberdeen*, United Kingdom, 7-10 September.

Tohidi, B., Chapoy, A. and Yang, J., Developing a Hydrate-Monitoring System. SPE Project, *Facilities & Construction* Journal, 4 (No. 1), pp:1-6 2009 .

Tohidi, B., Danesh, A., Todd, A.C., Burgass, R.W., 1996. Measurement and prediction of hydrate-phase equilibria for reservoir fluids. *SPE Production & facilities*, **11**, 69-76.

Tohidi-Kalorazi B., 1995, Gas hydrate equilibria in the presence of electrolyte solutions, Ph.D. thesis, Heriot-Watt University

Valderrama JO., 1990, A generalized Patel-Teja equation of state for polar and non-polar fluids and their mixtures, *J. Chem. Eng. Jpn*., 23, 87-91

Valderrama, J. O. A Generalized Patel-Teja Equation of State for Polar and Nonpolar Fluids and Their Mixtures, *Journal of Chemical Engineering of Japan*, 1990 23(1), 87-91

Van der Waals J.H., Platteeuw J.C., 1959, Clathrate solutions, Adv. *Chem. Phys*., **2**, 1–57

van Rossum, G. J., (ed.) Gas Quality. Proceeding of the congress, Specification and measurement of physical and chemical properties of natural gas, Groningen, Netherlands, 22-25 April 1986. Amsterdam: Elsevier Science Publishers B.V.

Vibhu, I., Singh, A.K, Gupta M., Shukla, J.P., 2004. Ultrasonic and IR investigation of N-H--N complexes in ternary mixtures, *Journal of Molecular Liquids*, 115, 1-3.

Von Stackelberg M. and Müller H.R. (1954) Feste Gashydrate II, Zeitschrift für Elektrochemie 58, Nr. 1, 104.

Von Stackelberg M., (1949) Feste Gashydrate, Naturwissenschaften 36, No. 11, 327-359.

Vyas, J.C., Katti, V.R., Gupta, S.K., Yakhmi J.V., 2006. A non-invasive ultrasonic gas sensor for binary gas mixtures, *Sensors and* Actuators B, 115, 28-32.

Vysniauskas A, Bishnoi PR. A kinetic study of methane hydrate formation. *chemical engineering Science* 1983; 38(7):1061-1972.

Wilcox, W.I., Carson, D.B., and Katz, D.L.: Natural Gas Hydrates, *Ind. Eng. Chem*. 1941, 33, 662.

Wright, M.R., 2007. *An Introduction to Aqueous Electrolyte Solutions*. Wiley. ISBN 978-0-470-84293-5.

Yang, J., Chapoy, A., Mazloum, S. and Tohidi, B., 2011. Development of a Hydrate Inhibition Monitoring System by Integration of Acoustic Velocity and Electrical Conductivity Measurements. *Journal of Exploration and Production: Oil and Gas Review*, 9 (1), pp.36-40.

Yousif, M.H, Young, D.B.1993.A Simple Correlation to Predict hydrate point Suppression in Drilling Fluid. *SPE/IADC Drilling conference*, Amsterdam, 23-25 FEB 1993.

Zain ZM, Yang J, Tohidi B, Cripps A, Hunt A. Hydrate Monitoring and Warning System: A New Approach for Reducing Gas Hydrate Risks, *SPE the 14th Europec Biennial Conference Spain*, 2005.

Appendix A

Natural Gas and produced water Compositions used in this work

Table A.72 Natural Gas

Component	Mole%
C_1	88.79
C_2	5.3
C_3	1.55
iC_4	0.17
nC_4	0.3
iC_5	0.07
nC_5	0.04
CO_2	1.68
N_2	2.04

Table A.55 Natural Gas

Component	Mole%
C_1	89.95
C_2	5.19
C_3	1.44
iC_4	0.18
nC_4	0.26
iC_5	0.05
nC_5	0.03
CO_2	1.48
N_2	1.37

Table A.56 Natural Gas

Component	Mole%
C_1	89.39
C_2	5.08
C_3	1.45
iC_4	0.18
nC_4	0.26
iC_5	0.06
nC_5	0.06
CO_2	2.24
N_2	1.93

Table A.57 Natural Gas

Component	Mole%
C_1	88.83
C_2	5.18
C_3	1.64
iC_4	0.16
nC_4	0.27
iC_5	0.04
nC_5	0.04
CO_2	2.24
N_2	1.6

Table A.58 Natural Gas

Component	Mole%
C_1	88.15
C_2	5.59
C_3	1.9
iC_4	0.24
nC_4	0.39
iC_5	0.07
nC_5	0.07
CO_2	1.86
N_2	1.7

Table A.59 Natural Gas

Component	Mole%
C_1	93.28
C_2	1.47
C_3	1.93
iC_4	0.1
nC_4	0.18
iC_5	0.06
nC_5	0.05
CO_2	1.23
N_2	1.7

Table A.11 Natural Gas

Component	Mole%
C_1	98.94
C_2	0.08
C_3	0.00
iC_4	0.00
nC_4	0.00
iC_5	0.00
nC_5	0.00

Table A.61 Natural Gas

Component	Mole%
C_1	88.21
C_2	5.78
C_3	1.78
iC_4	0.19
nC_4	0.3
iC_5	0.06
nC_5	0.07

Table A.62 Natural Gas

Component	Mole%
C_1	88.3
C_2	5.4
C_3	1.5
iC_4	0.2
nC_4	0.3
iC_5	0.1
nC_5	0.09

CO_2	0.17	CO_2	2.15	CO_2	1.72
N_2	0.77	N_2	1.4	N_2	2.39

Table A.14 Produced Water

Ion	Mg/L
Na^+	16350
Mg^{2+}	388
Ca^{2+}	1398
Sr^{2+}	157
Ba^{2+}	116
K^+	138
Fe^+	3.1
Cl^-	29913

Table A.16 Black Oil

Component	Mass%	Mole%
C_1	0.00	0.00
C_2	0.00	0.00
C_3	0.00	0.01
iC_4	0.00	0.00
nC_4	0.00	0.00
iC_5	0.00	0.00
nC_5	0.00	0.00
C_6s	0.02	0.05
C_7s	0.11	0.25
C_8s	0.54	1.07
C_9s	2.13	3.72
C_{10}s	3.42	5.38
C_{11}s	4.59	6.58
C_{12}s	6.34	8.30
C_{13}s	7.86	9.46
C_{14}s	8.71	9.66
C_{15}s	9.27	9.49
C_{16}s	9.09	8.63
C_{17}s	8.59	7.64
C_{18}s	8.43	7.07
C_{19}s	7.16	5.73
C_{20}s	6.61	5.06
C_{21}s	7.55	5.47
C_{22}s	3.85	2.70
C_{23}s	2.61	1.76
C_{24}s	1.69	1.10
C_{25}s	0.95	0.59
C_{26}^+	0.47	0.28

Table A.65 Composition of produced water systems

Salt	Produced water			
	Maya	Petronas	Forties	Scale
NaCl	9.000	3.316	6.993	2.231
KCl	0.000	4.468	0.066	0.037
CaCl2	0.800	0.174	0.735	0.133
MgCl2	0.200	0.014	0.186	0.041
Na2SO4	0.000	0.609	0.000	0.000
SrCl2	0.000	0.000	0.099	0.016

BaCl2	0.000	0.000	0.036	0.011
Total Salt	10.000	8.852	8.115	2.469